

Numerical methods for optimal control and parameter estimation in the life sciences



Jesse Aeden Sharp
BBus, BMath (hons)

Submitted in fulfilment of the requirement for the degree of
Doctor of Philosophy

Mathematical Sciences
Faculty of Science
Queensland University of Technology (QUT)

“Science is made up of so many things that appear obvious after they are explained.”

– Frank Herbert, Dune

Abstract

Mathematical models provide valuable insight into complex processes in the life sciences. Models can further our understanding of underlying mechanisms, facilitate development and testing of hypotheses, guide experimentation and data collection, and design intervention strategies that optimise resource allocation. Models must be sophisticated enough to adequately capture the behaviour of the underlying system, while ideally admitting parameters that carry a physical interpretation, that can be estimated from available or obtainable data. Often, closed-form analytical solutions are not available for such models, so numerical techniques are required to obtain approximate solutions. This thesis concerns numerical methods, with a focus on techniques for optimal control, and for parameter estimation and uncertainty quantification. In the first part of this thesis, we consider numerical methods for optimal control, with a particular focus on the forward-backward sweep method (FBSM) for solving two-point boundary value problems. Initially, we apply optimal control techniques to a model of acute myeloid leukaemia, and investigate the convergence behaviour of the FBSM. Then, motivated by combination therapies observed in cancer treatment, we consider the application of multiple optimal controls simultaneously. Finally, we discuss numerical techniques to improve and accelerate its convergence. Connecting models with data poses significant challenges, particularly in the life sciences; where data is often limited, noisy or incomplete. As such, we are interested not only in point-estimates of parameters but also information characterising the associated uncertainty. In the second part of this thesis we explore techniques from information geometry to supplement traditional likelihood-based uncertainty quantification for parameter inference. The outcomes of this thesis include four published papers. Code for implementing all of the numerical methods used in this work, and for reproducing the results of each chapter, is available on [GitHub](#).

Statement of Original Authorship

The work contained in this thesis has not been previously submitted to meet requirements for an award at this or any other higher education institution. To the best of my knowledge and belief, the thesis contains no material previously published or written by another person except where due reference is made.

Signature:

A handwritten signature in blue ink that appears to read "J Sharp".

Date: March 31, 2022

Acknowledgements

I must first thank my primary supervisor, Professor Matthew Simpson. Mat, your ongoing support: from my early days as an undergraduate vacation scholar, to today at the end of my PhD journey; has profoundly and positively shaped my experience as a researcher. Without your patient, compassionate and efficient supervision, none of this would have happened. Thank you for showing me the kind of researcher that I can aspire to be.

To my associate supervisor, Professor Kevin Burrage. Kevin, thank you for always encouraging me to try new ideas, and having confidence in my ability to push beyond what I thought were my limits. With your encouragement, I have travelled further than I thought possible along this journey. I also thank my other collaborators on the works in this thesis: Doctors Tarunendu Mapder and Chris Baker, and Mr Alexander Browning.

Without generous financial support, this journey would have been over before it began. I thank the Australian Research Council for my scholarship. My supervisors Mat and Kevin, and the AF Pillow Applied Mathematics Trust, for top-up scholarships. I extend this thanks to the School of Mathematical Sciences at QUT, the ANZIAM student support scheme and the Australian Research Council Centre of Excellence for Mathematical and Statistical Frontiers for travel funding.

To Liam, Ryan and Alex – Thank you for your stimulating discussions, insight, banter; and above all else, friendship. Without you, this would not have been nearly as enjoyable.

To my understanding wife Natassja and my becoming more understanding every day toddler Rosa; thank you both for your love, patience and support. To my parents; thank you for raising me to be strong, independent and inquisitive. Dad, thank you for always showing your pride. Mum, I have no doubt you would have believed in me all the way – I wish only that you were still here to share this accomplishment with me...

List of Publications

1. **Sharp JA**, Browning AP, Mapder T, Burrage K, Simpson MJ (2019). Optimal control of acute myeloid leukaemia. *Journal of Theoretical Biology*.
[doi:10.1016/j.jtbi.2019.03.006](https://doi.org/10.1016/j.jtbi.2019.03.006).
2. **Sharp JA**, Browning AP, Mapder T, Baker CM, Burrage K, Simpson MJ (2020). Designing combination therapies using multiple optimal controls. *Journal of Theoretical Biology*.
[doi:10.1016/j.jtbi.2020.110277](https://doi.org/10.1016/j.jtbi.2020.110277).
3. **Sharp JA**, Burrage K, Simpson MJ (2021). Implementation and acceleration of optimal control for systems biology. *Journal of the Royal Society Interface*.
[doi:10.1098/rsif.2021.0241](https://doi.org/10.1098/rsif.2021.0241).
4. **Sharp JA**, Browning AP, Burrage K, Simpson MJ (2022). Parameter estimation and uncertainty quantification using information geometry. *Journal of the Royal Society Interface* [in press].
[arXiv:2111.12201](https://arxiv.org/abs/2111.12201).

Contents

Abstract	i
Statement of Original Authorship	iii
Acknowledgements	v
1 Introduction	1
1.1 Overview	1
1.2 Research questions	10
1.3 Objectives and outcomes of this thesis	11
1.4 Thesis structure	15
1.5 Statement of joint authorship	17
2 Optimal control of acute myeloid leukaemia	19
2.1 Introduction	22
2.2 Acute myeloid leukaemia model	24
2.3 Incorporating the immune response	27
2.4 Methods	32
2.4.1 Optimal control theory	32
2.4.2 Continuous optimal control	33
2.4.3 Bang-bang optimal control	41
2.4.4 Convergence and control updating	45
2.5 Conclusion and Outlook	48
3 Designing combination therapies using multiple optimal controls	51
3.1 Introduction	54
3.2 Optimal control theory	57
3.3 Case study: combination therapy for acute myeloid leukaemia	59
3.3.1 Continuous chemotherapy, continuous stem cell transplant controls	64
3.3.2 Continuous chemotherapy, bang-bang stem cell transplant controls	64
3.3.3 Bang-bang chemotherapy, continuous stem cell transplant controls	65
3.3.4 Bang-bang chemotherapy, bang-bang stem cell transplant controls	65

3.4	Results and discussion	66
3.4.1	Optimal strategies respond non-linearly to control parameters	66
3.4.2	Interesting optimal strategies can be transient in parameter space	67
3.4.3	Practical insights	68
3.5	Conclusion	70
3.6	Acknowledgements	71
4	Implementation and acceleration of optimal control in systems biology	73
4.1	Introduction	76
4.2	Forward-backward sweep method	81
4.2.1	Adapted forward-backward sweep method	83
4.3	Control problems	85
4.3.1	Single-variable linear model	85
4.3.2	Multiple-variable nonlinear model	89
4.4	Iterative accelerators	96
4.4.1	Newton and Quasi-Newton methods	96
4.4.2	Wegstein method	97
4.4.3	Aitken-Steffensen method	98
4.4.4	Anderson Acceleration	100
4.4.5	Acceleration methods applied to typical fixed point problems	100
4.5	Acceleration results	101
4.5.1	Tuning	101
4.5.2	Wegstein method	103
4.5.3	Partial Aitken-Steffensen method	104
4.5.4	Anderson Acceleration	105
4.5.5	Method comparison with best tuning	105
4.6	Discussion	108
4.6.1	Acceleration outcomes	108
4.6.2	Convergence insights	112
4.6.3	Summary and outlook	113
5	Parameter estimation and uncertainty quantification using information geometry	117
5.1	Introduction	120
5.2	Methods	126
5.2.1	Parameter inference	127
5.2.2	Information geometry	128
5.2.3	Hypothesis testing	133
5.2.4	Numerical implementation	133

5.3	Results	134
5.3.1	Normal distributions	135
5.3.2	Population growth models	140
5.3.3	SIR epidemic model	151
5.3.4	Hypothesis testing	156
5.4	Discussion	159
6	Conclusions and future work	165
6.1	Summary and contribution	165
6.2	Future work	168
6.2.1	Optimal control	168
6.2.2	Inference and uncertainty quantification	170
6.3	Final remarks	171
2A	Supplementary material to Chapter 2	173
2A.1	Arbitrary initial conditions	173
2A.2	Control affects all proliferative cells	175
3A	Supplementary material to Chapter 3	179
3A.1	Supplementary results	179
3A.1.1	Continuous chemotherapy, continuous stem cell transplant controls	179
3A.1.2	Continuous chemotherapy, bang-bang stem cell transplant controls	184
3A.1.3	Bang-bang chemotherapy, continuous stem cell transplant controls	187
3A.1.4	Bang-bang chemotherapy, bang-bang stem cell transplant controls	191
3A.2	Steady state behaviour	194
3A.3	Sensitivity	194
3A.3.1	Initial conditions	195
3A.3.2	Model parameters	195
3A.3.3	Steady state assumption	198
3A.3.4	Control parameters impact sensitivity	200
3A.4	Supporting code	203
3A.5	Forward-backward sweep method	203
4A	Supplementary material to Chapter 4	205
4A.1	Forward-backward sweep method algorithm	205
4A.2	Single-variable linear continuous control analytical solution	206
4A.3	Steffensen derivation	209
4A.4	Acceleration algorithms	213
4A.4.1	Wegstein method	213
4A.4.2	Aitken-Steffensen method	214

4A.4.3 Anderson Acceleration	215
4A.5 Test nonlinear systems	217
4A.5.1 Results	218
4A.6 Control results	222
4A.6.1 Linear continuous control problem	224
4A.6.2 Linear bang-bang control problem	224
4A.6.3 AML continuous control problem with the Wegstein method . . .	225
4A.6.4 AML continuous control problem with the partial Aitken method	226
4A.6.5 AML continuous control problem with the partial Steffensen method	227
4A.6.6 AML continuous control problem with Anderson acceleration . . .	228
4A.6.7 AML bang-bang control problem with the Wegstein method . . .	229
4A.6.8 AML bang-bang control problem with the partial Aitken method	230
4A.6.9 AML bang-bang control problem with the partial Steffensen method	231
4A.6.10 AML bang-bang control problem with Anderson acceleration . .	232
4A.6.11 Linear fixed endpoint control problem	233
4A.6.12 AML fixed endpoint control problem	233

Chapter 1

Introduction

1.1 Overview

Throughout the life sciences, we encounter systems with behaviour that we seek to understand and influence. Whether we consider virus transmission [1, 238], cancer treatment [25, 59, 290], muscle contraction and gait regulation [103, 181, 254], cellular processes in synthetic biology [87, 139], cell population growth [78, 294], or biodiversity and invasive species management [31, 61, 72]; we are faced with decisions about how to design interventions to achieve the best outcomes with limited resources.

Mathematical and computational models provide significant insight into complex processes in the life sciences. These versatile tools enable the development and testing of novel hypotheses, guide experimentation and data collection, facilitate interpretation of data, assist in generating parameter estimates, improve our understanding of biological interactions, and aid in the design of interventions. Mathematical models are a convenient, inexpensive tool for investigating biological processes and interventions; for which experimental data may be scarce, incomplete, cost-prohibitive to obtain, or of poor quality (noisy). However, due to these issues with data, challenges arise when estimating the parameters of mathematical models. Often, this leads us to consider not only point-estimates of parameters, but also measures of the uncertainty associated with the point-estimates. The overarching objective of this thesis is to develop, implement and improve numerical methods in the life sciences, and increase their accessibility. This thesis comprises two parts; with three chapters devoted to optimal control, and one devoted to parameter inference and uncertainty quantification using information geometry.

Optimal control

Acute myeloid leukaemia (AML) is a cancer of the blood, characterised by haematopoietic stem cells in the bone marrow becoming leukaemic [82, 233]. Leukaemic cells do not respond to normal regulators of cell proliferation and do not undergo normal differ-

entiation or maturation [100, 135]. The presence of leukaemic cells in the bone marrow disrupts normal blood function leading to significant mortality rates [6]. There are several approaches to treatment and management of AML, such as chemotherapy, immunotherapy, leukapheresis (centrifugal separation of white blood cells from whole blood), and radiotherapy [19, 233, 265]. Often clinical approaches will implement multiple therapies concurrently. Key benefits derived from a combination therapy approach include a reduction of the toxicity and adverse effects of treatment, and improved outcomes in the presence of drug resistance and tumour cell heterogeneity [35, 152, 338]. Administering stem cell transplants between rounds of chemotherapy enables clinicians to administer a higher dose of chemotherapy, reduces adverse effects of the chemotherapy, and reduces the risk of recurrence [59, 207, 339].

An ordinary differential equation (ODE) model describing AML in terms of the interactions between leukaemic stem cells and haematopoietic stem cells within the bone marrow niche is given by [82]:

$$\begin{aligned} \frac{dS}{dt} &= \rho_s S(K_1 - Z_1) - \delta_S S, \\ \frac{dA}{dt} &= \delta_S S + \rho_A A(K_2 - Z_2) - \delta_A A, \\ \frac{dD}{dt} &= \delta_A A - \mu_D D, \\ \frac{dL}{dt} &= \rho_L L(K_2 - Z_2) - \delta_L L - \underbrace{\frac{\alpha L}{\gamma + L}}_{\text{immune response}}, \\ \frac{dT}{dt} &= \delta_L L - \mu_T T, \end{aligned} \tag{1.1}$$

where $S(t)$, $A(t)$, $D(t)$, $L(t)$ and $T(t)$ represent haematopoietic stem cells, blood progenitor cells, terminally differentiated blood cells, leukaemia stem cells and fully differentiated leukaemia cells, respectively. A schematic outlining the interspecies interactions in the model is presented in Figure 1.1, alongside descriptions of the model parameters. We introduce the immune response as it is both biologically relevant and mathematically convenient, as we discuss in Chapter 2. Determining optimal chemotherapy treatment regimes is of great practical and theoretical interest. But how do we determine the appropriate dose, and over what duration should it be administered? Optimal control theory provides a mathematical framework through which to address these questions.

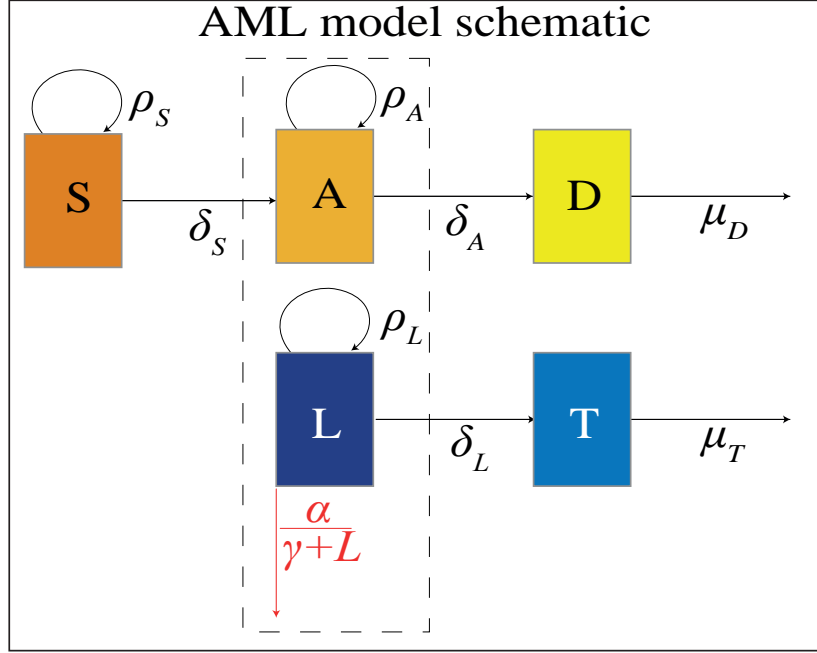


Figure 1.1: This schematic provides details of the interactions and associated parameters for the original model proposed in [82], with an immune response that we introduce in Chapter 2. Curved arrows represent proliferation, at rate ρ_i ; arrows between compartments represent cell differentiation at rate δ_i , with $i \in \{S, A, L\}$. Arrows out of the D and T compartments represent migration out of the bone marrow niche into the blood stream at rate μ_j , $j \in \{D, T\}$. The red arrow out of the L compartment represents death of leukaemic stem cells due to the immune response, at rate $\alpha/(\gamma + L)$. The grouping of $A(t)$ and $L(t)$ reflects resource competition between the leukaemic cells and the blood progenitor cells.

The seminal works of Pontryagin; through the Pontryagin Maximum Principle (PMP) [264], and Bellman; through dynamic programming and the Hamilton-Jacobi-Bellman equation [37], form the foundations of modern optimal control. These ideas build upon hundreds of years of development of the calculus of variations [125]. Optimal control is a science of trade-offs; whereby the benefits of control measures must be considered against their costs, to determine the best allocation of resources.

In the language of optimal control, the system of ODEs in Equation (1.1) constitute the *state equations*, expressed in vector form in Equation (1.2). The fundamental idea then, is to determine an intervention, the *control*, that causes the *state* to follow a more favourable trajectory, or arrive at a more desirable state. Specifically, the goal of optimal control is to identify the control that maximises or minimises a specified objective functional, the *pay-off*. In typical optimal control problems the state equations are expressed as functions of the state, $\mathbf{x}(t)$, and the control, $u(t)$, with either a fixed final time t_f , such that the final state is free to vary, or a fixed final state $\mathbf{x}(t_f)$, with the final time free to vary.

$$\frac{d\mathbf{x}}{dt} = f(t, \mathbf{x}(t), u(t)), \quad \mathbf{x}(t_0) = \mathbf{x}_0, \quad \mathbf{x}(t) \in \mathbb{R}^n. \quad (1.2)$$

The pay-off function, J , given in Equation (1.3), characterises what *optimal* means mathematically, within a given context. Typically the pay-off depends on some function, ϕ , of the final state, $\mathbf{x}(t_f)$, and/or a cumulative cost function, $\mathcal{L}(t, \mathbf{x}(t), u(t))$, integrated from initial time (t_0) to final time (t_f):

$$J = \phi(\mathbf{x}(t_f)) + \int_{t_0}^{t_f} \mathcal{L}(t, \mathbf{x}(t), u(t)) dt. \quad (1.3)$$

The optimal control, $u^*(t)$, is the control that minimises or maximises Equation (1.3). We illustrate key optimal control concepts in Figure 1.2, and through the following example. Suppose crop yield will grow from x_0 to $2x_0$ without intervention. To induce additional growth we may apply fertiliser. It is not obvious how much fertiliser should be applied, nor over what time period. The optimal application of fertiliser depends on the pay-off characterising optimality; the form of Equation (1.3) significantly impacts the dynamics of the optimal control. The optimal control may be continuous, such that the strength can be readily adjusted throughout time; or bang-bang (discontinuous), such that the control is applied exclusively at a lower or upper bound with finitely many discrete switching points.

To determine the optimal control, we apply Pontryagin's Maximum Principle (PMP) [264] to obtain necessary conditions for optimality. We construct the Hamiltonian, $H(t, \mathbf{x}, u, \boldsymbol{\lambda}) = \mathcal{L}(t, \mathbf{x}, u) + \boldsymbol{\lambda} \cdot f$, where $\boldsymbol{\lambda} = [\lambda_1(t), \lambda_2(t), \dots, \lambda_n(t)]$ for an n -dimensional state. The adjoint, $\boldsymbol{\lambda}$, links the state equations, f , to the pay-off via the Hamiltonian. The necessary conditions are obtained from the Hamiltonian [191]:

1. The optimality condition is obtained by minimising the Hamiltonian with respect to the control,

$$\frac{\partial H}{\partial u} = 0 \text{ gives } \left(\frac{\partial \mathcal{L}}{\partial u} + \boldsymbol{\lambda} \cdot \frac{\partial f}{\partial u} \right) = 0,$$

2. the adjoint is found by setting,

$$\frac{\partial H}{\partial \mathbf{x}} = -\frac{d\boldsymbol{\lambda}}{dt}, \text{ giving } \frac{d\boldsymbol{\lambda}}{dt} = -\left(\frac{\partial \mathcal{L}}{\partial \mathbf{x}} + \boldsymbol{\lambda} \cdot \frac{\partial f}{\partial \mathbf{x}} \right).$$

3. Finally, the transversality condition must be satisfied, namely

$$\boldsymbol{\lambda}(t_f) = \left. \frac{\partial \phi}{\partial \mathbf{x}} \right|_{t=t_f}.$$

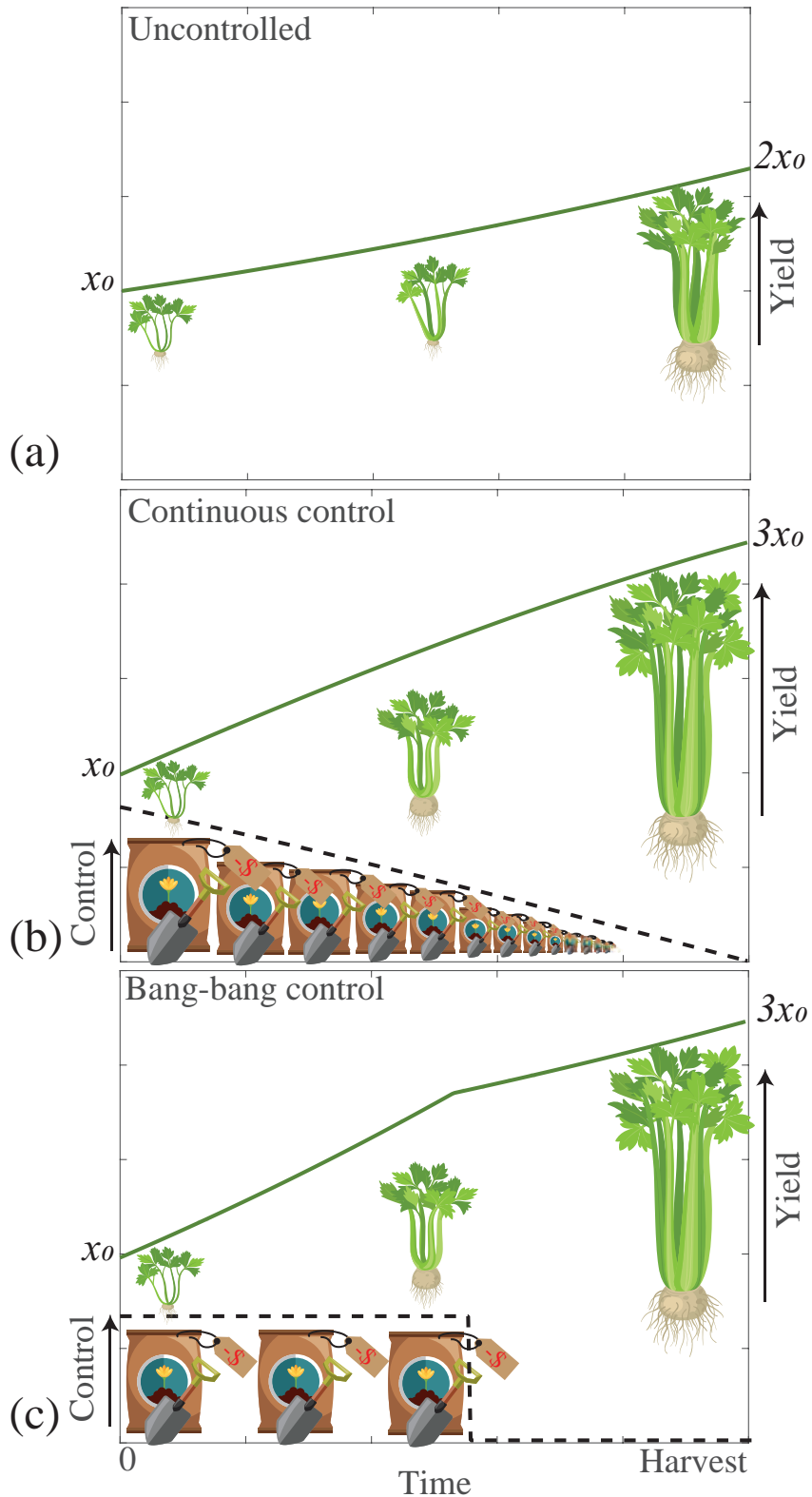


Figure 1.2: A pictorial example of optimal control for a growing crop. We want to grow this crop to increase the yield, represented by the green line. Actions taken to increase the growth rate of the crop; such as applying fertiliser, are the controls, represented using black dashed lines. Scenarios are presented for (a) no control, (b) continuous control, and (c) bang-bang control. Optimal control theory helps us determine how best to apply these controls. Illustrations adapted from ilyakalinin/iStock/Getty Images, johavel/iStock/Getty Images.

The adjoint, also referred to as the *co-state*, provides a link between our state and our pay-off function. The transversality condition defines a final-time condition on the co-state. Following these steps yields a two-point boundary value problem (TPBVP) for \mathbf{x} and $\boldsymbol{\lambda}$ that must be solved to determine the optimal control. A more detailed introduction to these optimal control concepts is provided in Chapter 2.

Underpinning the necessary conditions for optimality of the PMP is the assumption that an optimal control exists. For an optimal control to exist, the optimal control problem must have a solution; such that the pay-off is finite when evaluated at the optimal control and corresponding state [191]. Formally, existence of an optimal control requires that the *reachable set*—the set of all states traversed from all possible control sequences from an initial state \mathbf{x}_0 —is *compact*. A compact set is both bounded and closed [195]. For systems of ODEs of the form we consider in this thesis (Equation 1.2), compactness of the reachable set can be established via Filippov’s theorem [107]. This imposes requirements on the boundedness of the states and their derivatives. Throughout the work in this thesis, we assume the existence of an optimal control, and do not seek to treat it further. Additional information and examples concerning the existence of optimal controls can be sought in the following texts [171, 191, 195].

Seldom do the TPBVPs arising from optimal control problems admit closed-form analytical solutions. Instead, numerical methods are sought to obtain approximate solutions. Numerical methods for optimal control are generally classed as either indirect or direct methods. Indirect methods rely on deriving optimality conditions, such as via the PMP, often necessitating the solution to a two-point boundary value problem. For direct methods the control problem is discretised and reformulated as a nonlinear programming problem [275]. Early numerical methods in optimal control include gradient-based methods, Newton-Raphson methods, quasilinearisation, feasible direction algorithms and feedback solutions [56]. More recent developments include the forward-backward sweep method (FBSM), multiple-shooting methods, control parameterisation, collocation and pseudospectral methods and dynamic programming [275, 284].

The FBSM is a popular indirect method for solving optimal control problems in the life sciences—despite only satisfying necessary conditions for optimality, in contrast to the more powerful sufficient conditions satisfied by many direct methods—primarily because it scales well with system size and is conceptually relatively straightforward. Direct methods such as dynamic programming suffer significantly from the *curse of dimensionality*; use of this popular expression is particularly apt here, as it was originally coined by Bellman in direct relation to dynamic programming [38]. With a large number of state variables, as we frequently encounter in systems biology, the computational effort required to solve the control problem renders dynamic programming infeasible.

The FBSM starts from an initial guess for the control. The state equations are solved forwards in time, and the result is used to solve the co-state equations backwards

in time. This information is used in conjunction with the optimality condition obtained from the Hamiltonian to form an updated guess for the control. This procedure is applied iteratively. The forward-backward sweep method algorithm is presented in Algorithm 1.

Algorithm 1: Forward-backward sweep

- i. Make an initial guess for the control, $u^{(0)}(t)$.
- ii. Iterate for $k = 0, 1, \dots$, until converged or iteration limit met:
 - iii. Solve for $\mathbf{x}^{(k)}(t)$ forward in time using initial values $\mathbf{x}(0)$, and $u^{(k)}(t)$.
 - iv. Solve for $\boldsymbol{\lambda}^{(k)}(t)$ backwards in time from the transversality condition $\boldsymbol{\lambda}(t_N)$, using $u^{(k)}(t)$ and $\mathbf{x}^{(k)}(t)$.
 - v. Compute temporary update, $\hat{u}^{(k+1)}(t)$, using $\mathbf{x}^{(k)}(t)$, $\boldsymbol{\lambda}^{(k)}(t)$, and the optimality condition derived from minimising the Hamiltonian.
 - vi. Update $u^{(k+1)}(t) = \omega u^{(k)}(t) + (1 - \omega)\hat{u}^{(k+1)}(t)$.
 - vii. Check for convergence. If not converged, return to Step ii.

In Chapter 2 and Chapter 3 we apply this method to problems of practical and theoretical significance in the life sciences. In the course of these investigations, we identify and overcome challenges associated with numerical implementation and convergence of the algorithm; though such challenges are not the focus of these chapters. We demonstrate that the choice of ω , the control update weighting parameter in Step vi. of the FBSM, is a critically important factor in determining the convergence behaviour of the algorithm. Further, the appropriate choice of ω is problem dependent, and can be sensitive to model and control parameters. These issues are exacerbated where multiple controls are applied, as considered in Chapter 3. In Chapter 4 we comprehensively review the practical implementation of the FBSM and its convergence behaviour. We propose novel augmentations that improve the reliability and the rate of convergence.

Inference and information geometry

Significant challenges arise when calibrating models to data. Models should be sophisticated enough to adequately describe the behaviour of the system, while ideally admitting *identifiable* and physically interpretable parameters, that can be estimated from available or obtainable data [116, 199]. As previously noted, data can be scarce, incomplete, cost-prohibitive to obtain, or of poor quality. Due to these issues with data, there is uncertainty associated with parameter estimates. Quantifying and interpreting this uncertainty can improve our confidence in insights derived from models. Common approaches to uncertainty quantification include Bayesian methods, profile likelihood, asymptotic analysis and bootstrapping [114, 118, 231, 325, 330]. Uncertainty quantification also provides insight

into *identifiability*. Identifiability describes the degree to which model parameters can be determined from data [85], and is often considered in terms of *structural identifiability* and *practical identifiability* [28, 144, 298, 323, 324]. Structural identifiability relates to the underlying model structure and parameterisation; and refers to whether it is theoretically possible to determine unique parameter values, given an infinite amount of perfect noise-free data [50, 299]. Practical identifiability is less well defined, and depends on the quality and quantity of data available and prior knowledge of the parameters [50].

A standard method for parameter estimation is based on maximising the log-likelihood function, that represents the joint probability density of all the data for a given set of parameters. For a dataset $\mathcal{X} = [x_1, x_2, \dots, x_N]$ with unknown parameters, $\boldsymbol{\theta}$, the log-likelihood function is

$$\ell(\boldsymbol{\theta}; \mathcal{X}) = \sum_i^N \log f(x_i; \boldsymbol{\theta}), \quad (1.4)$$

where $f(x; \boldsymbol{\theta})$ is the probability density function associated with our observation process. The maximum likelihood estimate (MLE) is the point-estimate, $\hat{\boldsymbol{\theta}}$, that maximises $\ell(\boldsymbol{\theta}; \mathcal{X})$ in Equation (1.4).

Wilks' theorem states that asymptotically as $N \rightarrow \infty$, an approximate α -level confidence region is given by [255]:

$$\left\{ \boldsymbol{\theta} : \ell(\boldsymbol{\theta}) \geq \ell(\hat{\boldsymbol{\theta}}) - \frac{\Delta_{\nu, \alpha}}{2} \right\}, \quad (1.5)$$

where $\Delta_{\nu, \alpha}$ is the α th-quantile of the χ^2 distribution with ν degrees of freedom [52]. These confidence regions contour the log-likelihood function about the MLE, and their size in parameter space gives insight into the degree of uncertainty associated with the point-estimate. Using information geometry techniques we can explore the curvature of the parameter space, through an information metric derived from the likelihood function [11]. While likelihood-based approximate confidence regions rely on an asymptotic large sample argument [255], the geometric approach we consider provides data-agnostic insight into the *shape* and sensitivity of the parameter space. For example, we can compute *geodesic curves* describing geometrically the relationship between distributions with different parameters [228]; and we can compute the *scalar curvature* throughout parameter spaces to gain insight into uncertainty and identifiability.

Information geometry is a branch of mathematics connecting aspects of information theory including probability theory and statistics with concepts and techniques in differential geometry [11]. Central to information geometry in an inference context is the concept of a *statistical manifold*; an abstract geometric representation of a probability distribution space. For example, we can conceptualise the set of normal distributions parameterised by mean, μ , and standard deviation, $\sigma > 0$:

$$p(x; \mu, \sigma) = \frac{1}{\sigma\sqrt{2\pi}} \exp\left[-\frac{(x - \mu)^2}{2\sigma^2}\right], \quad x \in \mathbb{R},$$

as a two-dimensional surface with coordinates (μ, σ) [64]. The Fisher information describes the curvature of the log-likelihood function; incorporating information about the curvature induced by the observation process describing the data, and curvature induced by parameter sensitivities through a mathematical model linking parameter estimates to data. This highlights a link between sensitivity analysis, structural identifiability and practical identifiability [209].

In some areas of applied science, such as cosmology, information geometry techniques are used to supplement traditional likelihood-based uncertainty quantification [121]. However, these methods have not been widely adopted in the life sciences. We expect that the reason for this slow uptake in the life sciences is that the foundational theory of differential geometry is deeply rooted in the more formal mathematics literature that is seldom read by practitioners in the life sciences. In Chapter 5 we address this gap in the literature by outlining the key aspects of information geometry required for practical implementation of the techniques. We are cognisant that the majority of practitioners in the life sciences will not have prior knowledge of differential geometry, and present the techniques accordingly; using straightforward explanations and practical examples. We consider a combination of synthetic and publicly available data. By doing so, we open new avenues for uncertainty quantification in the life sciences.

1.2 Research questions

This thesis consists of two parts, each part within the purview of numerical methods in the life sciences. The first part pertains to optimal control. The second part relates to information geometry in the context of parameter inference and uncertainty quantification. We address the following research questions:

Part 1: Optimal control

- (1) Can we implement the PMP approach to solve optimal control problems that are of practical interest in mathematical biology?
- (2) How do the optimal control techniques we consider extend to more complex, clinically motivated treatment scenarios?
- (3) How can the disparate parts of the literature be unified, to improve accessibility of optimal control techniques to practitioners?
- (4) What can we do to improve and accelerate the convergence behaviour of the FBSM for optimal control?

Part 2: Parameter inference and information geometry

- (5) What insights emerge from combining techniques from information geometry with likelihood-based parameter inference?
- (6) How can we overcome the barriers preventing practitioners from applying information geometry techniques in the life sciences?
- (7) What do we learn from information geometry that is difficult to learn from standard likelihood-based methods?

1.3 Objectives and outcomes of this thesis

The objectives of this thesis are designed to address the research questions identified in Section 1.2. The key outcomes of this thesis are four published papers. The PhD candidate made significant contributions to all articles, and is recognised as the first author in each paper. As such, this work satisfies the Queensland University Technology requirements for thesis by publication.

The publications included in this thesis are:

1. **Sharp JA**, Browning AP, Mapder T, Burrage K, Simpson MJ (2019). Optimal control of acute myeloid leukaemia. *Journal of Theoretical Biology*.
[doi:10.1016/j.jtbi.2019.03.006](https://doi.org/10.1016/j.jtbi.2019.03.006).
2. **Sharp JA**, Browning AP, Mapder T, Baker CM, Burrage K, Simpson MJ (2020). Designing combination therapies using multiple optimal controls. *Journal of Theoretical Biology*.
[doi:10.1016/j.jtbi.2020.110277](https://doi.org/10.1016/j.jtbi.2020.110277).
3. **Sharp JA**, Burrage K, Simpson MJ (2021). Implementation and acceleration of optimal control for systems biology. *Journal of the Royal Society Interface*.
[doi:10.1098/rsif.2021.0241](https://doi.org/10.1098/rsif.2021.0241).
4. **Sharp JA**, Browning AP, Burrage K, Simpson MJ (2022). Parameter estimation and uncertainty quantification using information geometry. *Journal of the Royal Society Interface* [in press].
[arXiv:2111.12201](https://arxiv.org/abs/2111.12201).

We outline the objectives of this thesis and provide a brief summary of the outcomes of addressing each objective. Comprehensive details of each research outcome are provided in the main chapters of this thesis. For each objective, we identify the relevant chapter of the thesis where the work is documented and list the corresponding publication.

Part 1: Optimal control

- (1) Modify a stem cell model for AML to incorporate an immune response, and use optimal control techniques to investigate optimal chemotherapy treatment regimes.

We find a haematopoietic stem cell model of AML [82] that permits a stable steady state where populations of healthy and leukaemic cells coexist. The model also permits an unstable healthy steady state with no leukaemia. We modify the model by introducing a biologically appropriate and mathematically convenient immune response that is effective for small leukaemic populations and ineffective for large leukaemic populations, such that the modified model permits both healthy and

coexisting stable steady states. We apply continuous and bang-bang controls to the modified model under a range of parameter regimes to steer the system from a coexisting steady state to a healthy steady state. We investigate parameters that influence convergence behaviour of numerical optimal control techniques. The outcomes of this objective are presented in Chapter 2, and correspond to Paper 1: *Optimal control of Acute Myeloid Leukaemia*.

- (2) Extend the work with the model of AML from Objective 1 to investigate the application of multiple optimal controls to interacting species.

This objective is motivated by combination therapies for cancer treatment, where patients receive chemotherapy alongside radiotherapy and/or immunotherapy. We model the application of multiple optimal controls simultaneously, to interacting populations with resource competition; where abundance of one species is desirable and the other is undesirable. We find that the response of the optimal control strategy can be highly non-linear with respect to the parameters governing interaction between species. Interspecies interactions introduce complexity when designing optimal interventions, but also provide opportunities. The outcomes of this objective are presented in Chapter 3, and correspond to Paper 2: *Designing combination therapies using multiple optimal controls*.

- (3) Unify disparate parts of the optimal control and numerical methods literature and improve accessibility of optimal control techniques.

In addressing the first two objectives, we implement and develop a variety of optimal control techniques. Existing literature discussing practical implementation of these techniques is fragmented and sparse. Texts such as [168, 191] give an excellent overview of the theory of optimal control, and provide algorithms for numerical implementation. However, there is little discussion regarding practical implementation of the algorithms; such as potential issues with convergence of the numerical methods when applied to non-trivial examples. As such there is scope for a review paper that brings implementation of optimal control techniques to the forefront of the discussion in a practical and assimilable way. To address this objective, we provide a comprehensive review of optimal control theory and numerical methods, with a focus on the PMP approach to optimal control, and the implementation of the FBSM. We consider a single-variable linear model, and a multi-variable nonlinear model; and pose and solve continuous, bang-bang, and fixed endpoint control problems. Drawing on our experience in addressing the first two objectives, and insights scattered throughout the literature, we discuss practical considerations for numerical implementation, and consider in detail the convergence behaviour of the FBSM. To improve accessibility of the techniques to practitioners, we do not as-

sume any prior knowledge of optimal control, and we provide code with detailed and clear documentation for implementation of all numerical techniques considered. The outcomes of this objective are presented in Chapter 4, and correspond to Paper 3: *Implementation and acceleration of optimal control in systems biology*.

- (4) Develop novel improvements to the FBSM for optimal control, to achieve faster and more reliable convergence.

When considering iterative numerical methods, we are typically interested not only in whether or not they converge, but also how quickly. Achieving fast and reliable convergence of the FBSM is an open challenge. By conceptualising the FBSM as a fixed point iteration process, we provide novel augmentations of the FBSM to improve its convergence behaviour. We show that we can achieve improved convergence even without prohibitively costly tuning of the parameters of the acceleration techniques. We also demonstrate that in some instances the acceleration techniques can induce convergence where the underlying FBSM does not converge. The outcomes of this objective are presented in Chapter 4, and correspond to Paper 3: *Implementation and acceleration of optimal control in systems biology*.

Part 2: Parameter inference and information geometry

- (5) Demonstrate the insights that can be attained by supplementing likelihood-based parameter inference with information geometry techniques.

We investigate the insights that can be obtained via techniques from information geometry, including geodesic curves and the Ricci scalar curvature, to supplement likelihood-based parameter inference and uncertainty quantification. We implement the information geometry techniques for familiar pedagogical examples. We consider observational data that includes single and multiple observations at varying time-points. We demonstrate how these techniques can provide additional insights into uncertainty quantification and identifiability, and can be used to guide experimentation and data collection. The outcomes of this objective are presented in Chapter 5, and correspond to Paper 4: *Parameter estimation and uncertainty quantification using information geometry*.

- (6) Improve the accessibility of information geometry techniques to practitioners in the life sciences.

Using information geometry techniques to supplement traditional likelihood-based uncertainty quantification and gain insights into identifiability is currently an under-explored and inaccessible area, particularly in the life sciences. We attribute this partly to the underlying theory of differential geometry being deeply rooted in more formal mathematics literature. This area of the literature is seldom frequented

by practitioners in the life sciences. We make information geometry techniques accessible to practitioners in the life sciences by producing a review paper with a heavy focus on the practical implementation and interpretation of the techniques. We outline the fundamental aspects of information geometry required to support the techniques. However, we do so sparingly, and with no assumption of prior knowledge of inference or differential geometry. We implement the information geometry techniques to support likelihood-based parameter inference for linear and nonlinear ODE models, and systems of coupled nonlinear ODEs, with observational data that includes examples where single and multiple observations are recorded. We consider cases where combinations of model parameters, initial conditions, and the variability of observations are estimated. The outcomes of this objective are presented in Chapter 5, and correspond to Paper 4: *Parameter estimation and uncertainty quantification using information geometry*.

1.4 Thesis structure

This research program is presented as a thesis by published papers. Chapters 2-5 correspond, sequentially, to the four published papers listed in Section 1.3. Each chapter includes: an abstract; an introduction that motivates the study, identifies key areas of focus, provides background information and reviews relevant literature; a detailed overview of the methods implemented in the work and any mathematical modelling undertaken; results; conclusions and future avenues for investigation and extension. Each main chapter is a standalone publication, although the common themes introduce overlap in some sections, particularly in terms of literature review and methods. References from each chapter have been combined to produce a single alphabetised bibliography at the end of this thesis, to avoid duplication. Supplementary material is presented in Chapters 2A-4A at the end of this thesis. Content in each supplementary material chapter varies between publications, but typically includes: additional results and figures, sensitivity analysis, long analytical results and derivations, algorithms and details on numerical implementation.

In Chapter 2 we incorporate a biologically appropriate and mathematically convenient immune response into a haematopoietic stem cell model for AML, and discuss the impact this has on the steady states of the model. We use optimal control techniques to investigate both continuous and bang-bang optimal chemotherapy treatment regimes. We explore optimal controls under a range of scenarios, including varying the parameters in the pay-off that weight the relative importance of the negative effects of the disease and the negative effects of the treatment; and varying the maximum strength of the chemotherapy treatment. We investigate how the control update weighting parameter, ω , and the parameters weighting the importance of terms in the pay-off function, influence convergence behaviour of the FBSM. The corresponding supplementary material is provided in Chapter 2A.

In Chapter 3 we recast the haematopoietic stem cell model for AML presented in Chapter 2 in an ecological context; as a case study of a two species model with resource competition, where abundance of one species is desirable and abundance of the other is undesirable. We investigate the dynamics of optimal therapies where two controls are implemented simultaneously. In particular, we model a combination therapy intervention with one control that negatively affects healthy and leukaemic cells (chemotherapy), and another control that positively affects only the desirable species (stem cell transplant). We produce results for pay-off regimes corresponding to both controls being continuous, both controls being bang-bang, and a combination of continuous and bang-bang controls. The impact of key parameters influencing the combination therapy dynamics are also considered. The corresponding supplementary material is provided in Chapter 3A.

In Chapter 4 we review the theory of optimal control, and numerical methods for

solving control problems; with a focus on the PMP approach to optimal control, and the implementation of the FBSM. We apply optimal control techniques to solve continuous, bang-bang, and fixed endpoint control problems for both a single-variable linear model, and a multi-variable nonlinear model. Discussion is focused on practical considerations for numerical implementation, and the convergence behaviour of the FBSM. By conceptualising the FBSM as a fixed point iteration process, we propose novel augmentations to improve and accelerate its convergence behaviour. The corresponding supplementary material is provided in Chapter 4A.

In Chapter 5 we investigate the use of techniques from information geometry, including geodesic curves and the Ricci scalar curvature, to supplement likelihood-based parameter inference and uncertainty quantification. We review the fundamental aspects of information geometry required to support the implementation of these techniques. We implement the information geometry techniques for familiar pedagogical examples, including linear and nonlinear ODE models, and systems of coupled nonlinear ODEs. We consider observational data that includes single and multiple observations at varying time-points. We estimate combinations of model parameters, initial conditions, and the variability of observations.

1.5 Statement of joint authorship

Here, we outline the contribution of the PhD candidate and the co-authors to each piece of work included in the thesis. All co-authors have given permission for these publications to be presented in this thesis, and have confirmed their contributions, as follows:

Chapter 2: Optimal control of acute myeloid leukaemia

Sharp JA, Browning AP, Mapder T, Burrage K, Simpson MJ (2019). Optimal control of acute myeloid leukaemia. *Journal of Theoretical Biology*. [doi:10.1016/j.jtbi.2019.03.006](https://doi.org/10.1016/j.jtbi.2019.03.006).

- **Jesse A. Sharp (Candidate)**: designed the study, developed and implemented the computational algorithms, mathematical modelling, generated and interpreted results, produced figures, drafted the manuscript, revised the manuscript.
- Alexander P. Browning: aided development of the computational algorithms, interpreted results, provided comments on the manuscript.
- Tarunendu Mapder: aided development of the computational algorithms, interpreted results, provided comments on the manuscript.
- Kevin Burrage: designed the study, supervised the research, interpreted the results, and provided comments on the manuscript.
- Matthew J. Simpson: designed the study, supervised the research, interpreted the results, and provided comments on the manuscript.

Chapter 3: Designing combination therapies using multiple optimal controls

Sharp JA, Browning AP, Mapder T, Baker CM, Burrage K, Simpson MJ (2020). Designing combination therapies using multiple optimal controls. *Journal of Theoretical Biology*. [doi:10.1016/j.jtbi.2020.110277](https://doi.org/10.1016/j.jtbi.2020.110277).

- **Jesse A. Sharp (Candidate)**: designed the study, developed and implemented the computational algorithms, generated and interpreted results, produced figures, drafted the manuscript, revised the manuscript.
- Alexander P. Browning: interpreted results, provided comments on the manuscript.
- Tarunendu Mapder: interpreted results, provided comments on the manuscript.
- Chris M. Baker: interpreted results, provided comments on the manuscript.
- Kevin Burrage: designed the study, supervised the research, interpreted the results, and provided comments on the manuscript.

- Matthew J. Simpson: designed the study, supervised the research, interpreted the results, and provided comments on the manuscript.

Chapter 4: Implementation and acceleration of optimal control for systems biology

Sharp JA, Burrage K, Simpson MJ (2021). Implementation and acceleration of optimal control for systems biology. *Journal of the Royal Society Interface*.
[doi:10.1098/rsif.2021.0241](https://doi.org/10.1098/rsif.2021.0241).

- **Jesse A. Sharp (Candidate)**: designed the study, developed and implemented the computational algorithms, generated and interpreted results, produced figures, drafted the manuscript, revised the manuscript.
- Kevin Burrage: designed the study, supervised the research, interpreted the results, and provided comments on the manuscript.
- Matthew J. Simpson: designed the study, supervised the research, interpreted the results, and provided comments on the manuscript.

Chapter 5: Parameter estimation and uncertainty quantification using information geometry

Sharp JA, Browning AP, Burrage K, Simpson MJ (2022). Parameter estimation and uncertainty quantification using information geometry. *Journal of the Royal Society Interface* [in press].

[arXiv:2111.12201](https://arxiv.org/abs/2111.12201).

- **Jesse A. Sharp (Candidate)**: designed the study, developed and implemented the computational algorithms, generated and interpreted results, produced figures, drafted the manuscript, revised the manuscript.
- Alexander P. Browning: designed the study, advised on implementation of computational algorithms, interpreted results, provided comments on the manuscript.
- Kevin Burrage: designed the study, supervised the research, interpreted the results, and provided comments on the manuscript.
- Matthew J. Simpson: designed the study, supervised the research, interpreted the results, and provided comments on the manuscript.

Chapter 2

Optimal control of acute myeloid leukaemia

Statement of Contribution of Co-Authors

The authors listed below have certified that:

1. they meet the criteria for authorship and that they have participated in the conception, execution, or interpretation, of at least that part of the publication in their field of expertise;
2. they take public responsibility for their part of the publication, except for the responsible author who accepts overall responsibility for the publication;
3. there are no other authors of the publication according to these criteria;
4. potential conflicts of interest have been disclosed to (a) granting bodies, (b) the editor or publisher of journals or other publications, and (c) the head of the responsible academic unit, and
5. they agree to the use of the publication in the student's thesis and its publication on the [QUT's ePrints site](#) consistent with any limitations set by publisher requirements.

In the case of this chapter: Chapter 2

Please state the publication title and date of publication or status:

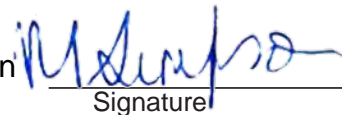
Optimal control of acute myeloid leukaemia. Published 2019 in Journal of Theoretical Biology.

Contributor	Statement of contribution*
Jesse A Sharp	Designed the study developed and implemented the computational algorithms, mathematical modelling, generated and interpreted results, produced figures, drafted the manuscript, revised the manuscript. 
08/12/2021	
AP Browning	Aided development of the computational algorithms, interpreted results, provided comments on the manuscript.
T Mapder	Aided development of the computational algorithms, interpreted results, provided comments on the manuscript.
K Burrage	Designed the study, supervised the research, interpreted the results, and provided comments on the manuscript.
MJ Simpson	Designed the study, supervised the research, interpreted the results, and provided comments on the manuscript.

Principal Supervisor Confirmation

I have sighted email or other correspondence from all Co-authors confirming their certifying authorship. (If the Co-authors are not able to sign the form please forward their email or other correspondence confirming the certifying authorship to the GRC).

Professor Matthew Simpson
Name


Signature

11/12/2021
Date

Article published 2019 in Journal of Theoretical Biology

Sharp JA, Browning AP, Mapder T, Burrage K, Simpson MJ (2019). Optimal control of acute myeloid leukaemia. *Journal of Theoretical Biology*. doi:[10.1016/j.jtbi.2019.03.006](https://doi.org/10.1016/j.jtbi.2019.03.006).

Abstract

Acute myeloid leukaemia (AML) is a blood cancer affecting haematopoietic stem cells. AML is routinely treated with chemotherapy, and so it is of great interest to develop optimal chemotherapy treatment strategies. In this work, we incorporate an immune response into a stem cell model of AML, since we find that previous models lacking an immune response are inappropriate for deriving optimal control strategies. Using optimal control theory, we produce continuous controls and bang-bang controls, corresponding to a range of objectives and parameter choices. Through example calculations, we provide a practical approach to applying optimal control using Pontryagin's Maximum Principle. In particular, we describe and explore factors that have a profound influence on numerical convergence. We find that the convergence behaviour is sensitive to the method of control updating, the nature of the control, and to the relative weighting of terms in the objective function. All codes we use to implement optimal control are made available on [GitHub](#).

2.1 Introduction

Acute Myeloid Leukaemia (AML) is a blood cancer that is characterised by haematopoietic stem cells, primarily in the bone marrow, transforming into leukaemic blast cells [82, 233]. These blast cells no longer undergo normal differentiation or maturation and stop responding to normal regulators of proliferation [100]; their presence in the bone marrow niche disrupts normal haematopoiesis [82]. AML has significant mortality rates, with a five-year survival rate of 24.5% [6], and challenges in treatment arise not only in eradication of the leukaemic cells but also prophylaxis and treatment of numerous life threatening complications that arise due to the absence of sufficient healthy blood cells [335]. Multiple interventions are employed in the management and treatment of AML, including: leukapheresis; haematopoietic stem cell transplants; radiotherapy; chemotherapy and immunotherapy [19, 233, 265].

Mathematical models are widely used to gain insight into complex biological processes [167, 235]. Mathematical models facilitate the development of novel hypotheses, allow us to test assumptions, improve our understanding of biological interactions, interpret experimental data and assist in generating parameter estimates. Furthermore, mathematical models provide a convenient, low-cost mechanism for investigating biological processes and interventions for which experimental data may be scarce, cost-prohibitive or difficult to obtain owing to ethical issues. Mathematical models are routinely used to interrogate a variety of processes relating to cancer research including: incidence; development and metastasis; tumour growth; immune reaction and treatment [63, 76, 82, 170, 211, 312]. Recently, mathematical models have been used to investigate various aspects of AML, including: incidence [201]; pathogenesis [83]; interactions between cancer and healthy haematopoietic stem cells within the bone marrow niche [82]; and recurrence following remission [247].

Determining how to apply optimally a treatment such as chemotherapy is of great practical and theoretical interest. Chemotherapy, a common treatment for AML [92], is associated with significant health costs related to the cytotoxicity of chemotherapeutic agents [60, 233], but also substantial economic cost [345]. Optimal control theory provides us with tools for determining the optimal way to apply a control to a model such that some desired quantities of interest are minimised or maximised. Further, it facilitates assessment of the efficacy of hypothetical treatment protocols relative to a theoretical optimal treatment. Optimal control has been applied to a range of medically motivated biological models recently; including vaccination, tumour therapy and drug scheduling [75, 77, 187, 188, 213].

In this work we consider a recent haematopoietic stem cell model of AML [82]. After examining the steady state behaviour associated with this model, we make a biologically appropriate and mathematically convenient modification by incorporating an immune

response in the form of a Michaelis-Menten kinetic function. Overall, in this work we pursue two broad aims:

1. Determine how to apply optimal control to the model, accounting for key clinical features such as the competition between the negative effects of the disease and the negative effects of the treatment;
2. Provide a concise and insightful discussion of the methodology and numerical implementation of optimal control, as we find that much of the existing literature is opaque with regard to practical implementation.

In addressing these aims, we provide a brief introduction to the theory of optimal control and apply optimal control techniques to the modified model, identifying optimal treatment strategies under a variety of circumstances. This leads us to consider both continuous and discontinuous bang-bang optimal controls. Our work provides a comprehensive discussion of practical issues that can arise when applying optimal control, and we explore key factors that influence numerical convergence when using a forward-backward sweep algorithm to solve two-point boundary value problems that arise. The code we use to implement the algorithms associated with the optimal control solutions is freely available on [GitHub](#).

In Section 2.2 we present a haemotopoietic stem cell model of AML [82], and discuss the steady states. In Section 2.3 the importance of an immune response is outlined, and the model is modified to include such a response. In Section 2.4, we present discussion and results of optimal control applied to the modified AML model. Finally, concluding remarks are provided in Section 2.5. In the supplementary material document we extend the work in this document to consider: (i) arbitrary initial conditions, and; (ii) controls that impact multiple species.

2.2 Acute myeloid leukaemia model

Crowell, MacLean and Stumpf [82] propose a system of ordinary differential equations (ODEs) to model AML. Their model can be written as,

$$\begin{aligned}\frac{dS}{dt} &= \rho_s S(K_1 - Z_1) - \delta_S S, \\ \frac{dA}{dt} &= \delta_S S + \rho_A A(K_2 - Z_2) - \delta_A A, \\ \frac{dD}{dt} &= \delta_A A - \mu_D D, \\ \frac{dL}{dt} &= \rho_L L(K_2 - Z_2) - \delta_L L, \\ \frac{dT}{dt} &= \delta_L L - \mu_T T.\end{aligned}\tag{2.1}$$

Here $S(t)$, $A(t)$, $D(t)$, $L(t)$ and $T(t)$ represent haematopoietic stem cells, progenitor cells, terminally differentiated cells of $S(t)$, leukaemia stem cells and fully differentiated leukaemia cells, respectively. $Z_1(t) = S(t)$ and $Z_2(t) = A(t) + L(t)$, where $A(t)$ and $L(t)$ are coupled as the proliferating leukaemia population ($L(t)$) competes with the haematopoietic progenitor cell population ($A(t)$). This competition is motivated in [82] by the hypothesis that leukaemic stem cells and haematopoietic stem cells occupy the same niche within the bone marrow [149, 301] and hence compete for resources. This niche interaction has been demonstrated as being crucial to similar haematopoietic and leukaemic cell models of chronic myeloid leukaemia [211]. Throughout this work we present numerical solutions to this model and other related models. In all solutions presented the parameters are dimensionless, such that the time scale is arbitrary and cell population sizes within the bone marrow are expressed as a portion of the carrying capacities; $K_1 = K_2 = 1$. Setting these carrying capacities to be of equal size is a simplifying assumption in our analysis, though we note that this is not required, and could be relaxed if suitable alternative estimates of the carrying capacities were identified.

Crowell, MacLean and Stumpf use numerical solutions of Equation (2.1) to identify parameter values that lead to particular long-time steady state solutions of the model [82]. In this work we will use standard variables to denote time dependent quantities, such as $S(t)$, and an overbar to denote long-time steady quantities, such as $\lim_{t \rightarrow \infty} S(t) = \bar{S}$. The parameters we use are summarised in Table 2.1, and we note that the model supports three non-trivial steady states:

1. The *coexisting* steady state requires $\bar{S}, \bar{A}, \bar{D}, \bar{L}, \bar{T} > 0$ simultaneously. In this work we are interested in modelling the optimal application of an intervention (or control) such as chemotherapy to the system that shifts it from the coexisting steady state towards the healthy steady state. Examples trajectories resulting in the coexisting

steady state are given in Figure 2.2a and Figure 2.2b.

2. The *healthy* steady state consists of $\bar{S}, \bar{A}, \bar{D} > 0$ and $\bar{L} = \bar{T} = 0$, such that there is a population of each healthy cell species and no leukaemia is present. The healthy steady state is demonstrated in Figure 2.2c.
3. The third steady state is *leukaemic*, characterised by $\bar{S} = \bar{A} = \bar{D} = 0$ and $\bar{L}, \bar{T} > 0$, such that only leukaemic cells are present. The leukaemic steady state is demonstrated in Figure 2.2d.

The leukaemic steady state is less interesting from an intervention perspective as it cannot be steered towards the healthy steady state via a control such as chemotherapy alone; requiring in addition a source of healthy cells.

Table 2.1: Parameters values used in this work.

Parameter description	Value
Proliferation of S	$\rho_S = 0.5$
Proliferation of A	$\rho_A = 0.43$
Proliferation of L	$\rho_L = 0.27$
Differentiation of S into A	$\delta_S = 0.14$
Differentiation of A into D	$\delta_A = 0.44$
Differentiation of L into T	$\delta_L = 0.05$
Migration of D into the blood stream	$\mu_D = 0.275$
Migration of T into the blood stream	$\mu_T = 0.3$
Carrying capacity of the compartment with S	$K_1 = 1$
Carrying capacity of the compartment with A and L	$K_2 = 1$
Characteristic rate of the immune response	$\alpha = 0.015$
Half saturation constant of the immune response	$\gamma = 0.1$

Parameter values in Table 2.1 are used in all numerical solutions presented in this work, unless otherwise indicated. These values match those specified in [82] to produce a healthy steady state, with the exception of δ_L , noting that [82] included parameter sweeps over ρ_S, ρ_A, δ_S and δ_A . We have set $\delta_L = 0.05$ to produce the coexisting steady state, although other values for δ_L also produce this coexisting steady state.

Schematics showing the key features of the original model, a modified model that incorporates an immune response (Section 2.3), and the modified model subject to a control (Section 2.4) are presented in Figure 2.1. Typical numerical solutions of the original model are presented in Figure 2.2. All numerical results presented in this study are obtained using a fourth-order Runge-Kutta method [269] with a constant time step of $\delta t = 0.001$. We find that this choice is sufficient to produce numerical solutions that are grid-independent. From the numerical results we observe that for the parameter values given in Table 2.1, provided that initially $S(0) > 0$ and $L(0) > 0$, the system will tend towards the coexisting steady state. In Section 2.3 we modify the model to incorporate an immune response, such that sufficiently small leukaemic populations will decay without intervention.

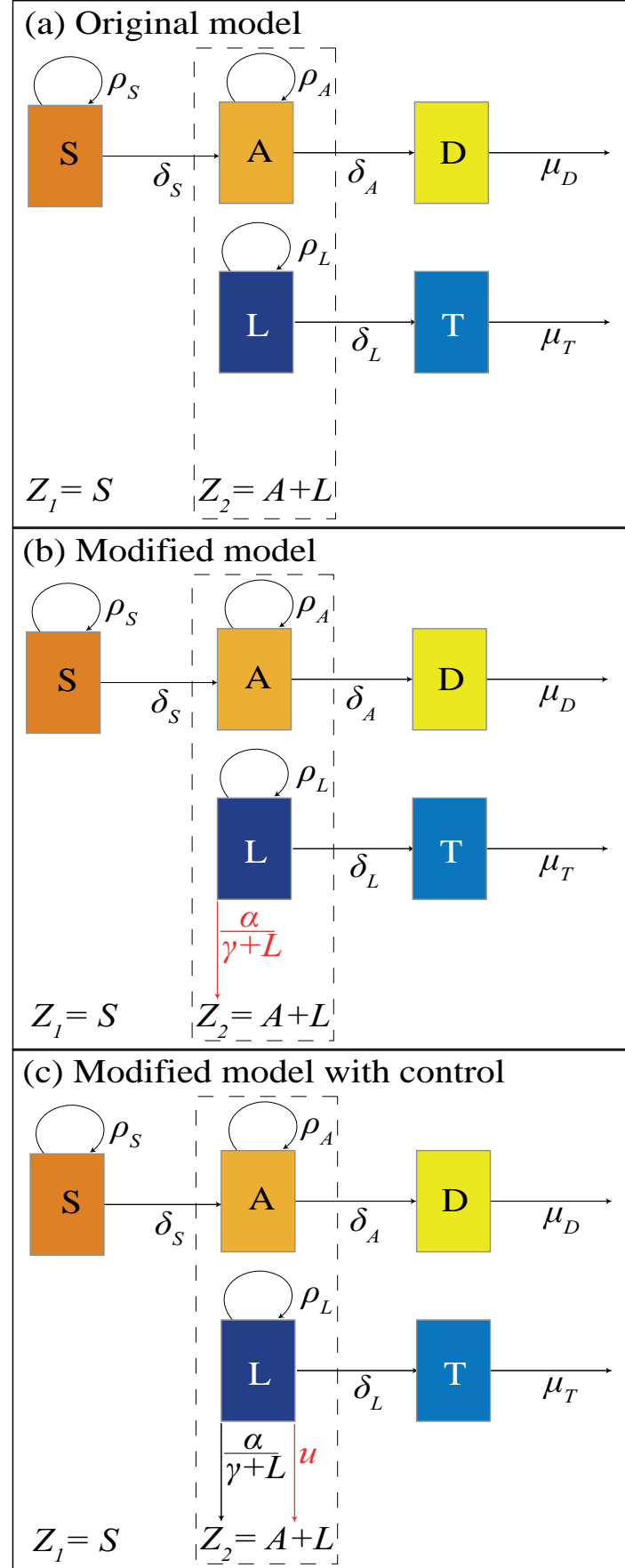


Figure 2.1: Schematics present the interactions and associated parameters for the (a) original model [82], (b) modified model with immune response and (c) modified model subject to a control, u . In each schematic the additional response is highlighted in red.

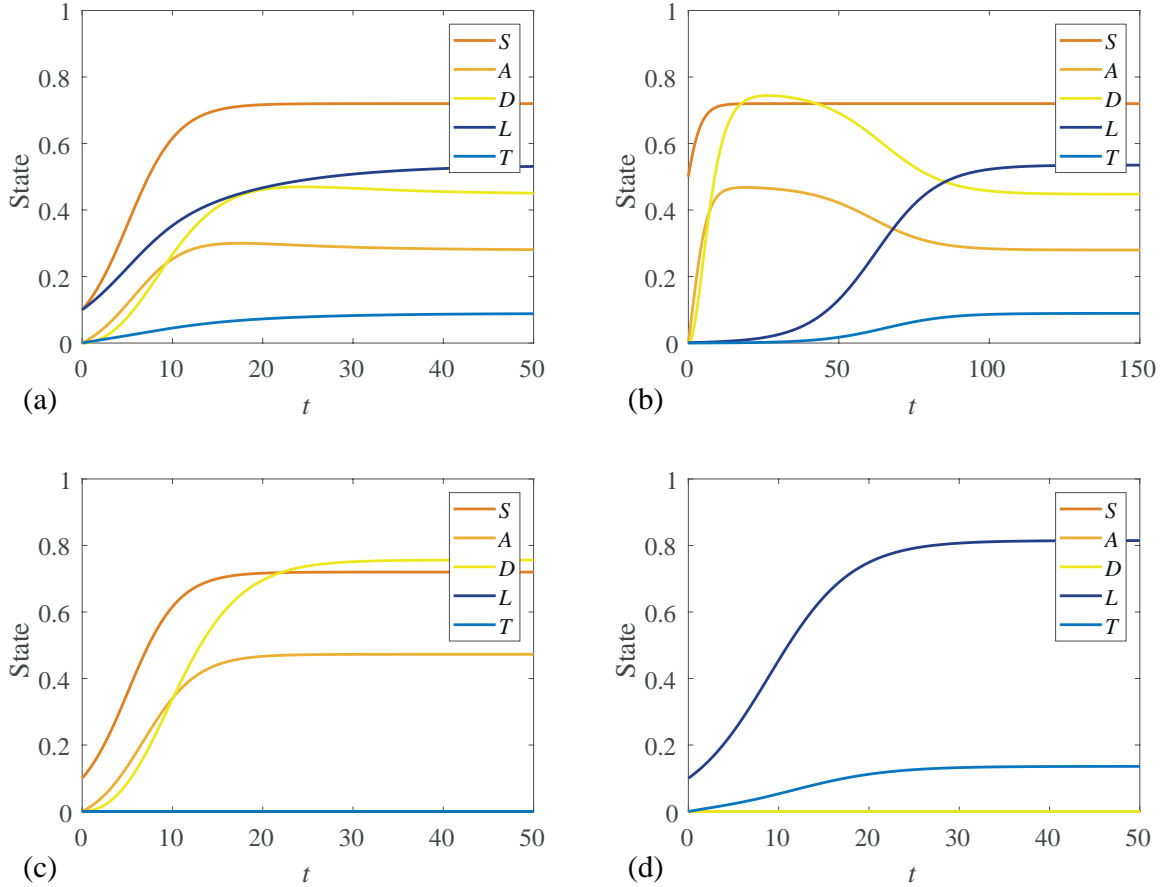


Figure 2.2: Numerical solutions of Equations 2.1 for various initial conditions: (a) Coexisting steady state solution with $[S(0), A(0), D(0), L(0), T(0)] = [0.1, 0, 0, 0.1, 0]$. (b) Coexisting steady state with $[0.5, 0, 0, 10^{-3}, 0]$. (c) Healthy steady state with $[0.1, 0, 0, 0, 0]$. (d) Leukaemic steady state with $[0, 0, 0, 0.1, 0]$.

In Figure 2.2b we note that although the initial leukaemia stem cell population is small compared to the initial haematopoietic stem cell population, the system eventually evolves to the same coexisting steady state as in Figure 2.2a. However, this steady state condition requires a longer timescale to develop from the different initial conditions.

2.3 Incorporating the immune response

The immune system is known to play a critical role in the development, metastasis, treatment and recurrence of cancers [117, 159]. This knowledge is supported by a range of clinical evidence, including a well-documented increased risk of cancer incidence in patients with immunodeficiency [79]. This is exemplified by experimental mouse models where mice are typically immunocompromised to avoid transplanted cancers being destroyed by the immune response in xenograft studies [86]. Furthermore, tumours found in immunocompetent hosts are observed to exhibit mechanisms for avoiding immune response [226].

The behaviour exhibited in Figure 2.2b indicates that the system cannot reach a healthy non-leukaemic steady state in the presence of even small leukaemic stem cell populations. It is reasonable to expect that under some circumstances a small leukaemic population may be outcompeted by healthy cells occupying the same niche [210], without intervention. Therefore, we consider a modification to the model proposed by Crowell, MacLean and Stumpf [82] to incorporate an immune response. We expect this immune response to be effective for small L and ineffective for large L , and so we mimic this by introducing a Michaelis-Menten term to represent the immune response, giving,

$$\begin{aligned}\frac{dS}{dt} &= \rho_s S(K_1 - Z_1) - \delta_S S, \\ \frac{dA}{dt} &= \delta_S S + \rho_A A(K_2 - Z_2) - \delta_A A, \\ \frac{dD}{dt} &= \delta_A A - \mu_D D, \\ \frac{dL}{dt} &= \rho_L L(K_2 - Z_2) - \delta_L L - \underbrace{\frac{\alpha L}{\gamma + L}}_{\text{immune response}}, \\ \frac{dT}{dt} &= \delta_L L - \mu_T T.\end{aligned}\tag{2.2}$$

Including an immune response in the model is not only mathematically convenient in that it provides desirable steady states that we discuss later in this section, but also biologically relevant. Immune responses are widely studied in both the theoretical and experimental biology literature and acknowledged as an important contributor to pathogenesis and tumour dynamics in AML [29, 173, 328]. Additionally, immunotherapy is being investigated as an alternative to chemotherapy for treatment of AML and many other cancers [44, 196, 220].

Michaelis-Menten terms are commonly used to incorporate immune responses in other biologically motivated models [9, 111, 192]. However, it is unclear, simply by inspection, what parameter values are required to obtain two stable steady states: one coexisting and one healthy. For $\gamma \ll \alpha$ the Michaelis-Menten term behaves as exponential decay at a rate of α , while for $\gamma \gg L$ it behaves as a linear sink term [296, 297]. Intuitively, we expect setting $\gamma = \mathcal{O}(L)$ will produce the desired dynamics whereby the immune response is effective for small L and ineffective for large L .

We investigate further by considering the potential steady states permitted by Equation (2.2). We note that S is governed by a logistic growth mechanism that does not depend on any of the other species so we have $\bar{S} = 1 - \delta_S/\rho_S$. Similarly, D and T do not influence the other populations and hence can be neglected in the consideration of the steady states. Therefore, we consider a reduced system in terms of A , L with

$\bar{S} = 1 - \delta_S/\rho_S$, recalling that $Z_2 = A + L$, and through scaling $K_2 = 1$,

$$\frac{dA}{dt} = f(A, L) = \delta_S \left(1 - \frac{\delta_S}{\rho_S}\right) + \rho_A A(1 - A - L) - \delta_A A, \quad (2.3)$$

$$\frac{dL}{dt} = g(A, L) = \rho_L L(1 - A - L) - \delta_L L - \frac{\alpha L}{\gamma + L}. \quad (2.4)$$

By inspection, there is a trivial L-nullcline at $\bar{L} = 0$. We can find the A-nullcline by setting $f(A, L) = 0$ in Equation (2.3),

$$\bar{L} = \frac{\delta_S \bar{S}}{\rho_A A} + 1 - A - \frac{\delta_A}{\rho_A}. \quad (2.5)$$

Similarly, we can find the non-trivial L-nullcline by setting $g(A, L) = 0$ in Equation (2.4),

$$\bar{A} = 1 - L - \frac{\delta_L}{\rho_L} - \frac{\alpha}{\rho_L(\gamma + L)}. \quad (2.6)$$

The nullclines, given by Equations (2.5) and (2.6), are hyperbolas. In Figure 2.3 we present phase planes for both the modified (with immune response) and unmodified (no immune response) models showing dynamics of the A and L populations within the physically meaningful region, $A + L \leq 1$.

This system has the desired property that we outlined previously, namely that there is a stable steady state of coexistence that we aim to steer to the stable state with no leukaemia through applying optimal control. Numerical solutions of the modified model with no control are presented in Figure 2.4.

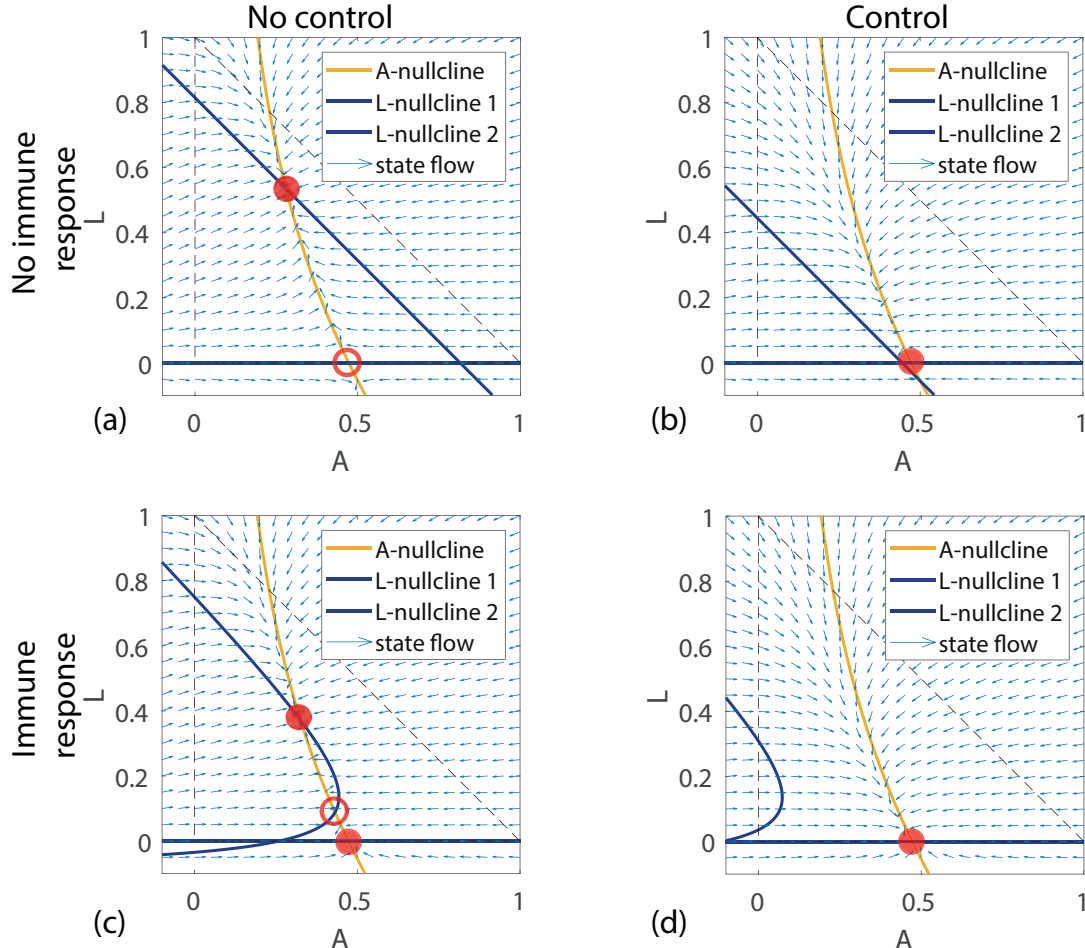


Figure 2.3: Nullclines and steady states of the model with (a) no immune response and no control, (b) no immune response with control, (c) immune response with no control and (d) immune response with control, using parameters for a coexistence steady state; $[\rho_S, \rho_A, \rho_L, \delta_S, \delta_A, \delta_L] = [0.5, 0.43, .027, 0.14, 0.44, 0.05]$. Physically realistic fixed points are marked with closed discs if stable or open discs if unstable. The application of a control in (b) and (d) corresponds to $u \equiv 0.1$, effectively increasing δ_L to 0.15 (a control could be a treatment such as chemotherapy that increases the rate of decay of leukaemic stem cells, this is discussed in Section 2.4). In (c), for particular choices of the introduced parameters α and γ it is possible for the hyperbolas to intersect twice within the physically realistic region (dashed triangle). Figures (c) and (d) are produced with $\alpha = 0.015$, $\gamma = 0.1$. Without an immune response, as illustrated in (a) and (b), application of a control can steer the system towards a stable healthy steady state, however this fixed point becomes unstable if the control is ceased, causing the system to revert to the coexisting steady state. With an immune response, as illustrated in (c) and (d), once the control steers the system into the attractor region of the healthy fixed point, the system does not revert to the coexisting steady state upon ceasing the control.

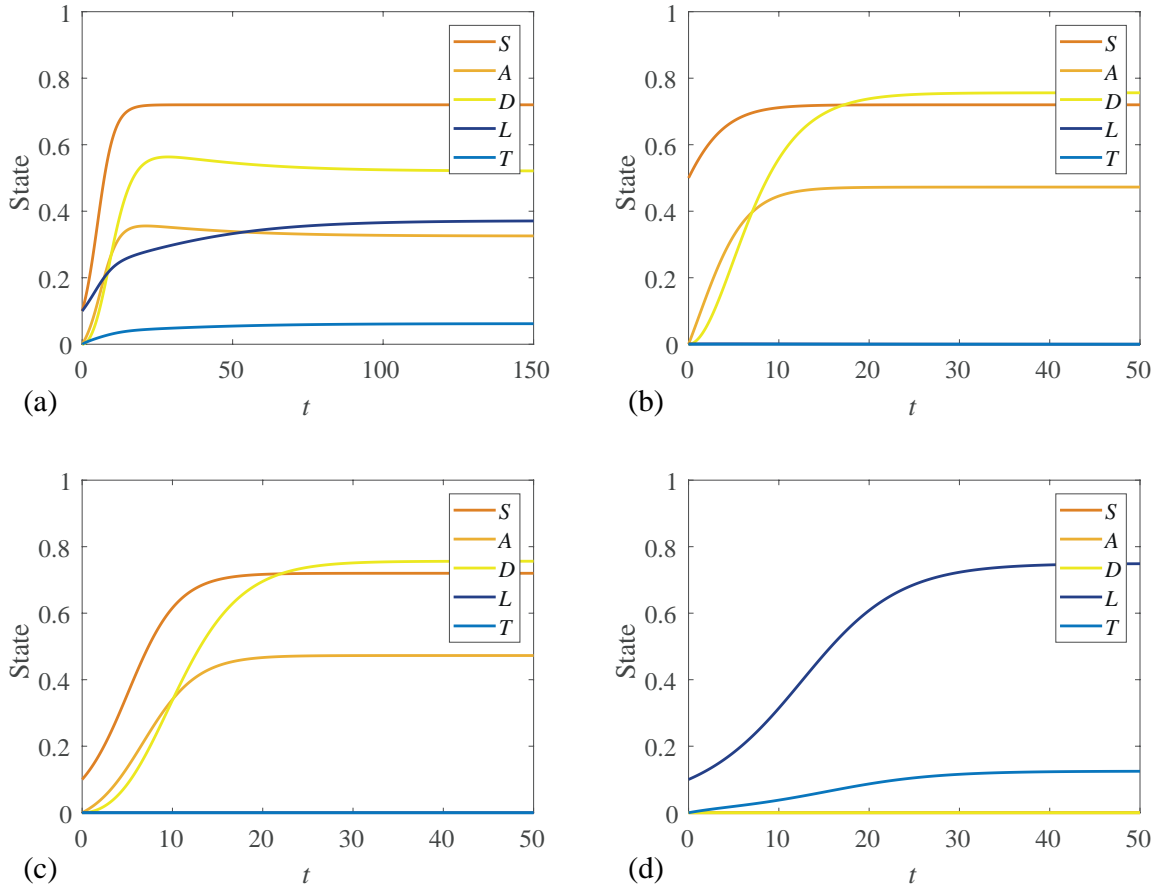


Figure 2.4: Numerical solutions to the modified model with an immune response for initial conditions corresponding to Figure 2.2. In (a) we observe coexistence, though it takes longer for the solutions to approach steady state when compared with the original model (Figure 2.2a). This result is presented over a larger time-scale. With the introduction of the Michaelis-Menten style immune response to leukaemia, we observe in (b) that a small leukaemia stem cell population does not survive in the presence of a haematopoietic stem cell population. This is in contrast to Figure 2.2b, where a minute population of leukaemic stem cells was sufficient to grow to a coexisting steady state. These figures are produced with immune response parameters $\alpha = 0.015$, $\gamma = 0.1$.

2.4 Methods

In this section we provide a concise overview of the theory of optimal control. Methods for solving optimal control problems are discussed. We determine optimal controls to the model presented in Section 2.3. Specifically, we consider continuous optimal controls corresponding to quadratic pay-off functions and discontinuous bang-bang optimal controls corresponding to linear pay-off functions. Numerical solutions are produced for several different pay-off weighting parameter combinations.

2.4.1 Optimal control theory

The basic principle of optimal control is to apply an external force, the *control*, to a system of differential equations, the *state equations*, to cause the solution, the *state*, to follow a new trajectory and/or arrive at a different final state. The goal of optimal control is to select a particular control that maximises or minimises a chosen objective functional, the *pay-off*; typically a function of the state and the control. The pay-off is chosen such that the new trajectory/final state are preferred to that of the uncontrolled state, accounting for any cost associated with applying the control.

A typical optimal control problem will introduce the state equations as functions of the state $\mathbf{x}(t)$ and the control $u(t)$, with initial state $\mathbf{x}(0) = \mathbf{x}_0$,

$$\frac{d\mathbf{x}}{dt} = f(t, \mathbf{x}(t), u(t)), \quad \mathbf{x}(t) \in \mathbb{R}^n. \quad (2.7)$$

It is also necessary to specify either a final time t_f with the final state free, or a final state $\mathbf{x}(t_f)$, with the final time free.

A pay-off function J is defined as a function of the final state, $\mathbf{x}(t_f)$, and a cost function $\mathcal{L}(t, \mathbf{x}(t), u(t))$ integrated from initial time (t_0) to final time (t_f). Through choosing an optimal control $u^*(t)$ and solving for the corresponding optimal state $\mathbf{x}^*(t)$, we seek to maximise or minimise this objective function. Selecting the pay-off enables us to incorporate the context of our application and determine the meaning of *optimality*. In general, the pay-off function can be written as,

$$J = \phi(\mathbf{x}(t_f)) + \int_{t_0}^{t_f} \mathcal{L}(t, \mathbf{x}(t), u(t)) dt. \quad (2.8)$$

Depending on the form of ϕ , it may be possible to incorporate ϕ into \mathcal{L} by restating the final state constraint in terms of an integral expression using the Fundamental Theorem of Calculus, and noting that $\phi(\mathbf{x}(t_0))$ is constant and hence does not impact the optimal control. The resulting unconstrained optimal control problem is often more straightforward to solve than the constrained problem.

The optimal control can be found by solving necessary conditions obtained through

application of Pontryagin's Maximum Principle (PMP) [264], or a necessary and sufficient condition by forming and solving the Hamilton-Jacobi-Bellman partial differential equation; a dynamic programming approach [37]. In this work we use the PMP and we construct the Hamiltonian, $H(t, \mathbf{x}, u, \boldsymbol{\lambda}) = \mathcal{L}(t, \mathbf{x}, u) + \boldsymbol{\lambda} \cdot f$, where $\boldsymbol{\lambda} = [\lambda_1(t), \lambda_2(t), \dots, \lambda_n(t)]$ are the adjoint variables for an n -dimensional state. The adjoint is analogous to Lagrange multipliers for constrained optimisation problems. Through the Hamiltonian, the adjoint allows us to link our state to our pay-off function. The necessary conditions can be expressed in terms of the Hamiltonian,

1. The optimality condition is obtained by minimising the Hamiltonian,

$$\frac{\partial H}{\partial u} = 0 \text{ gives } \left(\frac{\partial \mathcal{L}}{\partial u} + \boldsymbol{\lambda} \cdot \frac{\partial f}{\partial u} \right) = 0, \quad (2.9)$$

2. the adjoint, also referred to as *co-state*, is found by setting,

$$\frac{\partial H}{\partial \mathbf{x}} = -\frac{d\boldsymbol{\lambda}}{dt}, \text{ giving } \frac{d\boldsymbol{\lambda}}{dt} = -\left(\frac{\partial \mathcal{L}}{\partial \mathbf{x}} + \boldsymbol{\lambda} \cdot \frac{\partial f}{\partial \mathbf{x}} \right), \text{ and} \quad (2.10)$$

3. satisfying the transversality condition (a final time condition on the co-state),

$$\boldsymbol{\lambda}(t_f) = \left. \frac{\partial \phi}{\partial \mathbf{x}} \right|_{t=t_f}. \quad (2.11)$$

2.4.2 Continuous optimal control

In this section we consider optimal control applied to the AML model presented in Section 2.3. From this point we omit the implied time dependence of all control, state and co-state variables for notational convenience. Consider the steady states we observed for the coexistent parameter values of model 1. Suppose we wish to apply an optimal control that steers the system from a steady state observed in Figure 2.4a towards a healthy steady state (Figure 2.4b). This could be achieved by applying a drug $u(t)$, the dosage of which may vary over time, that kills leukaemic stem cells,

$$\begin{aligned} \frac{dS}{dt} &= \rho_S S(K_1 - Z_1) - \delta_S S, \\ \frac{dA}{dt} &= \delta_S S + \rho_A A(K_2 - Z_2) - \delta_A A, \\ \frac{dD}{dt} &= \delta_A A - \mu_D D, \\ \frac{dL}{dt} &= \rho_L L(K_2 - Z_2) - \delta_L L - \frac{\alpha L}{\gamma + L} - uL, \\ \frac{dT}{dt} &= \delta_L L - \mu_T T. \end{aligned} \quad (2.12)$$

A potential pay-off function for this optimal control problem is to minimise,

$$J = \int_0^{t_f} (a_1 u^2 + a_2 L^2) dt, \quad (2.13)$$

where the control problem is assumed to start at time zero and run until a fixed end time of t_f . Note that we have not included a function of the final state in the pay-off: $\phi = 0$. In defining a pay-off function there is significant scope for flexibility, and what constitutes an appropriate choice depends on the application. The parameters $a_1 > 0$ and $a_2 > 0$ are chosen to weight the importance of each term in the pay-off, and can be adjusted to best suit a particular application. Through scaling it can be seen that for this example only the relative weighting (a_1/a_2) is important, however we specify a_1 and a_2 separately for clarity.

Quadratic pay-off functions have several desirable mathematical properties that increase the ease of finding optimal solutions; they are smooth and have only a single extremum. Furthermore, quadratic pay-off functions help to avoid non-physical controls that may otherwise be found. For example; if the pay-off was a cubic function of u , setting u to be large and negative may minimise the pay-off but be physically unrealisable. Quadratic pay-off functions also have some desirable physical properties; a quadratic term will apply a harsher penalty to large amounts of control than small amounts [26], which in many treatments, such as chemotherapy, is desirable [169]. In control engineering applications, the control, u , is thought to be proportional to a voltage or current, in which case a quadratic pay-off has a convenient interpretation, as u^2 is proportional to power, and the integral of this power over an interval is proportional to the energy expended [26]. Pay-off functions that are quadratic in the control variable are used in many biological [193, 270] and engineering applications [17, 246].

We can construct the Hamiltonian as $H = \mathcal{L} + \boldsymbol{\lambda} \cdot f$; where f is the right hand side of Equation (2.12), $\boldsymbol{\lambda} = [\lambda_1, \lambda_2, \lambda_3, \lambda_4, \lambda_5]$, and from Equation (2.13), we have $\mathcal{L} = a_1 u^2 + a_2 L^2$, giving,

$$\begin{aligned} H = & a_2 L^2 + a_1 u^2 + \lambda_1 [\rho_S S(1 - S) - \delta_S S] \\ & + \lambda_2 [\delta_S S + \rho_A A(1 - A - L) - \delta_A A] \\ & + \lambda_3 (\delta_A A - \mu_D D) \\ & + \lambda_4 [\rho_L L(1 - A - L) - \delta_L L - \alpha L / (\gamma + L) - u L] \\ & + \lambda_5 (\delta_L L - \mu_T T). \end{aligned} \quad (2.14)$$

From Equation (2.9), we find the optimal control by setting $\partial H / \partial u = 0$, giving $u^* = \lambda_4 L / 2a_1$. Following Equation (2.10), the co-state equations for $\boldsymbol{\lambda}$ are found by setting $d\boldsymbol{\lambda}/dt = -\partial H / \partial \mathbf{x}$,

$$\begin{aligned}
\frac{d\lambda_1}{dt} &= 2S\lambda_1\rho_S + \delta_S\lambda_1 - \delta_S\lambda_2 - \lambda_1\rho_S, \\
\frac{d\lambda_2}{dt} &= 2A\lambda_2\rho_A + L\lambda_2\rho_A + L\lambda_4\rho_L + \delta_A\lambda_2 - \delta_A\lambda_3 - \lambda_2\rho_A, \\
\frac{d\lambda_3}{dt} &= \mu_D\lambda_3, \\
\frac{d\lambda_4}{dt} &= -2a_2L + \rho_AA\lambda_2 + \lambda_4\rho_LA + 2\rho_LL\lambda_4 - \lambda_4\rho_L \\
&\quad + \lambda_4\delta_L + \frac{\alpha\gamma\lambda_4}{(\gamma+L)^2} + \lambda_4u - \delta_L\lambda_5, \\
\frac{d\lambda_5}{dt} &= \mu_T\lambda_5.
\end{aligned} \tag{2.15}$$

The transversality condition, Equation (2.11), gives final time conditions on the co-state, Equation (2.15); $\boldsymbol{\lambda}(t_f) = [0, 0, 0, 0, 0]$. Assuming that the initial state is known; $[S(0), A(0), D(0), L(0), T(0)]$, it is now possible to determine the optimal control and corresponding state and co-state through solving a two-point boundary value problem (BVP).

We solve Equation (2.2) numerically to reach the stable coexisting steady state of the uncontrolled model. These steady state values in the absence of the control are used as the initial state conditions to solve the BVP to find the optimal control solution. The initial condition for the optimal control problem is $[S(0), A(0), D(0), L(0), T(0)] = [0.7200, 0.3255, 0.5207, 0.3715, 0.0619]$. Initialising the optimal control solution from the uncontrolled steady state is not necessary, however it helps to illustrate the role of the control. We demonstrate this flexibility by generating results for a range of arbitrary initial conditions and control start times. These results are presented and discussed in the supplementary material.

There are a range of analytical methods available for solving some forms of BVP under certain conditions [5, 337]. However, in this work we focus on numerical solutions with a view to identifying and discussing typical issues that may arise in implementation. Common numerical solution techniques include shooting and forward-backward sweep methods (FBSM) [165, 191]. The most effective numerical method depends on the particular BVP. The single shooting method is relatively straightforward, but can be sensitive to the initial guess of the co-state. Forming a suitable guess for the initial values of the co-state is challenging, as the co-state does not have a straightforward physical interpretation. Although the FBSM calls for an initial guess for the control over the entire interval, this can often be straightforward to determine, as we will demonstrate.

We apply the FBSM using an initial guess for the control, $u(t) \equiv 0$, to solve for the state variables forward in time. The co-state is then solved backward in time. In each case a fixed step fourth order Runge-Kutta method is applied to solve the relevant system of ODEs. Using these solutions, the control is updated and the process is repeated until convergence is achieved. The algorithm for the FBSM is given in Algorithm 1.

Algorithm 1: Forward-backward sweep

- i. Make an initial guess of $u(t)$.

Typically $u(t) \equiv 0$ is sufficient, though a more thoughtful choice may result in fewer iterations required for convergence.

- ii. Using the initial condition $\mathbf{x}(0) = \mathbf{x}_0$, solve for $\mathbf{x}(t)$ forward in time using the initial guess of $u(t)$.

- iii. Using the transversality condition $\boldsymbol{\lambda}(t_f)$, solve for $\boldsymbol{\lambda}(t)$ backwards in time, using the values for $u(t)$ and $\mathbf{x}(t)$.

- iv. Calculate $u_{\text{new}}(t)$ by evaluating the expression for the optimal control $u^*(t)$ using the updated $\mathbf{x}(t)$ and $\boldsymbol{\lambda}(t)$ values.

- v. Update $u(t)$ based on a combination of $u_{\text{new}}(t)$ and the previous $u(t)$. *For continuous controls applied to relatively simple systems, it may be possible to use $u_{\text{new}}(t)$ directly ($u(t) = u_{\text{new}}(t)$), however this is not sufficient to achieve convergence in general. We discuss this further in Section 2.4.4.*

- vi. Check for convergence.

If $\mathbf{x}(t)$, $\boldsymbol{\lambda}(t)$ and $u(t)$ are within a specified absolute or relative tolerance of the previous iteration, accept $\mathbf{x}(t)$, $\boldsymbol{\lambda}(t)$ and $u(t)$ as having converged, otherwise return to Step ii. and repeat the process using the updated $u(t)$.

Solutions are provided in Figure 2.5 for various weighting on the control parameters. As expected, when $a_1 > a_2$, placing a greater weighting on the negative impact of the control than the negative impact of the leukaemic stem cells we observe that the control is applied at a lower level than when $a_1 < a_2$. When the pay-off weightings are equal, as shown in Figure 2.5b, the continuous control is applied at an amount similar to the level of the leukaemic stem cell population. Similarly, when the amount of control applied is larger, we observe that the leukaemic stem cell population declines at a faster rate. With $a_1 > a_2$, as in Figure 2.5c, we observe that the leukaemic population is effectively eradicated by t_f , whereas when $a_1 < a_2$ we see, in Figure 2.5d, that a leukaemic population remains at t_f . A limitation of specifying a fixed final time, as opposed to a fixed final state, is that the optimal outcome is dependent on the specified final time, and there is no consideration for what may happen *after* t_f . In many applications, the notion of what happens beyond the control interval is not of interest, though in some instances specifying a final state may be more sensible. In this work we consider fixed final time problems for ease of comparison between controls under different parameter regimes, though we acknowledge that specifying a final state, such as *no leukaemic stem cells*, may be more biologically appropriate.

For each of the optimal controls presented in Figure 2.5, we include an estimate of J , calculated by evaluating Equation (2.13) with the trapezoid rule. It is critical to note that these pay-offs should not be directly compared with each other. This kind of comparison would be meaningless as each result corresponds to different choices of a_1 and a_2 , and these values explicitly contribute to J . For example; suppose an optimal control with pay-off weightings a_1 and a_2 is computed to have a pay-off of J_1 . Recomputing the optimal control with weightings $2a_1$ and $2a_2$ would produce a near identical optimal control and corresponding state, with slight deviation due to floating-point error. However, the corresponding pay-off J_2 would be twice as large.

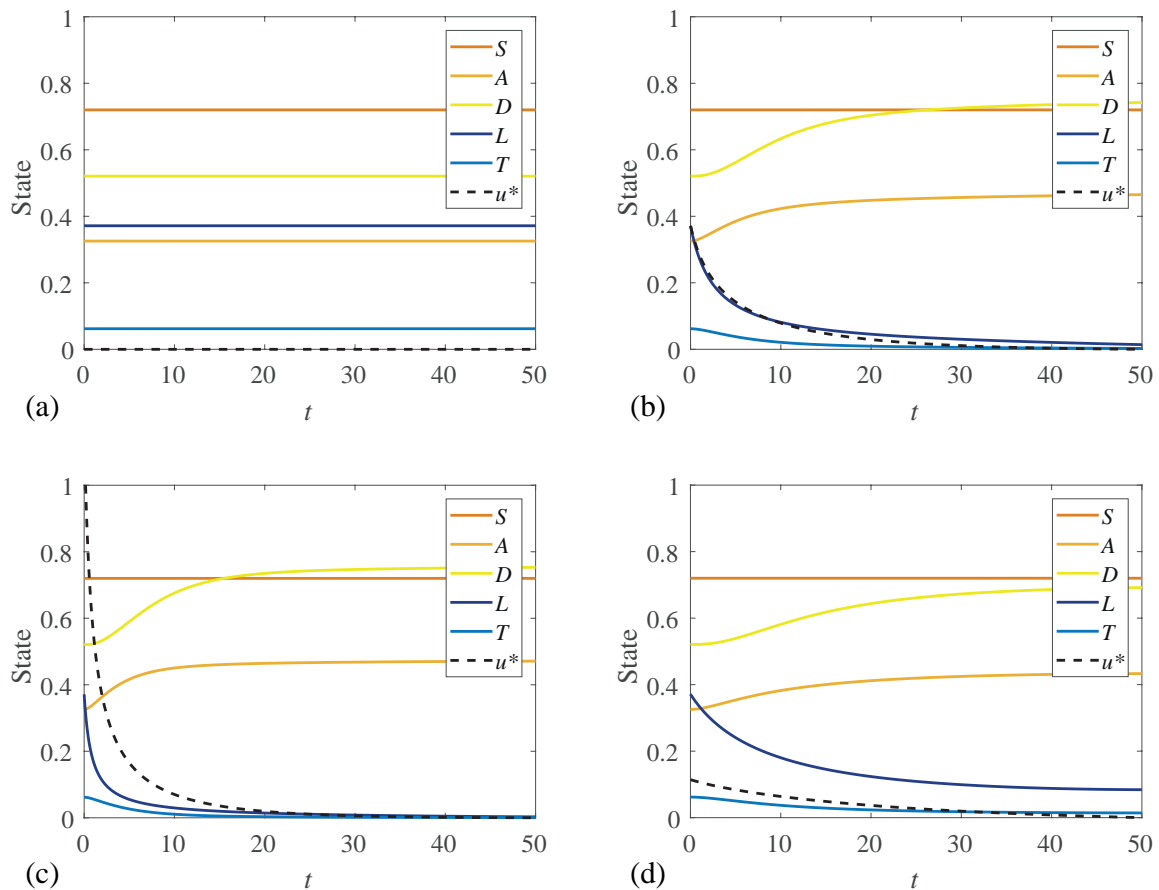


Figure 2.5: Application of a continuous optimal control (black dashed line) for various pay-off weightings a_1 and a_2 . The corresponding pay-off, J , is also given. (a) Coexisting steady state solution with no control applied. (b) Equal weighting $[a_1, a_2] = [1, 1]$, $J = 0.7167$. (c) Leukaemia weighted more heavily $[a_1, a_2] = [0.1, 1]$, $J = 0.2288$. (d) Control weighted more heavily $[a_1, a_2] = [1, 0.1]$, $J = 0.2262$. These figures are produced with immune response parameters $\alpha = 0.015$, $\gamma = 0.1$.

No pay-off is calculated for the uncontrolled steady state solution (Figure 2.5a) as the choice of a_1 and a_2 would be arbitrary. In this sense, computed pay-offs are not useful for comparing the outcome of *treatment* versus *no treatment* as there is no meaningful pay-off associated with no treatment. Rather, computed pay-offs can be used for comparison with other controls applied to a system with identical parameters to check whether or not they are comparable in outcome to the optimal control, noting that the response of the state will also change if the control changes.

To illustrate this point, we compare the optimal control obtained in Figure 2.5b to other potential treatment scenarios. In Figure 2.6 we compare four different dosing strategies where the same total amount of drug is applied using different temporal regimes. Our calculations of J provide a measure of how much the optimal result (Figure 2.6a) outperforms the other heuristically-determined dosing strategies. Applying the control at a constant rate for the full duration of the simulation (Figure 2.6b) produces a worse outcome than clinically-motivated cyclic treatment designs; applying the control at a greater level for a shorter duration in one (Figure 2.6c) or two (Figure 2.6d) cycles [24]. Due to the quadratic control term in Equation (2.13), despite applying the same total dosage, the control contributes more to the pay-off in Figure 2.6c than 2.6d, but this is outweighed by the benefit of reducing the leukaemic population more quickly. The optimal control framework provides us with tools to generate treatment hypotheses and assess the efficacy of different treatment protocols relative to one another and to the theoretical optimum for a given set of parameters.

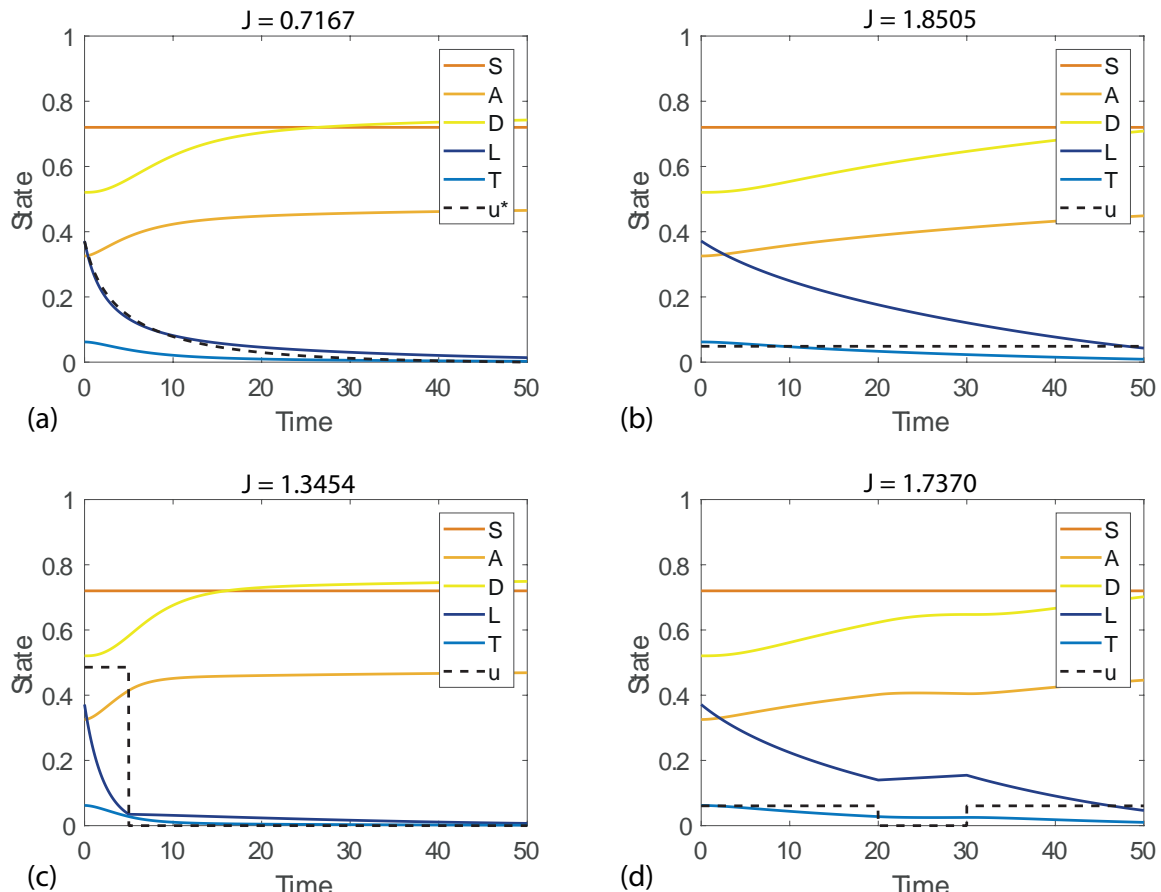


Figure 2.6: Comparison of (a) continuous optimal control with other possible controls of the same total dosage; (b) control applied at a constant rate over the entire duration, (c) control applied at a higher rate over a short cycle and (d) control applied in two cycles. These figures are produced with $a_1 = a_2 = 1$ and immune response parameters $\alpha = 0.015$, $\gamma = 0.1$.

2.4.3 Bang-bang optimal control

In addition to considering continuous controls, it is also relevant to consider discontinuous bang-bang controls as this kind of *on-off* control could be thought to be more clinically relevant than a continuous setting. Bang-bang control problems require a specified bound on the control variable. A bang-bang optimal control takes the value of either the upper or lower bound with finitely many switching points over an interval. As a starting point we re-consider Equation (2.12) and note that a control will be either bang-bang optimal or singular if the pay-off function is linear in the control term. A pay-off that should produce a bang-bang or singular optimal control of Equation (2.12) is to minimise

$$J = \int_0^{t_f} (a_1 u + a_2 L) dt, \quad (2.16)$$

subject to $b_1 \leq u \leq b_2$. We can construct the Hamiltonian as $H = \mathcal{L} + \boldsymbol{\lambda} \cdot f$, where \mathcal{L} is the integrand of Equation (2.16), $\boldsymbol{\lambda} = [\lambda_1, \lambda_2, \lambda_3, \lambda_4, \lambda_5]$ and f is the right hand side of Equation (2.12), giving

$$\begin{aligned} H = & a_2 L + a_1 u + \lambda_1[\rho_S S(1 - S) - \delta_S S] \\ & + \lambda_2[\delta_S S + \rho_A A(1 - A - L) - \delta_A A] \\ & + \lambda_3(\delta_A A - \mu_D D) \\ & + \lambda_4[\rho_L L(1 - A - L) - \delta_L L - \alpha L/(\gamma + L) - u L] \\ & + \lambda_5(L\delta_L - T\mu_T). \end{aligned} \quad (2.17)$$

As for the continuous control case, we differentiate the Hamiltonian with respect to our control variable u . With a linear pay-off, however, the result no longer contains u . Rather than solving for u , we define a switching function, $\psi(t)$, given by

$$\psi(t) = \frac{\partial H}{\partial u} = -\lambda_4(t)L(t) + a_1. \quad (2.18)$$

From PMP [264], it is implied that the Hamiltonian will be minimised under the following conditions,

$$u^*(t) = \begin{cases} b_1, & \text{if } \psi(t) > 0, \\ b_2, & \text{if } \psi(t) < 0. \end{cases} \quad (2.19)$$

Conditions in Equation (2.19) produce a bang-bang control. Here, the control variable takes a value of either its upper or lower bound. Notably, Equation (2.19) omits the case where $\psi(t) = 0$, as a bang-bang optimal control requires that $\psi(t) = 0$ only at discrete points, if at all [71]. If $\psi(t) = 0$ for any finite interval aside from isolated points, the control is singular. Singular controls are most commonly encountered in cases where the Hamiltonian is linear in the control variable but non-linear in some state variables [55].

When $\psi(t) = 0$ over an interval, the Hamiltonian is not a function of the control, so the state and co-state variables no longer determine the control [55]; over this interval the control is determined by requiring $\partial H/\partial u = 0$. Our control problem defined by Equation (2.12) and Equation (2.16) is not singular, so we do not discuss singular controls further.

Our co-state equations for $\boldsymbol{\lambda}$ are found as $\partial H/\partial \mathbf{x} = -d\boldsymbol{\lambda}/dt$. The co-state in the bang-bang control problem is given by,

$$\begin{aligned}\frac{d\lambda_1}{dt} &= 2S\lambda_1\rho_S + \delta_S\lambda_1 - \delta_S\lambda_2 - \lambda_1\rho_S, \\ \frac{d\lambda_2}{dt} &= 2A\lambda_2\rho_A + L\lambda_2\rho_A + L\lambda_4\rho_L + \delta_A\lambda_2 - \lambda_2\rho_A, \\ \frac{d\lambda_3}{dt} &= \mu_D\lambda_3, \\ \frac{d\lambda_4}{dt} &= -a_2 + \rho_AA\lambda_2 + \lambda_4\rho_LA + 2\rho_LL\lambda_4 - \lambda_4\rho_L \\ &\quad + \lambda_4\delta_L + \frac{\alpha\gamma\lambda_4}{(\gamma+L)^2} + \lambda_4u - \delta_L\lambda_5, \\ \frac{d\lambda_5}{dt} &= \mu_T\lambda_5,\end{aligned}\tag{2.20}$$

and we note that Equation (2.20) is subtly different to Equation (2.15), as the first term of the fourth line of Equation (2.20) is the constant $-a_2$, and no longer depends on L .

The transversality condition, Equation (2.11), gives the final time conditions on the co-state, $[\lambda_1(t_f), \lambda_2(t_f), \lambda_3(t_f), \lambda_4(t_f), \lambda_5(t_f)] = [0, 0, 0, 0, 0]$. Assuming again that the initial state is known; $[S(0), A(0), D(0), L(0), T(0)]$, it is now possible to determine the optimal bang-bang control and corresponding optimal state and co-state through a two-point BVP that we solve using the FBSM, as in the continuous control case. It is not necessary to modify the FBSM algorithm to find bang-bang optimal controls, though care must be taken in how the control is updated between iterations. This is discussed further in Section 2.4.4. Depending on the numerical scheme used to integrate the state and co-state equations through time, the discontinuous nature of the bang-bang control may require careful handling. Solutions are provided in Figure 2.7 for various weighting on the control parameters. In the continuous control case, when $a_1 > a_2$, placing a greater weighting on the negative impact of the control than the negative impact of the leukaemic stem cells; we observed that the control is applied at a lower level than when $a_1 < a_2$. The optimal bang-bang control must take either the upper or lower bound of the specified range. As such, in the bang-bang control case the pay-off weighting parameters determine not the level at which the control is applied, but rather the times at which the control switches from one bound to the other, hence the name *switching function* given to Equation (2.19).

In Figure 2.7 it is clear that when the upper bound on the control is higher, meaning in this context the maximum amount of chemotherapy that can be applied at any given

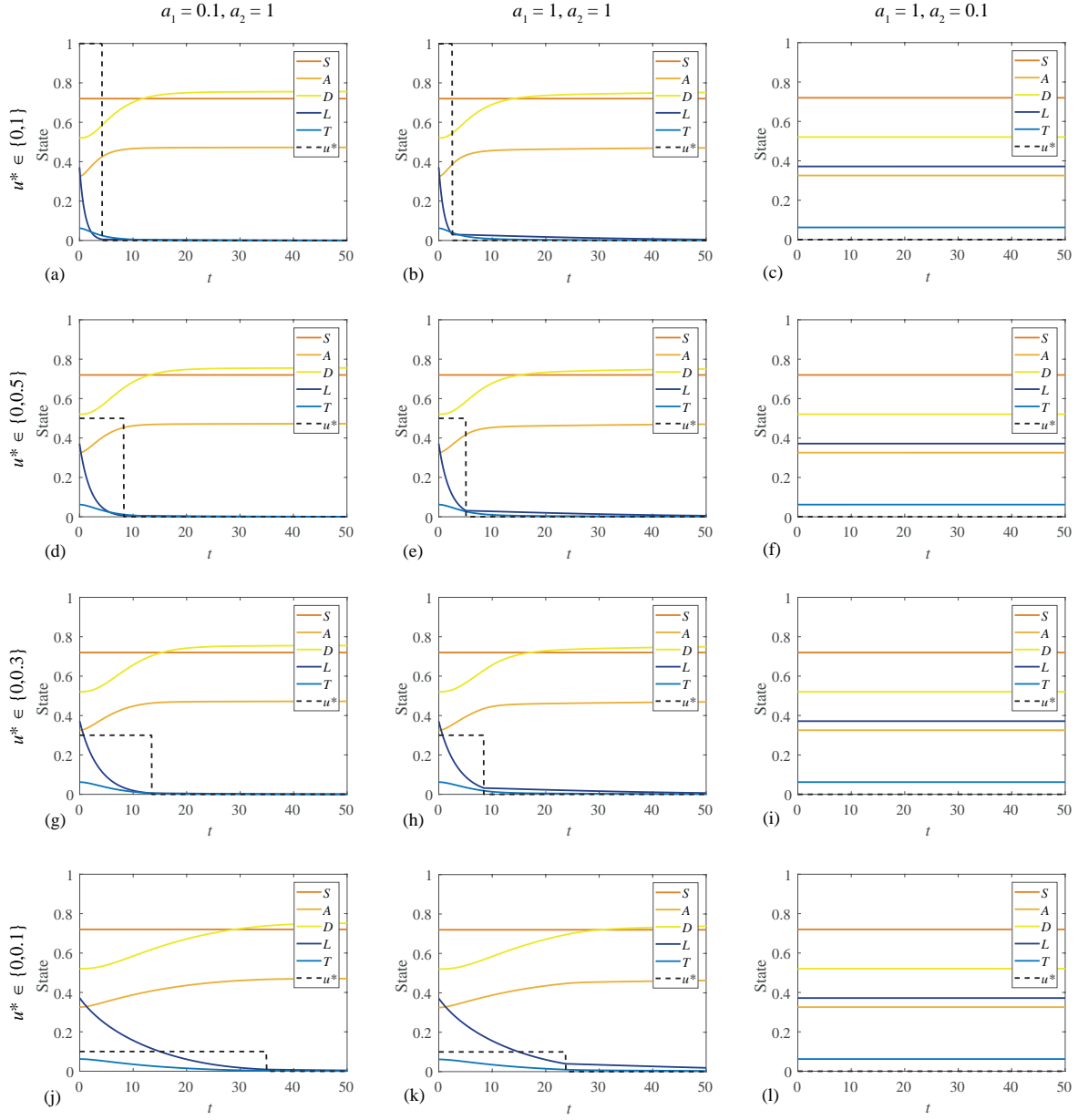


Figure 2.7: Bang-bang control solutions for various weightings on control and leukaemia in the pay-off (a_1 and a_2 respectively), with different control upper bounds. These figures are produced with immune response parameters $\alpha = 0.015$, $\gamma = 0.1$.

time is higher, the control switches to the lower bound earlier. In this case the lower bound corresponds to $u = 0$, or no chemotherapy being applied (control *switched off*), though this is not required of the method. The interaction between the control and state in Equation (2.20) means that the cumulative amount of control applied is not the same for different bounds on the control. In Figure 2.5 we demonstrate that for a continuous control with $a_1 = 1$, $a_2 = 0.1$, a small amount of control is applied. For the bang-bang case with the same weighting, we observe in the rightmost column of Figure 2.7 that for a range of control upper bounds, the control is not switched on at all - implying that with such a pay-off, it is optimal not to apply the control. One may suppose that for

a sufficiently small upper bound that the control would turn on even with this pay-off, however a lower upper bound on the control also reduces the impact the control has on the state.

Due to the immune response incorporated in Section 2.3, a sufficiently small leukaemic population will tend towards extinction rather than grow back to a coexisting steady state. Because of this, we observe in Figure 2.7 that the control switches off before the leukaemic stem cells are totally eradicated - the immune response is sufficient once the leukaemic population is sufficiently low. This is most evident in Figure 2.7k, where we can see that the population of leukaemic stem cells is declining but has not become extinct by the final time, $t = 50$. In absence of the immune response incorporated in Section 2.3, we would observe the leukaemic population increasing as soon as the control is switched off, since the healthy steady state would be unstable; applying fixed final time bang-bang optimal control to the original model produces outcomes that are mathematically optimal but physically undesirable.

In our discussion of continuous controls, we note the fixed final time as a limitation, since changing the final time can change the profile of the optimal control and state. In general the same is true of bang-bang controls with fixed final times, though in some instances that we consider the optimal bang-bang control does not change significantly if the final time is changed. For example; the optimal switching times and corresponding optimal states in the leftmost column of Figure 2.7 do not change significantly if the final time is increased to $t = 100$, because by $t = 50$ we see that $L \approx 0$ and $u = 0$, so neither contributes significantly to the pay-off in the interval $50 < t \leq 100$. For these cases the control is not costly relative to the leukaemia ($a_1 < a_2$) so it is applied at the upper bound until the leukaemic stem cell population is virtually eradicated before switching off.

For this particular system, we only obtain bang-bang optimal controls with a single switching time. We are able to verify these bang-bang optimal controls through an exhaustive search of all possible bang-bang controls by specifying the switching time, directly calculating the pay-off and determining the switching time that minimises the pay-off. For all cases considered in Figure 2.7 the switching time identified via exhaustive search is in agreement. It is also possible that the optimal bang-bang control may switch between the upper and lower bounds numerous times, producing multiple ‘bangs’. Bang-bang optimal controls that exhibit multiple bangs can be identified using the FBSM without modification, though it is more difficult to find a convergent bang-bang optimal control with multiple bangs. Similarly, without knowing a priori how many switching times to expect, an exhaustive search for multiple bangs is not computationally feasible.

2.4.4 Convergence and control updating

In this section we examine the convergence behaviour of solutions to the optimal control problems presented in this work. Convergence behaviour of numerical solutions to optimal control problems is influenced by multiple factors. In particular, we discuss the initial guess of the control, convergence criteria, control updating and pay-off weightings. These factors influence not only the number of iterations required to reach a converged numerical solution, but also whether or not a converged solution will be reached at all.

Holding all other factors constant, provided that the initial guess for the control is sensible, the initial guess does not have a significant impact on whether or not a converged result is reached for the control problems considered in this work. However, convergence is typically reached with fewer iterations when the initial guess is relatively closer to the true value of the optimal control. For simplicity we use the initial guess $u \equiv 0$ for all results presented in this work, while acknowledging that more thoughtful choices may deliver convergence in fewer iterations.

For optimal control results presented in the previous sections, we determine whether convergence has been achieved after each iteration based on the relative difference between the updated control, u_{updated} , and the old control, u_{old} . If this relative difference is sufficiently small, the updated control is accepted as the optimal control. A typical relative difference convergence criterion requires

$$\frac{|u_{\text{updated}} - u_{\text{old}}|}{|u_{\text{updated}}|} \leq \varepsilon, \quad (2.21)$$

where $0 < \varepsilon \ll 1$ is the desired relative tolerance. Following [191], we adjust Equation (2.21) to allow for a control of the form $u \equiv 0$, giving

$$\varepsilon \sum_{i=1}^n |u_{\text{updated}}(i\Delta t)| - \sum_{i=1}^n |u_{\text{updated}}(i\Delta t) - u_{\text{old}}(i\Delta t)| \geq 0, \quad (2.22)$$

where $t = i\Delta t$, Δt is the numerical time step and n is the number of nodes in the time discretisation. The absolute value is taken to ensure that positive differences are not offset by negative differences that could otherwise result in incorrectly detecting convergence. The choice of convergence criterion and acceptable tolerance depends on the particular problem at hand, and may need to be adjusted to be appropriate for another control problem. In some instances, it may be necessary to check convergence of the state and co-state as well as the control, particularly if the state response to control is sensitive. For the control problems studied in this work, we find that state and co-state respond predictably to the control, and convergence of the control is accompanied by convergence of that state and co-state. As such we do not explicitly check for convergence of the state and co-state.

In each iteration of the FBSM we recalculate the control, u_{new} , based on the newly calculated state and co-state solutions and associated optimality criterion, as discussed in Section 2.4.2 for the continuous control and Section 2.4.3 for the bang-bang control. Typically, u_{new} is not used directly as the control for the next iteration of the FBSM, but rather we form an updated control u_{updated} as a weighted combination of u_{new} and the control from the previous iteration, u_{old} . The motivation for this is two-fold; first, an appropriately weighted control updating scheme can speed up convergence; and second, for many optimal control problems, a direct update of $u_{\text{updated}} = u_{\text{new}}$ will fail to produce converging results at all. A common approach is to update the control based on a convex combination, such that the total weightings sum to one, of the new and previous control(s). In this work we use a constant linear weighting, with $0 < \omega < 1$, giving

$$u_{\text{updated}} = \omega u_{\text{old}} + (1 - \omega)u_{\text{new}}. \quad (2.23)$$

We find that the best choice for ω depends not only on the form of the control, continuous or bang-bang, but also on model parameters such as the pay-off weightings. There is a trade-off between the number of iterations required to obtain convergence, and actually converging at all; a larger ω typically is more likely to produce converging solutions, but this also means that the control changes less each iteration, so more iterations are required. For example, a weighting of $\omega = 0.7$ was sufficiently large that all continuous control solutions presented in Figure 2.5 converged to a relative tolerance of $\varepsilon = 1 \times 10^{-3}$. For $\omega = 0.6$ only Figure 2.5d converges, and for $\omega = 0.8$, all solutions in Figure 2.5 converge but require more iterations than when $\omega = 0.7$.

Convergence in the bang-bang control case typically requires larger ω and more iterations than the continuous controls. In the rightmost column of Figure 2.7, there is no concept of convergence as the control never switches on. Only Figure 2.7j and Figure 2.7k converge to a relative tolerance of 1×10^{-3} for $\omega = 0.7$, with $\omega = 0.9$ being sufficient for convergence of all remaining solutions aside from Figure 2.7b, where we set $\omega = 0.95$.

It is clear that the best control updating scheme depends on the particular problem; and a scheme that works well for one problem may not necessarily work at all for another. When solving control problems, it may be necessary to try a range of updating schemes to achieve convergence. In this work we only consider constant weighted updating, though there are more sophisticated updating schemes that shift the weighting towards u_{new} as the number of iterations increase [191]. In Figure 2.8 we examine the influence of the control update weighting ω , and the pay-off weightings, a_1 and a_2 , on the convergence behaviour of the bang-bang control problem studied in Section 2.4.3. Specifically, we consider the case where $0 \leq u \leq 0.5$, and determine that a solution has converged if it meets a relative tolerance of $\varepsilon = 1 \times 10^{-3}$ within 250 iterations. In each panel of Figure 2.8 we observe three *regions*: in region I we have no concept of convergence as the

control never switches on; in region II we find that the optimal control problem does not converge; and in region III we observe convergence. Not all simulations conform strictly to these regions since the boundary between the different regions is not always sharp and well-defined. However, broadly speaking, these three regions capture the essence of the convergence behaviour that we observe. These regions are constructed based on discrete simulations of the problem for $0 < a_1 \leq 10$ and $0 \leq a_2 \leq 10$, each in increments of 0.1. The case where $a_1 = 0$ is excluded as this corresponds to no cost associated with applying the control, so there is no sense of convergence.

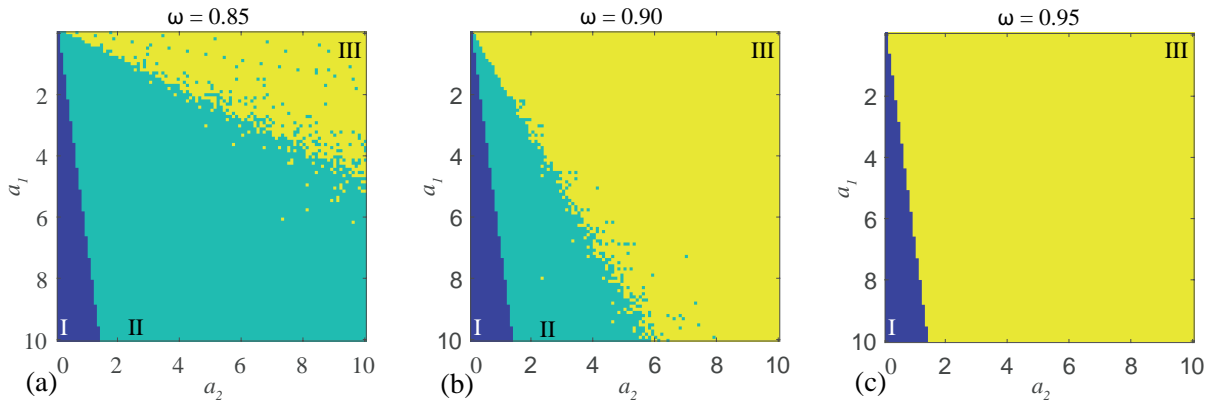


Figure 2.8: Convergence behaviour for (a) $\omega = 0.85$, (b) $\omega = 0.9$, and (c) $\omega = 0.95$, with a_1 and a_2 ranging from 0 to 10 in increments of 0.1, excluding $a_1 = 0$. In region I (dark blue) we have no concept of convergence as the control never switches on. In region II (light blue) we find that the optimal control problem does not converge, and in region III (yellow) we observe convergence. These figures are produced with immune response parameters $\alpha = 0.015$, $\gamma = 0.1$.

From Figure 2.8 it is clear that convergence is achieved in a larger region of the (a_1, a_2) parameter space when ω is increased. However, it is important to note that achieving convergence in this context only implies that Equation (2.22) is satisfied, and does not necessarily mean that a suitable bang-bang control is obtained. While some controls corresponding to individual simulations in Figure 2.8c are suitable bang-bang controls; a portion are approaching bang-bang but require additional iterations to accurately calculate the control around the switching point. The weighting applied in Equation (2.23) has the effect of smoothing u during intermediate iterations of the FBSM; this smoothness is gradually reduced as the control converges to the optimal switching point. Since ω explicitly influences the relative amount that the control can differ between iterations, if a larger ω is required to achieve convergence for a given problem, it may also be necessary to reduce the convergence tolerance ε to ensure that the resulting control is sufficiently bang-bang.

2.5 Conclusion and Outlook

In this work we consider a haematopoietic stem cell model of AML that incorporates competition between leukaemic stem cells and blood progenitor cells within the bone marrow niche. We incorporate a biologically appropriate immune response in the form of a Michaelis-Menten term. This modification is mathematically convenient because of the impact it has on the steady states, and biologically relevant because the immune response is known to play an important role in cancer progression and treatment. With a view to identifying the optimal way to apply a treatment such as chemotherapy to the model, we formulate and solve optimal control problems corresponding to multiple objectives and constraints. This includes quadratic pay-off functions, yielding continuous controls, as well as linear pay-off functions, yielding discontinuous bang-bang controls.

We provide a brief overview of optimal control theory, with a focus on the necessary conditions derived from Pontryagin's Maximum Principle. This approach formulates the optimal control problem as a coupled multi-species two-point boundary value problem. The resulting optimal control problem is solved numerically using the iterative FBSM. The algorithm for the FBSM is discussed, with a focus on highlighting typical issues that may arise in implementing optimal control. Suggestions are provided for overcoming these issues. In particular, we focus on factors that influence the convergence of the FBSM; not only in terms of the number of iterations required, but also whether it converges at all. These factors include the initial guess for the control, the convergence criterion, the method of updating the control, the associated weighting placed on controls from prior iterations and parameters such as pay-off weightings, and in the bang-bang control case, the control bounds.

For the model we consider, a well informed initial guess for the control may reduce the number of iterations required for convergence; but any sensible guess should not prevent convergence. Most critically, we show that the method of updating the control and the associated weight placed on the control from the previous iteration has a significant impact on whether or not convergence will be achieved, as do the weights in the pay-off function. In the bang-bang control case, we observe that increasing the upper bound on the control can prevent convergence, holding all other factors constant; in this case, placing a greater weight on the solution from the previous iteration may produce convergence.

There are many potential avenues to extend the ideas explored in this work. Here, we have incorporated the control via a simple mechanism, and more sophisticated pharmacokinetic processes such as drug absorption and metabolism could be incorporated to increase the biological detail captured by the model, but this additional biological detail comes at the cost of increasing the number of unknown, and possibly unmeasurable parameters. Therefore, care must be exercised in following up this kind of extension. In the main document we consider the most fundamental case of a control that only impacts

leukaemic cells, however the methodology extends to a control affecting multiple species. We demonstrate this extension in the supplementary material. The control problems presented in this work could be reformulated as fixed final state problems, leaving the final time free to vary which could be more clinically relevant than specifying the final time. With the introduction of an immune mechanism to the model, it is also possible to consider a control based around immunotherapy.

A recent idea of great interest in clinical cancer research is the possibility of introducing an interval of time during treatment in which no chemotherapy is applied. This kind of intervention is reminiscent of a bang-bang control, and is often referred to as a *drug holiday* [313]. There is some evidence to suggest that drug resistance of tumour cells may reduce with time so that patients experience an improved response to chemotherapy following a drug holiday [174, 180, 287]. This application of a drug in an *on-off* fashion parallels the idea of the bang-bang controls we consider in this work and so it would be interesting to formulate the concept of designing a drug holiday in terms of a bang-bang optimal control problem by extending the model to include acquired drug resistance and using the algorithms and concepts demonstrated in this work.

Acknowledgements

This work is supported by the United States Air Force Office of Scientific Research (BAA-AFRL-AFOSR-2016-0007) and the Australian Research Council (DP170100474). Computational resources were provided by the eResearch Office at QUT. We appreciate the helpful referee comments.

Chapter 3

Designing combination therapies using multiple optimal controls

Statement of Contribution of Co-Authors

The authors listed below have certified that:

1. they meet the criteria for authorship and that they have participated in the conception, execution, or interpretation, of at least that part of the publication in their field of expertise;
2. they take public responsibility for their part of the publication, except for the responsible author who accepts overall responsibility for the publication;
3. there are no other authors of the publication according to these criteria;
4. potential conflicts of interest have been disclosed to (a) granting bodies, (b) the editor or publisher of journals or other publications, and (c) the head of the responsible academic unit, and
5. they agree to the use of the publication in the student's thesis and its publication on the [QUT's ePrints site](#) consistent with any limitations set by publisher requirements.

In the case of this chapter: Chapter 3

Please state the publication title and date of publication or status:

Designing combination therapies using multiple optimal controls. Published 2020 in Journal of Theoretical Biology.

Contributor	Statement of contribution*
Jesse A Sharp 	Designed the study developed and implemented the computational algorithms, generated and interpreted results, produced figures, drafted the manuscript, revised the manuscript.
08/12/2021	
AP Browning	Interpreted results, provided comments on the manuscript.
T Mapder	Interpreted results, provided comments on the manuscript.
CM Baker	Interpreted results, provided comments on the manuscript.
K Burrage	Designed the study, supervised the research, interpreted the results, and provided comments on the manuscript.
MJ Simpson	Designed the study, supervised the research, interpreted the results, and provided comments on the manuscript.

Principal Supervisor Confirmation

I have sighted email or other correspondence from all Co-authors confirming their certifying authorship. (If the Co-authors are not able to sign the form please forward their email or other correspondence confirming the certifying authorship to the GRC).

Professor Matthew Simpson
Name


Signature

11/12/2021
Date

Article published 2020 in Journal of Theoretical Biology

Sharp JA, Browning AP, Mapder T, Baker CM, Burrage K, Simpson MJ (2020). Designing combination therapies using multiple optimal controls. *Journal of Theoretical Biology*. doi:[10.1016/j.jtbi.2020.110277](https://doi.org/10.1016/j.jtbi.2020.110277).

Abstract

Strategic management of populations of interacting biological species routinely requires interventions combining multiple treatments or therapies. This is important in key research areas such as ecology, epidemiology, wound healing and oncology. Despite the well developed theory and techniques for determining single optimal controls, there is limited practical guidance supporting implementation of combination therapies. In this work we use optimal control theory to calculate optimal strategies for applying combination therapies to a model of acute myeloid leukaemia. We consider various combinations of continuous and bang-bang (discrete) controls, and we investigate how the control dynamics interact and respond to changes in the weighting and form of the pay-off characterising optimality. We demonstrate that the optimal controls respond non-linearly to treatment strength and control parameters, due to the interactions between species. We discuss challenges in appropriately characterising optimality in a multiple control setting and provide practical guidance for applying multiple optimal controls. Code used in this work to implement multiple optimal controls is available on [GitHub](https://github.com/Mapder/CombinationTherapies).

3.1 Introduction

Determining appropriate interventions for managing populations of interacting species poses significant challenges. A wide variety of biological processes are characterised by interactions between species, ranging from mutualistic to antagonistic. Mutualistic interactions benefit all species involved: for example, the acacia-ant and acacia tree have a mutualistic interaction; the ants are provided food and shelter by the tree, and in turn protect the tree from herbivores, insects and other plants [155]. Antagonistic interactions occur where one species gains at the expense of others, or where all species are disadvantaged; such as the predation of rabbits by foxes [105], competition for prey between lions and hyenas occupying the same ecological niche [305], or in acute myeloid leukaemia (AML) where progenitor blood cells and leukaemic stem cells in the bone marrow niche compete for resources [149, 210, 301]. These interactions, coupled with the reality that many interventions impact multiple species within an environment, increase the difficulty of designing intervention strategies. We use optimal control techniques to explore the dynamics of multi-species systems subject to multiple intervention strategies. We present a case study considering a combination therapy approach to treatment; analysing a stem cell model of acute myeloid leukaemia (AML). We subject the system to a chemotherapy control that destroys both leukaemic stem cells and progenitor blood cells, and a stem cell transplant control that replenishes progenitor blood cells. This is an informative system to study as the complexity makes it unclear how to best apply these interventions without applying optimal control techniques, and the antagonistic dynamics of AML are representative of many other systems in biology.

Where available intervention mechanisms incur different costs, target different species or have a level of efficacy that varies based on the state of the system, it is reasonable to consider a strategy with multiple interventions applied in combination. We are interested in applying interventions to interacting multi-species processes to influence the outcomes. Example situations where multiple interventions are employed include aerial baiting and animal trapping for invasive species management in ecology [31]; vaccination, rehydration, antibiotics and sanitation for outbreak control in epidemiology [238]; growth hormone and hyperbaric oxygen therapy for wound healing [4]; and chemotherapy and stem cell transplants for cancer treatment in oncology [59].

Interactions between species increase the complexity involved when considering interventions, but can also provide opportunities. Failure to understand the interactions between species can result in unintended effects of intervention. In the Boodarie National Park in south-eastern Australia, intensive fox baiting was implemented to curb population decline of native animals through predation by foxes. This significantly increased the abundance of wallabies, with the unintended consequence of reducing abundance of some tree species [90]. Conversely, understanding interspecies interactions can provide

exploitable opportunities in designing interventions. In cancer research, particular genes have been shown to exhibit cancer-promoting functions. There are significant challenges associated with targeting these genes directly, prompting investigation into means of targeting the upstream signalling pathways that activate the genes [277, 342]. Understanding the dynamics of interactions between species and the influence of proposed treatments improves our ability to determine effective intervention strategies.

Mathematical models provide a low-cost, low-risk way of exploring the dynamics of biological processes (and valuably, understanding the risks of proposed interventions) [33, 76, 170, 232]. In cancer research mathematical models have been used to explore key processes such as incidence; pathogenesis; tumour growth; metastasis; immune reaction and treatment [63, 82, 83, 177, 211, 312]. Optimal control techniques are widely applied, not only in mathematical biology broadly [77, 187, 188, 213], but also in cancer therapy [75, 150, 285] and AML specifically [290]. Likewise, mathematical models have been used to study stem cell dynamics [215, 250], including optimal control of cancer via chemotherapy with consideration for bone marrow destruction [109]. Optimal control techniques have been applied to study various cancer therapies, including: chemotherapy and immunotherapy [57], and combined broad spectrum and targeted chemotherapy [237], for chronic myeloid leukemia; chemotherapy and anti-angiogenic therapy to control tumour volume [95, 185, 285]; hormone therapy for prostate cancer [84]; chemotherapy in the presence of drug resistant tumours [74]; and chemotherapy and radiotherapy treatments for bone metastatic cancer [66].

Many interacting population dynamics can be explored through studying coupled systems of differential equations. As a starting point, we could consider two species, $S_1(t)$ and $S_2(t)$ with general growth and decay functions g_1 , g_2 and d_1 , d_2 , respectively. These systems are readily extended to incorporate multiple interventions or controls, say $u(t)$ and $v(t)$, that result in some net impacts c_1 and c_2 on each species. Such a model could take the following form, with all variables implicitly functions of time:

$$\begin{aligned} \frac{dS_1}{dt} &= \underbrace{g_1(S_1, S_2)}_{\text{growth of } S_1} - \underbrace{d_1(S_1, S_2)}_{\text{decay of } S_1} + \underbrace{c_1(S_1, S_2, u, v)}_{\text{interventions}}, \\ \frac{dS_2}{dt} &= \underbrace{g_2(S_1, S_2)}_{\text{growth of } S_2} - \underbrace{d_2(S_1, S_2)}_{\text{decay of } S_2} + \underbrace{c_2(S_1, S_2, u, v)}_{\text{interventions}}. \end{aligned} \quad (3.1)$$

In Equation (3.1) all growth and decay terms are presented as functions of both species. These terms can be reduced to functions of a single species to capture the range of interactions from mutualism to antagonism. For example, the classic Lotka-Volterra model for predator-prey interaction [40, 205] can be recovered if $g_1(S_1, S_2)$ reduces to $g_1(S_1)$, and $d_2(S_1, S_2)$ reduces to $d_2(S_2)$. The intervention terms are expressed as functions of both species and controls for generality, but can also be reduced to model specific

interventions. We note that this formulation permits modelling of complex interactions between species and provides flexibility in the application of controls, for example allowing us to implement a control that impacts both species simultaneously.

This paper presents a case study of a two species model with resource competition, where abundance of one species is desirable and the other is undesirable. We consider the dynamics of optimal therapies involving two controls. In particular, we model the dynamics of a combination therapy intervention with one control that negatively affects both species, and another control that positively affects only the desirable species. Results are obtained under pay-off regimes corresponding to continuous applications of both controls; combinations of continuous and bang-bang (discrete) controls; and bang-bang applications of both controls [191, 290]. The impact of key parameters on the combination therapy dynamics are also considered. We find that the response of the optimal control strategy to interaction parameters can be highly non-linear, with behaviour that exhibits significant variation across the parameter space. We identify dynamics reflective of clinical practice under some parameter regimes, and note that some interesting solution dynamics are transient, existing only over small regions of control parameter space. We also demonstrate that the response of the system under optimal control dynamics can provide insights into the quality of the underlying model. Finally, we comment on the challenges involved in selecting appropriate pay-off weightings, and the flexibility it affords.

There are two key aspects of novelty in this work. First, we have completed a novel mathematical modelling exercise in which acute myeloid leukaemia is treated using a combination of chemotherapy and stem cell transplants, determined using optimal control theory. Secondly, we present a versatile framework, and make code available, for designing combination therapy protocols using optimal control. We note that this framework can be readily adapted to problems beyond oncology involving multiple interacting species subject to multiple interventions.

In Section 3.2 we outline the optimal control approach taken in this work. In Section 3.3 we introduce a model of AML [82, 290] to examine as a case study on combination therapy; we subject the model to both a chemotherapy control and a stem cell transplant control. We identify candidate pay-off functions characterising optimality for the AML model. Results and discussion corresponding to these candidate pay-off functions are presented in Section 3.4. Concluding remarks are provided in Section 3.5. In the supplementary material we present a broad collection of results corresponding to a wide range of control parameter regimes, we provide a phase portrait illustrating the steady state behaviour of the model, and we explore sensitivity of the optimal control regimes to parameters, assumptions and initial conditions.

The code used to produce the optimal control results in this work is freely available on [GitHub](#). Our implementation of the FBSM uses a fourth-order Runge-Kutta

method to generate numerical solutions to ordinary differential equations [191, 269]. A sufficiently small constant time step is chosen to produce numerical solutions that are grid-independent.

3.2 Optimal control theory

When considering a system with inputs that we can control, we are naturally interested in determining the particular amount and timing of these inputs that produces the *best* outcome. In the context of optimal control, *best* corresponds to a control that minimises or maximises a specified pay-off. The pay-off is also modelled; as such it has assumptions, and in complex systems it is not always clear how to appropriately represent objectives. This is particularly evident when controls are designed to meet multiple objectives; there is not necessarily a single way to value outcomes [218, 282]. When considering optimal control for disease treatment, the pay-off typically incorporates factors such as reducing the negative effect of the disease, and minimising the resources used and any adverse effects of the treatment.

For the interacting multi-species system given by Equation (3.1) a general pay-off functional, J , to be minimised over a fixed time interval is:

$$J = \int_{t_0}^{t_f} \mathcal{L}(S_1(t), S_2(t), u(t), v(t)) dt,$$

where $u(t)$ and $v(t)$ represent the treatments or interventions applied. The integral captures cumulative costs over time, such as disease burden, side effects or toxicity of a treatment, or resource costs. The particular form chosen for \mathcal{L} determines the dynamics of the optimal strategy, as we discuss later.

In this work, we determine optimal controls through applications of Pontryagin's Maximum Principle (PMP) [264]. Although multiple interventions are commonly applied in ecology, epidemiology, wound healing and oncology [4, 31, 59, 238], there is limited discussion of optimal control problems with multiple controls. The theory and practice of modelling a single optimal control using the PMP approach has been thoroughly explored in texts such as [17, 26, 55, 191], and extends readily to multiple control problems. As such, we present here only a brief outline of the process, and focus this work on insights and issues of practical implementation of multiple optimal controls. We construct the Hamiltonian and appropriate co-state equations that couple the objective and cost to the multi-species system. Applying the PMP produces a two-point boundary value problem (TPBVP) that we must solve, in combination with known initial conditions for the *state*, $\{S_1(t_0), S_2(t_0)\}$, to minimise the Hamiltonian and hence determine the optimal controls and corresponding optimal state trajectories. The TPBVPs arising in optimal control are typically characterised as being a system of differential equations where some ini-

tial conditions and some final time conditions are known. As such, they are commonly solved using iterative approaches such as the forward-backward sweep method (FBSM) or shooting methods [165, 191].

We apply the FBSM, an iterative process involving the following steps: an initial guess is made for the controls over the interval; using this guess the state is solved forwards in time from t_0 to t_f ; with this information and the transversality condition (a final time constraint on the co-state variables, derived from the pay-off function), the co-state equations are solved backwards in time from t_f to t_0 , and; the guess for the controls are updated based on the solutions for the state and co-state. This process is repeated until the state, co-state and controls are deemed to have converged to some tolerance. Practical guidance and code for implementation of the FBSM for optimal control problems is available in the literature [191, 290]. The FBSM readily generalises to problems with multiple controls with no modification beyond including the additional equations, though typically incorporating additional controls also increases the computational cost. An algorithm for the FBSM for multiple controls is provided in the supplementary material.

The pay-off functions we consider vary in regard to whether each of the terms in the integrand are linear or quadratic. Linear and quadratic forms are prevalent in the literature [17, 193, 246, 270], although other forms are also considered, such as a logarithmic pay-off to represent investor utility in mathematical finance [8, 178]. Quadratic control terms in the pay-off produce continuous controls. Having the control term appear only linearly in both the pay-off and the state produces bang-bang or singular controls. Bang-bang controls require specified lower and upper bounds, are applied at either bound, and switch based on the sign of the derivative of the Hamiltonian with respect to the control variable. Singular controls arise when this derivative is zero over any finite interval excluding isolated points. Over such intervals the optimal control cannot be determined by simply looking for the value that minimises the Hamiltonian [55, 191]. In this work we focus on control parameter regimes where the linear pay-off terms correspond to non-singular bang-bang optimal control problems.

The functional form of state variables in the pay-off has a less clear impact on the control dynamics. Quadratic terms attribute a disproportionately greater cost to large quantities than small; this can be desirable when modelling leukaemia, as a larger leukaemic burden can be disproportionately more damaging than a smaller one [100]. The downside of this is that very little cost is ascribed to a small leukaemic burden, meaning optimal control regimes derived from a pay-off with a quadratic leukaemia term may reach a state where significant leukaemia remains. Conversely, the penalty applied by a linear term is proportional to the size of the leukaemic burden; optimal control regimes derived under this type of pay-off will typically produce final states with less leukaemia remaining.

In the following sections, we explore the dynamics of multiple controls through a model of AML subject to combination therapy. We present select results in this document to

highlight key features of multiple control dynamics, and present a broad selection of additional results in the supplementary material.

3.3 Case study: combination therapy for acute myeloid leukaemia

Acute Myeloid Leukaemia (AML) is a blood cancer characterised by the transformation of haematopoietic stem cells into leukaemic blast cells, primarily in the bone marrow [82, 233]. The presence of leukaemic cells in the bone marrow niche disrupts haematopoiesis [82], as these cells stop responding to normal regulators of proliferation and no longer undergo normal differentiation or maturation [100, 135]. Typical treatments for AML include chemotherapy; immunotherapy; haematopoietic stem cell transplants; radiotherapy and leukapheresis [19, 233, 265]. Treatment strategies often incorporate multiple therapies concurrently, these combination therapies can be intramodal; such as chemotherapy with multiple chemotherapeutic agents, or intermodal; such as chemotherapy in combination with stem cell transplantation. Combination therapies offer a range of potential advantages over individual therapies, including reduction of toxicity and adverse effects of treatment, improved outcomes in the presence of drug resistance and tumour cell heterogeneity and potentiation of chemotherapy [35, 152, 338].

In a clinical setting, AML treatment may involve both chemotherapy to reduce the leukaemic cell population and stem cell transplants to bolster the healthy cell populations. This has been shown to allow a higher dose of chemotherapy to be given, reduce adverse effects of the chemotherapy, reduce the risk of relapse and improve long-term survival [59, 207, 339]. When treating cancer via chemotherapy the exact mechanisms depend on the type of cancer and the particular chemotherapeutic drug, but typically, cytotoxic drugs are administered that target highly proliferative cells. Unfortunately, this commonly includes not only cancer cells, but also healthy cells in the bone marrow, hair, skin and digestive system [233]. The loss of these healthy cells contributes to the significant side effects experienced by chemotherapy patients. A stem cell transplant can mitigate these side effects by giving a patient allogeneic (from a matched donor) or autologous (from the person receiving the transplant) stem cells, typically collected from the bone marrow or the peripheral blood. Transplants are most often administered in remission, following preparative high-dose chemotherapy and/or radiotherapy [59, 67]. Side effects arising from stem cell transplants can also be significant, including complications related to the liver, kidneys and lungs, heightened risk of bacterial and viral infections, and graft-versus-host disease [93, 127, 207].

Development, progression and response to treatment of AML is highly heterogeneous, due to its distinct genetic variation [100, 307]. Measuring individual biological parameter

values directly from experiments is challenging, and fitting models to clinical data produces parameter estimates that are not unique or with significant uncertainty [128, 307]. Further, clinical data is often only collected at a course-grained level, sufficient to describe only the collective behaviour of the system [82, 128]. In Ommen et al. (2014), patient data is analysed to investigate the doubling time of the leukaemic burden in relapse of AML [248]. The results are delineated according to molecular subgroups. The median doubling times for these subgroups range from 12 to 24 days. There was significant variance between samples however, with doubling times ranging from 3 days to around 70 days. Another study of patients with untreated, newly diagnosed AML calculates the median potential tumour doubling time to be 8 days, with a range of 3 to 48.9 days [48].

In treating AML with chemotherapy, the timing and dose of chemotherapeutic agents is a critical factor in determining patient outcomes [263]. It follows that the dosages applied in combination therapy are also critical, particularly with studies indicating that synergistic relationships may exist between treatments in particular ratios and schedules but not others [35, 223]. As such, it is important to understand the dynamics of systems subject to multiple treatments, and identify key factors that impact the optimal treatment schedules and dosages. Different aspects of treatment schedules interact in a complex way and models are a useful way to investigate the relationship [32].

We consider a stem cell model of AML first presented by Crowell, MacLean and Stumpf [82], modified to incorporate an immune response to leukaemia [290]. The model consists of five species; haematopoietic stem cells $S(t)$, progenitor cells $A(t)$, terminally differentiated blood cells $D(t)$, leukaemic stem cells $L(t)$, and fully differentiated leukaemia cells $T(t)$. All dependent variables are functions of t , and rates have dimension [T^{-1}]. We do not explicitly specify a time scale. For notational convenience we often omit the explicit time-dependence of $S(t)$, $A(t)$, $D(t)$, $L(t)$ and $T(t)$ from this point forward:

$$\begin{aligned}\frac{dS}{dt} &= \rho_S S(1 - S) - \delta_S S, \\ \frac{dA}{dt} &= \delta_S S + \rho_A A(1 - A - L) - \delta_A A, \\ \frac{dD}{dt} &= \delta_A A - \mu_D D, \\ \frac{dL}{dt} &= \rho_L L(1 - A - L) - \delta_L L - \frac{\alpha L}{\gamma + L}, \\ \frac{dT}{dt} &= \delta_L L - \mu_T T.\end{aligned}\tag{3.2}$$

The competition between progenitor blood cells and leukaemic stem cells is based on the hypothesis that these cells occupy the same niche within the bone marrow [149, 301]. Motivation for incorporating this kind of interaction in models of AML and other similar leukaemias has been detailed in the literature [82, 211].

The steady state behaviour of the original model has been thoroughly explored in [82], and the effect of the incorporated immune response on these steady states is outlined in [290]. Briefly, the original model supports healthy (no leukaemia cells), leukaemic (no healthy cells) and coexisting (both progenitor blood cells and leukaemia cells) steady states, and the immune response incorporated in [290] has the effect of introducing a stable healthy steady state in place of the previously unstable healthy steady state. A phase portrait illustrating this steady state behaviour is included in the supplementary material.

The haematopoietic stem cells in the original model grow logistically to steady state: $\lim_{t \rightarrow \infty} S(t) = \bar{S} = 1 - \delta_S/\rho_S$, independent of the other cell types. As such, in this work we make a simplifying assumption that the haematopoietic stem cell population is held constant at this steady state. Provided that $S(0)$ is of a similar scale to $A(0)$ and $L(0)$, relaxing this assumption does not significantly impact the results. Prior to $S(t)$ reaching steady state, the production of A from S is proportionally reduced, resulting in less competitive pressure exerted on L by A , promoting an increased application of control. This is demonstrated in the supplementary material. We neglect the terminally differentiated cell populations as they do not feed back to the progenitor or leukaemic stem cell populations, and as such will not influence the design of optimal combination therapy based on progenitor and leukaemic stem cell populations.

The chemotherapy control, $u(t)$, is modelled as an additional death term for both progenitor blood cells and leukaemic stem cells. The additional death rate of each type of cell depends on the amount of control applied and the size of the population. The stem cell transplant control, $v(t)$, is modelled as an increase in the progenitor blood cell population, depending only on the amount of control applied. These assumptions reduce Equation (3.2) to Equation (3.3). We consider scaled populations such that $0 \leq A + L \leq 1$ in absence of control, for suitably chosen initial conditions: $A(0) + L(0) < 1$ and $L(0) \lesssim 0.9$.

$$\begin{aligned} \frac{dA(t)}{dt} &= \delta_S \bar{S} + \rho_A A(t)(1 - A(t) - L(t)) - \delta_A A(t) + \underbrace{v(t)}_{\text{stem cell transplant}} - \underbrace{\kappa u(t) A(t)}_{\text{chemotherapy}}, \\ \frac{dL(t)}{dt} &= \rho_L L(t)(1 - A(t) - L(t)) - \delta_L L(t) - \frac{\alpha L(t)}{\gamma + L(t)} - \underbrace{u(t) L(t)}_{\text{chemotherapy}}. \end{aligned} \quad (3.3)$$

The significant heterogeneity of AML development, progression and response to treatment makes identifying realistic individual parameter values challenging; as such the parameter values in Table 3.1 are selected such that the qualitative behaviour we observe from the uncontrolled model is consistent with previous studies [82, 290]. For illustrative purposes we treat the rates presented to be per day, and present solutions over a potentially typical time-scale of days. We note that there is significant uncertainty in the parameter values, and stress that the focus of this work is on the dynamics and interactions of multiple controls, and in particular, how these dynamics change in response to

varying control parameters. We provide additional results in the supplementary material exploring parameter sensitivity.

In the context of applying multiple interventions, particularly when an intervention impacts multiple species, understanding interactions between species and controls is crucial for determining appropriate management strategies. As such, we are particularly interested in the parameter κ , that describes the effectiveness of the chemotherapy in killing progenitor blood cells, relative to leukaemic stem cells; $\kappa < 1$ corresponds to chemotherapy that is more effective at killing leukaemic stem cells than progenitor blood cells, $\kappa = 1$ corresponds to chemotherapy that is equally effective at killing either cell type and $\kappa > 1$ corresponds to chemotherapy that is more effective at killing progenitor blood cells than leukaemic stem cells. This parameter can be adjusted to reflect the clinically observed heterogeneity in response to treatment. A description of the other model parameters and the values used to produce results in this work are presented in Table 3.1. In absence of control, these parameters can give rise to the coexisting steady state. Dynamics of this model, for various initial conditions, and without any control, are presented in Figure 3.1. Solutions in this work are initialised at the coexisting steady state values for A and L unless otherwise specified, however this is not a requirement of the technique. This is a sensible choice as it corresponds to a reasonable treatment scenario, whereby a patient initially has some healthy cells and some leukaemic cells. It also best allows us to investigate interplay between the interspecies interaction and the control dynamics. In the supplementary material we present additional results demonstrating that the optimal controls are relatively insensitive to moderate variation in the initial conditions.

Table 3.1: Parameters

Parameter description	Variable	Value	Dimensions
Haematopoietic stem cell (S) steady state	\bar{S}	0.72	[\cdot]
Proliferation of S	ρ_S	0.5	[T^{-1}]
Proliferation of A	ρ_A	0.43	[T^{-1}]
Proliferation of L	ρ_L	0.27	[T^{-1}]
Differentiation of S into A	δ_S	0.14	[T^{-1}]
Differentiation of A	δ_A	0.44	[T^{-1}]
Differentiation of L	δ_L	0.05	[T^{-1}]
Characteristic rate of the immune response	α	0.015	[T^{-1}]
Half saturation constant of the immune response	γ	0.1	[\cdot]

Parameters correspond to those presented with the original model [82], with immune response parameters introduced in subsequent work [290].

Due to the significant cost and side effects associated with each treatment, we typically define pay-offs that minimise not only the leukaemic burden but also the amount of each control applied. In the remainder of this section we identify and discuss several

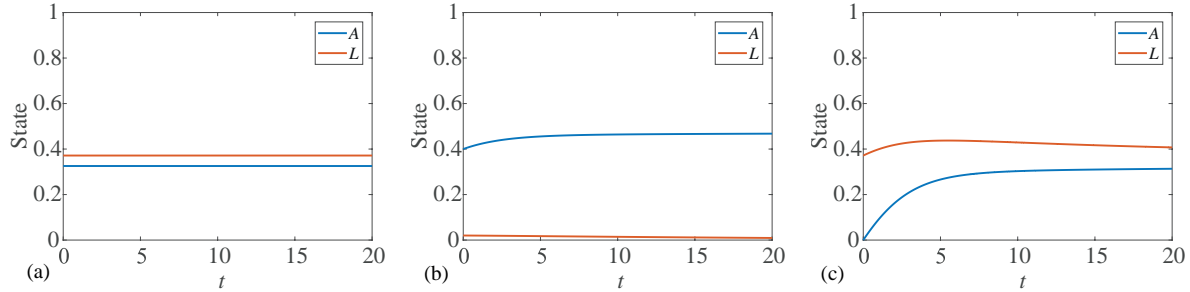


Figure 3.1: Numerical solutions are presented for Equation (3.3) to demonstrate the model dynamics for different initial conditions, in absence of control ($u(t) \equiv v(t) \equiv 0$). Parameter values are given in Table 3.1. Initial conditions in (a) correspond to the coexisting steady state. In (b) we observe that a small leukaemic population is depleted through the immune response and competition with progenitor blood cells. In (c) we observe that a small progenitor blood cell population is replenished from haematopoietic stem cells, such that the model tends toward the coexisting steady state.

reasonable choices of pay-off. We model two controls and explore the dynamics of each possible combination of continuous and bang-bang. This produces four distinct sets of control dynamics. In the supplementary material we present numerical solutions for each combination of control dynamics and investigate the impact of various parameters.

Bang-bang controls require lower and upper bounds on the control variable, and are named as such because the optimal control takes either the lower or upper bound, with finitely many discontinuous switching points throughout the interval. We also apply bounds on the continuous controls. Bounds are used to incorporate practical constraints such as a maximum tolerated dose. In this work, we apply a lower bound of zero to all controls, corresponding to no treatment. The control techniques are general and do not require the lower control bound to be zero. However, this is a practical choice in a treatment context. Unless otherwise specified we choose upper bounds on continuous controls to be arbitrarily large; such that they do not constrain the control dynamics. There is no requirement for any relationship between the upper bounds on the chemotherapy and stem cell transplant controls, u_b and v_b , respectively.

The pay-offs we consider in this work can be expressed in a general form as:

$$J = \int_0^{t_f} (a_1 u(t)^p + a_2 v(t)^q + a_3 L(t)^r) dt, \quad 0 \leq u(t) \leq u_b, \quad 0 \leq v(t) \leq v_b. \quad (3.4)$$

We focus our investigation on the combinations of continuous and bang-bang controls possible with $p \in \{1, 2\}$ and $q \in \{1, 2\}$. Linear control terms in the pay-off, corresponding to $p = 1$ for chemotherapy control and $q = 1$ for stem cell transplant control, produce bang-bang controls. Quadratic control terms in the pay-off, corresponding to $p = 2$ for chemotherapy control and $q = 2$ for stem cell transplant control, produce continuous controls. In each case we also explore the impact of a linear or quadratic leukaemic term

in the pay-off, through choosing $r \in \{1, 2\}$.

Parameters $a_1, a_2, a_3 > 0$ are chosen to weight the relative importance of each contribution to the pay-off. For example, if we want to assign a greater penalty to the chemotherapy control than to the stem cell transplant control and the leukaemia, we increase a_1 relative to a_2 and a_3 . When mixing quadratic and linear control terms care must be exercised when selecting weighting parameters. For the model given by Equation (3.3), with $0 \leq A + L \leq 1$, linear pay-off terms are proportionally more penalising than quadratic terms ($x > x^2$ for $x \in (0, 1)$).

The weighting parameters and exponents in the pay-off do not have a direct clinical interpretation, but rather need to be considered in the context of how optimality is characterised in a clinical setting. For example, the simplest fully linear pay-off, with $p = q = r = 1$ and $a_1 = a_2 = a_3 = 1$, implies that one unit of chemotherapy control imposes the same cost or harm as one unit of stem cell transplant control or one unit of leukaemia. For practical applications, these pay-off weightings and exponents could be estimated through expert opinion of clinicians [120, 219, 245]. The combination of parameters that best characterise optimality may vary between cases, and depend on factors such as the particular controls and their side effects, and how a particular patient is impacted by the leukaemia. Since the aim of this work is to present a general framework rather than a specific application of that framework, we leave these constants unspecified and note that code is provided on [GitHub](#) to facilitate particular applications.

3.3.1 Continuous chemotherapy, continuous stem cell transplant controls

For a continuous chemotherapy control and continuous stem cell transplant control we consider a pay-off that minimises the cumulative amount of leukaemia and the controls, with each term squared. This corresponds to Equation (3.4) with $p = 2$ and $q = 2$.

Results investigating the effect of varying the parameter κ ; the rate that the chemotherapy control depletes progenitor blood cells relative to leukaemic cells, are presented in Figure S1 of the supplementary material. Results exploring the impact of changing the final time are presented in Figure S2 of the supplementary material.

3.3.2 Continuous chemotherapy, bang-bang stem cell transplant controls

A pay-off that minimises the cumulative amount of chemotherapy control squared, with the stem cell transplant control term entering the pay-off linearly, will produce a continuous chemotherapy control with bang-bang stem cell transplant control. This corresponds to Equation (3.4) with $p = 2$ and $q = 1$.

Results investigating greater variations in the parameter κ are presented in Figure S3 of the supplementary material. Upper bounds on the continuous chemotherapy control are considered in Figure S4 of the supplementary material.

3.3.3 Bang-bang chemotherapy, continuous stem cell transplant controls

Bang-bang chemotherapy control with continuous stem cell transplant control arises from the pay-off in Equation (3.4) with $p = 1$ and $q = 2$. Noting that each control impacts the state differently (u reduces both A and L while v increases A only), we can expect this to produce different dynamics to the combination considered in the previous part with $p = 2$ and $q = 1$.

We present results exploring the effect of the final time on the dynamics of the bang-bang chemotherapy control in Figure S5 of the supplementary material. In Figure S6 of the supplementary material we investigate how different upper bounds on the continuous stem cell transplant control impact the dynamics.

3.3.4 Bang-bang chemotherapy, bang-bang stem cell transplant controls

Finally, we investigate the case where both controls enter the pay-off linearly, such that both optimal controls are bang-bang. This corresponds to Equation (3.4) with $p = 1$ and $q = 1$.

In Figure S7 of the supplementary material, we investigate the impact of increasing the upper bound on each of the bang-bang controls, effectively allowing for stronger doses of each treatment to be applied. In Figure S8 of the supplementary material we consider how the parameter κ impacts the dynamics when all controls are bang-bang.

3.4 Results and discussion

In this section we draw insights about the behaviour of the model when subject to interventions, and also more broadly investigate key factors influencing the dynamics of multiple controls. In particular, we focus on the strength of interaction between controls and species, the form and strength of the controls applied, the duration of the treatment interval and the control weighting parameters. Suites of results investigating these aspects are presented in the supplementary material. In the remainder of this section, we highlight key insights.

3.4.1 Optimal strategies respond non-linearly to control parameters

Due in part to the heterogeneity of AML, there is significant uncertainty around how an individual will respond to treatment [100, 176], which is represented by κ in our model. This poses challenges in determining appropriate intervention strategies, as it is unclear how heavily chemotherapy treatment will deplete healthy blood cells. As such, a key aspect of this work is to investigate how the optimal control dynamics change as we vary κ . Varying κ allows us to change the rate that the chemotherapy control depletes progenitor blood cells relative to leukaemic cells. Increasing κ makes chemotherapy more damaging to the progenitor blood cells; intuitively one might expect this to promote a reduced application of chemotherapy control. This occurs under some circumstances, but the dynamics are non-linear due to the interactions between the progenitor blood cells and leukaemic cells. In Figure 3.2 we present results demonstrating that adjusting κ can both increase and decrease the duration of both chemotherapy and stem cell transplant controls, depending on the control weighting parameters. Changing control weighting parameters could be thought of as representing the way that different individuals may be more or less heavily impacted by the (side) effects of leukaemia or the treatments [237]. These results agree with the clinically observed heterogeneity in response to regimented treatment, and highlight a key challenge in managing the interacting populations. Even when the nature of an interaction is known, the optimal intervention strategy can vary significantly with changes to the strength of the relationship, the strength of the treatment and the form of the controls.

The upper bound on a control represents the maximum strength of the treatment, and can be used to enforce a practical constraint such as a maximum tolerated dose. For bang-bang controls with a lower bound of zero, the optimal treatment is to apply the drug at the maximum tolerated dose (over one or many intervals) or not at all. Bounds can also be used to enforce a dosage threshold on continuous optimal controls, while still

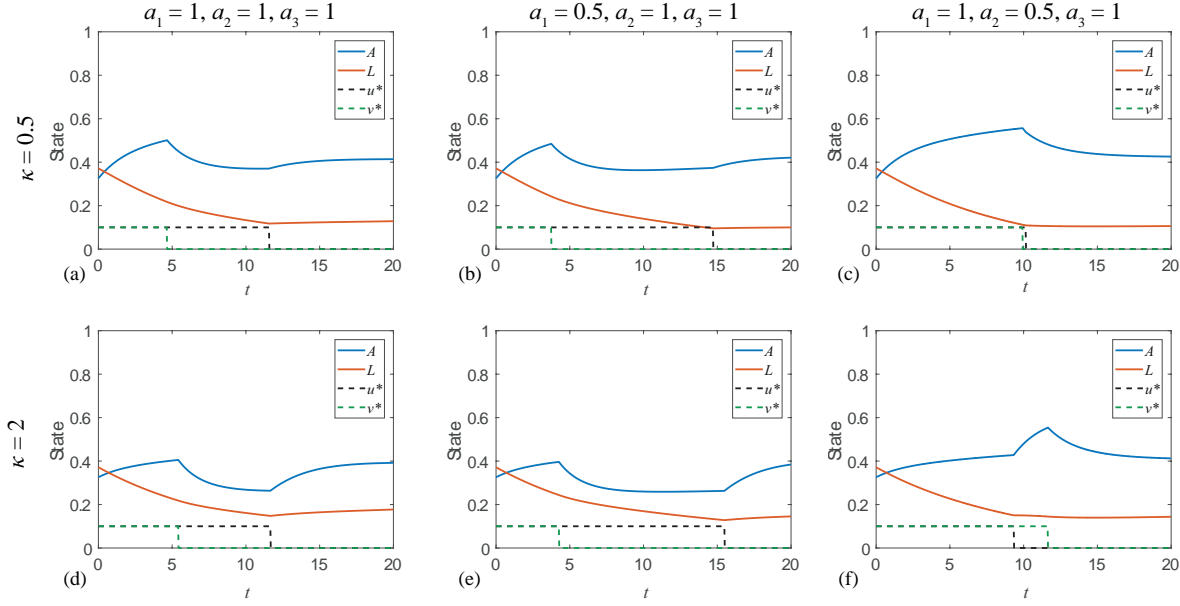


Figure 3.2: The control dynamics respond non-linearly to the parameter κ . Solutions are presented corresponding to the linear pay-off given in Equation (3.4) with $p = 1$, $q = 1$, $r = 1$ and upper control bounds $u_b = v_b = 0.1$. With equal weightings ($a_1 = a_2 = a_3 = 1$), increasing κ from $\kappa = 0.5$ to $\kappa = 2$ extends the duration of the stem cell transplant control and has little effect on the chemotherapy control. With a reduced weight on the chemotherapy control in the pay-off ($a_1 = 0.5$), increasing κ from $\kappa = 0.5$ to $\kappa = 2$ extends the duration of both controls. With a reduced weight on the stem cell transplant control in the pay-off ($a_2 = 0.5$), increasing κ from $\kappa = 0.5$ to $\kappa = 2$ increases the application of the stem cell transplant control and reduces the application of the chemotherapy control.

admitting intermediate doses. In Figure 3.3 we observe that increasing the treatment strength results in a reduced duration of application of both controls. For sufficiently high maximum doses only chemotherapy control is applied. At lower κ , we observe that the maximum doses must be higher before combination therapy is abandoned in favour of solely chemotherapy. This demonstrates that the strength of a treatment can influence whether or not it is applied, indicating a non-linear response of the optimal control strategy to treatment strength.

3.4.2 Interesting optimal strategies can be transient in parameter space

Optimal control dynamics that resemble clinical practice are recovered under particular pay-off weighting parameters. If a stem cell transplant is administered in practice, it typically follows high-dose chemotherapy or radiotherapy to reduce the level of leukaemic cells, suppress the immune system and condition the patient for the introduction and growth of the new blood cells [68, 224]. In Figure 3.4(b) we observe that for particular

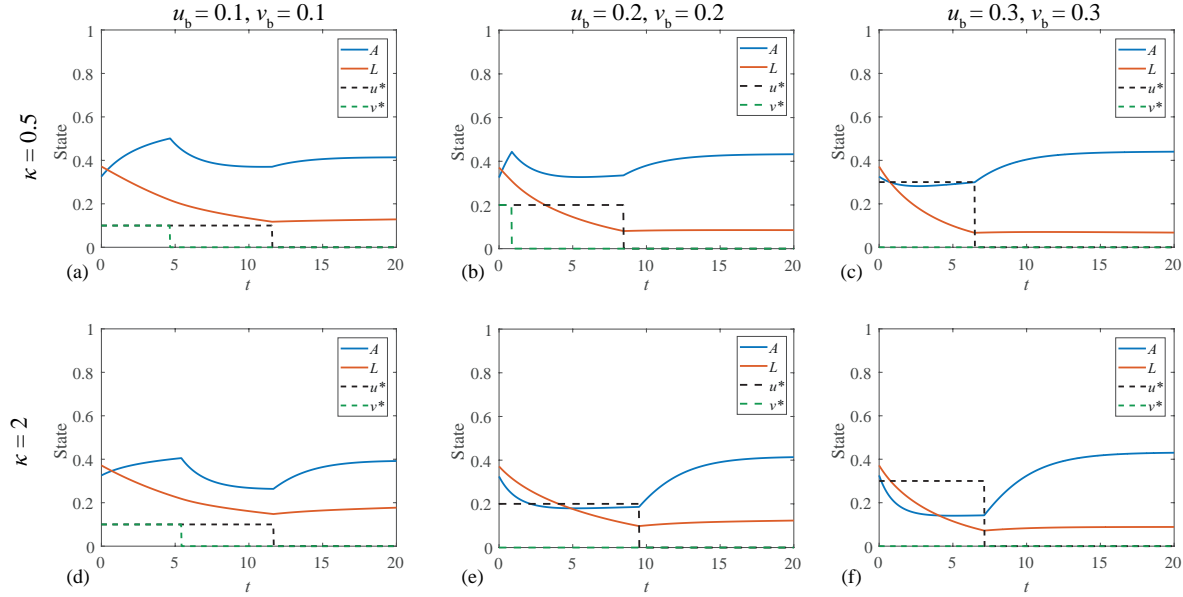


Figure 3.3: Increasing the upper bound of the bang-bang controls can significantly alter the dynamics. Solutions are presented corresponding to the linear pay-off given in Equation 3.4 with $p = 1$, $q = 1$, $r = 1$ and equal pay-off weightings ($a_1 = a_2 = a_3 = 1$). When the chemotherapy control is more effective at killing leukaemia cells than progenitor blood cells ($\kappa = 0.5$), we observe that increasing the upper bound of each control from $u_b = v_b = 0.1$ to $u_b = v_b = 0.2$ results in a reduced duration of application of both controls. Increasing the bounds further to $u_b = v_b = 0.3$ leads to the result in panel (c) where only the chemotherapy control is applied. When the chemotherapy control is more effective at killing progenitor blood cells than leukaemia cells ($\kappa = 2$), the stem cell transplant control is no longer applied after increasing the upper bound of each control from $u_b = v_b = 0.1$ to $u_b = v_b = 0.2$.

pay-off weightings it is possible to recover similar behaviour through optimal control solutions to the model. It is also interesting to note the transience of this result within the pay-off weighting parameter space. In Figure 3.4(a) a small decrease in the weighting on the stem cell transplant control in the pay-off causes the stem cell transplant control to be applied earlier and for longer. Conversely, the small increase in the weighting on the stem cell transplant control demonstrated in Figure 3.4(c) results in no stem cell transplant control being applied at all. However, under these parameters the optimal control results exhibit a significant leukaemia population remaining at final time.

3.4.3 Practical insights

Optimal control results can provide insight into the quality of the underlying model and its assumptions. In this work we consider a simplified stem cell model of acute myeloid leukaemia. In reducing this model, it is assumed that the haematopoietic stem cell population is held constant at its steady state, allowing us to focus on the dynamics of the

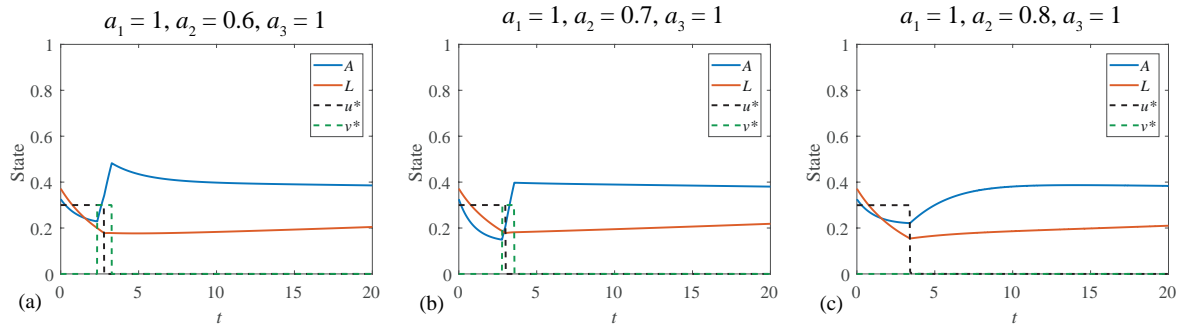


Figure 3.4: Under particular pay-off weightings, we observe that the stem cell transplant control is applied as the chemotherapy treatment is stopped. Solutions are presented corresponding to the pay-off given in Equation 3.4 with $p = 1$, $q = 1$, $r = 2$ and upper control bounds $u_b = v_b = 0.3$.

progenitor blood cells (that are replenished at a constant rate due to the haematopoietic stem cell population) and the leukaemic cells. This assumption is reasonable for a large region of control parameter space, although it is quite restrictive when we are considering control regimes that would significantly deplete the progenitor population, such as where κ and u_b are large. This can be observed in Figure 3.3(e) where the progenitor blood cell population remains almost constant from $t \approx 5$ to $t \approx 10$ despite the chemotherapy control being applied up to $t \approx 10$, due to the constant rate of replenishment of progenitor blood cells. This causes the stem cell transplant control to be devalued in these circumstances, suggesting that the model could be improved by reintroducing the haematopoietic stem cell population, and having it also negatively impacted by the chemotherapy control.

It is clear that the optimal control strategy entirely depends on the form and weighting of the pay-off. The results in the main text and the associated supplementary material demonstrate that these choices can produce fundamentally different optimal control dynamics and outcomes. Selecting an appropriate pay-off form and weighting is therefore a significant and recurring challenge in applied optimal control. An ideal pay-off encodes how each factor is truly valued relative to each other factor, although determining this is often not feasible or requires subjective judgement. Determining appropriate pay-off functions becomes increasingly complicated when dealing with multiple controls; it introduces the need for relative weighting, and in some cases scaling or normalisation of pay-off terms. Control problems in biology typically include non-monetary costs; such as side effects of treatment, which are not easily valued [290, 314]. Even for problems where all elements of a pay-off are readily expressed in monetary terms, there can be challenges associated with economic uncertainty [184].

When determining the form of a control term in the pay-off function it may be tempting to consider how the control can be applied practically. For example, if it is only possible for the control to be active or not active (with no intermediate levels of acti-

vation) using a linear term ensures that the optimal control is bang-bang. Particular care must be taken in employing this approach for a multi-objective pay-off, as a linear term implies a different cost weighting to (for example) a quadratic term, which penalises disproportionately; ($x > x^2$ for $x \in (0, 1)$, $x < x^2$ for $x \in (1, \infty)$). A standard approach in the literature is to consider a practical range of parameter values, often guided by the literature or expert opinion, and examine how sensitive the control strategy is to changes in these parameters [158, 238]. The parameters can also be tuned to produce optimal control strategies that satisfy additional external constraints [30]. An alternative approach feasible for some problems is to construct the simplest possible pay-off (for example, the sole objective of minimising leukaemia), at the cost of requiring a more sophisticated model that explicitly accounts for the negative impacts or costs of the controls.

In some regions of the parameter space, the FBSM fails to converge. Convergence can often be achieved by adjusting the parameter that weights the contribution of the control from previous iteration to the control in the next iteration [290]. However, there are some regions of the parameter space where the control does not converge for any value of this parameter. Interestingly, this non-convergence does not always occur at the extremities of a parameter space. For example, comparing Figure S3(h) with Figure S3(i) of the supplementary material, we show that increasing the rate that the chemotherapy control kills progenitor blood cells relative to leukaemic cells from $\kappa = 1$ to $\kappa = 10$ moves the optimal control solution from a moderate application of both controls, to a solution dominated by stem cell transplant control. For intermediate values, $5.5 \lesssim \kappa \lesssim 7.5$, this control problem does not converge. This may correspond to a region where the optimal control is not bang-bang, but rather is singular. Singular control problems arise when the first order conditions derived from the PMP do not provide sufficient information over an interval to determine the optimal control [55]. Singular controls can sometimes be determined from higher order optimality conditions—for example, conditions involving second order derivatives of the Hamiltonian—although this is non-trivial [110, 124].

3.5 Conclusion

In this work we study the application of multiple optimal controls to a stem cell model of AML. We consider a chemotherapy control that reduces the population of both progenitor blood cells and leukaemic stem cells, and a stem cell transplant control that replenishes progenitor blood cells. To investigate the dynamics arising from different forms of control and interspecies interaction, we generate results corresponding to each of the possible combinations of continuous and bang-bang controls, with pay-off functions containing linear or quadratic leukaemia terms. The dynamics of multiple controls are further explored through varying control parameters, treatment strengths and the rate at which the chemotherapy control depletes progenitor blood cells relative to leukaemic

stem cells.

We determine optimal controls through application of PMP, yielding two-point boundary value problems. Numerical solutions to these problems are generated using an implementation of the forward-backward sweep method. The method readily generalises to solving problems with multiple controls, and we observe only a modest increase in computational resources required beyond a comparable single optimal control problem.

Through investigating how optimal control dynamics change in response to the relative effectiveness of the chemotherapy control, the maximum strength of the controls and other control and weighting parameters we show that the behaviour can be highly non-linear. We observe that interesting and clinically reflective optimal control strategies can be transient, existing only over small regions of control parameter space. We also demonstrate how optimal control results can provide insight into the quality of the underlying model.

Modelling multiple interventions that incur costs naturally increases the complexity involved in determining appropriate pay-off functions. A pragmatic approach is to consider a range of weighting parameters and observe the optimal control dynamics. The sensitivity of these dynamics to the weighting parameters can provide insight into how carefully a pay-off must be chosen. If the optimal control dynamics under a particular set of control parameters do not represent a desirable outcome to the practitioner, then the pay-off function may need to be modified [168].

The primary avenues for extending this work are model refinement and control approach. The model could be extended to incorporating a delay to the impact of the stem cell transplant on the system, either through a delay differential equation, or an additional state equation acting as a reservoir of A cells produced by the stem cell transplant. This is biologically motivated as it can take multiple weeks for the production of blood cells to occur following a transplant [69]. This extension would also facilitate relaxing the assumption of a constant reservoir of haematopoietic stem cells replenishing the stem cell population. The control approach in this work focuses on fixed terminal time problems. Although informative, this can result in optimal control results that are clinically undesirable under some parameter regimes, such as having a significant amount of leukaemia remaining at the terminal time. Alternatively, optimal controls can be determined for problems with free terminal times and fixed final states; for example no leukaemia remaining [191]. The problems explored in this work could be recast as fixed final state problems to determine how significantly this alters the optimal control dynamics.

3.6 Acknowledgements

This work is supported by the Air Force Office of Scientific Research (BAA-AFRL-AFOSR-2016-0007) and the Australian Research Council (DP170100474). Computa-

tional resources were provided by the eResearch Office at QUT. J.A.S gratefully acknowledges support from the Australian Government Research Training Program and the AF Pillow Applied Mathematics Trust. We thank the three referees for their helpful comments and suggestions.

Chapter 4

Implementation and acceleration of optimal control in systems biology

Statement of Contribution of Co-Authors

The authors listed below have certified that:

1. they meet the criteria for authorship and that they have participated in the conception, execution, or interpretation, of at least that part of the publication in their field of expertise;
2. they take public responsibility for their part of the publication, except for the responsible author who accepts overall responsibility for the publication;
3. there are no other authors of the publication according to these criteria;
4. potential conflicts of interest have been disclosed to (a) granting bodies, (b) the editor or publisher of journals or other publications, and (c) the head of the responsible academic unit, and
5. they agree to the use of the publication in the student's thesis and its publication on the [QUT's ePrints site](#) consistent with any limitations set by publisher requirements.

In the case of this chapter: Chapter 4

Please state the publication title and date of publication or status:

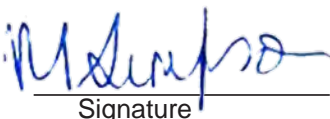
Implementation and acceleration of optimal control for systems biology. Published 2021 in Journal of the Royal Society Interface.

Contributor	Statement of contribution*
Jesse A Sharp 	Designed the study developed and implemented the computational algorithms, generated and interpreted results, produced figures, drafted the manuscript, revised the manuscript.
08/12/2021	
K Burrage	Designed the study, supervised the research, interpreted the results, and provided comments on the manuscript.
MJ Simpson	Designed the study, supervised the research, interpreted the results, and provided comments on the manuscript.

Principal Supervisor Confirmation

I have sighted email or other correspondence from all Co-authors confirming their certifying authorship. (If the Co-authors are not able to sign the form please forward their email or other correspondence confirming the certifying authorship to the GRC).

Professor Matthew Simpson
Name


Signature

11/12/2021
Date

Article published 2021 in Journal of the Royal Society Interface.

Sharp JA, Burrage K, Simpson MJ (2021). Implementation and acceleration of optimal control for systems biology. *Journal of the Royal Society Interface*.
[doi:10.1098/rsif.2021.0241](https://doi.org/10.1098/rsif.2021.0241).

Abstract

Optimal control theory provides insight into complex resource allocation decisions. The forward-backward sweep method (FBSM) is an iterative technique commonly implemented to solve two-point boundary value problems (TPBVPs) arising from the application of Pontryagin's Maximum Principle (PMP) in optimal control. The FBSM is popular in systems biology as it scales well with system size and is straightforward to implement. In this review we discuss the PMP approach to optimal control and the implementation of the FBSM. By conceptualising the FBSM as a fixed point iteration process, we leverage and adapt existing acceleration techniques to improve its rate of convergence. We show that convergence improvement is attainable without prohibitively costly tuning of the acceleration techniques. Further, we demonstrate that these methods can induce convergence where the underlying FBSM fails to converge. All code used in this work to implement the FBSM and acceleration techniques is available on [GitHub](#).

4.1 Introduction

Across the life sciences, we encounter systems over which we wish to exert control. Whether we consider outbreak control in epidemiology [1, 238], chemotherapy in oncology [25, 59, 290], muscle contraction and gait regulation in biomechanics [103, 181, 254], engineering cellular processes in synthetic biology [87, 139], cell population growth in tissue engineering [78, 294], or biodiversity and invasive species management in ecology [31, 61, 72], we face decisions around how a particular intervention should be applied to best achieve desired outcomes. Using mathematical models of such systems, optimal control theory provides insight into these resource allocation decisions.

Optimal control is a science of trade-offs; between competing objectives, or in weighing up the benefits of control measures against their costs. We illustrate some key concepts of optimal control in Figure 4.1. Suppose that without intervention, a crop yield will double, from x_0 to $2x_0$, between now and harvest time. We might consider applying a control, such as fertiliser, to increase the growth rate of the crop; thereby increasing the yield at harvest to $3x_0$. Of course, applying fertiliser comes at a cost, and this must be considered against the increase in crop yield. As such, it is not immediately apparent how much fertiliser should be applied, and over what time period. This depends entirely on our characterisation of optimality; the *pay-off*. Depending on the pay-off, the optimal control may be continuous; whereby the strength can be readily and continuously adjusted throughout time, or bang-bang (discontinuous); whereby the control is applied at either a lower or upper bound with finitely many discrete switches between the two. The pay-off determines the objective(s) of control; which in our stylised example may be to maximise profits after cost of fertilising is considered, or achieve a specific yield, for example $3x_0$, using the minimum amount of fertiliser.

Much of modern day optimal control theory stems from the seminal works of Pontryagin; through the Pontryagin Maximum Principle (PMP) [264], and Bellman; through the advent of dynamic programming and the Hamilton-Jacobi-Bellman equation [37], in the 1950s and 1960s. These foundations of optimal control are built upon centuries of development in the calculus of variations [125]. For brief but broad expositions of the theoretical roots of optimal control and developments following these seminal works, we direct the reader to articles such as [56, 284].

Often we are unable to solve optimal control problems analytically, so we pursue computational approaches. Broadly, the numerical methods for optimal control can be classed as either indirect or direct methods; for indirect methods optimality conditions are derived in the calculus of variations fashion via the PMP, leading to a two-point boundary value problem (TPBVP), while for direct methods the control problem is discretised and reformulated as a nonlinear programming problem [275]. For an early history of numerical methods in optimal control, including gradient and conjugate gradient methods,

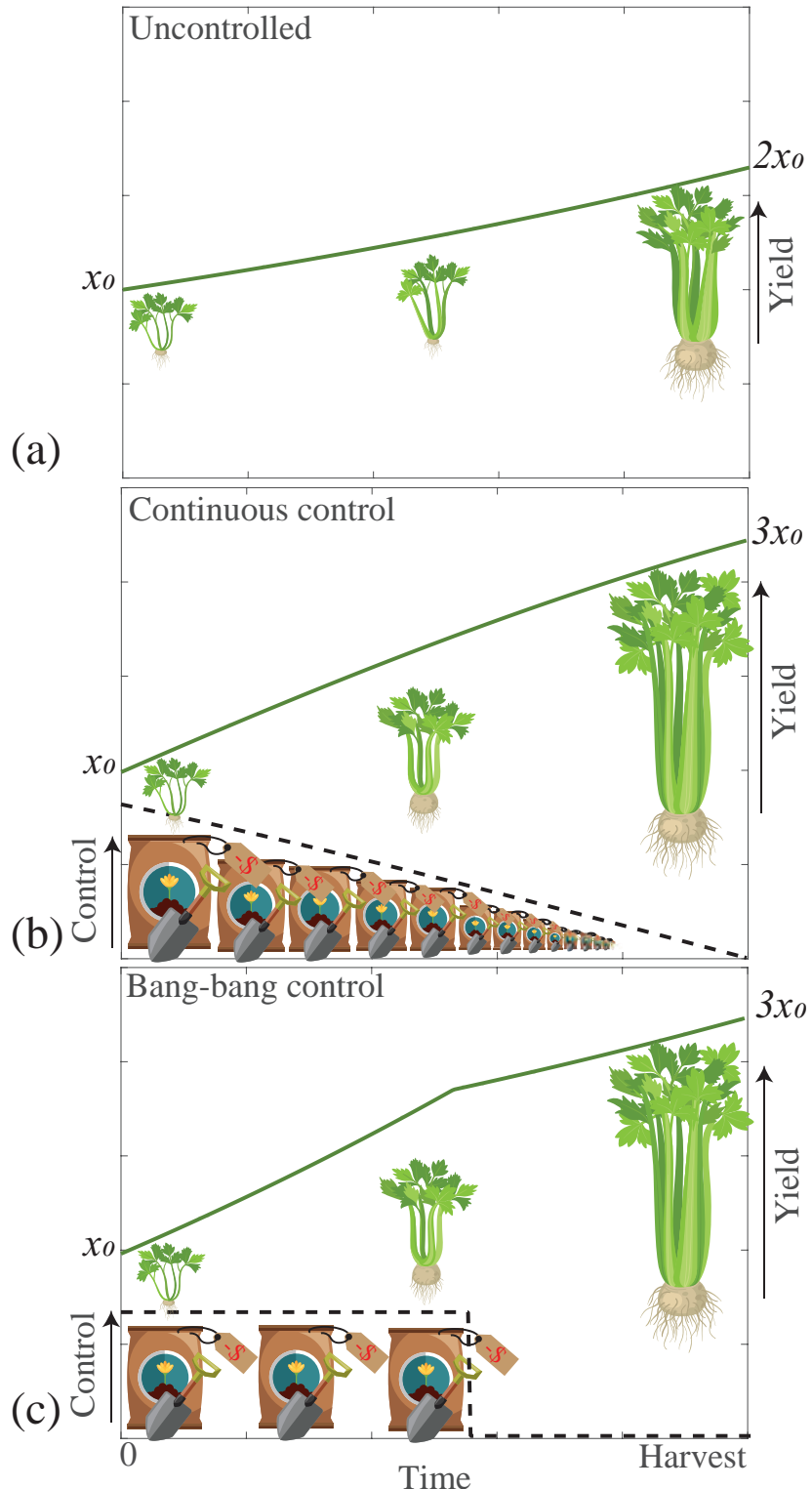


Figure 4.1: A pictorial example of optimal control for a growing crop. Suppose that initially, the crop yield is x_0 . We want to grow this crop to increase the yield, represented by the green line, come harvest time. Actions taken to increase the growth rate of the crop; such as applying fertiliser, are the controls, represented in black dash. Scenarios are presented for (a) no control, (b) continuous control, and (c) bang-bang control. Optimal control theory helps us determine how best to apply these controls. Illustrations adapted from ilyakalinin/iStock/Getty Images, johavel/iStock/Getty Images.

Newton-Raphson methods, quasilinearisation, feasible direction algorithms and feedback solutions we suggest [262]. Surveys [275, 284] give an excellent overview of more recent developments in relevant numerical methods, including the forward-backward sweep method (FBSM), multiple-shooting methods, control parameterisation, collocation and pseudospectral methods and complete discretisation into finite-dimensional nonlinear programming problems.

Optimal control methodology and numerical solution techniques are continually being developed and improved. The growing popularity of artificial intelligence, machine learning and related disciplines has precipitated significant advances in computational techniques for handling large-scale systems with many variables, and related infinite-dimensional optimisation problems. Nonlinear approximators, including neural networks, can be used to reduce infinite-dimensional optimisation problems to finite-dimensional nonlinear programming problems. This approach is presented in [348], alongside other techniques that arise through unifying aspects of decision science, dynamic optimisation, statistical and deterministic machine learning, nonlinear approximation theory and other fields. One example of control paired with machine learning arises in autonomous vehicles, where machine learning techniques can accelerate obtaining approximately optimal controls where computational power on-board is limited and controls satisfying strict safety constraints must be obtained rapidly [148]. Reinforcement learning, a technique from artificial intelligence resembling a model-free analogue of dynamic programming, has shown promising simulation results for the control of multi-species microbial communities in bioreactors [317].

Formulation and approximate solutions of fractional optimal control problems (FOCP); optimal control of systems involving fractional derivatives, has also garnered wide interest recently within the control, numerical methods and applied mathematics communities. This has resulted in the development of new numerical approaches such as the non-standard two-step Lagrange interpolation method [46, 309]; and amalgamations of new and existing techniques, such as pairing predictor-corrector methods for solving fractional differential equations with the FBSM for optimal control [153, 154]. Applications involving FOCPs arise in areas of systems biology including epidemiology, where the incorporation of memory effects through fractional time derivatives may better describe disease transmission, by modelling the capacity for the population to learn from past outbreaks [46, 311]; and in cancer therapy for determining optimal chemotherapeutic and immunotherapeutic treatment regimens [136, 310].

The field of optimal control has historically focused on determining optimal interventions to apply to systems to meet specified objectives. More recently, however, optimal control techniques have been applied in a systems biology context to further our understanding of the underlying mechanisms or processes involved in a given system; for example via inverse optimal control, whereby exhibited behaviour observed in a system

is used to elicit the underlying optimality principles that may guide the system [318]. Optimality principles have been employed to investigate mechanisms in metabolism; for example in [251], where optimal control techniques provide rationalisation for experimentally and numerically observed sequential activation of metabolic pathways; in [319] where optimal control techniques predict enzyme activation times and metabolite concentrations; and in other work reviewed in [101], where further insights are gained regarding metabolic pathway activation and regulation. Optimal control has also provided insight into the emergence of persister cells in the presence of environmental volatility [51].

The FBSM is an iterative method for solving the TPBVPs that arise from the indirect PMP approach to optimal control. In systems biology the FBSM for optimal control is very popular, owing particularly to its straightforward scalability to large systems, and to its moderate computational cost and mathematical complexity [191]. In this work we review the implementation of the FBSM to solve optimal control problems, and investigate means of accelerating the convergence. To contextualise our discussion of the FBSM, we first consider the more familiar technique of successive over-relaxation (SOR). SOR is a generalisation of the Gauss-Seidel method, and is widely applied in numerical linear algebra to accelerate convergence when solving linear systems iteratively [322]. Essentially, the process of SOR involves specifying an acceleration or relaxation parameter, $\beta \in (0, 2)$; a weighting factor that serves to reduce the spectral radius of the iterative matrix operator [279]. The error and rate of convergence of SOR is sensitive to this (problem dependent) choice of β , prompting investigation into theoretical convergence results and methods of determining β [73, 175, 279]. Despite challenges in identifying the optimal β , the SOR has historically been widely applied and studied in the literature due to the ease with which it can be implemented, and the rapid convergence it can deliver; even without identifying the optimal β [131, 341].

This narrative closely parallels that of the FBSM in optimal control, where a weighting factor ω can be applied when updating the control between iterations to aid convergence. The optimal choice of ω is problem dependent, and significantly impacts the rate of convergence, or whether the FBSM converges at all. Nonetheless, the FBSM is frequently used in applied optimal control work as it is relatively straight-forward to implement, and can still converge in absence of the optimal ω . Theoretical convergence results of the FBSM are available in the literature [130, 225], although the focus is on the FBSM without weighted updating, with no consideration for choosing ω . Using regularisation techniques, the FBSM is modified in [194] to improve convergence properties for large systems in a continuous setting, with a view to training deep neural networks in machine learning. These convergence results have recently been extended to the numerically discretised setting through symplectic Runge-Kutta discretisation; taking advantage of the variational structure of optimal control problems [203]. The authors also demonstrate that the rate of convergence of the regularised FBSM with symplectic discretisation can

be improved with Anderson acceleration, an iterative acceleration technique. Although promising, this regularisation introduces a regularisation parameter, ρ . Similar to ω , the choice of ρ impacts convergence, and its choice is problem dependent. Understanding and implementing the regularisation and symplectic techniques is not trivial, and introduces conceptual complexity beyond what is necessary for many applied optimal control problems. As such, the standard FBSM remains an attractive choice for practitioners.

To this end, we aim to review acceleration techniques that can be paired with the standard FBSM. We implement such techniques alongside the FBSM with the goals of: (1) increasing the rate and frequency of convergence, and (2) reducing the importance of, and challenges associated with, selecting ω . A graphical overview of the optimal control process we employ in this work, including the incorporation of acceleration methods, is presented in Figure 4.2. We note that all code used to implement the algorithms presented in this review; the FBSM and the Wegstein, Aitken-Steffensen and Anderson acceleration methods, is available on [GitHub](#).

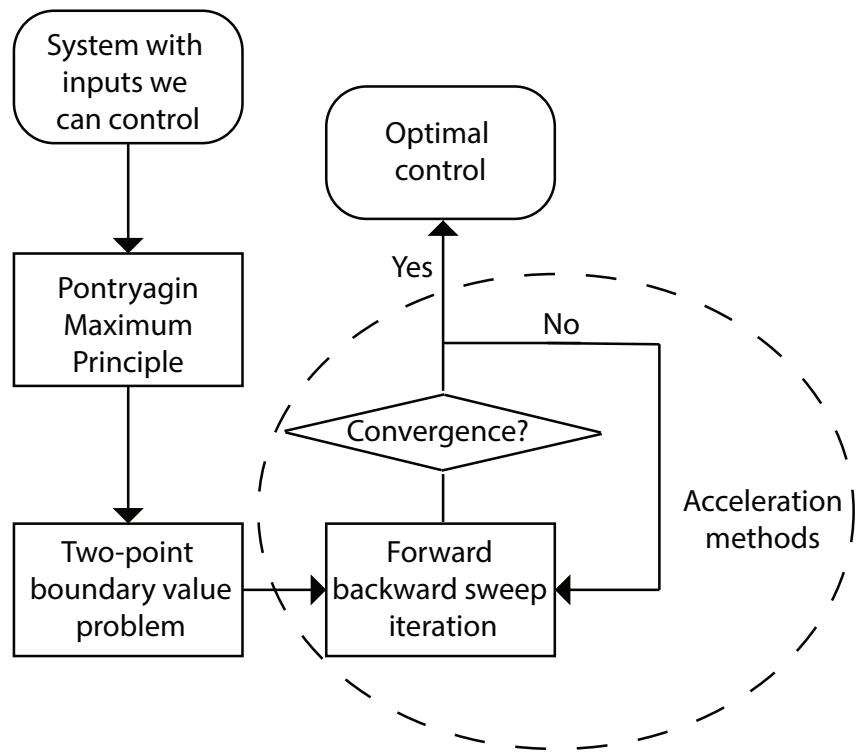


Figure 4.2: The process of optimal control via the Pontryagin Maximum Principle approach, with the incorporation of acceleration methods.

Throughout this work we consider optimal control in the systems biology context. However, we note that optimal control is relevant to a wide variety of fields including chemical engineering [204], aeronautics and astronautics [275], management science and economics [289]. The FBSM, and by extension, the acceleration techniques we consider in this work, can be readily applied in any of these areas.

In §4.2 we review the PMP approach to optimal control, and the implementation of the

FBSM. We provide a single-variable linear model, and a multi-variable nonlinear model in §4.3; and pose and solve example continuous, bang-bang (discontinuous), and fixed endpoint control problems. We review potential iterative acceleration methods in §4.4, and present the results of selected techniques in §4.5. We discuss the performance of these techniques in §4.6, and identify opportunities for application and further investigation.

4.2 Forward-backward sweep method

In an optimal control problem with one state variable, $x(t)$, one control, $u(t)$, over a fixed time interval, $t \in [t_0, t_N]$; such as the crop growth example presented in Figure 4.1, we seek the optimal control $u^*(t)$ that minimises or maximises a specified pay-off function, J , subject to the dynamics of the state. In this section we briefly review the Pontryagin Maximum Principle approach to such an optimal control problem, and the standard implementation of the FBSM for solving the resulting two-point boundary value problem. The FBSM is readily extended to problems with multiple state variables, multiple controls, state constraints and free end-times [191, 225, 290, 291], however for this overview we restrict ourselves to the single variable, single control, fixed end-time case for clarity.

The pay-off typically comprises a cost function $\mathcal{L}(t, x(t), u(t))$ integrated over the time interval, and/or a function, ϕ , of the state at final time: $\phi(x(t_N))$. As such, we seek to minimise or maximise J , subject to

$$J = \phi(x(t_N)) + \int_{t_0}^{t_N} \mathcal{L}(t, x(t), u(t)) dt. \quad (4.1)$$

$$\frac{dx}{dt} = f(x(t), u(t), t), \quad x(t_0) = x_0. \quad (4.2)$$

By the PMP, we construct the Hamiltonian; $H(t, x(t), u(t), \lambda(t)) = \mathcal{L}(t, x(t), u(t)) + \lambda(t)f(x(t), u(t), t)$, where $\lambda(t)$ is the co-state variable linking our state to our pay-off. The necessary conditions for optimal control are obtained from the Hamiltonian:

1. The optimal control, $u^*(t)$, is obtained by minimising the Hamiltonian,

$$\frac{\partial H}{\partial u} = 0. \quad (4.3)$$

2. The co-state is found by setting,

$$\frac{d\lambda}{dt} = -\frac{\partial H}{\partial x},$$

3. satisfying the transversality condition,

$$\lambda(t_N) = \lambda_N = \left. \frac{\partial \phi}{\partial x} \right|_{t=t_N}. \quad (4.4)$$

Following these steps yields a TPBVP to solve for $x(t)$, $\lambda(t)$, subject to $x(t_0) = x_0$, and $\lambda(t_N) = \lambda_N$. To solve this numerically, we discretise t into $N + 1$ time points separated by a step-size $dt = (t_N - t_0)/N$; $\mathbf{t} = [t_0, t_0 + dt, \dots, t_0 + Ndt] = [t_0, t_1, \dots, t_N]$. Here, we consider a uniform discretisation in time; although this is not strictly necessary, as discussed in §4.3. Using superscripts to denote the iteration number, provide an initial guess of the control at each t ; $\mathbf{u}^{(0)} = [u_0^{(0)}, u_1^{(0)}, \dots, u_N^{(0)}]$. From $\mathbf{u}^{(0)}$, solve Equation (4.2) numerically from t_0 to t_N to obtain $\mathbf{x}^{(0)} = [x_0^{(0)}, x_1^{(0)}, \dots, x_N^{(0)}]$. Now, using $\mathbf{x}^{(0)}$, solve for $\boldsymbol{\lambda}^{(0)} = [\lambda_0^{(0)}, \lambda_1^{(0)}, \dots, \lambda_N^{(0)}]$ backwards in time from t_N to t_0 , starting from λ_N . With the optimality condition from Equation (4.3), generate a temporary update for the control, $\hat{\mathbf{u}}^{(1)}$. The next iteration begins with an updated guess for the control, $\mathbf{u}^{(1)}$. These steps are repeated until a convergence condition is satisfied. The algorithm for the FBSM is summarised in §1 of the supplementary material.

In some instances, directly updating the control, such that

$$\mathbf{u}^{(k)} = \hat{\mathbf{u}}^{(k)}, \quad k = 1, 2, \dots \quad (4.5)$$

is sufficient, however more commonly a weighted update is performed [191, 290], such that in the $(k + 1)$ th iteration,

$$\mathbf{u}^{(k+1)} = \omega \mathbf{u}^{(k)} + (1 - \omega) \hat{\mathbf{u}}^{(k+1)}, \quad k = 1, 2, \dots, \quad \omega \in [0, 1]. \quad (4.6)$$

This weighted updating is also referred to as applying a relaxation factor, similar to SOR as discussed in §4.1. An appropriate choice of ω in Equation (4.6) can accelerate convergence relative to Equation (4.5), or in some cases induce convergence where Equation (4.5) leads to divergence. The weighting parameter, ω , can be held constant between iterations, although faster convergence may be achieved by updating ω . For example, by reducing ω as the system approaches convergence, a greater portion of the updated control is maintained relative to the control from the previous iteration [191], possibly accelerating convergence. A challenge commonly faced in implementing this control updating scheme is that the best choice for ω is problem dependent, and often is determined heuristically in practice. We address the extent to which the proposed acceleration algorithms address this issue in §4.4.

To facilitate the following discussion regarding acceleration, we note that the FBSM can be thought of as a generalised fixed point iteration [225], where each iteration com-

prises a forward and backward sweep and a control update. As such, for a control problem with one control, discretised into $N + 1$ time points, each iteration of the FBSM can be thought of as the application of a nonlinear operator, \mathcal{F} , of dimension $N + 1$, such that $\mathbf{u}^{(k+1)} = \mathcal{F}(\mathbf{u}^{(k)})$, or:

$$\begin{bmatrix} u_0^{(k+1)} \\ u_1^{(k+1)} \\ \vdots \\ u_N^{(k+1)} \end{bmatrix} = \begin{bmatrix} f_0(u_0^{(k)}, u_1^{(k)}, \dots, u_N^{(k)}) \\ f_1(u_0^{(k)}, u_1^{(k)}, \dots, u_N^{(k)}) \\ \vdots \\ f_N(u_0^{(k)}, u_1^{(k)}, \dots, u_N^{(k)}) \end{bmatrix},$$

where $\mathcal{F} = (f_0, f_1 \dots f_N)^T$. However, in general we are not able to write down an explicit expression for \mathcal{F} . Viewing the FBSM as a fixed point iteration process informs the choice of acceleration methods discussed in §4.4.

Importantly, we use the term *function evaluation* in this work to refer to the process of solving the system of ODEs for the state forward in time and the system of ODEs for the co-state backwards in time, once. This aligns with a single iteration of the standard FBSM. The function evaluation nomenclature becomes convenient when discussing the FBSM in the context of acceleration algorithms, that typically focus on reducing the number of times expensive functions are evaluated. Producing numerical solutions to the ODE systems is by far the most computationally expensive component of the FBSM. This computational expense increases with the size and complexity of the systems; reducing the number of times these systems must be solved becomes more advantageous as the size and complexity of the systems increases. The function evaluation description also facilitates comparison between acceleration methods that require solving the ODE systems a different number of times per iteration. Throughout this work, we use \mathcal{N} to denote the total number of function evaluations a given method takes to achieve convergence.

4.2.1 Adapted forward-backward sweep method

The FBSM can be extended to handle problems where we aim not only to minimise or maximise a given quantity over time, but also ensure that a specific state is reached at final time. This aligns with the crop growth example from Figure 4.1 if the objective is to achieve a specific yield of $3x_0$ at harvest, rather than to maximise yield. In this case we may have an integral term in the pay-off as described in Equation (4.1), however the function of the final state, $\phi(x(t_N))$, is redundant in a control problem with a prescribed final state. Equation (4.2) is also modified to incorporate the additional constraint:

$$J = \int_{t_0}^{t_N} \mathcal{L}(t, x(t), u(t)) dt, \quad \text{subject to,}$$

$$\frac{dx}{dt} = f(x(t), u(t), t), \quad x(t_0) = x_0, \quad x(t_N) = x_N. \quad (4.7)$$

Here, x_N is the specified state that must be reached at final time. Since we have introduced an additional boundary value to the system, we no longer obtain the transversality condition from Equation (4.4). Instead, we seek the final time condition on the co-state, λ_N , and associated optimal control that satisfies Equation (4.7). We proceed by considering an adapted FBSM that takes as an input a guess for this final time condition, $\hat{\lambda}_N$, and solves the corresponding control problem. If we denote this application of the FBSM as the function $V(\hat{\lambda}_N)$, and the corresponding final value of the state, \hat{x}_N , then the adapted FBSM is an iterative process that solves for the root of $V(\hat{\lambda}_N)$; the value of $\hat{\lambda}_N$ for which $x_N - \hat{x}_N = 0$. This outer iterative process can be solved using standard techniques such as the bisection method or secant method; the former converging more reliably provided that the initial guesses for $\hat{\lambda}_N$ form an interval that brackets the root, the latter converging in fewer iterations [191]. Each of these outer iterations necessitates solving a boundary value problem to convergence, often involving numerous iterations of the FBSM. In this work we apply the secant algorithm as presented in [191] without modification, for the adapted FBSM. The acceleration techniques described in §4.4 are applied only to the inner FBSM processes, reducing \mathcal{N} for each internal FBSM problem, leaving the outer secant iterations unchanged. Using $\mathcal{N}^{(k)}$ to denote the number of function evaluations in the k th internal FBSM problem, we can express the cumulative function evaluations required for convergence of the adapted FBSM as Σ , such that $\Sigma = \mathcal{N}^{(1)} + \mathcal{N}^{(2)} + \dots$.

The adapted FBSM can also be used to solve control problems with isoperimetric constraints; integral constraints of the form

$$\int_{t_0}^{t_N} h(t, x(t), u(t)) dt = K,$$

where K is a prescribed constant. For example, if $h(t, x(t), u(t)) = u(t)$, then K represents a specific and known amount of control that must be applied. The approach to solve problems with isoperimetric constraints, as outlined in [191], is to introduce an additional state variable, z , with

$$\frac{dz}{dt} = h(t, x(t), u(t)), \quad z(t_0) = 0, \quad z(t_N) = K.$$

This transforms the problem with an isoperimetric constraint into a problem with a fixed endpoint, that can be solved using the adapted FBSM as described.

4.3 Control problems

To investigate the robustness and effectiveness of the iterative acceleration techniques that we will discuss in §4.4, we consider two distinct systems, and for each system we study three example control problems. The first system is a single species linear differential equation subject to a control. We later demonstrate that under certain conditions we are able to obtain exact solutions for control problems applied to this model. The second system is a three species model for acute myeloid leukaemia (AML) governed by a coupled nonlinear system of differential equations, subject to a control. We construct the linear model to examine the behaviour of the acceleration techniques as applied to a simple idealised set of control problems. We include the AML model, variations upon which have been considered in the literature [82, 290, 291], to examine how the acceleration techniques perform when applied to problems more reflective of those considered in applied optimal control. For each model, we consider three distinct control problems; continuous control, bang-bang control and continuous control with fixed endpoint.

For all control results presented in this work, convergence is deemed to be achieved when the error, ε , measured as the Euclidean norm of the difference between subsequent controls, falls below a tolerance of 1×10^{-10} . Numerical solutions to ODEs are obtained using a fourth-order Runge-Kutta method [269] with constant time-stepping. A uniform time discretisation is sufficient for all control problems considered in this work. However, the FBSM and acceleration methods readily generalise to a non-uniform discretisation. If the desired discretisation for the state equations differs from that of the co-state equations, it is necessary to perform interpolation within each iteration of the FBSM to obtain values at corresponding time points. This can be computationally expensive and introduce an additional source of error. Where the desired discretisations for the state and co-state differ, numerical schemes with internal interpolation such as Continuous Runge-Kutta methods may be appropriate [36, 346].

4.3.1 Single-variable linear model

The linear model is a single species model for the growth of $x(t)$, subject to control $u(t)$ that increases the growth rate. This model could represent our stylised crop growth example presented in §4.1. We suppress the explicit time dependence of the state and co-state variables and the control in the following equations for notational convenience. For numerical results, we solve the linear problems on the domain $0 \leq t \leq 1$, with time-step $dt = 3.91 \times 10^{-3}$, giving $N = 257$ time points.

$$\frac{dx(t)}{dt} = \gamma x(t) + u(t), \quad x(0) = x_0, \quad \gamma > 0, \quad 0 \leq t \leq 1. \quad (4.8)$$

In absence of control, $u(t) \equiv 0$, this model admits the solution $x(t) = x_0 \exp(\gamma t)$, describing exponential growth.

Continuous control

We seek to maximise a quadratic cost function J , subject to

$$J = \int_0^1 (ax^2 - bu^2) dt, \quad a > 0, b > 0. \quad (4.9)$$

Following the standard Pontryagin Maximum Principle approach for solving optimal control problems, we form the Hamiltonian and derive the co-state equation, transversality condition and optimality condition. The Hamiltonian is given by

$$H = ax^2 - bu^2 + \lambda(\gamma x + u). \quad (4.10)$$

The co-state equation is

$$\frac{d\lambda}{dt} = -\frac{\partial H}{\partial x} = -2ax - \lambda\gamma, \quad (4.11)$$

with transversality condition $\lambda(1) = 0$. In this case the optimality condition is

$$\frac{\partial H}{\partial u} = \lambda - 2bu = 0,$$

such that the optimal control is given by

$$u^*(t) = \frac{\lambda(t)}{2b}. \quad (4.12)$$

For model parameter $\gamma = 0.5$ and pay-off weightings $a = b = 1$, with initial condition $x_0 = 1$, we are able to solve the control problem analytically using standard techniques for linear systems with complex eigenvalues [160]. The process is laborious so we present the approach and analytical solution in §2 of the supplementary material. In the supplementary material we also plot the analytical results against the numerical results to demonstrate the excellent agreement. The numerical solution to the linear continuous control problem is presented in Figure 4.3. Convergence via the FBSM requires $\mathcal{N} = 57$ iterations.

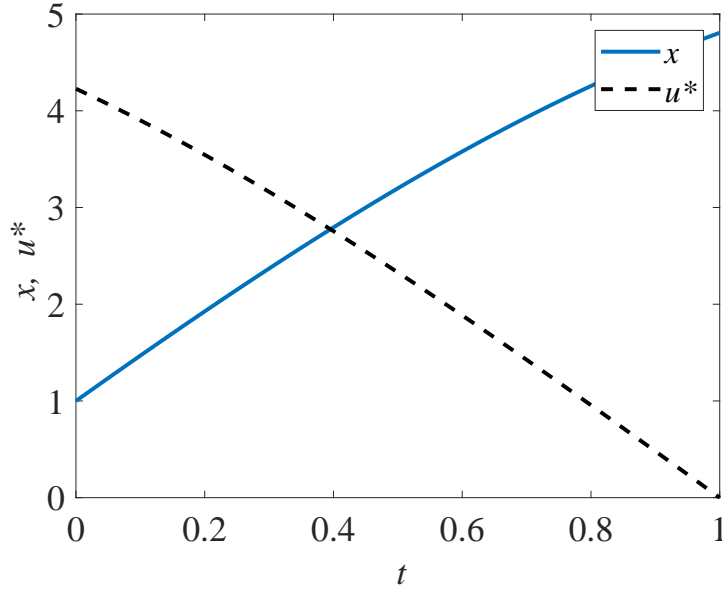


Figure 4.3: Solution to the linear continuous control problem. The optimal control, $u^*(t)$, is shown in black dash and the corresponding state, $x(t)$, in blue. This solution is produced with model parameter $\gamma = 0.5$, time-step $dt = 3.91 \times 10^{-3}$, over the interval $0 \leq t \leq 1$. The contributions of the state and the control to the pay-off are equally weighted, with $a = b = 1$.

Bang-bang control

For the bang-bang control we consider the same state equation as in Equation (4.8), and incorporate bounds on the control.

$$\frac{dx(t)}{dt} = \gamma x(t) + u(t), \quad x(0) = x_0, \quad \gamma > 0, \quad 0 \leq t \leq 1, \quad 0 \leq u(t) \leq 2.$$

We seek to maximise a cost function J that is linear in u ,

$$J = \int_0^1 (ax^2 - bu) dt, \quad a > 0, b > 0.$$

We form the Hamiltonian and derive the co-state equation and transversality condition:

$$H = ax^2 - bu + \lambda(\gamma x + u).$$

The co-state equation is

$$\frac{d\lambda}{dt} = -\frac{\partial H}{\partial x} = -2ax - \lambda\gamma,$$

with transversality condition $\lambda(1) = 0$.

In seeking the optimality condition we find

$$\frac{\partial H}{\partial u} = \lambda - b. \quad (4.13)$$

As Equation (4.13) does not depend on u , we define a switching function

$$\psi(t) = \lambda - b,$$

and produce an expression for the control, based on the bounds on u and the sign of the switching function:

$$u^*(t) = \begin{cases} 0, & \psi(t) < 0, \\ 2, & \psi(t) > 0. \end{cases} \quad (4.14)$$

If $\psi(t)$ is zero over any finite interval excluding isolated points, the optimal control is singular rather than bang-bang. Over such intervals, minimisation of the Hamiltonian does not provide sufficient information to determine the optimal control, and further conditions must be considered. [55, 191]. We restrict our focus in this work to non-singular bang-bang optimal control problems. The numerical solution to the linear bang-bang control problem is presented in Figure 4.4. Convergence to this solution via the FBSM required $\mathcal{N} = 8$ iterations.

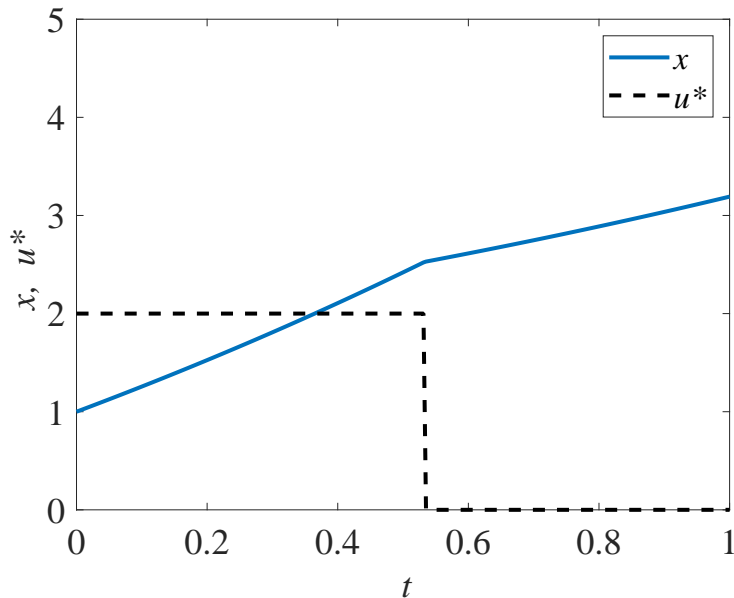


Figure 4.4: Solution to the linear bang-bang control problem. The optimal control, $u^*(t)$, is shown in black dash and the corresponding state, $x(t)$, in blue. This solution is produced with model parameter $\gamma = 0.5$, time-step $dt = 3.91 \times 10^{-3}$, over the interval $0 \leq t \leq 1$, with pay-off weightings of $a = 1$ for the state, and $b = 3$ for the control. The bang-bang control has prescribed bounds of $0 \leq u^*(t) \leq 2$.

Continuous control with fixed endpoint

For the fixed endpoint problem, we proceed with the same state equation, however we now impose a terminal condition on x .

$$\frac{dx(t)}{dt} = \gamma x(t) + u(t), \quad x(0) = x_0, \quad x(1) = 10, \quad \gamma > 0, \quad 0 \leq t \leq 1.$$

We seek to maximise the same quadratic cost function J , as considered in Equation (4.9). As such, we form the same Hamiltonian given in Equation (4.10) and derive the same co-state, Equation (4.11), and expression for the control, Equation (4.12). Note however that we do not prescribe a final time condition on the co-state equation via the transversality condition; as the system already has two boundary conditions, doing so would cause it to be overdetermined. Instead, we make two guesses for $\lambda(1)$; for example, $\lambda^{(0)}(1) = -10$ and $\lambda^{(1)}(1) = 10$. We proceed by applying the adapted FBSM outlined in §4.2, using these guesses to initialise the secant method. Numerical results for the linear fixed endpoint control problem are presented in Figure 4.5. Convergence of the adapted FBSM is achieved after $\Sigma = 177$ iterations.

4.3.2 Multiple-variable nonlinear model

The AML model is a nonlinear coupled multi-species model describing the interactions between progenitor blood cells, $A(t)$, and leukaemic stem cells, $L(t)$, that occupy the same niche in the bone marrow; thereby competing for space and resources. Haematopoietic stem cells, $S(t)$, act as upstream production of $A(t)$. These dynamics have been explored in the literature both experimentally [149, 301], and through mathematical modelling [82, 210]. We subject the model to a chemotherapy-like control, $u(t)$, that acts as an additional death term for $L(t)$. The state can be expressed as $\mathbf{x}(t) = [S(t), A(t), L(t)]^T$. As there are now three state equations, we require three co-state equations; $\boldsymbol{\lambda}(t) = [\lambda_1(t), \lambda_2(t), \lambda_3(t)]^T$. We suppress the explicit time dependence of the state and co-state variables and the control in the following equations for notational convenience:

$$\begin{aligned} \frac{dS}{dt} &= \underbrace{\rho_S S(1 - S)}_{\text{logistic growth}} - \underbrace{\delta_S S}_{\text{differentiation}}, \\ \frac{dA}{dt} &= \underbrace{\delta_S S}_{\text{upstream production}} + \underbrace{\rho_A A(1 - A - L)}_{\text{logistic growth with competition}} - \underbrace{\delta_A A}_{\text{differentiation}}, \\ \frac{dL}{dt} &= \underbrace{\rho_L L(1 - A - L)}_{\text{logistic growth with competition}} - \underbrace{\delta_L L}_{\text{differentiation}} - \underbrace{\frac{\alpha L}{\gamma + L}}_{\text{immune response}} - \underbrace{uL}_{\text{chemotherapy control}}. \end{aligned} \quad (4.15)$$

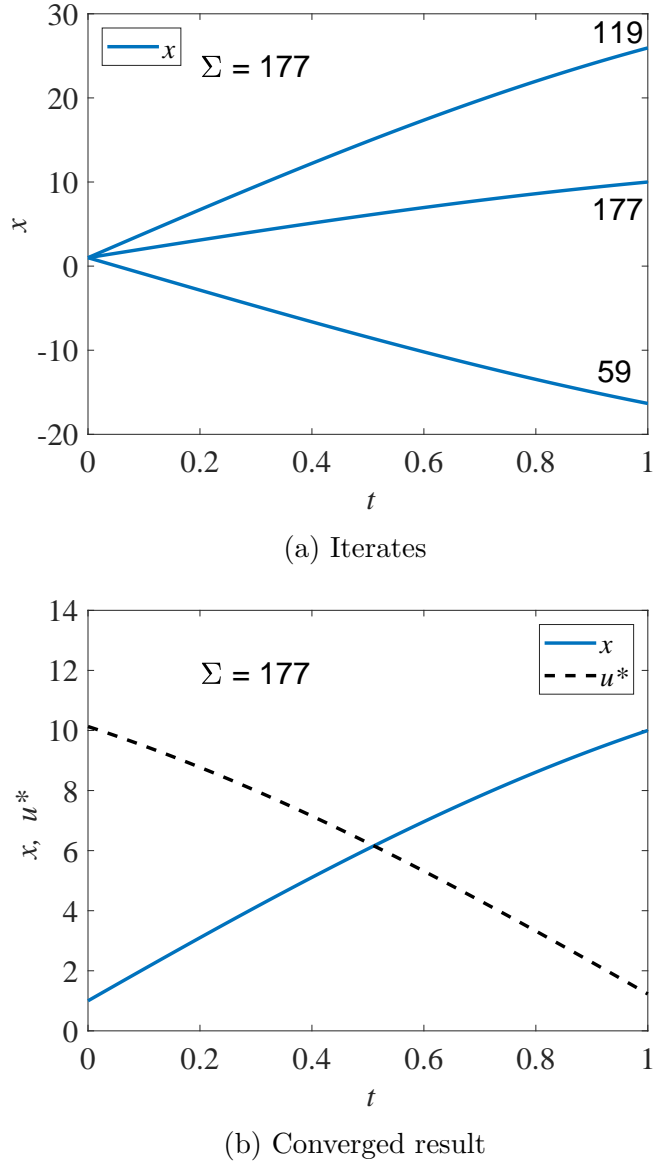


Figure 4.5: Results are presented for the linear problem with specified terminal state value, $x(t_N) = 10$, solved using the adapted FBSM. Underlying FBSM problems are solved with time-step $dt = 3.91 \times 10^{-3}$, over the interval $0 \leq t \leq 1$, with pay-off weightings of $a = b = 1$. In (a) the $x(t)$ iterates of the adapted FBSM are presented. We annotate the cumulative function evaluations after the first ($\mathcal{N}^{(1)} = 59$) and second ($\mathcal{N}^{(1)} + \mathcal{N}^{(2)} = 119$) iterations of the adapted FBSM, based on initial guesses for $\lambda(t_N)$ of $\lambda(t_N) = -10$ and $\lambda(t_N) = 10$. The total cumulative function evaluations required for convergence of the adapted FBSM, $\Sigma = \mathcal{N}^{(1)} + \mathcal{N}^{(2)} + \mathcal{N}^{(3)} = 177$, is indicated. The converged result for $x(t)$, satisfying $|x(t_N) - 10| \leq 1 \times 10^{-10}$ is presented in (b); this figure also includes the optimal control, $u^*(t)$.

For each control problem associated with the AML model, we use initial conditions that yield a coexisting steady state in absence of control (all three species non-zero); $S(0) = 1 - \delta_S/\rho_S$, $A(0) = 0.3255$, and $L(0) = 0.3715$. We solve the AML problems numerically on the domain $0 \leq t \leq 10$, with time-step $dt = 4.88 \times 10^{-4}$, giving $N = 20481$ time points. Model parameters are specified in Table 4.1.

Table 4.1: AML model parameters

Description	Variable	Value	Dimension
Proliferation of S	ρ_S	0.5	[T ⁻¹]
Proliferation of A	ρ_A	0.43	[T ⁻¹]
Proliferation of L	ρ_L	0.27	[T ⁻¹]
Differentiation of S into A	δ_S	0.14	[T ⁻¹]
Differentiation of A	δ_A	0.44	[T ⁻¹]
Differentiation of L	δ_L	0.05	[T ⁻¹]
Characteristic rate of the immune response	α	0.015	[T ⁻¹]
Half saturation constant of the immune response	γ	0.1	[\cdot]

Parameters correspond to those presented with the original model [82], with immune response parameters introduced in subsequent work [290].

Continuous control

For the AML continuous control problem we seek to minimise a quadratic cost function J , that accounts for both the cost of applying the control and the cost of the leukaemic burden, subject to

$$J = \int_0^{10} (a_1 u^2 + a_2 L^2) dt, \quad a_1 > 0, a_2 > 0. \quad (4.16)$$

We form the Hamiltonian and derive the co-state equation, transversality condition and optimality condition. The Hamiltonian is given by

$$\begin{aligned} H = & a_1 u^2 + a_2 L^2 + (\rho_S S(1 - S) - \delta_S S) \lambda_1 \\ & + (\delta_S S + \rho_A A(1 - A - L) - \delta_A A) \lambda_2 \\ & + (\rho_L L(1 - A - L) - \delta_L L - \frac{\alpha L}{\gamma + L} - u L) \lambda_3. \end{aligned} \quad (4.17)$$

The co-state equations are

$$\begin{aligned}\frac{d\lambda_1}{dt} &= -\frac{\partial H}{\partial S} = -\rho_S \lambda_1 + 2\rho_S \lambda_1 S + \delta_S \lambda_1 - \delta_S \lambda_2, \\ \frac{d\lambda_2}{dt} &= -\frac{\partial H}{\partial A} = -\rho_A \lambda_2 + 2\rho_A \lambda_2 A + \rho_A \lambda_2 L + \delta_A \lambda_2 + \rho_L \lambda_3 L, \\ \frac{d\lambda_3}{dt} &= -\frac{\partial H}{\partial L} = -2a_2 L + \rho_A \lambda_2 A - \rho_L \lambda_3 + \rho_L \lambda_3 A + 2\rho_L \lambda_3 L \\ &\quad + \delta_L \lambda_3 + \frac{\alpha \gamma \lambda_3}{(\gamma + L)^2} + \lambda_3 u,\end{aligned}\tag{4.18}$$

with transversality conditions $\lambda_1(10) = \lambda_2(10) = \lambda_3(10) = 0$, obtained in the usual way. In this case the optimality condition is

$$\frac{\partial H}{\partial u} = 2a_1 u - \lambda_3 L = 0,\tag{4.19}$$

such that the optimal control is given by

$$u^*(t) = \frac{\lambda_3 L}{2a_1}.\tag{4.20}$$

Numerical solutions for the AML continuous control problem are presented in Figure 4.6. These solutions are obtained via the FBSM, requiring $\mathcal{N} = 38$ iterations with $\omega = 0.55$. This choice of ω minimises \mathcal{N} for the AML continuous control problem solved with the FBSM without acceleration techniques. We discuss the choice of ω further in §4.5.

Bang-bang control

For the bang-bang AML problem we consider the same states as in Equation (4.15), and incorporate bounds, $0 \leq u \leq 0.3$, on the control. We seek to minimise a cost function J that is linear in the control and the state variable L :

$$J = \int_0^{10} (a_1 u + a_2 L) dt, \quad a_1 > 0, a_2 > 0.\tag{4.21}$$

We form the Hamiltonian and derive the co-state equations, transversality conditions and optimality condition. The Hamiltonian is given by

$$\begin{aligned}H &= a_1 u + a_2 L + (\rho_S S(1 - S) - \delta_S S)\lambda_1 \\ &\quad + (\delta_S S + \rho_A A(1 - A - L) - \delta_A A)\lambda_2 \\ &\quad + (\rho_L L(1 - A - L) - \delta_L L - \frac{\alpha L}{\gamma + L} - uL)\lambda_3.\end{aligned}\tag{4.22}$$

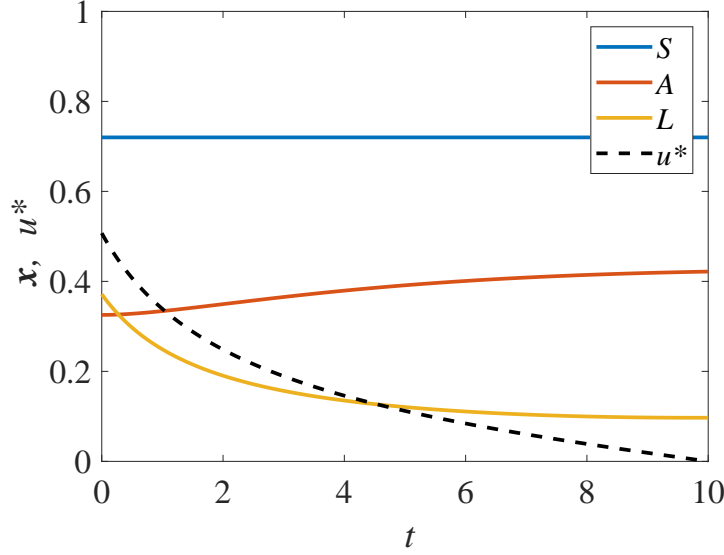


Figure 4.6: Solution to the AML continuous control problem. The optimal control, $u^*(t)$, is shown in black dash and the corresponding state equations for $S(t)$, $A(t)$ and $L(t)$ are shown in blue, red and yellow, respectively. This solution is produced with model parameters given in Table 4.1, time-step $dt = 4.88 \times 10^{-4}$, over the interval $0 \leq t \leq 10$, with pay-off weightings of $a_1 = 1$ for the control, and $a_2 = 2$ for state variable $L(t)$.

The co-state equations are

$$\begin{aligned} \frac{d\lambda_1}{dt} &= -\rho_S \lambda_1 + 2\rho_S \lambda_1 S + \delta_S \lambda_1 - \delta_S \lambda_2, \\ \frac{d\lambda_2}{dt} &= -\rho_A \lambda_2 + 2\rho_A \lambda_2 A + \rho_A \lambda_2 L + \delta_A \lambda_2 + \rho_L \lambda_3 L, \\ \frac{d\lambda_3}{dt} &= -a_2 + \rho_A \lambda_2 A - \rho_L \lambda_3 + \rho_L \lambda_3 A + 2\rho_L \lambda_3 L \\ &\quad + \delta_L \lambda_3 + \frac{\alpha \gamma \lambda_3}{(\gamma + L)^2} + \lambda_3 u, \end{aligned} \tag{4.23}$$

with transversality conditions $\lambda_1(10) = \lambda_2(10) = \lambda_3(10) = 0$. In this case the switching function is

$$\psi(t) = \frac{\partial H}{\partial u} = a_1 - \lambda_3 L, \tag{4.24}$$

such that the optimal control is given by

$$u^*(t) = \begin{cases} 0, & \psi(t) > 0, \\ 0.3, & \psi(t) < 0. \end{cases} \tag{4.25}$$

Note that the correspondence between the sign of $\psi(t)$ and the chosen bound is reversed in Equation (4.25) relative to Equation (4.14) as we are now performing minimisation rather than maximisation. Numerical solutions for the AML bang-bang control problem

are presented in Figure 4.7. These solutions are obtained via the FBSM, requiring $\mathcal{N} = 34$ iterations with $\omega = 0.4$. This choice of ω minimises \mathcal{N} for the AML bang-bang control problem solved with the FBSM without acceleration techniques. We discuss the choice of ω further in §4.5.

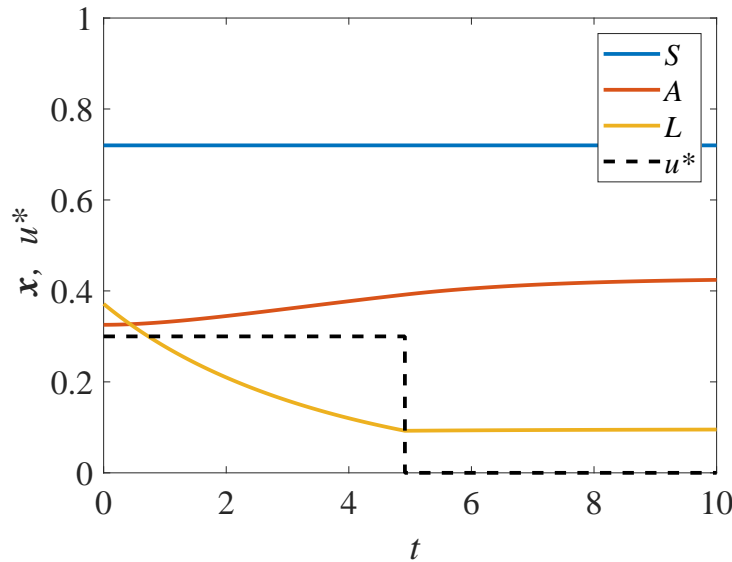


Figure 4.7: Solution to the AML bang-bang control problem. The optimal control, $u^*(t)$, is shown in black dash and the corresponding state equations for $S(t)$, $A(t)$ and $L(t)$ are shown in blue, red and yellow, respectively. This solution is produced with model parameters given in Table 4.1, time-step $dt = 4.88 \times 10^{-4}$, over the interval $0 \leq t \leq 10$, with pay-off weightings of $a_1 = 1$ for control, and $a_2 = 2$ for the state variable $L(t)$.

Continuous control with fixed endpoint

For the fixed endpoint problem, we proceed with the same state equations as for the AML continuous control problem given in Equation (4.15), however we now impose a terminal condition on the leukaemic population; $L(10) = 0.05$. We seek to minimise the same quadratic cost function J , as considered in Equation (4.16). We form the same Hamiltonian given in Equation (4.17) and derive the same co-state, Equation (4.18), and expression for the control, Equation (4.20).

We obtain final time conditions, $\lambda_1(10) = \lambda_2(10) = 0$, via the transversality conditions as usual, however we do not prescribe $\lambda_3(10)$. Instead, we make two guesses for $\lambda_3(10)$; for instance, $\lambda_3^{(0)}(10) = 0$ and $\lambda_3^{(1)}(10) = 10$. We then proceed by applying the adapted FBSM outlined in §4.2, using these guesses to initialise the secant method. Numerical results for the AML fixed endpoint control problem are presented in Figure 4.8. These results are produced using the adapted FBSM with $\omega = 0.55$ in $\Sigma = 434$ iterations. This choice of ω minimises Σ for the AML fixed endpoint control problem solved with the FBSM without acceleration techniques. We discuss this further in §4.5.

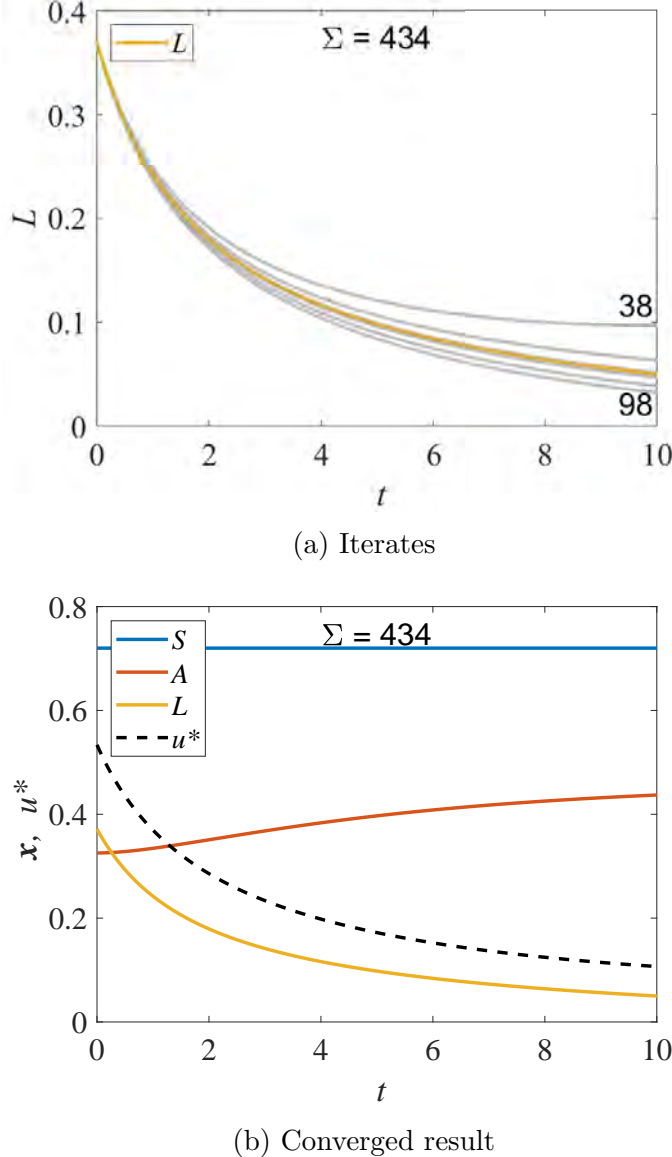


Figure 4.8: Results are presented for the AML problem with specified terminal state, $L(t_N) = 0.05$, solved using the adapted FBSM. Each underlying FBSM problem is solved with model parameters given in Table 4.1, time-step $dt = 4.88 \times 10^{-4}$, over the interval $0 \leq t \leq 10$, with pay-off weightings of $a_1 = 1$ for the control, and $a_2 = 2$ for the state variable $L(t)$. In (a) the $L(t)$ iterates of the adapted FBSM are presented in grey; the converged solution satisfying $L(t_N) = 0.05$ is plotted in yellow. We annotate \mathcal{N} for the first ($\mathcal{N}^{(1)} = 38$) and second ($\mathcal{N}^{(1)} + \mathcal{N}^{(2)} = 98$) iterations of the adapted FBSM, based on initial guesses for $\lambda_3(t_N)$ of $\lambda_3(t_N) = 0$ and $\lambda_3(t_N) = 10$. Due to the close proximity, subsequent iterations are not annotated. The cumulative function evaluations required for convergence of the adapted FBSM ($\Sigma = 434$) is indicated. The converged result for $L(t)$, satisfying $-L(t_N) - 0.05| \leq 1 \times 10^{-10}$, is presented in (b); this figure also includes the optimal control, $u^*(t)$ and trajectories for $S(t)$ and $A(t)$.

4.4 Iterative accelerators

In this section we outline several techniques for acceleration of iterative schemes. Where appropriate, we first present the univariate/scalar version of the method for familiarity, then provide the multivariate/vector analogue of the method for use with accelerating the FBSM. We attempt to use notation that aligns most closely with commonly used notation in the literature, while maintaining internal consistency in this work. In the scalar case, we consider the iterative process $x^{(k+1)} = f(x^{(k)})$, where $x^{(k)}$ is the k th iterate and f is the iterating function. In the vector case we consider $X^{(k+1)} = F(X^{(k)})$, where $X^{(k)} = [x_0^{(k)}, x_1^{(k)}, \dots, x_N^{(k)}]^T$ is the k th iterate, consisting of $N + 1$ values, and $F = [f_0, f_1, \dots, f_N]^T$ is the $N + 1$ dimensional operator of the iterative process. For clarity, we stress that in the context of the acceleration algorithms applied to the FBSM, $X^{(k)}$ is the discretised control in the k th iteration.

The acceleration methods considered in this work apply either to problems stated as fixed point iterations (as above), or as root-finding problems. For acceleration via root-finding algorithms, we can consider the complementary problems in the scalar and vector setting, respectively; $g(x) := x - f(x) = 0$ and $G(X) := X - F(X) = \mathbf{0}$, where $\mathbf{0}$ is the zero column vector of length $N + 1$.

We note that many of the methods presented here can be written in several different forms. While some forms better facilitate analysis of aspects such as convergence speed and numerical stability, others emphasise ease of understanding and implementation. In this work we prioritise usability and present methods and algorithms in forms reflective of their implementation where possible. For the purpose of this work, we feel it is sufficient to present the methods and discuss their implementation without delving into their derivation or rigorous theoretical convergence results. For readers interested in these aspects, we suggest these articles [47, 273], and numerical analysis texts [58, 141].

4.4.1 Newton and Quasi-Newton methods

Newton's method is one of the most prevalent root-finding algorithms, due to its relatively straightforward implementation and potential for quadratic convergence [141]. For a univariate function Newton's method is given by

$$x^{(k+1)} = x^{(k)} - \frac{f(x^{(k)})}{f'(x^{(k)})}. \quad (4.26)$$

We arrive at the scalar secant method by replacing the derivative term, $f'(x^{(k)})$, in Equation (4.26) with a finite difference approximation:

$$x^{(k+1)} = x^{(k)} - f(x^{(k)}) \frac{x^{(k)} - x^{(k-1)}}{f(x^{(k)}) - f(x^{(k-1)})}.$$

Newton's method for multivariate systems is

$$\begin{aligned} X^{(k+1)} &= X^{(k)} + \Delta X^{(k)}, \\ \text{where } \Delta X^{(k)} &\text{ is obtained by solving} \\ J_k \Delta X^{(k)} &= -F(X^{(k)}). \end{aligned}$$

Here, J_k is the Jacobian matrix of F evaluated at $X^{(k)}$ [141]. Setting aside the interpretation of the Jacobian in the context of the FBSM; numerically approximating an $N \times N$ Jacobian matrix using finite differences requires $\mathcal{O}(N^2)$ FBSM iterations at each Newton step. A range of Quasi-Newton methods have been developed to minimise the computational expense associated with computing the Jacobian at each Newton step. It is not immediately apparent how the secant method should be extended to multivariate systems, but one such interpretation is the Quasi-Newton Broyden's method. Broyden's method reduces the number of function evaluations required at each Newton step by forming the full Jacobian only initially, then updating the Jacobian matrix via a rank-one update based on the secant method [54, 58]. We later discuss the Wegstein method [334], which is another interpretation of the secant method in multivariate settings.

In the context of accelerating the FBSM, techniques that require forming or approximating a full Jacobian, even once, are not appropriate. We have an $N + 1$ dimensional system, where $N + 1$ is the number of time points in the discretisation of the ODEs, so we expect N to be large, relative to the number of iterations required for the FBSM to converge without acceleration techniques, via Equation (4.6). As such, we restrict our focus to Jacobian-free methods in the remainder of this section; in particular, we discuss and implement the Wegstein and Aitken-Steffensen methods and Anderson acceleration. We provide a broad overview alongside the key equations here, and provide complete algorithms alongside notes for implementation in §4 of the supplementary material.

4.4.2 Wegstein method

Wegstein's method can be thought of as an element-wise extension of the secant method to multivariate systems [129]. Although Wegstein's method appears less popular than other methods considered in this work, it has found practical utility, particularly in chemical and process engineering software [214, 303]. We include it here due to the striking similarity it bears to the control update with relaxation presented in Equation (4.6). It is also one

of the more straightforward techniques, both in conception and implementation:

$$\hat{x}^{(k+1)} = f(x^{(k)}), \quad (4.27)$$

$$x^{(k+1)} = q^{(k)}x^{(k)} + (1 - q^{(k)})\hat{x}^{(k+1)}, \quad (4.27)$$

$$\text{where } q^{(k)} = \frac{a^{(k)}}{a^{(k)} - 1}, \text{ and } a^{(k)} = \frac{f(x^{(k)}) - f(x^{(k-1)})}{x^{(k)} - x^{(k-1)}}. \quad (4.28)$$

In implementation, from an initial value x_0 it is necessary to perform two function evaluations; i.e. $x_1 = f(x_0)$, and $f(x_1)$, before it is possible to compute Equation (4.28) for the Wegstein method [334]. In subsequent iterations only one new function evaluation is required.

The extension of Wegstein's method to multivariate systems follows exactly the process outlined in Equations (4.27) and (4.28), as it is extended element-wise. While convergence is guaranteed when using Wegstein's method for a single nonlinear equation, the uncoupling implied by the element-wise extension can lead to divergence [249].

In Equations (4.27) and (4.28) $q^{(k)}$ denotes q in the k th iteration, however, we note that it is not necessarily most effective to update q every iteration. As such, in this work we explore various updating regimes. There is also the option of applying bounds on q . Bounds of $-5 < q_i < 0$, $\forall i$, where i denotes the i th element of the system, are frequently applied when implementing Wegstein's method [21, 283]. This bounding appears to work reasonably well for the small nonlinear test systems we consider in §5 of the supplementary material, although we were not able to identify a theoretical result supporting this specific choice. For the control problems we consider, this bounding is not effective, so we apply different bounds, discussed further in §4.5. The univariate Wegstein method can be thought of as a modification of the Aitken method, which at the time the Wegstein method was developed, was only understood for the univariate case [81].

4.4.3 Aitken-Steffensen method

Aitken's Δ^2 method, also referred to as Aitken's delta-squared process or Aitken extrapolation, was originally posed by Aitken in 1927 as a means of extending Bernoulli's method of approximating the largest root of an algebraic equation. This extension facilitates numerically approximating not only the largest root, but all roots of the equation [7]. Aitken's method generates a new sequence, \hat{x} , in parallel to the fixed point iteration.

$$\begin{aligned} \hat{x}^{(k)} &= x^{(k)} - \frac{(x^{(k+1)} - x^{(k)})^2}{x^{(k+2)} - 2x^{(k+1)} + x^{(k)}}, \quad \text{or} \\ \hat{x}^{(k)} &= x^{(k)} - \frac{(\Delta x^{(k)})^2}{\Delta^2 x^{(k)}}, \end{aligned} \quad (4.29)$$

where Δ is the difference operator; $\Delta x^{(k)} = x^{(k+1)} - x^{(k)}$, and the higher order operator is applied recursively; $\Delta^2 x^{(k)} = \Delta(\Delta x^{(k)}) = \Delta x^{(k+1)} - \Delta x^{(k)}$ [141]. From an initial value, $x^{(0)}$, two function evaluations; iterations of the underlying fixed point process, must be performed to obtain $x^{(1)}$ and $x^{(2)}$, before Equation (4.29) can be computed.

The derivation of Aitken's method assumes an underlying linearly converging series of iterates. The order of convergence of the resulting Aitken accelerated series is still linear, however this series converges faster than the original series [58]. We discuss Aitken's Δ^2 method and Steffensen iteration together, as Steffensen iteration is a straightforward extension of Aitken's method, whereby the Aitken value, $\hat{x}^{(k)}$, is used to continue the fixed point iteration, i.e. $x^{(k+1)} = \hat{x}^{(k)}$. Despite the striking similarity, Steffensen's method was seemingly developed shortly after (1933) and without knowledge of Aitken's method [306]. Steffensen iteration can achieve quadratic convergence [2, 141, 240]. Further theoretical convergence results for the Steffensen method are established by Nievergelt [241] and in a series of papers by Noda [242–244].

Aitken and Steffensen iteration can be extended to multivariate systems [141]. In the following statements we outline the method for an $N + 1$ dimensional system; $X^{(k)} = [x_0^{(k)}, x_1^{(k)}, \dots, x_N^{(k)}]^T \in \mathbb{R}^{N+1}$, as appropriate for use with the FBSM:

$$\hat{X}^{(k)} = X^{(k)} - \Delta \mathcal{X}^{(k)} (\Delta^2 \mathcal{X}^{(k)})^{-1} \Delta X^{(k)}, \quad (4.30)$$

where $\Delta X^{(k)} = X^{(k+1)} - X^{(k)}$, and $\mathcal{X}^{(k)}$ is a matrix constructed with columns $(X^{(k)}, X^{(k+1)}, \dots, X^{(k+N)})$, such that $\mathcal{X}^{(k)}$ is a square matrix of dimension $N + 1$, with $\Delta \mathcal{X}^{(k)} = \mathcal{X}^{(k+1)} - \mathcal{X}^{(k)}$, and $\Delta^2 \mathcal{X}^{(k)} = \Delta \mathcal{X}^{(k+1)} - \Delta \mathcal{X}^{(k)}$.

In the form given by Equation (4.30) there are glaring issues with using the Steffensen method to accelerate convergence of the FBSM. Setting aside the question of whether $\Delta^2 \mathcal{X}^{(k)}$ is invertible, forming $\mathcal{X}^{(k)}$ would require $\mathcal{O}(N)$ iterations of the FBSM to be performed, and since N relates to the number of time points in the discretisation of the ODEs in the FBSM, we expect N to be large, relative to the number of iterations required for the FBSM to converge without acceleration.

We instead consider a modification of the Steffensen method, requiring fewer function evaluations per iteration. Introduce $m < N$, and define $\Delta X^{(k)} = X^{(k+1)} - X^{(k)}$ as before, $\mathcal{X}^{(k)}$ is now a rectangular matrix constructed with columns $(X^{(k)}, X^{(k+1)}, \dots, X^{(k+m+1)})$, such that $\mathcal{X}^{(k)} \in \mathbb{R}^{(N+1) \times (m+2)}$, with $\Delta \mathcal{X}^{(k)} = \mathcal{X}^{(k+1)} - \mathcal{X}^{(k)}$, and $\Delta^2 \mathcal{X}^{(k)} = \Delta \mathcal{X}^{(k+1)} - \Delta \mathcal{X}^{(k)}$, both of dimension $(N+1) \times m$. We now interpret the matrix inverse in Equation (4.30) as the Moore-Penrose pseudoinverse [257], a generalisation of the matrix inverse for singular and rectangular matrices; we discuss this further in §3 of the supplementary material. This partial implementation requires only $m + 1$ function evaluations per iteration. For the remainder of this document when referring to the Steffensen method we are specifically referring to this partial Steffensen implementation. We present the

derivation of the multivariate Aitken-Steffensen method and outline where the partial implementation differs, in §3 of the supplementary material.

4.4.4 Anderson Acceleration

Anderson Acceleration or Anderson Mixing, originally denoted as the extrapolation algorithm by Anderson in the 1960s [16], is a technique developed for accelerating convergence of fixed point iteration problems with slowly converging Picard iterations [18]. Anderson Acceleration is of particular interest in this work, as it has recently been implemented to accelerate the convergence of a regularised version of the FBSM [203]. In contrast to a standard fixed point iteration; whereby the next iterate depends only on the immediately preceding iterate, Anderson Acceleration has ‘memory’ through the inclusion of previous iterates [102]. Unlike other methods considered in this work, Anderson Acceleration explicitly utilises the differences between residuals of subsequent iterates alongside iterates and their differences in computing future iterates.

Anderson Acceleration involves solving a least-squares problem at each iteration. The problem can be expressed in both constrained and unconstrained forms, with the updating step dependent on the form [104, 326]. We solve the following unconstrained least-squares problem in each iteration of Anderson Acceleration:

$$\gamma = \arg \min_{\gamma} (\|G - \gamma dG\|), \quad (4.31)$$

where $\arg \min(\cdot)$ returns the argument, γ , that minimises the expression in Equation (4.31). The corresponding updating step is

$$X^{(k+1)} = X^{(k)} + G^{(k)} - (dX^{(k-1)} + dG^{(k-1)})\gamma, \quad (4.32)$$

where $G^{(k)} = F(X^{(k)}) - X^{(k)}$ is the residual, $dX^{(k)}$ is a matrix with columns $(\Delta X^{(k-m)}, \Delta X^{(k-m+1)}, \dots, \Delta X^{(k)})$, and $dG^{(k)}$ is a matrix with columns $(\Delta G^{(k-m)}, \Delta G^{(k-m+1)}, \dots, \Delta G^{(k)})$, and m indicates the number of previous iterates that are incorporated.

4.4.5 Acceleration methods applied to typical fixed point problems

As a precursor to implementing these acceleration methods for control problems, we apply them to solve example nonlinear systems of dimension 2×2 , 3×3 , and 4×4 . We provide these systems and the results of the acceleration methods compared to standard fixed point iteration in §5 of the supplementary material. We do not discuss these results in

detail, although broad comparisons regarding the application of the acceleration methods to these systems and to control problems are made in §4.6. We provide code on [GitHub](#) for implementing the acceleration algorithms to solve systems of arbitrary size.

4.5 Acceleration results

In this section we discuss the results of applying the acceleration algorithms. When discussing results we are solely focused on reducing \mathcal{N} , the number of function evaluations required for the control problems to reach convergence; as in all convergent cases we arrive at the same optimal control results. We first discuss the aspects of each method that can be tuned, then outline the results of the standard FBSM with the best choice of ω but without acceleration methods applied, to establish a baseline against which to compare the acceleration methods. A detailed suite of results for each control problem and each acceleration method, for various combinations of tuning parameters, is provided in §6 of the supplementary material.

4.5.1 Tuning

Each method we consider has parameters that can be tuned to improve performance for a given problem. For the FBSM without acceleration, we can select $\omega \in [0, 1]$; the parameter that weights the contribution of the control from the previous iteration, and the newly calculated control, to the control used in the next iteration, as stated in Equation (4.6). Control problems based on the linear model are able to converge via direct updating, as given in Equation (4.5), equivalent to $\omega = 0$. Increasing ω in this case only serves to increase \mathcal{N} , so we do not attempt to tune ω when considering the linear model. Using the standard FBSM without acceleration the continuous linear problem requires $\mathcal{N} = 57$ while the bang-bang linear problem requires only $\mathcal{N} = 8$.

In Figure 4.9 we plot \mathcal{N} against $\omega \in [0, 1]$, for the continuous and bang-bang AML problems. As expected, for small ω we find that the problem does not converge, and for large ω , \mathcal{N} increases. For the continuous AML problem we identify $\omega = 0.55$ as the best choice, with $\mathcal{N} = 38$. For the bang-bang AML problem we find that $\omega = 0.4$ is best, with $\mathcal{N} = 34$.

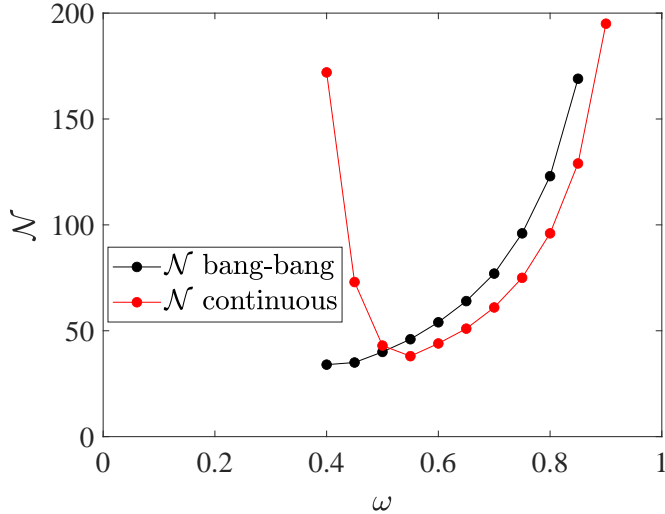


Figure 4.9: Here we plot \mathcal{N} against $\omega \in [0, 1]$ in increments of 0.05, for the AML continuous (in red) and bang-bang (in black) control problems, using FBSM with no acceleration. Results correspond to model parameters given in Table 4.1, time-step $dt = 4.88 \times 10^{-4}$, over the interval $0 \leq t \leq 10$. The continuous problem is solved with payoff weightings of $a_1 = 1$ for control, and $a_2 = 2$ for the state variable $L(t)$, while the bang-bang problem is solved with $a_1 = 1$ and $a_2 = 3$. Where an ω value does not have a corresponding marker, this indicates that the procedure fails to converge within $\mathcal{N} = 200$.

Recall that fixed endpoint problems are solved using the adapted FBSM; this entails solving several control problems to convergence with the FBSM. Each of these control problems can have a different optimal ω . In this instance, $\omega = 0.55$ also happens to be best for the AML fixed endpoint problem if holding ω constant, when considering $\omega \in [0, 1]$ at increments of 0.05. These ω values will not coincide in general. When applying the acceleration methods to the fixed endpoint problems, we employ the tuning parameters that perform best for the continuous problem. This does not imply that we are using the best tuning parameters for the acceleration methods in the context of the fixed endpoint problem. Importantly, this demonstrates whether or not the techniques can effectively reduce Σ , the cumulative function evaluations required for convergence of the adapted FBSM for fixed endpoint problems, without requiring prohibitive tuning.

With the Wegstein method, we only select ω for the two FBSM iterations required for initialisation, and specify n , such that we update q every n th iteration. We generate results for $n \in \{1, 2, \dots, 10\}$. We also bound q , however identifying suitable bounds is challenging. In this work we select bounds that perform reasonably, but acknowledge that we do not search for optimal bounds, nor do we think that attempting to do so is realistic. This drawback of Wegstein's method contributes to its inconsistent performance relative to other methods. For the partial Aitken-Steffensen methods, we choose ω , and the parameter m that specifies the dimension of the $(N + 1) \times m$ matrices in the updating step, requiring $m + 1$ function evaluations per iteration. We generate results

for $m \in \{1, 2, \dots, 10\}$. Similarly, for Anderson Acceleration we select ω and M ; where M determines the maximum number of previous iterations to retain when solving the least squares problem and performing the updating step. We produce results for $M \in \{1, 2, \dots, 10\}$.

4.5.2 Wegstein method

For the continuous linear problem, we apply bounds of $-2 \leq q \leq 0$. For the bang-bang linear problem, we leave q unbounded. For both AML problems we apply bounds $-1 \leq q \leq 1$. We explore the effect of updating q every n th iteration, $n \in \{1, 2, \dots, 10\}$. For the continuous linear problem, $n = 4$ minimises \mathcal{N} , although $n \in \{1, 2, \dots, 5\}$ all perform well. For the linear bang-bang problem, the Wegstein method converges without bounding on q , and varying n does not affect convergence. The Wegstein method outperforms other acceleration methods for the linear bang-bang problem with $\mathcal{N} = 9$, but does not improve upon $\mathcal{N} = 8$ for the FBSM without acceleration.

For the continuous AML problem, the performance of Wegstein's method is inconsistent. With $n = 6$ and $\omega = 0.55$, the Wegstein method achieves convergence with $\mathcal{N} = 26$, outperforming the FBSM; however, almost every other combination of tuning parameters considered with $\omega \in [0, 1)$ and $n \in \{1, 2, \dots, 10\}$ require larger \mathcal{N} than the FBSM without acceleration. Generally, increasing n produces worse outcomes. We do, however, observe that the Wegstein method can induce convergence for $\omega < 0.4$, where the standard FBSM does not converge. For the bang-bang AML problem, the Wegstein method appears more robust; consistently outperforming the standard FBSM across most of the tuning parameter space. The best result requires only $\mathcal{N} = 9$, with $\omega = 0$ and $n = 7$, although several other combinations of tuning parameters are similarly successful. For $\omega \geq 0.4$, corresponding to values that the underlying FBSM converges, we find that moderate $n \in \{3, 4, \dots, 7\}$ produces the best results; while for smaller ω , larger $n \in \{6, 7, \dots, 10\}$ consistently performs best. Once again we observe that convergence is achieved for ω values where the underlying FBSM would not converge.

For the linear fixed endpoint problem the adapted FBSM with the Wegstein method consistently generates a moderate reduction in Σ , compared to the adapted FBSM without acceleration, for all $n \in \{1, 2, \dots, 10\}$, $-2 \leq q \leq 0$. For the AML fixed endpoint problem we do not observe improvement. Using the tuning parameters that perform best for the continuous AML problem, we find that Σ for the adapted FBSM with Wegstein's method is more than double that of the adapted FBSM without acceleration. This results from the inconsistency of Wegstein's method with poor tuning. In §6 of the supplementary material it can be seen that some control problems within the adapted FBSM that require $\mathcal{N} \approx 50$ without Wegstein's method, require $\mathcal{N} \approx 200$ with the specified Wegstein tuning parameters.

4.5.3 Partial Aitken-Steffensen method

Both Aitken and Steffensen methods significantly and consistently outperform the FBSM without acceleration for the continuous linear problem. The Aitken method performs best for $m \in \{1, 2, 3\}$, requiring $\mathcal{N} = 12$. Steffensen's method performs best when $m = 6$, requiring only $\mathcal{N} = 8$. In the linear bang-bang case, both Aitken and Steffensen methods perform marginally worse than the FBSM without acceleration, which requires only $\mathcal{N} = 8$. In the best cases, with $m = 1$ the Aitken method requires $\mathcal{N} = 10$, and with $m = 7$ the Steffensen method requires $\mathcal{N} = 9$.

For the continuous AML problem, we observe a stark difference between the Aitken and Steffensen methods; while the Steffensen method is able to achieve convergence for values of ω where the underlying FBSM fails to converge; $\omega \leq 0.35$, particularly for $m \in \{1, 2, 3, 4\}$, the Aitken method only converges to the optimal control for ω values where the underlying FBSM converges. For $\omega \leq 0.35$ the Aitken method achieves apparent convergence; the iterative procedure terminates as the convergence criteria is met. However, explicitly calculating the pay-off associated with these controls via Equation (4.16), and comparing this result to the pay-off associated with the control obtained via the standard FBSM, indicates that the controls obtained via the Aitken method for $\omega \leq 0.35$ are not optimal, as they fail to minimise J . The best result for the Aitken method, with $\omega = 0.5$ and $m = 5$, requires $\mathcal{N} = 30$, marginally improving on the FBSM without acceleration, requiring $\mathcal{N} = 38$. Steffensen's method produces more significant improvements, requiring only $\mathcal{N} = 19$ with $\omega = 0.5$ and $m = 5$. In each case neighbouring combinations of tuning parameters also yield equivalent or comparable improvement over the standard FBSM. In the bang-bang AML problem, we observe similar behaviour; for ω values that the underlying FBSM fails to converge, the Steffensen method consistently converges. The Aitken method achieves apparent convergence for these values of ω ; the iterative procedure terminates as the convergence criteria is met, however the resulting controls contain intermediate values between the lower and upper bounds. As such the resulting controls are not bang-bang, so we treat these results as failing to converge. At best, Aitken's method requires $\mathcal{N} = 8$, with $\omega = 0.5$ and $m = 1$, while Steffensen's requires only $\mathcal{N} = 7$, with $\omega = 0.5$ and $m = 5$. The vast majority of tuning parameter combinations yield improvements over the $\mathcal{N} = 34$ of the standard FBSM.

Aitken and Steffensen methods consistently offer significant improvement over the standard adapted FBSM for the linear fixed endpoint problem for $m \in \{1, 2, \dots, 10\}$, with the exception of $m = 1$ for the Steffensen method, which yields only marginal improvement. Using the best performing tuning parameters for the continuous AML problem, we find that both Aitken and Steffensen methods improve upon the standard adapted FBSM for the AML fixed endpoint problem. Relative to $\Sigma = 434$ required without acceleration, the $\Sigma = 360$ required with Aitken's method reflects a modest improvement, while the

$\Sigma = 238$ required with the Steffensen method is a significant improvement.

4.5.4 Anderson Acceleration

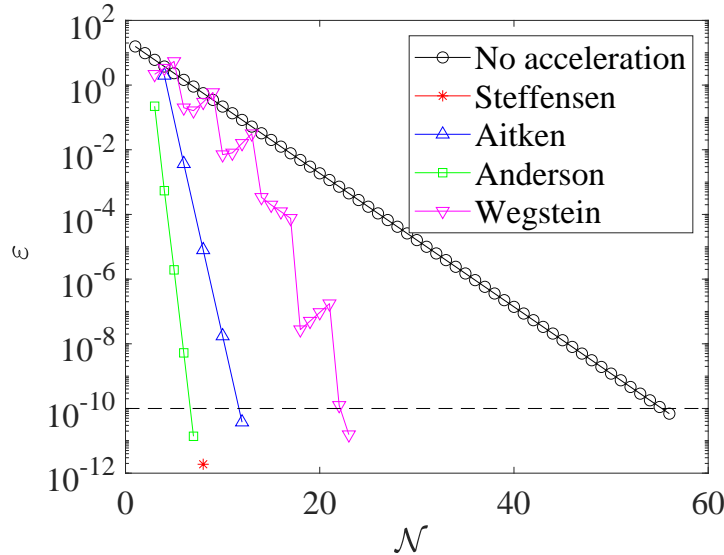
Anderson Acceleration performs exceptionally well on the continuous linear problem, requiring only $\mathcal{N} = 7$ for $M \in \{4, 5, \dots, 10\}$ compared to $\mathcal{N} = 57$ for the standard FBSM. For the linear bang-bang problem however, it is the worst performing acceleration method; achieving at best $\mathcal{N} = 11$, with $M = 1$.

Similarly to the Wegstein and Steffensen methods, Anderson Acceleration achieves convergence in both the continuous and bang-bang AML problems for ω values where the underlying FBSM fails to converge. Anderson Acceleration achieves the best individual result for the continuous AML problem, requiring only $\mathcal{N} = 17$, with $\omega = 0.85$ and $M = 6$. Again, we observe comparable improvement over a wide range of tuning parameters. For the bang-bang AML problem Anderson Acceleration consistently outperforms FBSM without acceleration, particularly for $\omega < 0.7$, at best requiring $\mathcal{N} = 17$, with $\omega = 0.35$ and $M \in \{7, 8, 9, 10\}$, with other non-neighbouring tuning parameter combinations also yielding $\mathcal{N} = 17$.

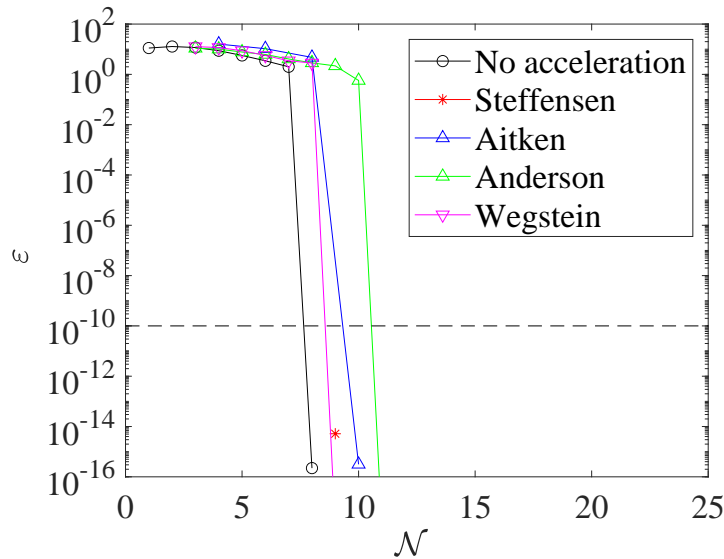
For both the linear and AML fixed endpoint problems Anderson Acceleration produces the most significant reduction in Σ , and improves upon the adapted FBSM over a wide range of tuning parameters. In the linear case, Anderson Acceleration requires only $\Sigma = 24$ for $M \in \{4, 5, \dots, 10\}$. In the AML fixed endpoint problem, using the tuning parameters that perform best for the continuous AML problem, Anderson Acceleration converges in only $\Sigma = 204$; less than half as many as the standard adapted FBSM.

4.5.5 Method comparison with best tuning

Results presented in Figure 4.10 and Figure 4.11 provide comparison of the error, ε , as each method approaches convergence, for the linear and AML problems, respectively. Error is measured as the Euclidean norm of the difference between subsequent controls; $\varepsilon = \|F(X^{(k)}) - X^{(k)}\|$, with the exception of Aitken's method, where error is measured as the difference between subsequent values in the Aitken series; $\varepsilon = \|\hat{X}^{(k)} - \hat{X}^{(k-1)}\|$. Convergence is achieved when $\varepsilon \leq 1 \times 10^{-10}$, marked in black dash. In each case, we are plotting the result that minimises \mathcal{N} for each method, over the space of tuning parameters considered, including the best tuning of ω for the FBSM without acceleration. Error is plotted on a logarithmic scale. For the linear bang-bang problem with the Wegstein and Anderson methods, and the AML bang-bang problem with the Wegstein method, the error after the final iteration is $\varepsilon = 0$, as two subsequent iterates for the control are identical. This is represented on the logarithmic scale as a line that intersects the horizontal axis.

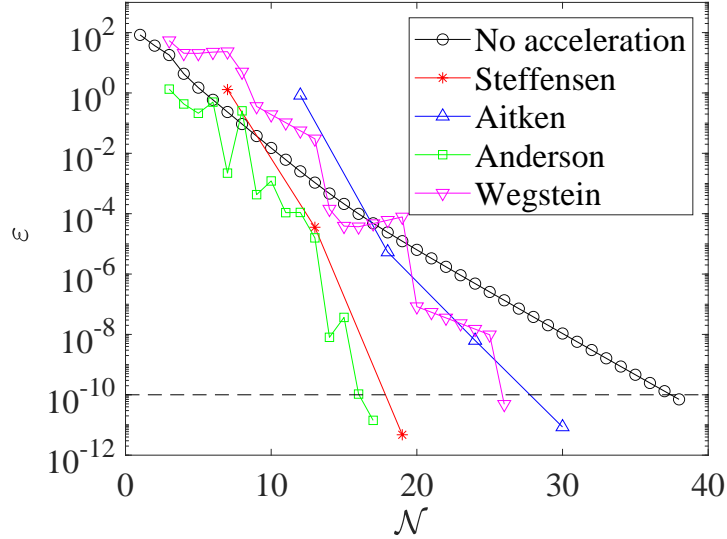


(a) Linear model continuous control

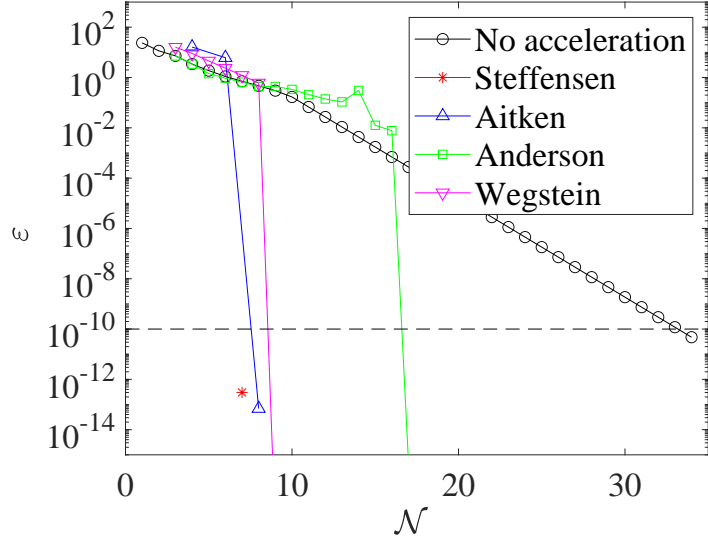


(b) Linear model bang-bang control

Figure 4.10: Convergence rates for the result that minimises \mathcal{N} , for each acceleration method, when applied to the linear control problems. Results in this plot are produced with model parameter $\gamma = 0.5$, time-step $dt = 3.91 \times 10^{-3}$, over the interval $0 \leq t \leq 1$, with pay-off weighting $a = b = 1$ for the continuous control (a), and $a = 1, b = 3$ for the bang-bang control (b). The tolerance of 1×10^{-10} required for convergence is marked in black dash. As the methods do not necessarily use the same number of function evaluations per iteration, markers indicate each time ε is computed. Continuous control results correspond to the FBSM with no acceleration, the partial Steffensen method with $m = 6$, partial Aitken method with $m = 1$, Anderson Acceleration with $M = 4$ and Wegstein with bounds $-2 \leq q \leq 0$, updating q every 4th iteration. Bang-bang results correspond to the FBSM with no acceleration, the partial Steffensen method with $m = 7$, partial Aitken method with $m = 1$, Anderson Acceleration with $M = 1$ and Wegstein without bounds on q , updating q every iteration. The standard FBSM outperformed all acceleration methods in solving the linear bang-bang control problem. We attribute this to how few iterations were required ($\mathcal{N} = 8$) for convergence without acceleration.



(a) AML model continuous control



(b) AML model bang-bang control

Figure 4.11: Convergence rates for the converged result that minimises \mathcal{N} , for each acceleration method, when applied to the AML control problems. Results in this plot are produced with model parameter $\gamma = 0.5$, time-step $dt = 4.88 \times 10^{-4}$, over the interval $0 \leq t \leq 1$, with pay-off weighting $a = b = 1$ for the continuous control (a), and $a = 1$, $b = 3$ for the bang-bang control (b). The tolerance of 1×10^{-10} required for convergence is marked in black dash. As the methods do not necessarily use the same number of function evaluations per iteration, markers indicate each time ε is computed. Continuous control results correspond to the FBSM with no acceleration, $\omega = 0.55$, the partial Steffensen and partial Aitken methods with $m = 5$ and $\omega = 0.5$, Anderson Acceleration with $M = 6$ and $\omega = 0.85$, and Wegstein method with $\omega = 0.55$, bounds $-1 < q < 1$, updating q every 6th iteration. Bang-bang results correspond to the FBSM with no acceleration, $\omega = 0.4$, the partial Steffensen method with $m = 5$ and $\omega = 0.5$, partial Aitken method with $m = 1$ and $\omega = 0.5$, Anderson Acceleration with $M = 7$ and $\omega = 0.35$, and Wegstein method with $\omega = 0$, bounds $-1 < q < 1$, updating q on the 7th iteration.

4.6 Discussion

Modelling processes in systems biology is complex; frequently involving large state systems consisting of several ODEs [39, 94, 304], including canonical examples such as the mitogen-activated protein kinase (MAPK) cascade [147], Wnt/ β -catenin signalling pathway [230], early incarnations of whole-cell models [27, 161], and other cellular signalling, metabolic and regulatory processes and mechanisms [186, 300]. The acceleration methods we implement act only on the control term; the number and form of state equations has no bearing on the mathematical and computational complexity of the acceleration methods. As such, the methods scale excellently with system complexity. In this section we discuss the results presented in §4.5, and draw insights into the convergence behaviour of the FBSM when augmented with acceleration techniques. We highlight opportunities for application of these methods, and outline several avenues for further investigation.

4.6.1 Acceleration outcomes

In evaluating the performance of each acceleration method, we are interested in: (1) how significantly they are able to reduce \mathcal{N} , (2) method robustness, and (3) method accessibility. In this context we use robustness to refer to how consistently the method outperforms the best tuned FBSM over the range of tuning parameters considered. We judge the accessibility of each method based on implementation and conceptual complexity. Overall, we find that the acceleration methods, particularly Anderson and Steffensen, significantly and robustly reduce \mathcal{N} . Anderson Acceleration appears most effective for continuous control, while the Steffensen method appears best for bang-bang control. The Aitken method occasionally outperforms Steffensen, but overwhelmingly the Steffensen method appears to be the better option of the two for the range of parameters we consider. Implementing the Anderson and Steffensen methods introduces challenge beyond that of the underlying FBSM, although it is not prohibitively difficult; particularly with reference to the code where we implement these methods, that we make available on [GitHub](#). Both methods introduce conceptual complexity, perhaps marginally less-so for the Steffensen method due to the similarities it shares with the familiar Newton's method.

We produce heatmaps to visualise the convergence behaviour of the acceleration methods across the range of tuning parameters considered. Figure 4.12 corresponds to the AML continuous control problem, while Figure 4.13 corresponds to the AML bang-bang control problem. Recall that with the tuning of ω that minimises \mathcal{N} , the FBSM with no acceleration requires $\mathcal{N} = 38$ for the AML continuous control problem, and $\mathcal{N} = 34$ for the AML bang-bang control problem. Tuning parameter combinations that reflect a reduction in \mathcal{N} relative to the these FBSM results are shaded in the green spectrum, while worse performing combinations are shaded in the red spectrum. The midpoint of the colour spectra, yellow, corresponds to the FBSM result with the best tuning, without

acceleration. Simulations are terminated when \mathcal{N} exceeds 100; reflecting a combination of tuning parameters that do not yield convergence within this specified maximum. Data supporting these heatmaps, and similar results for the linear control problems are provided in §6 of the supplementary material.

In identifying tuning parameter combinations that yield significant reductions in \mathcal{N} , we are looking for bright green areas in the heatmaps. We assess the robustness of each method by considering whether we observe large contiguous areas in the green spectrum, such as in Figure 4.12(c), indicating robustness, or patchy areas with both green spectrum and red spectrum, such as Figure 4.13(d), suggesting a lack of robustness.

In Table 4.2 we provide our subjective but informed rating of the methods against the criteria of reduction in \mathcal{N} , robustness and accessibility. We consider the continuous and bang-bang control cases separately in terms of reduction in \mathcal{N} and robustness.

Table 4.2: Method comparison

Method	Reduction in \mathcal{N}		Robustness		Accessibility	
	Cts	BB	Cts	BB	Imp	Complexity
FBSM	~	~	✓	✓	✓	✓
Wegstein	~	✓✓	✗	✓	✓	~
Aitken	✓	✓	~	✓	~	~
Steffensen	✓✓	✓✓	✓	✓✓	~	~
Anderson	✓✓	✓	✓	✓	~	✗

We rate the methods considered in this work against key factors such as the reduction in \mathcal{N} that they deliver and how robustly they perform over the range of tuning parameters considered, for both continuous (Cts) and bang-bang (BB) control problems. We also consider how accessible the methods are from the standpoints of ease of implementation (Imp) and conceptual complexity. Methods are rated as being either strongly positive (✓✓), positive (✓), neutral (~), negative (✗) against each aspect.

Despite its conceptual simplicity and straightforward implementation, Wegstein's method is significantly hampered by the difficulty in choosing bounds. If there were a more informed approach for identifying suitable bounds, Wegstein's method could be particularly useful for bang-bang control problems. Due to the effect of ω , intermediate control iterates of the FBSM do not appear bang-bang; as such the bulk of \mathcal{N} are incurred in refining the control about the switching points. Wegstein's method can accelerate this refinement by adaptively setting $q_i = 0$ where appropriate.

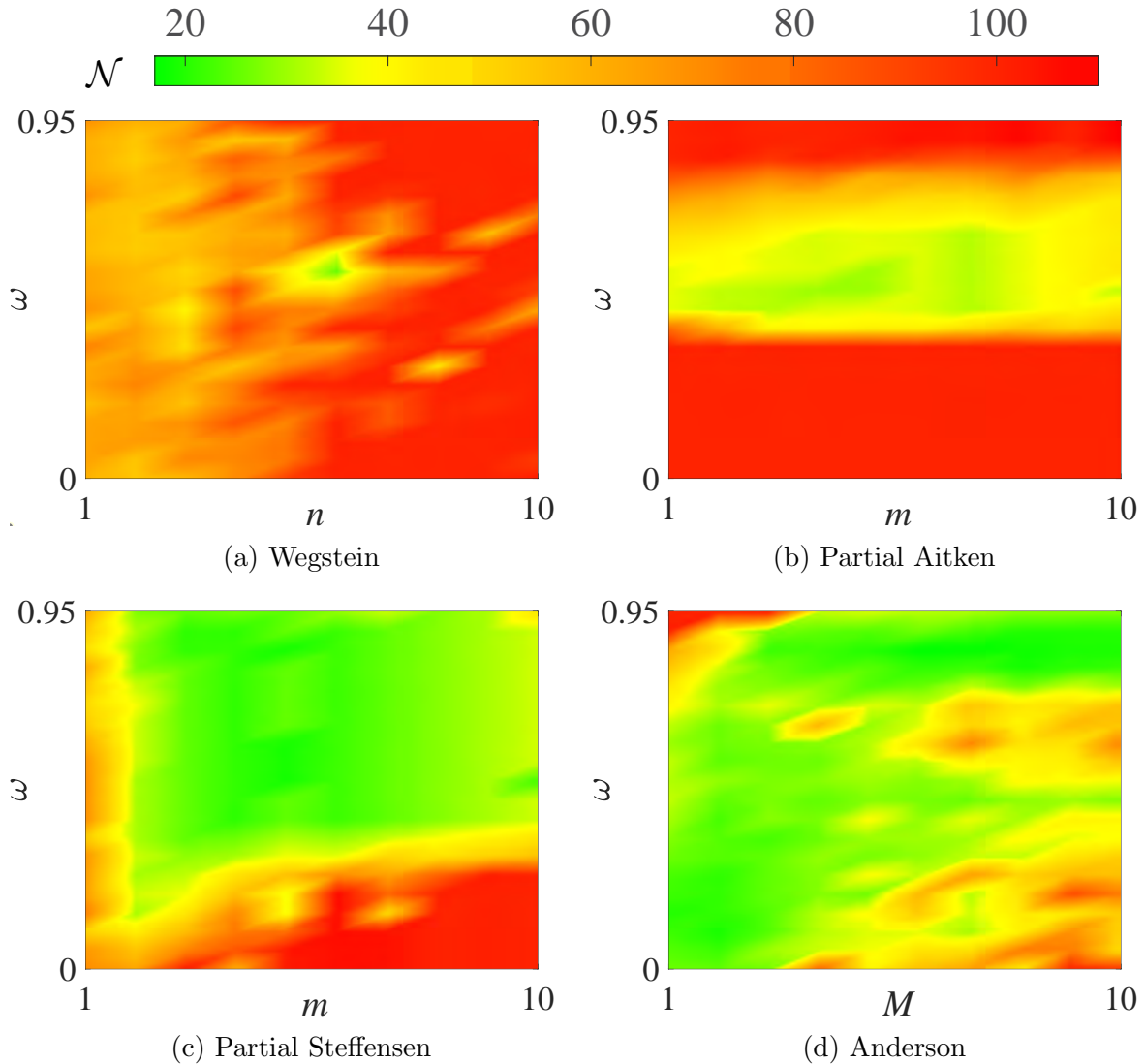


Figure 4.12: This heatmap provides insight into the convergence behaviour of the acceleration methods for the AML continuous control problem. Here we visualise \mathcal{N} against ω and the method specific tuning parameter; n for Wegstein (a), m for partial Aitken (b) and partial Steffensen (c), and M for Anderson Acceleration (d). Tuning parameter combinations requiring $\mathcal{N} = 38$, equivalent to the best tuned FBSM without acceleration, are shaded yellow. Colours in the green-yellow spectrum represent a reduction in \mathcal{N} relative to FBSM without acceleration, while colours in the yellow-red spectrum represent an increase in \mathcal{N} .

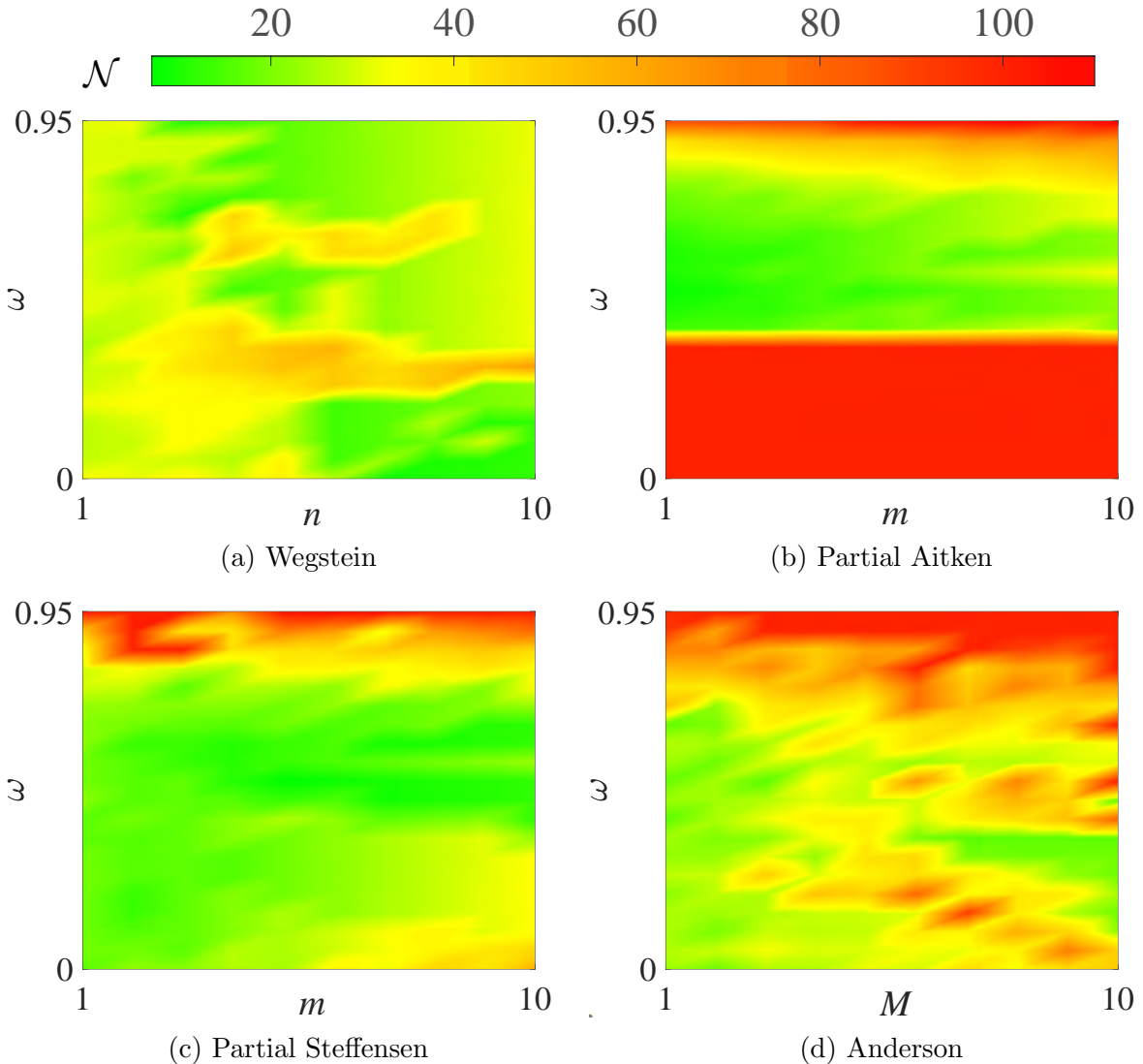


Figure 4.13: This heatmap provides insight into the convergence behaviour of the acceleration methods for the AML bang-bang control problem. Here we visualise \mathcal{N} against ω and the method specific tuning parameter; n for Wegstein (a), m for partial Aitken (b) and partial Steffensen (c), M for Anderson Acceleration (d). Tuning parameter combinations requiring $\mathcal{N} = 34$, equivalent to the best tuned FBSM without acceleration, are shaded yellow. Colours in the green-yellow spectrum represent a reduction in \mathcal{N} relative to FBSM without acceleration, while colours in the yellow-red spectrum represent an increase in \mathcal{N} .

4.6.2 Convergence insights

As outlined in §4.5, the linear model control problems converge with $\omega = 0$. It may at first seem counter-intuitive that Wegstein’s method can improve upon this, given that the computed q in Wegstein’s method acts as a stand-in for ω . There are two aspects of distinction that enable Wegstein’s method to generate improvement in this case; first, while ω is held constant both within the time discretisation and between iterations, the element-wise nature of Wegstein’s method enables each element of the discretisation to have a different value, $q_i, i \in \{0, 1, \dots, N\}$, and q can be updated between iterations; secondly, observing the values of q_i in Wegstein’s method indicates that $q < 0$ can be appropriate. This suggests that $\omega < 0$ could also be used to accelerate the standard implementation of the FBSM. Preliminary investigation suggests that this is true for the linear model, however we do not pursue this further as we expect it to be of limited applicability beyond contrived problems.

We apply the acceleration methods to small nonlinear test systems in §5 of the supplementary material. We know these systems have multiple fixed points; all methods we consider aside from Aitken’s method, in some of our examples, reach different fixed points to fixed point iteration. In contrast, when applied to accelerate control problems, we observe only the Aitken method converging to a result other than the optimal control obtained via the FBSM, as discussed in §4.5. This apparent convergence of the Aitken method to controls that are not optimal is a significant deterrent to using the Aitken method in situations where the optimal control is not known a priori. Outside of this issue with the Aitken method, each acceleration method produces the same optimal control for a given problem. However, they each approach the converged control differently. In Figure 4.14 we plot the control as it converges for the FBSM and acceleration methods. In the code we provide on [GitHub](#), users can view the control iterates of each method as they approach convergence. Visualising these methods as they converge gives insight into how they may be able to arrive at different fixed points; under certain circumstances the accelerated series of iterates may leave the basin of attraction for the fixed point found via fixed point iteration.

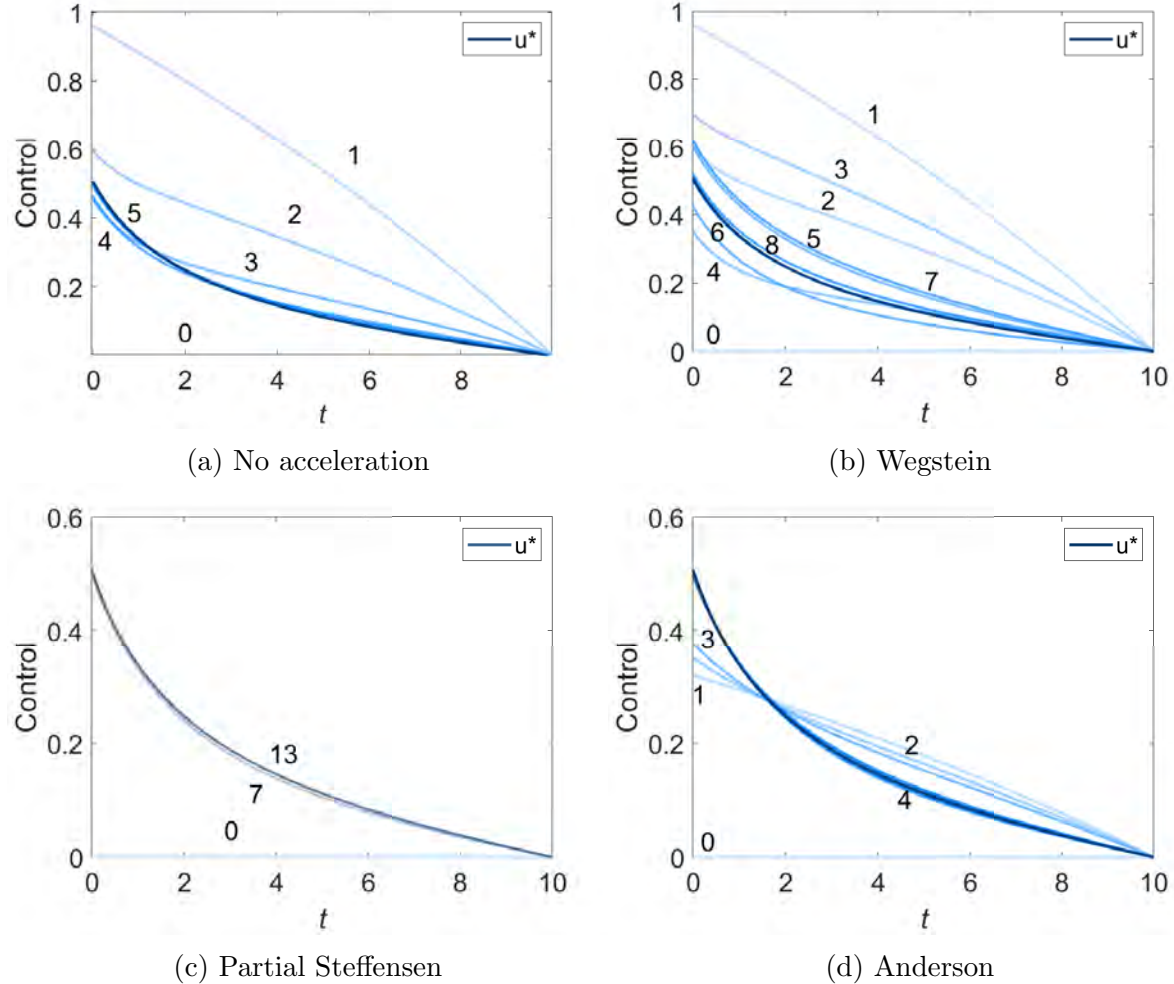


Figure 4.14: Here we observe the iterates of the control in the AML continuous control problem as it converges, for (a) the FBSM with no acceleration, (b) the Wegstein method, (c) the partial Steffensen method and (d) Anderson Acceleration. Initial iterates are shown in light blue, while darker blue denotes later iterates. Results for the Aitken method are not shown as they are visually similar to the Steffensen result. We present the results corresponding to the tuning parameters that minimise \mathcal{N} , outlined in §4.5. Where it is visually distinguishable, we indicate the number of function evaluations corresponding to a particular iterate. While all methods produce the same eventual result for u^* , they follow considerably different series of iterates. Note that the vertical scale in (a) and (b) differs from that of (c) and (d).

4.6.3 Summary and outlook

In this work, we review the theory and implementation of the FBSM for solving TPBVPs that arise from application of PMP in solving optimal control problems. We study a single-variable linear model and a multiple-variable nonlinear model and consider continuous, bang-bang and fixed endpoint control problems. Conceptualising the FBSM as a fixed point iteration, we leverage and adapt existing acceleration methods to significantly and robustly increase the convergence rate of the FBSM for a range of optimal control

problems. The Anderson and partial Steffensen methods appear to perform best, without requiring prohibitive tuning.

Accelerating the convergence of the FBSM, and reducing the importance of appropriately selecting ω for a single control problem, is promising. That said, the real utility of the robust acceleration methods in this work is in application to families of control problems. We provide a glimpse of this benefit through considering fixed endpoint control problems, though other excellent opportunities for application arise due to the uncertainty prevalent in the life sciences. First, it is common for there to be uncertainty around model parameters and structure [96, 128]. In this case solving optimal control problems over several model structures and sets of model parameters provides insight into the sensitivity of the control strategy [45, 134, 236, 278]. Secondly, when performing multi-objective optimisation, a trade-off is made between objectives. For example, in Equation (4.21) we seek to minimise the cumulative negative impact of leukaemia and of the control; parameters a_1 and a_2 weight the relative important of each objective. In practical applications, it is not always clear how to determine these weightings. It can therefore be useful to generate a family of optimal controls that are each optimal for their specific combination of pay-off weighting parameters, akin to a Pareto frontier [10, 164, 204]. Producing these sets of control results benefits significantly from acceleration techniques such as the Anderson and Steffensen methods, where a consistent reduction in \mathcal{N} is obtained without optimal tuning.

In this work multi-objective optimisation is considered in the form of a control problem with a single cost function comprising a scalar combination of state and control terms. More generally, multi-objective optimisation can be formulated as a control problem with a vector-valued cost function, with the goal of minimising each component simultaneously. There are a range of strategies for handling multi-objective optimal control problems formulated in this way, and we direct readers to [256] for a recent and extensive survey.

Here, we have only considered systems subject to a single control. While this is reflective of the vast majority of applications featured in the control literature, there are instances where we are interested in applying multiple controls simultaneously [31, 61, 291]. The FBSM can be readily applied to solve problems with multiple controls [291]; a logical extension of this work is to adapt the acceleration methods or identify suitable alternative methods for accelerating convergence of the FBSM for problems with multiple controls.

Over a range of tuning parameters the Wegstein, Steffensen, and Anderson methods are able to induce convergence where the underlying FBSM fails to converge; such as in the AML control problems with $\omega = 0$. This behaviour has been documented for Anderson acceleration [326] and Wegstein's method [129] when applied to standard fixed point iteration problems. This presents an opportunity for future exploration, in identifying control problems that cannot be solved via the FBSM for any ω , and attempting to produce solutions using these acceleration techniques.

The examples we consider in this work include a variety of control problem formulations that arise in systems biology. However, it is worth noting that the examples are not exhaustive. Further challenges can be introduced; either through the formulation of the control problem, or as a result of the behaviour of the underlying system. Examples of such challenges include control problems with singular arcs, path constraints, multiple local solutions, discontinuous dynamics and sensitivity to the initial guess of the control [319]. These challenges can introduce numerical difficulties, and complications in terms of the optimal control theory; for example, control problems with singular arcs typically require additional necessary conditions for optimality beyond those obtained from the PMP [191]. A thorough assessment of the appropriateness of the FBSM as a method for solving control problems with such complications is an avenue for further investigation. We stress that the acceleration techniques that we develop and survey in this work are able to accelerate convergence when compared to a naive FBSM implementation, and in some cases induce convergence where the naive FBSM fails to converge. We anticipate that these trends will persist if these acceleration techniques are applied to appropriately conceived implementations of the FBSM for the various complications outlined here.

Acknowledgements

JAS acknowledges support from the Australian Government Research Training Program and the AF Pillow Applied Mathematics Trust. JAS and KB acknowledge support from the Australian Centre of Excellence for Mathematical and Statistical Frontiers (CE140100049). MJS is supported by the Australian Research Council (DP200100177).

We also thank two anonymous referees for their helpful comments.

Chapter 5

Parameter estimation and uncertainty quantification using information geometry

Statement of Contribution of Co-Authors

The authors listed below have certified that:

1. they meet the criteria for authorship and that they have participated in the conception, execution, or interpretation, of at least that part of the publication in their field of expertise;
2. they take public responsibility for their part of the publication, except for the responsible author who accepts overall responsibility for the publication;
3. there are no other authors of the publication according to these criteria;
4. potential conflicts of interest have been disclosed to (a) granting bodies, (b) the editor or publisher of journals or other publications, and (c) the head of the responsible academic unit, and
5. they agree to the use of the publication in the student's thesis and its publication on the [QUT's ePrints site](#) consistent with any limitations set by publisher requirements.

In the case of this chapter: Chapter 5

Please state the publication title and date of publication or status:

Parameter estimation and uncertainty quantification using information geometry. Accepted for publication in *Journal of the Royal Society Interface* (2022) [in press].

Contributor	Statement of contribution*
Jesse A Sharp	Designed the study, implemented the computational algorithms, generated and interpreted results, produced figures, drafted the manuscript, revised the manuscript. 
08/12/2021	
AP Browning	Advised on implementation of computational algorithms, interpreted results, provided comments on the manuscript.
K Burrage	Designed the study, supervised the research, interpreted the results, and provided comments on the manuscript.
MJ Simpson	Designed the study, supervised the research, interpreted the results, and provided comments on the manuscript.

Principal Supervisor Confirmation

I have sighted email or other correspondence from all Co-authors confirming their certifying authorship. (If the Co-authors are not able to sign the form please forward their email or other correspondence confirming the certifying authorship to the GRC).

Professor Matthew Simpson
Name


Signature

11/12/2021
Date

Article published 2022 in Journal of the Royal Society Interface.

Sharp JA, Browning AP, Burrage K, Simpson MJ (2022). Parameter estimation and uncertainty quantification using information geometry. *Journal of the Royal Society Interface* [in press]. [arXiv:2111.12201](https://arxiv.org/abs/2111.12201).

Abstract

In this work we: (1) review likelihood-based inference for parameter estimation and the construction of confidence regions; and, (2) explore the use of techniques from information geometry, including geodesic curves and Riemann scalar curvature, to supplement typical techniques for uncertainty quantification such as Bayesian methods, profile likelihood, asymptotic analysis and bootstrapping. These techniques from information geometry provide data-independent insights into uncertainty and identifiability, and can be used to inform data collection decisions. All code used in this work to implement the inference and information geometry techniques is available on [GitHub](https://github.com/joshuasharp/information-geometry-inference).

5.1 Introduction

Computational and mathematical models are versatile tools, providing valuable insight into complex processes in the life sciences. Models can further our understanding of mechanisms and processes, facilitate development and testing of hypotheses, guide experimentation and data collection and aid design of targeted interventions [52, 235, 291, 327, 331]. However, there are considerable challenges associated with calibrating these models to data. For example, models need to be sufficiently sophisticated to adequately reflect the behaviour of the underlying system, while ideally admitting *identifiable* parameters that are interpretable, and that can be estimated from available or obtainable data [116, 199]. Further, available data can be limited and often is not collected for the express purpose of parameter estimation; data may be noisy, incomplete, or may not provide the level of detail or sample size required to obtain precise parameter estimates [114, 145, 286, 315, 325].

Due to the challenges associated with parameter estimation, we are often interested not only in point-estimates, but also the associated uncertainty [89, 216, 329]. Quantifying and interpreting this uncertainty establishes a level of confidence in parameter estimates; and by extension, in the insights derived from the model. Further, this uncertainty quantification can give insights into *identifiability*: whether the information in a data set can be used to infer unique or sufficiently precise parameter estimates for a given model [299]. Often we are concerned with both *structural identifiability* and *practical identifiability* [28, 144, 298, 323, 324]. Structural identifiability can be thought of as a property of the underlying model structure and parameterisation; and refers to whether it is theoretically possible to determine unique parameter values, given an infinite amount of perfect noise-free data [50, 299, 340]. Structural identifiability requires that unique parameter combinations precipitate distinct model outputs. Structural identifiability occurs if and only if the Fisher information matrix, which we soon discuss, is of full rank [172]. In contrast, practical identifiability is less well defined, and depends on the quality and quantity of data available and existing knowledge of the parameters [50]. In the context of profile likelihood methods, practical non-identifiability can manifest as contours of the log-likelihood function that do not admit closed levels; the log-likelihood does not reach a predetermined statistical threshold within the physical parameter regime [200]. If a model is not structurally identifiable, it cannot be practically identifiable.

Practical non-identifiability may be addressed either through improving data quantity or data quality [50, 298]. Data quantity can be improved by increasing the number of observations; such as by making additional observations at different time points. Data quality may be improved through reducing the noise present in the data, for example by obtaining a dataset with reduced measurement error or repeating measurements across identically-prepared experiments [49, 276]. It is also possible to resolve practical non-identifiability through incorporating existing knowledge about parameters, such as

physical constraints or information established in previous studies; or specifically in the Bayesian inferential framework, through informative priors [119]. Addressing structural non-identifiability is more challenging, for example this may necessitate a change to the underlying model structure [123, 276, 323].

Uncertainty quantification takes many forms, with common examples including Bayesian methods, profile likelihood, asymptotic analysis and bootstrapping [114, 118, 231, 325, 330]. Bayesian methods are widely used for parameter estimation and uncertainty quantification, with Bayesian computation being employed throughout the mathematical biology and systems biology literature. Broadly, these methods involve repeated sampling of parameter values from a prior distribution and invoking Bayes theorem to approximate the *posterior* distribution; the posterior distribution describes knowledge about the probability of parameter combinations after taking into account the observed data and any prior information [50, 330]. Well-known approaches include rejection sampling, Markov Chain Monte Carlo (MCMC) and sequential Monte Carlo (SMC) or particle filtering. In rejection sampling, parameters drawn from a prior distribution are used to simulate the model; simulated data is compared to the observed data based on some distance metric, and if this metric is within a prescribed tolerance, the parameters are accepted as a sample from the approximate posterior distribution, otherwise they are rejected [118, 183]. Rejection sampling can be computationally expensive as the rejection rate can be significant with an uninformative prior [197, 268]. In MCMC the parameter space is sampled following a Markov chain—a memoryless stochastic process where the probability of the next state depends only on the previous state [255]—with a stationary distribution corresponding to the posterior distribution. Samples are accepted or rejected based on the relative likelihood between the current configuration and proposed sample [20, 202, 315, 330]. For SMC, rejection sampling can be used to produce an initial coarse approximation of the posterior distribution. This coarse approximation informs further (sequential) sampling efforts in the region of parameter space corresponding to high likelihood, reducing the rejection rate when compared to rejection sampling alone [151, 197, 315]. MCMC and SMC approaches can offer significantly improved efficiency in comparison to rejection sampling [197, 330], but both involve specifying hyperparameters and these choices are not always obvious.

In situations where the likelihood function is intractable or not easily evaluated, Approximate Bayesian Computation (ABC) provides a range of related likelihood-free methods for estimating posterior distributions [308]. Popular approaches include ABC rejection sampling [151, 179, 268, 308, 336], ABC MCMC [217, 295, 302], and ABC SMC [197, 315]; we do not focus on ABC methods here, as the approaches we explore in this work are applied to problems with tractable likelihoods. We direct interested readers to the wealth of information in the references provided.

For Bayesian inference methods, uncertainty can be quantified based on features such

as the coefficient of variation and probability intervals of the posterior distribution [325]. There are a variety of approaches for uncertainty quantification for frequentist inference methods. In profile likelihood, a parameter of interest is varied over a fixed set of values, while re-estimating the other parameters; providing insight into identifiability and uncertainty [52]. In asymptotic analysis, confidence regions can be constructed based on local information via a Taylor expansion of the Fisher information about the maximum likelihood estimate (MLE) [114, 200]. In bootstrapping, data is repeatedly sampled and parameter estimates are computed from the samples; these estimates are used to construct confidence intervals [231].

Through the geometric approaches we review in this work, more akin to traditional approaches for sensitivity analysis [216, 229, 344], we explore the curvature of the parameter space through an information metric induced by the likelihood function. Whereas likelihood-based approximate confidence regions provide insight into specific level curves of the likelihood function—the levels of which depend on an asymptotic large sample argument [255]—this geometric approach provides insight into the *shape* and sensitivity of the parameter space. For example, we compute *geodesic curves* that describe the geometric relationship between distributions with different parameters [228]; and explore the *scalar curvature* throughout parameter spaces. We review ideas from *information geometry* in the context of inference and uncertainty quantification; not with a view to replacing established methods such as profile likelihood, asymptotic analysis, bootstrapping and Bayesian methods [114, 231, 325, 330], but rather to supplement them where additional insight may prove useful.

Information geometry is a branch of mathematics connecting aspects of information theory including probability theory and statistics with concepts and techniques in differential geometry [11]. In this exposition we seek to outline only the key concepts required to understand the information geometric analysis in this work. However, we note that more thorough and rigorous treatments of the concepts introduced in this section, and mathematical foundations of information geometry, can be found in texts and surveys such as [11, 64, 239]. Central to the information geometry ideas explored in this work is the concept of a *statistical manifold*; an abstract geometric representation of a distribution space, or a Riemannian manifold consisting of points that correspond to probability distributions, with properties that we later discuss. For example, the set of normal distributions parameterised by mean, μ , and standard deviation, $\sigma > 0$:

$$p(x; \mu, \sigma) = \frac{1}{\sigma\sqrt{2\pi}} \exp\left[-\frac{(x - \mu)^2}{2\sigma^2}\right], \quad x \in \mathbb{R}, \quad (5.1)$$

can be thought of as a two-dimensional surface with coordinates (μ, σ) [64]. In this work we will use $\boldsymbol{\theta}$ to refer to the parameters of interest that we seek to estimate; i.e. $\boldsymbol{\theta} = (\mu, \sigma)$ for the univariate normal distribution with unknown mean and standard deviation. In

Section 5.3, we consider various combinations of components of $\boldsymbol{\theta}$; including model parameters, variability in observations characterised by a separate observation noise model, and initial conditions associated with a differential equation-based process model. When referring to all possible parameters, rather than solely the unknown parameters to be estimated, we denote this Θ .

In applications where we consider multiple data sets, or different candidate models or candidate parameter values, we are interested in methods of comparing distributions. A well-known measure for comparing a probability distribution, P , to another, Q , is the Kullback-Leibler (KL) divergence from P to Q , denoted $\mathcal{D}_{KL}(P, Q)$ [99]. The KL divergence, or *relative entropy*, can be computed as [99]:

$$\mathcal{D}_{KL}(P, Q) = \int p(x) \log \frac{p(x)}{q(x)} dx = \mathbb{E}_p \left[\log \frac{p(x)}{q(x)} \right], \quad (5.2)$$

where $p(x)$ and $q(x)$ are the respective probability density functions of P and Q . Consider two sets of parameters, $\boldsymbol{\theta}^*$ and $\hat{\boldsymbol{\theta}}$; let $\log(p(x)) = \log(p(x|\boldsymbol{\theta}^*)) = \ell(\boldsymbol{\theta}^*)$ and $\log(q(x)) = \log(p(x|\hat{\boldsymbol{\theta}})) = \ell(\hat{\boldsymbol{\theta}})$, where $\ell(\cdot)$ denotes the log-likelihood, discussed in detail in Section 5.2. If $p(x|\boldsymbol{\theta}^*)$ is the true distribution and $p(x|\hat{\boldsymbol{\theta}})$ is our estimate, then (5.2) is the expected log-likelihood ratio and the relationship between MLE and KL divergence becomes evident; maximising the likelihood is equivalent to minimising KL divergence [234].

An issue with the KL divergence is asymmetry; $\mathcal{D}_{KL}(P, Q) \neq \mathcal{D}_{KL}(Q, P)$. It is not necessarily obvious in a given situation which orientation of the KL divergence will most appropriately inform decisions such as model selection [288]. Due to the aforementioned asymmetry, and its failure to satisfy the triangle inequality, the KL divergence is not a *metric*—it is not a measure of distance in a differential geometric sense—on a given manifold [64]. One means of addressing this asymmetry is through devising various symmetrised forms of the KL divergence to inform model selection criteria [288]. Alternatively, we may approach the issue from a geometric perspective. It is natural to think of geometry in terms of objects or shapes in Euclidean, or *flat*, space. Euclidean space is characterised by orthonormal basis vectors; the standard basis in three-dimensions being $\mathbf{e}_1 = (1, 0, 0)^T$, $\mathbf{e}_2 = (0, 1, 0)^T$, $\mathbf{e}_3 = (0, 0, 1)^T$, where superscript T denotes the transpose. In the n -dimensional orthonormal basis, we can compute the squared infinitesimal distance between the points \mathcal{S} and $\mathcal{S} + ds$, where ds has components ds_i , as [12]:

$$\|ds\|^2 = \sum_{i=1}^n (ds_i)^2. \quad (5.3)$$

Differential geometry extends ideas from Euclidean geometry to manifolds. Manifolds are topological spaces that resemble flat space about each individual point in the space; they can be considered *locally flat*, but have a different topology globally. The sphere is

a classic example, whereby points on the surface are locally topologically equivalent to two-dimensional Euclidean space, but globally the sphere is curved and has a compact topology; it is bounded and closed [15]. In particular, we are interested in Riemannian manifolds; differentiable manifolds—sufficiently locally smooth that our typical notions of calculus remain valid—upon which we are able to measure geometric quantities such as distance, through the existence of a Riemannian metric on the tangent space of the manifold, that generalises the notion of an inner product from Euclidean geometry [189].

A Riemannian metric is a smooth covariant 2-tensor field; on a differentiable manifold M , the Riemannian metric is given by an inner product on the tangent space of the manifold, $T_p M$, which depends smoothly on the base point p [156, 189]. A tangent space can be thought of as a multidimensional generalisation of a tangent plane to a three-dimensional surface. Each point p on a manifold is associated with a distinct tangent space. An n -dimensional manifold has infinitely many n -dimensional tangent spaces; the collection of these tangent spaces is referred to as the tangent bundle of the manifold. On a manifold each tangent space can have different basis vectors, in contrast to Euclidean geometry where tangent vectors at any point have the same basis vectors. A consequence of the distinct basis vectors of tangent spaces on manifolds is that tangent vectors at different points on the manifold cannot be directly added or subtracted. Introducing an *affine connection* on the manifold connects nearby tangent spaces, such that the manifold looks infinitesimally like Euclidean space, facilitates differentiation of tangent vectors [13]. Formally, we introduce the unique, torsion free Levi-Civita connection, ∇ ; an affine connection on the Riemannian manifold that yields isometric parallel transport, such that inner products between tangent vectors, defined by the metric, are preserved [121]. The coefficients of this connection are the Christoffel symbols, which we discuss further in Section 5.2. Readers are directed to [13, 23, 121] for further detail regarding the Levi-Civita connection, and how it relates to other concepts discussed in this work. A manifold equipped with such a connection and a Riemann metric is a Riemann manifold.

Metric tensors can be thought of as functions that facilitate computation of quantities of interest such as distances on a manifold. A metric matrix with elements g_{ij} , $G = [g_{ij}]$, is positive definite and symmetric [189]. The metric matrix defines an inner product between u and v as $\langle u, v \rangle_G = u^T G v$, and the length of u as $\|u\|_G = \sqrt{\langle u, u \rangle_G}$ [80]. On a Riemannian manifold we consider a generalisation of the square of the infinitesimal distance element (5.3), appropriate for non-orthonormal bases [12], given by

$$\|ds\|^2 = \sum_{i,j=1}^n g_{ij} ds_i ds_j.$$

Foundational to information geometry is the notion that the Fisher information matrix defines a Riemannian metric on a statistical manifold [274]. The Fisher information,

denoted $\mathcal{I}(\boldsymbol{\theta})$, describes the expected curvature of the log-likelihood and gives information about the precision and variance of parameter estimates. Therefore, $\mathcal{I}(\boldsymbol{\theta})$ can incorporate information about both the curvature induced by the data through the observation process, as well as the curvature induced by parameter sensitivities through a mathematical model that links parameter estimates to data. In the examples we consider, deterministic model predictions are connected to the data through the probabilistic observation process, yielding a general formula for the Fisher information [190]:

$$\mathcal{I}(\boldsymbol{\theta}) = N \mathbf{J}(\boldsymbol{\theta})^T \underbrace{\mathcal{O}(\mathbf{m})}_{\substack{\text{Curvature induced} \\ \text{by parameter sensitivities}}} \underbrace{\mathbf{J}(\boldsymbol{\theta})}_{\substack{\text{Curvature induced} \\ \text{by data}}}. \quad (5.4)$$

Here, we denote $\mathcal{O}(\mathbf{m})$ the Fisher information matrix of the observation process, given a model, $\mathbf{m} = \mathbf{m}(\boldsymbol{\theta})$, where $\mathbf{J}(\boldsymbol{\theta})$ is the Jacobian of the model with respect to the parameters. The number of independent, identically distributed (iid) observations in the likelihood is given by N ; with statistical independence, the Fisher information is additive [112].

Expression (5.4) highlights a link between sensitivity analysis, structural identifiability and practical identifiability [209]. For sensitivity analysis and structural identifiability, only the curvature of the model space is studied through $\mathbf{J}(\boldsymbol{\theta})$. In practical identifiability analysis, the sensitivity of the model is linked to the data through an observation process, and the curvature of the parameter space is studied through, for example, $\mathcal{I}(\boldsymbol{\theta})$.

In this review, we present and explore fundamental techniques in inference and information geometry, including confidence regions, geodesic curves, and scalar curvature. Through application to standard distributions and canonical models in the life sciences, including population growth processes and epidemic transmission, we demonstrate how these techniques can be combined to provide additional insights into parameter estimation and uncertainty quantification. Starting with parameter estimates inferred from real data, we use mathematical models to generate synthetic data with different numbers of observations and at varying points in time, to explore the impact that these aspects have on the inference and information geometry results. Specifically, we consider univariate and multivariate normally distributed observation processes; linear, exponential and logistic models of population growth; and the classical susceptible, infectious, recovered (SIR) model of epidemic transmission [97, 166]. Although the examples considered in this work are based on ODE process models drawn from the life sciences, the techniques we consider are general and can be applied in the context of parameter estimation and uncertainty quantification in any discipline and for other model formulations.

By considering standard distributions and canonical models we are able to explore the inference and information geometry techniques through a series of examples with

incremental increases in complexity. Through this approach, we consider the techniques as applied to both linear and nonlinear ordinary differential equation (ODE) models, coupled nonlinear ODE systems, and data with both one and many observed variables. We consider cases where model parameters, initial conditions, and the standard deviation of the data, are to be estimated from data. The inference and information geometry techniques considered in this work are general, and can be applied far more widely than the examples we consider here. To improve the accessibility of these methods, code used to implement the inference and information geometry techniques applied in this work is written in the open source Julia language [41]; and is available on [GitHub](#).

In Section 5.2 we describe the inference and information geometry methods implemented in this work, including maximum likelihood estimation, profile-likelihood based approaches, geodesic curves and scalar curvature calculations. Results of applying these techniques to univariate and multivariate normal distributions, linear, exponential and logistic growth models and the SIR model, are presented in Section 5.3. We discuss the utility of these techniques, and identify opportunities for extension and further consideration in Section 5.4.

5.2 Methods

Here we describe the parameter inference and information geometry methods used to produce results in this work. We also describe the numerical methods used to implement these techniques. The techniques we discuss in this section readily generalise to parameter spaces with an arbitrary number of dimensions, so we discuss the techniques here for arbitrary dimensions. However, for the sake of exploring the techniques through visualisation in Section 5.3, we restrict ourselves to two-dimensional manifolds. In context, this means we consider only two parameters to be inferred in any given example, treating other parameters as known and fixed; for example, as if they are drawn from prior knowledge or pre-estimated.

Although we consider deterministic mathematical models, data used to estimate parameters can exhibit significant variability. We follow a standard approach and assume that the mathematical models describe the expected behaviour, and that our observations are normally distributed about this expected behaviour [144]. This allows us to think about a statistical model, $\mathbf{m}(\boldsymbol{\theta}, t)$, in terms of its expected behaviour, $\boldsymbol{\mu}$ and the standard deviation of the observations, σ .

$$\mathbf{m}(\boldsymbol{\theta}, t) = (\boldsymbol{\mu}(\boldsymbol{\theta}, t), \sigma(\boldsymbol{\theta}, t)).$$

We restrict the examples in this work to cases where σ is constant; setting $\sigma(\boldsymbol{\theta}, t) = \sigma$.

In this work we focus on the most commonly employed additive noise model [144, 276, 298, 315, 331]. Additive noise implies that the variance of the data is independent of the mean behaviour. In cases where variance scales with mean behaviour, multiplicative noise may be more appropriate. The information geometric methods presented here are applicable in cases where the Fisher information can be obtained; including models with multiplicative noise, and parameter or time dependent standard deviation. However, obtaining the Fisher information is a separate challenge, and can be difficult when considering different process and noise models.

5.2.1 Parameter inference

In this work, parameter estimates are inferred from data following a standard maximum log-likelihood based approach. We make observations at L time-points, $T = (t_1, t_2, \dots, t_L)$. At each time-point we make N observations, $\mathcal{X} = (\mathbf{x}_1(T), \mathbf{x}_2(T), \dots, \mathbf{x}_N(T))$. With this notation the log-likelihood function is

$$\ell(\boldsymbol{\theta}; \mathcal{X}) = \sum_{j=1}^L \sum_{i=1}^N \log f(\mathbf{x}_i(t_j); \boldsymbol{\mu}(\boldsymbol{\theta}, t_j), \sigma^2), \quad (5.5)$$

where $f(\mathbf{x}; \boldsymbol{\mu}, \sigma^2)$ is the probability density function associated with our observation process. In this work we hold N constant across time-points, though non-constant N is easily incorporated into Equation (5.5) as N_j . The likelihood function can be thought of as the joint probability density of all the data for a given set of parameters. In examples where σ is unknown, we treat σ as an element of $\boldsymbol{\theta}$, but note that the expected model behaviour is independent of σ . The MLE is the point estimate, $\hat{\boldsymbol{\theta}}$, that satisfies

$$\hat{\boldsymbol{\theta}} = \arg \max_{\boldsymbol{\theta}} \ell(\boldsymbol{\theta}; \mathcal{X}), \quad (5.6)$$

where $\arg \max(\cdot)$ returns the argument, $\boldsymbol{\theta}$, that maximises $\ell(\boldsymbol{\theta}; \mathcal{X})$ in (5.6). The associated maximum log-likelihood is $\ell(\hat{\boldsymbol{\theta}})$. MLEs of the parameters of interest are obtained by solving (5.6) numerically as outlined later in Section 5.2. For an iid sample from a univariate normal distribution, $\mathcal{N}(\mu, \sigma^2)$, maximising the likelihood function of μ is equivalent to performing least-squares estimation [50], although having access to the likelihood function facilitates uncertainty quantification.

Presenting confidence regions alongside MLEs enhances our interpretation of the likelihood function, while still acknowledging that the estimates carry uncertainty [255]. We apply a probability-based log-likelihood approach when constructing confidence regions for model parameters. From Wilks' theorem [255], asymptotically as $N \rightarrow \infty$, an ap-

proximate α -level confidence region is given by

$$\left\{ \boldsymbol{\theta} : \ell(\boldsymbol{\theta}) \geq \ell(\hat{\boldsymbol{\theta}}) - \frac{\Delta_{\nu,\alpha}}{2} \right\}, \quad (5.7)$$

where $\Delta_{\nu,\alpha}$ is the α th-quantile of the $\chi^2(\nu)$ distribution; with ν degrees of freedom [52]. In this work the degrees of freedom correspond to the number of parameters of interest, i.e. $\nu = \dim(\boldsymbol{\theta})$. To enable comparison between different data sets and models in Section 5.3, we consider the normalised log-likelihood, $\hat{\ell}(\boldsymbol{\theta}) = \ell(\boldsymbol{\theta}) - \ell(\hat{\boldsymbol{\theta}})$. This forms the basis for log-likelihood ratio based hypothesis tests [255]. The normalised log-likelihood is zero at the MLE: $\hat{\ell}(\hat{\boldsymbol{\theta}}) \equiv 0$.

5.2.2 Information geometry

As outlined in Section 5.1, the Fisher information describes the curvature of the log-likelihood function. It describes how much information a random variable, X , contains about a parameter, $\boldsymbol{\theta}$. For unbiased estimators, the inverse of the Fisher information provides a lower bound on the covariance matrix, via the Cramer-Rao inequality [333]. Formally, the Fisher information is the covariance of the score, where the score is defined as the partial derivative of the log-likelihood with respect to $\boldsymbol{\theta}$ [190, 255]. The Fisher information matrix can be written as [163, 255]:

$$[\mathcal{I}(\boldsymbol{\theta})]_{ij} = \mathbb{E}_X \left[\left(\frac{\partial}{\partial \theta_i} \log f(X; \boldsymbol{\theta}) \right) \left(\frac{\partial}{\partial \theta_j} \log f(X; \boldsymbol{\theta}) \right) \right]. \quad (5.8)$$

We can recover our expression for the Fisher information in Equation (5.4) from Equation (5.8), by considering how Equation (5.8) changes under reparameterisation, and via application of the chain-rule for differentiation [190].

With observations at L unique times, $T = (t_1, t_2, \dots, t_L)$, we can think of a model as a mapping between the parameters and the outputs that we can observe:

$$\mathbf{m}(\boldsymbol{\theta}) : \boldsymbol{\theta} \rightarrow \left((\boldsymbol{\mu}_1(\boldsymbol{\theta}, t_1), \sigma), (\boldsymbol{\mu}_2(\boldsymbol{\theta}, t_2), \sigma), \dots, (\boldsymbol{\mu}_L(\boldsymbol{\theta}, t_L), \sigma) \right). \quad (5.9)$$

We consider some examples where σ is unknown and is estimated as a part of the analysis; in these instances $\sigma \in \boldsymbol{\theta}$, however we express σ explicitly in the mapping presented in (5.9) to emphasise that it behaves somewhat differently to a model parameter. The expected behaviour of the model does not depend on σ , and variability in the data maps directly to σ . In all the examples we consider, σ is constant. This could be extended to incorporate variability dependent on the expected behaviour, for example logistic growth with standard deviation that depends on the population density [53]. In the mapping, this could be expressed as $\sigma(\boldsymbol{\mu}(\boldsymbol{\theta}, t))$.

Following Equation (5.4), we can form the Fisher information as a combination of the Fisher information matrix of the observation process, $\mathcal{O}(\mathbf{m})$, and the Jacobian of the model with respect to the parameters, $\mathbf{J}(\boldsymbol{\theta})$. From (5.9), with ν unknown parameters ($\dim(\boldsymbol{\theta}) = \nu$), we can view the model Jacobian as

$$\mathbf{J}(\boldsymbol{\theta}) = \begin{pmatrix} \frac{\partial \boldsymbol{\mu}_1}{\partial \theta_1} & \frac{\partial \boldsymbol{\mu}_1}{\partial \theta_2} & \cdots & \frac{\partial \boldsymbol{\mu}_1}{\partial \theta_\nu} \\ \frac{\partial \boldsymbol{\mu}_1}{\partial \sigma} & \frac{\partial \boldsymbol{\mu}_1}{\partial \sigma} & \cdots & \frac{\partial \boldsymbol{\mu}_1}{\partial \sigma} \\ \frac{\partial \boldsymbol{\mu}_2}{\partial \theta_1} & \frac{\partial \boldsymbol{\mu}_2}{\partial \theta_2} & \cdots & \frac{\partial \boldsymbol{\mu}_2}{\partial \theta_\nu} \\ \frac{\partial \boldsymbol{\mu}_2}{\partial \sigma} & \frac{\partial \boldsymbol{\mu}_2}{\partial \sigma} & \cdots & \frac{\partial \boldsymbol{\mu}_2}{\partial \sigma} \\ \vdots & \vdots & \ddots & \vdots \\ \frac{\partial \boldsymbol{\mu}_j}{\partial \theta_1} & \frac{\partial \boldsymbol{\mu}_j}{\partial \theta_2} & \cdots & \frac{\partial \boldsymbol{\mu}_j}{\partial \theta_\nu} \\ \frac{\partial \boldsymbol{\mu}_j}{\partial \sigma} & \frac{\partial \boldsymbol{\mu}_j}{\partial \sigma} & \cdots & \frac{\partial \boldsymbol{\mu}_j}{\partial \sigma} \end{pmatrix}. \quad (5.10)$$

Noting that we are taking σ to be independent of model parameters, all of the partial derivatives of σ in (5.10) are zero, except the case where $\theta_i = \sigma$, for some $i \in \{1, 2, \dots, \nu\}$, whereby the corresponding partial derivative is unity. Given a set of N normally distributed observations at a single point in time, we have an observation process characterised by a mean, μ , and standard deviation, σ . The Fisher information for such an observation is given by

$$\mathcal{I}(\mu, \sigma) = \frac{N}{\sigma^2} \mathbf{D}, \quad \text{where } \mathbf{D} = \text{diag}(1, 2). \quad (5.11)$$

This can be verified by applying Equation (5.8) to (5.1). For data at L time-points with N_1, N_2, \dots, N_L observations at each time, with constant standard deviation, the Fisher information for the observation process is a $2L \times 2L$ (block) diagonal matrix:

$$\mathcal{I}(\mu, \sigma) = \text{diag} \left(\frac{N_1}{\sigma^2} \mathbf{D}, \frac{N_2}{\sigma^2} \mathbf{D}, \dots, \frac{N_L}{\sigma^2} \mathbf{D} \right). \quad (5.12)$$

Similarly, for a model with M species, where we have observations of all M species at only one time-point we recover Fisher information in the form of (5.12). For observations of M species at L time-points we form a $2LM \times 2LM$ (block) diagonal matrix from (5.12). Assuming a constant standard deviation, for the computations in this work we could more simply express (5.12) as the diagonal matrix $\text{diag}(N_1/\sigma^2, N_2/\sigma^2, \dots, N_L/\sigma^2, 2 \sum N_i/\sigma^2)$, where $\sum N_i$ is the total number of observations contributing to our information regarding the standard deviation, and the factor of two comes from (5.11). In this case, the model Jacobian as presented in (5.10) is modified such that only the final row includes the partial derivatives with respect to the standard deviation.

Before outlining specific techniques of information geometry, we present a conceptual example to develop some intuition for information geometric concepts. Consider the manifold corresponding to the family of univariate normal distributions parameterised

by mean, μ , and standard deviation, $\sigma > 0$. Let $P \sim \mathcal{N}(\mu_1, \sigma)$ and $Q \sim \mathcal{N}(\mu_2, \sigma)$ be two normal distributions. Geometrically speaking, increasing σ reduces the distance between P and Q ; this corresponds to a contraction of the space. Conversely, decreasing the variance dilates the space; as $\sigma \rightarrow 0$, the Fisher information, $\text{diag}(1/\sigma^2, 1/\sigma^2)$, is degenerate and the distance between P and Q tends to infinity.

Equipped with the Fisher information, we may begin to explain some foundational ideas from information geometry; including geodesic curves, geodesic distances between distributions for statistical models, and scalar curvature [11]. We denote the elements of the Fisher information as $\mathcal{I}(\boldsymbol{\theta}) = [g_{ij}(\boldsymbol{\theta})]$, and its inverse $\mathcal{I}(\boldsymbol{\theta})^{-1} = [g^{ij}(\boldsymbol{\theta})]$, where $\boldsymbol{\theta} = (\theta_1, \theta_2, \dots, \theta_\nu)$ are the coordinates of the manifold. While uncertainty in estimates is typically characterised by the Fisher information at only a single point, based on the Cramer-Rao inequality [333], information geometry utilises the Fisher information throughout the parameter space. A Riemann geodesic is a curve forming the shortest path between two points in a Riemannian manifold [14]. The length of this shortest curve is referred to as the Fisher or Fisher-Rao distance [259]. We soon discuss a relationship between confidence regions and the length of geodesic curves. Informally, with greater information supporting a MLE, coinciding with an increase in its relative likelihood, confidence regions tighten. This also corresponds to a dilation of the parameter manifold; thereby increasing the geodesic distance between the MLE and other parameter combinations, reflecting their relatively reduced likelihood.

A curve $\mathbf{z}(s)$, parameterised by s , connecting the points $\mathbf{z}_1 = \mathbf{z}(s_1)$ and $\mathbf{z}_2 = \mathbf{z}(s_2)$ on a Riemannian manifold, has length [156]:

$$L(\mathbf{z}) = \int_{s_1}^{s_2} \sqrt{\sum_{i,j=1}^n \left(g_{ij}(\boldsymbol{\theta}(\mathbf{z}(s))) \frac{d\theta_i(\mathbf{z}(s))}{ds} \frac{d\theta_j(\mathbf{z}(s))}{ds} \right)} ds. \quad (5.13)$$

A Riemann geodesic is a curve that minimises $L(\mathbf{z})$ (5.13), such that the distance between two points on a Riemannian manifold is given by the curve that satisfies

$$d(\mathbf{z}_1, \mathbf{z}_2) = \min\{L(\mathbf{z}) : \mathbf{z}(s_1) = \mathbf{z}_1, \mathbf{z}(s_2) = \mathbf{z}_2\}.$$

For Gaussian likelihoods, there is an asymptotic relationship between the geodesic distance between the MLE, $\hat{\boldsymbol{\theta}}$, and a point $\boldsymbol{\theta}_\alpha$ that corresponds to an α -level confidence region on the manifold [22]. The geodesic distance between $\hat{\boldsymbol{\theta}}$ and $\boldsymbol{\theta}_\alpha$: $d(\hat{\boldsymbol{\theta}}, \boldsymbol{\theta}_\alpha)$; can be written in terms of the α th-quantile of the $\chi^2(\nu)$ distribution

$$d(\hat{\boldsymbol{\theta}}, \boldsymbol{\theta}_\alpha) = \sqrt{\Delta_{\nu, \alpha}}. \quad (5.14)$$

Pairing Equations (5.7) and (5.14) yields an asymptotic relationship between confi-

dence regions and geodesic length [22]:

$$2 \left(\ell(\hat{\boldsymbol{\theta}}) - \ell(\boldsymbol{\theta}) \right) \sim d(\hat{\boldsymbol{\theta}}, \boldsymbol{\theta}_\alpha)^2 \quad \text{as } N \rightarrow \infty. \quad (5.15)$$

In Section 5.3 we present likelihood-based confidence regions alongside geodesic curves of the corresponding length, as characterised by (5.14), and comment on the validity of Equation (5.15) in a range of scenarios.

Geodesic curves satisfy the following system of differential equations in n dimensions [260]:

$$\frac{d^2\theta_m}{ds^2} + \sum_{i,j=1}^n \Gamma_{ij}^m \frac{d\theta_i}{ds} \frac{d\theta_j}{ds} = 0, \quad m = 1, \dots, n, \quad (5.16)$$

where s is the parameterisation of the geodesic curve, in accordance with Equation (5.13), and Γ_{ij}^m are the Christoffel symbols of the second kind [64], defined as

$$\Gamma_{ij}^m = \frac{1}{2} \sum_{l=1}^n g^{ml} \left(\frac{\partial g_{lj}}{\partial \theta_i} + \frac{\partial g_{li}}{\partial \theta_j} - \frac{\partial g_{ij}}{\partial \theta_l} \right). \quad (5.17)$$

We can convert from Christoffel symbols of the second kind to Christoffel symbols of the first kind by lowering the contravariant (upper) index through multiplication by the metric: $\Gamma_{kij} = g_{km} \Gamma_{ij}^m$ [140]. Here, repeated indices, in this case m , imply a summation is to be performed over the repeated index, following the Einstein summation convention [15]. Conversely, we can recover Christoffel symbols of the first kind from Christoffel symbols of the second kind via the inverse metric: $g^{km} \Gamma_{kij} = \Gamma_{ij}^m$. Christoffel symbols of the second kind are the connection coefficients of the Levi-Civita connection; the Christoffel symbols are symmetric in the covariant (lower) indices [121]. On an n -dimensional manifold, the Christoffel symbol is of dimension $n \times n \times n$. Geodesics can be used to construct theoretical confidence regions, to measure the geometric distance between probability distributions, and to perform hypothesis testing, for example to test equality of parameters [162, 228, 239].

Under certain conditions, analytical expressions can be obtained for the solutions of the geodesic equations, and the corresponding Fisher-Rao distances, for example in the case of the univariate (5.1) and multivariate (5.25) normal distributions [65, 259]. However, we solve Equation (5.16) numerically, after converting the second order ODE to a first order system of ODEs using standard techniques.

We are also interested in exploring the scalar curvature, also known as the *Ricci scalar*, of our manifolds. To compute the scalar curvature, we must first construct the Riemann tensor, and subsequently the Ricci tensor. As we only require these tensors for computation of the scalar curvature, and do not attempt to interpret these tensors

directly in this work, we provide only a limited outline of their interpretation. The Riemann curvature tensor is constructed from the Christoffel symbols and their first partial derivatives. Here, it is convenient to think about these partial derivatives as being with respect to the parameters of interest. Due to the possibility of raising or lowering indices of Christoffel symbols and tensors via the metric, there are several equivalent expressions for computing the Riemann curvature tensor [140]. The elements of the Riemann tensor of the first kind can be written as

$$R_{ijkl} = \frac{\partial \Gamma_{jli}}{\partial k} - \frac{\partial \Gamma_{jki}}{\partial l} + \Gamma_{ilr}\Gamma_{jk}^r - \Gamma_{ikr}\Gamma_{jl}^r. \quad (5.18)$$

The Riemann tensor of the first kind is a (0,4) tensor (with no contravariant indices and four covariant indices), and can be converted to the (1,3) Riemann tensor of the second kind via the inverse of the metric: $g^{im}R_{ijkl} = R_{jkl}^m$. On an n -dimensional manifold, the Riemann tensor is of dimension $n \times n \times n \times n$; due to various symmetries however, there are far fewer independent elements [208]. The Riemann tensor provides information about the intrinsic curvature of the manifold. A geometric interpretation is that a vector from a point on the manifold, parallel transported around a parallelogram, will be identical to its original value when it returns to its starting point if the manifold is flat. In this case, the Riemann tensor vanishes. If the manifold is not flat, the Riemann tensor can be used to quantify how the vector differs following this parallel transport [206].

From the Riemann tensor of the second kind, we can compute the Ricci tensor of the first kind. The Ricci tensor, R_{ij} , is obtained by contracting the contravariant index with the third covariant index of the Riemann tensor of the second kind; that is,

$$R_{ij} = R_{ijm}^m. \quad (5.19)$$

On an n -dimensional manifold, the Ricci tensor is of dimension $n \times n$, and is symmetric [206]. The Ricci tensor can quantify the changes to a volume element as it moves through the manifold, relative to Euclidean space [206].

The scalar curvature, Sc , can be obtained as a contraction of the Ricci tensor

$$Sc = g^{ij}R_{ij}. \quad (5.20)$$

The scalar curvature is invariant; it does not change under a change of coordinates (re-parameterisation). For Gaussian likelihoods, the corresponding manifold is flat; characterised by zero scalar curvature everywhere. As such, the scalar curvature provides a measure of how the likelihood of the underlying statistical model deviates from being Gaussian—often referred to as *non-Gaussianity* in the physics and cosmology literature—irrespective of the parameterisation [121]. As we will explore in Section 5.3, it can also provide insights into parameter identifiability.

5.2.3 Hypothesis testing

Here we outline the approach for performing likelihood-ratio-based hypothesis tests, and hypothesis tests based on geodesic distance. As we consider synthetic data in this work, we know the *true* parameter values, $\boldsymbol{\theta}_t$. In practical applications this is not the case. As such, we may seek to test whether some previously held notion about the true parameters, $\boldsymbol{\theta}_t = \boldsymbol{\theta}_0$, is supported by the data, based on the computed MLE. This could be investigated via the following hypothesis test:

$$\begin{cases} H_0 : \boldsymbol{\theta}_t = \boldsymbol{\theta}_0, \\ H_1 : \boldsymbol{\theta}_t \neq \boldsymbol{\theta}_0. \end{cases} \quad (5.21)$$

From Equation (5.7) the test statistic for such a likelihood-ratio-based hypothesis test can be expressed as

$$\lambda_{LR} = -2(\ell(\boldsymbol{\theta}_0) - \ell(\hat{\boldsymbol{\theta}})), \quad (5.22)$$

where asymptotically as $N \rightarrow \infty$, $\lambda_{LR} \sim \chi^2(\nu)$, following Wilk's theorem [255]. From the asymptotic relationship given in Equation (5.15), it follows that under the same asymptotic relationship the test statistic for a hypothesis test based on geodesic distance is [162]:

$$\lambda_{GD} = d(\boldsymbol{\theta}_0, \hat{\boldsymbol{\theta}})^2. \quad (5.23)$$

The likelihood values required to compute Equation (5.22) can be obtained directly by evaluating Equation (5.5). To compute the geodesic distance between two specific points in parameter space, as required by Equation (5.23), it is necessary to solve a boundary value problem to obtain the geodesic curve between $\boldsymbol{\theta}_0$ and $\hat{\boldsymbol{\theta}}$. Approximate p-values can be computed from these test statistics as $1 - F_{\chi^2(\nu)}(\lambda_{LR})$ and $1 - F_{\chi^2(\nu)}(\lambda_{GD})$, respectively, where $F_{\chi^2(\nu)}$ is the cumulative distribution function of $\chi^2(\nu)$ [52]. We provide practical examples of each of these approaches to hypothesis testing in Section 5.3.

5.2.4 Numerical implementation

All numerical techniques used to produce the results in this work are implemented in the open source Julia language [41]; we use a combination of existing Julia packages and bespoke implementations. There are several aspects of numerical computation in this work, including approximate solutions to systems of ODEs, differentiation with both finite differences and forward mode automatic differentiation, likelihood computation and nonlinear optimisation. Nonlinear optimisation for obtaining MLEs and parameter combinations corresponding to particular confidence levels is performed with the Julia pack-

age NLOpt.jl, using the Bound Optimisation by Quadratic Approximation (BOBYQA) algorithm. BOBYQA is a derivative-free algorithm for solving bound constrained optimisation problems [266]. Approximate solutions to ODEs are obtained using the Julia package DifferentialEquations.jl [272]. The second order Heun’s method [91]; a two-stage Runge–Kutta method, is used for obtaining contours of the log-likelihood function to form approximate likelihood-based confidence regions [52]. Heun’s method is implemented as `Heun()` in DifferentialEquations.jl. Approximate solutions to geodesic differential equations are obtained using the Tsitouras implementation of the Runge–Kutta method, that employs Runge–Kutta pairs of orders 5 and 4 [320], implemented as `Tsit5()` in DifferentialEquations.jl. Boundary value problems for geodesic-distance-based hypothesis tests are solved using the DifferentialEquations.jl implementation of a shooting method, utilising `Tsit5()`. Code for reproducing all examples in this work is available on [GitHub](#).

5.3 Results

In this section we present results combining likelihood based parameter inference and uncertainty quantification with ideas from information geometry, including geodesic curves and scalar curvature. We apply these techniques to univariate and multivariate normal distributions, linear, exponential and logistic population growth models and the SIR model. Through these canonical examples, we explore pedagogically differences in the inference and information geometry results that arise as we consider parameter estimation and uncertainty for increasingly complex systems.

Synthetic data for the univariate and multivariate normal distributions are generated by sampling from the respective distributions given in Equation (5.24). For simplicity, in this work we consider synthetic data from uncorrelated observation processes with constant standard deviation in both time and parameter space. However, we note that the techniques presented in this work can be generalised to handle data with non-constant variance and for other distributions where the Fisher information is available [53].

$$\text{Univariate} : x_i \sim \mathcal{N}(\mu, \sigma^2), \quad \text{Multivariate} : \mathbf{x}_i \sim \text{MVN}(\boldsymbol{\mu}, \boldsymbol{\Sigma}), \quad (5.24)$$

where $\boldsymbol{\Sigma} = \text{diag}(\sigma^2)$ is the covariance matrix. For the population growth and SIR models considered in this work, synthetic data is generated by drawing from a normal distribution with mean described by the model solution and a prescribed standard deviation; effectively substituting $\mu = \mu(\boldsymbol{\theta}, t)$ in Equation (5.24) for observation processes with a single variable, and $\boldsymbol{\mu} = \boldsymbol{\mu}(\boldsymbol{\theta}, t)$ for observation processes with several variables. When σ is one of the parameters to be estimated, $\sigma \in \boldsymbol{\theta}$, but $\boldsymbol{\mu}$ does not depend on σ . Parameter values that we use to generate synthetic data correspond to parameter estimates inferred from field data in the literature [235, 299].

We present a series of figures in this section visualising the normalised log-likelihood, $\hat{\ell}$, and scalar curvature, Sc , as heatmaps, with likelihood-based 95% confidence regions and geodesics with a length corresponding to a 95% confidence distance superimposed. All results are computed numerically, as outlined in Section 5.2, with code available on [GitHub](#). Unless otherwise indicated, each set of geodesics includes 20 geodesics with initial velocities corresponding to equidistant points uniformly distributed on the circumference of a unit circle. As such, the apparent clustering of geodesics in some examples highlights differences in the scaling and stretching of parameter spaces. Each scalar curvature and log-likelihood heatmap is computed on a uniformly discretised 100×100 grid.

5.3.1 Normal distributions

We first consider parameter inference and information geometry techniques applied to observations drawn directly from univariate and bivariate normal distributions, with no underlying process model. In Figure 5.1 we present results for the univariate normal distribution (5.1), estimating $\boldsymbol{\theta} = (\mu, \sigma)$. The true mean and standard deviation used to generate data are $(\mu, \sigma) = (0.7, 0.5)$. Estimates are obtained via maximum likelihood estimation. MLEs of normal variance are known to provide biased underestimates [255], and the derivation of the Fisher information assumes an unbiased estimator [113]. This may partially explain the particular differences observed between the likelihood-based confidence region and the endpoints of the geodesics in Figure 5.1, wherein the geodesics appear not only to suggest a tighter confidence region, but also appear to be biased towards parameter space with smaller standard deviation. As the number of observations increases from $N = 10$ to $N = 100$, we observe not only that the MLE more precisely estimates the true parameter values, but also the endpoints of the geodesic curves more closely correspond to the likelihood-based confidence regions. This is consistent with both the theoretical asymptotic relationship between geodesic length and likelihood-based confidence regions given in Equation (5.15), and also the bias of the MLE for standard deviation decreasing, as N increases.

The manifold representing the family of normal distributions parameterised by $\boldsymbol{\theta} = (\mu, \sigma)$ has constant scalar curvature $Sc = -1$. Due to the additive nature of the Fisher information, having N observations results in a constant scalar curvature of $Sc = -1/N$, as presented in Figure 5.1(c,d). It is straightforward, although tedious, to verify this result through combining Equations (5.4), (5.17), (5.18), (5.19) and (5.20).

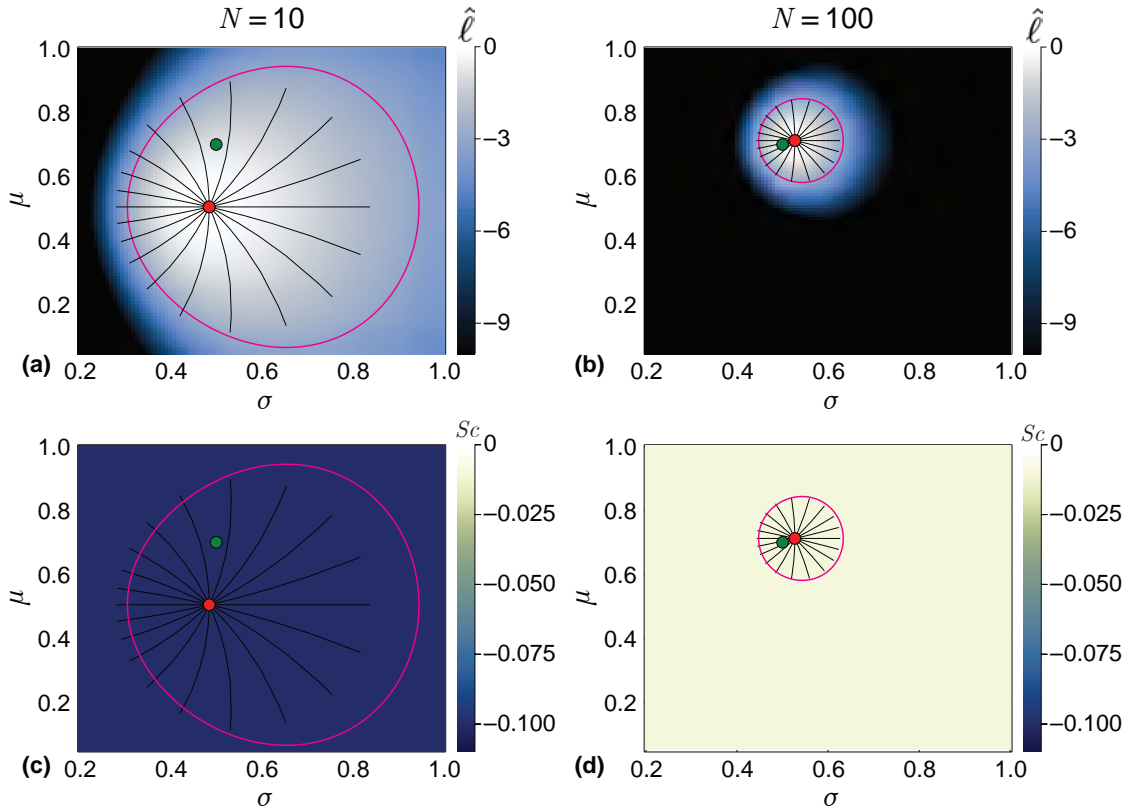


Figure 5.1: Univariate normal distribution with inferred mean, μ , and standard deviation, σ . Heatmaps visualise the normalised log-likelihood, $\hat{\ell}$, (a,b) and the scalar curvature, S_c , (c,d). True parameter values, $(\mu, \sigma) = (0.7, 0.5)$, are marked with green discs, with the MLEs indicated using red discs. Magenta curves correspond to likelihood-based 95% confidence regions. Black lines are geodesic curves emanating from the MLEs, with a geodesic length corresponding to a theoretical 95% confidence region. Increasing the number of data points, N , tightens the confidence regions, improves the correspondence between geodesic curves and likelihood-based confidence regions, and reduces the scalar curvature.

The probability density function for the multivariate normal distribution with two independent variables; $x, y \in \mathbb{R}$, with constant standard deviation σ is

$$p(x, y; \mu_1, \mu_2, \sigma) = \frac{1}{2\pi\sigma^2} \exp\left(-\left(\frac{(x - \mu_1)^2 + (y - \mu_2)^2}{2\sigma^2}\right)\right). \quad (5.25)$$

In Equation (5.25) there are 3 parameters that we could estimate from data; $\Theta = (\mu_1, \mu_2, \sigma)$. As we estimated the mean and standard deviation for the univariate normal distribution in Figure 5.1, we consider inference of both means for the multivariate normal; $\theta = (\mu_1, \mu_2)$. Results are presented in Figure 5.2. Even with a small number of observations ($N = 10$), we observe an excellent match between the likelihood-based confidence regions and geodesics when only estimating means. As expected, increasing N results in a MLE closer to the true values, and tighter confidence regions. We also observe that the confidence regions are symmetric with respect to each mean parameter. When estimating only the mean parameters of the multivariate normal distribution, we see that the scalar curvature is zero everywhere. This is to be expected, as the Fisher information for normally distributed observation processes, Equation (5.11), depends only on the standard deviation and not the mean. As such all of the partial derivatives used to construct the Christoffel symbols, (5.17), are zero; this vanishing of the Christoffel symbols translates to zero scalar curvature through Equations (5.18), (5.19) and (5.20). We also observe that, in contrast to the evident curvature of the geodesics for the univariate normal case presented in Figure 5.1, the geodesic curves in Figure 5.2 appear perfectly straight when plotted in Euclidean geometry. The Riemann tensor (5.18) is zero everywhere when inferring multivariate normal means. This suggests that the manifold is flat.

Results presented in this work predominantly feature 95% confidence regions. We note that although this choice is common [108], it is also arbitrary, and equivalent analysis could be performed at different confidence levels. In examples where the geodesic endpoints approximately align with the likelihood-based confidence regions at the 95% level, we expect intermediate points along the geodesics to also approximately align with corresponding likelihood contours, in accordance with Equation (5.15). However, in examples where we observe a mismatch between geodesic endpoints and likelihood-based confidence intervals at the 95% level, we do not expect intermediate points along geodesics to correspond to likelihood contours. This is demonstrated in Figure 5.3.

Having considered the techniques as applied directly to distributions, we now incorporate ODE-based process models, such that our observations are normally distributed about the solution of a mathematical model.

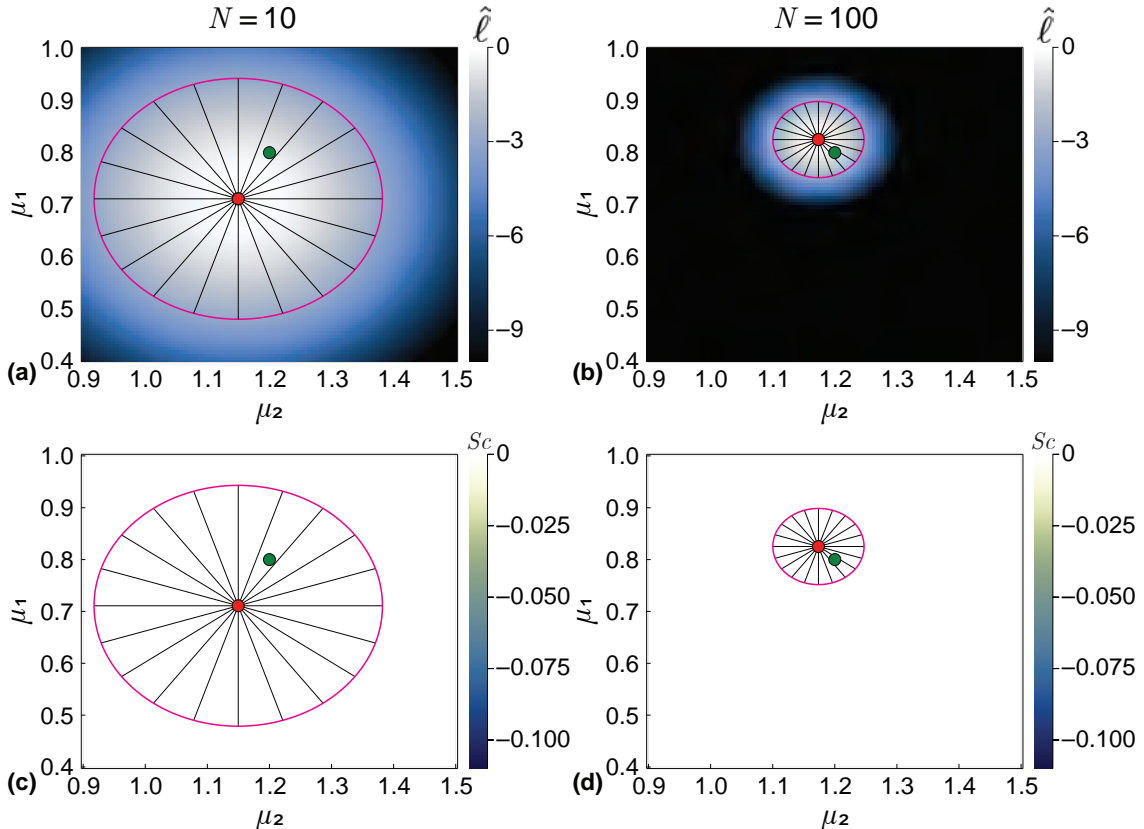


Figure 5.2: Multivariate normal distribution with inferred means, μ_1 , and μ_2 , with known constant standard deviation, $\sigma = 0.3$. Heatmaps visualise the normalised log-likelihood, $\hat{\ell}$, (a,b) and the scalar curvature, Sc , (c,d). True parameter values, $(\mu_1, \mu_2) = (0.8, 1.2)$, are marked with green discs, with the MLEs indicated using red discs. Magenta curves correspond to likelihood-based 95% confidence regions. Black lines are geodesic curves emanating from the MLEs, with geodesic lengths corresponding to a theoretical 95% confidence region. Increasing the number of data points, N , tightens the confidence regions. In contrast to the univariate case where we infer standard deviation in Figure 5.1, when only inferring the mean parameters of the multivariate normal distribution, we see that even with few observations, $N = 10$, the geodesics and likelihood-based confidence regions match closely. As we are estimating means only, and there is no model-induced curvature, the scalar curvature is zero everywhere.

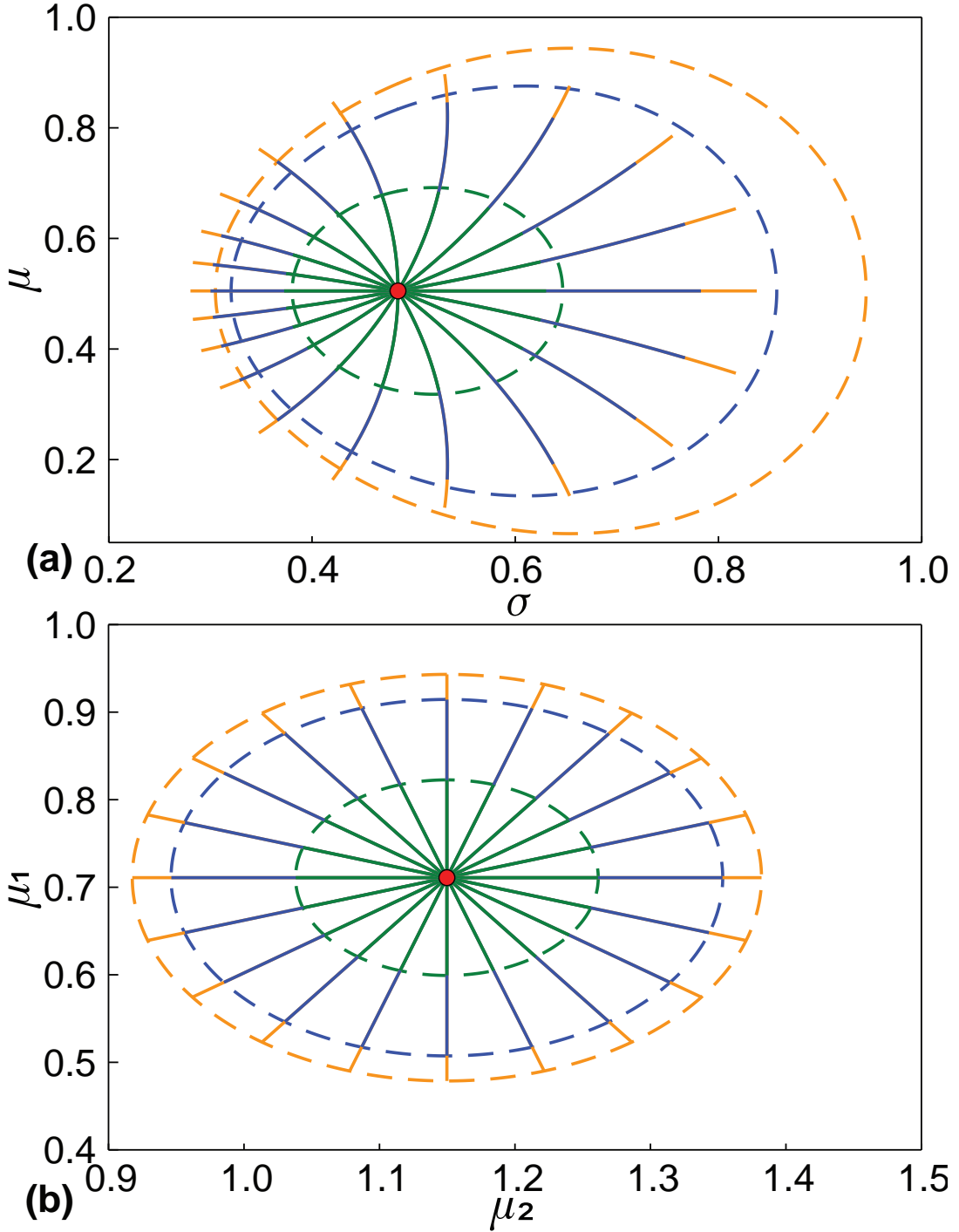


Figure 5.3: Comparison of confidence regions at intermediate likelihood values and geodesic distances. Results correspond to (a) univariate normal distribution with inferred mean, μ , and standard deviation, σ , as considered in Figure 5.1a, and (b) multivariate normal distribution with inferred means, μ_1 , and μ_2 , as considered in Figure 5.2a. MLEs are indicated using red discs. Dashed curves correspond to likelihood-based 50% (green), 90% (blue), and 95% (orange) confidence regions. Solid lines are geodesic curves emanating from the MLEs, with geodesic lengths within a theoretical 50% (green), 90% (blue), and 95% (orange) confidence distance.

5.3.2 Population growth models

The canonical logistic growth model, alongside generalisations and related sigmoid models such as Gompertz and Richards' models, have been extensively applied to study population growth dynamics in the life sciences [252, 299]. In Figure 5.4 we present data from the literature describing the area covered by hard corals in a region as they regrow following an adverse event. This can be modelled as a logistic growth process [299]. Logistic growth of a population with density, $C(t)$, is characterised by a growth rate, $r > 0$, initial condition, $C(0) > 0$, and carrying capacity, $K > 0$. Treating parameters values $(r, C(0), K) = (0.9131 \text{ [year}^{-1}], 0.7237\%, 79.74\%)$, and standard deviation $\sigma = 2.301\%$, inferred in the literature from this field data as the *true* values, we generate various synthetic data sets with multiple observations at various time-points.

The logistic growth model is well approximated by the exponential growth model when $C(t) \ll K$ [321], and early time exponential growth is approximately linear. Before considering the inference and information geometry techniques as applied to the logistic model, we first consider the more fundamental linear and exponential growth models. In Figure 5.5 we present example synthetic linear and exponential data, and in Figure 5.6 synthetic logistic data. In the context of population growth models, the presence of variability in observations at a single time-point could reflect, for example; measurement error, variability in population estimates, or expert judgement [106].

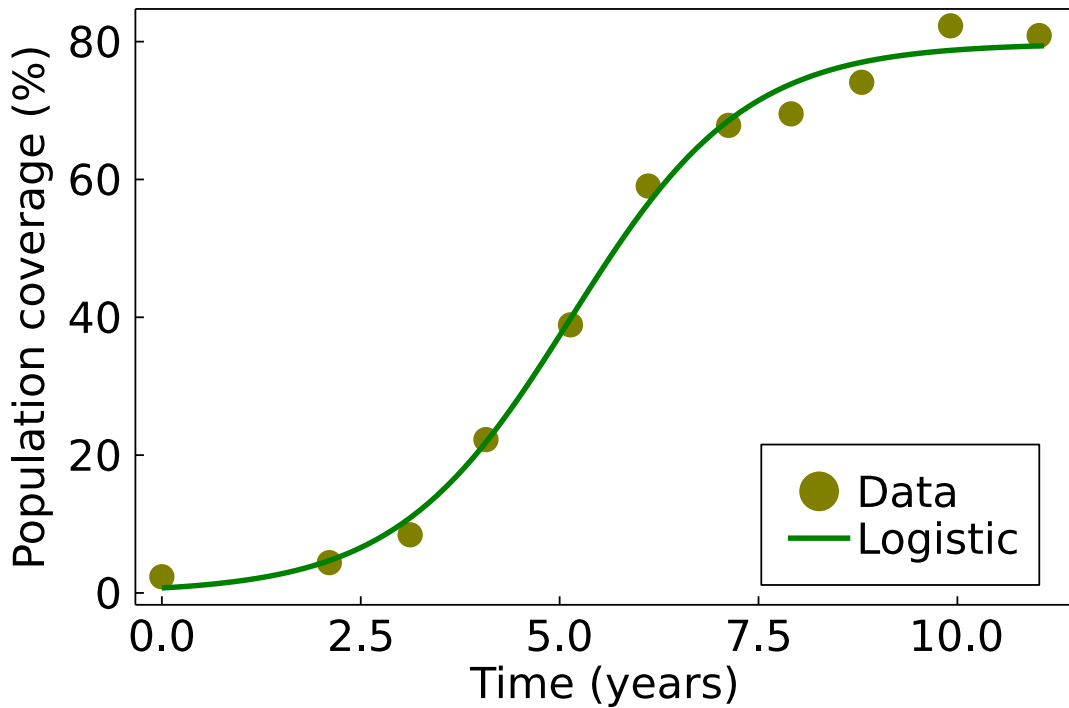


Figure 5.4: Markers correspond to data from field studies, representing the % of area in a region covered by hard corals, as the coral population regrows following depletion by an external event [299]. Data originally extracted from the Australian Institute of Marine Science (AIMS) Long Term Monitoring Program (LTMP) eAtlas (eatlas.org.au/gbr/ltmp-data). A logistic model is fit to the data in [299], with inferred parameters: $r = 0.9131 \text{ [year}^{-1}]$, $C(0) = 0.7237\%$, $K = 79.74\%$ and standard deviation $\sigma = 2.301$; this is reproduced here as the green curve.

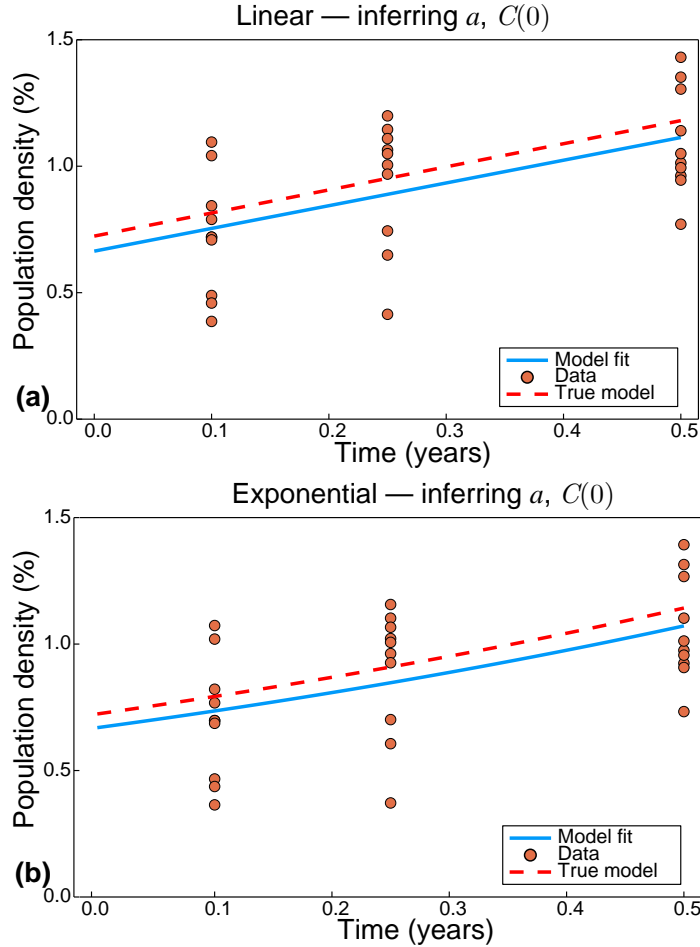


Figure 5.5: Example synthetic data generated from the linear and exponential models with comparison of early time linear and exponential model fits, inferring a and $C(0)$. $N = 10$ observations per time-point, with time-points $T = (0.1, 0.25, 0.5)$. True parameter values are $a = 0.9131$, $C(0) = 0.7237$, with known standard deviation, $\sigma = 0.2301$. For generating synthetic early time linear and exponential data, we reduce the standard deviation relative to the $\sigma = 2.301$ computed from the logistic model, as early time data produced with $C(0) = 0.7237$ and $\sigma = 2.301$ produces negative population density observations. Inference produces MLEs of $(\hat{a}, \hat{C}(0)) = (0.8988, 0.6642)$ for the linear model, and $(\hat{a}, \hat{C}(0)) = (0.9412, 0.6695)$ for the exponential model.

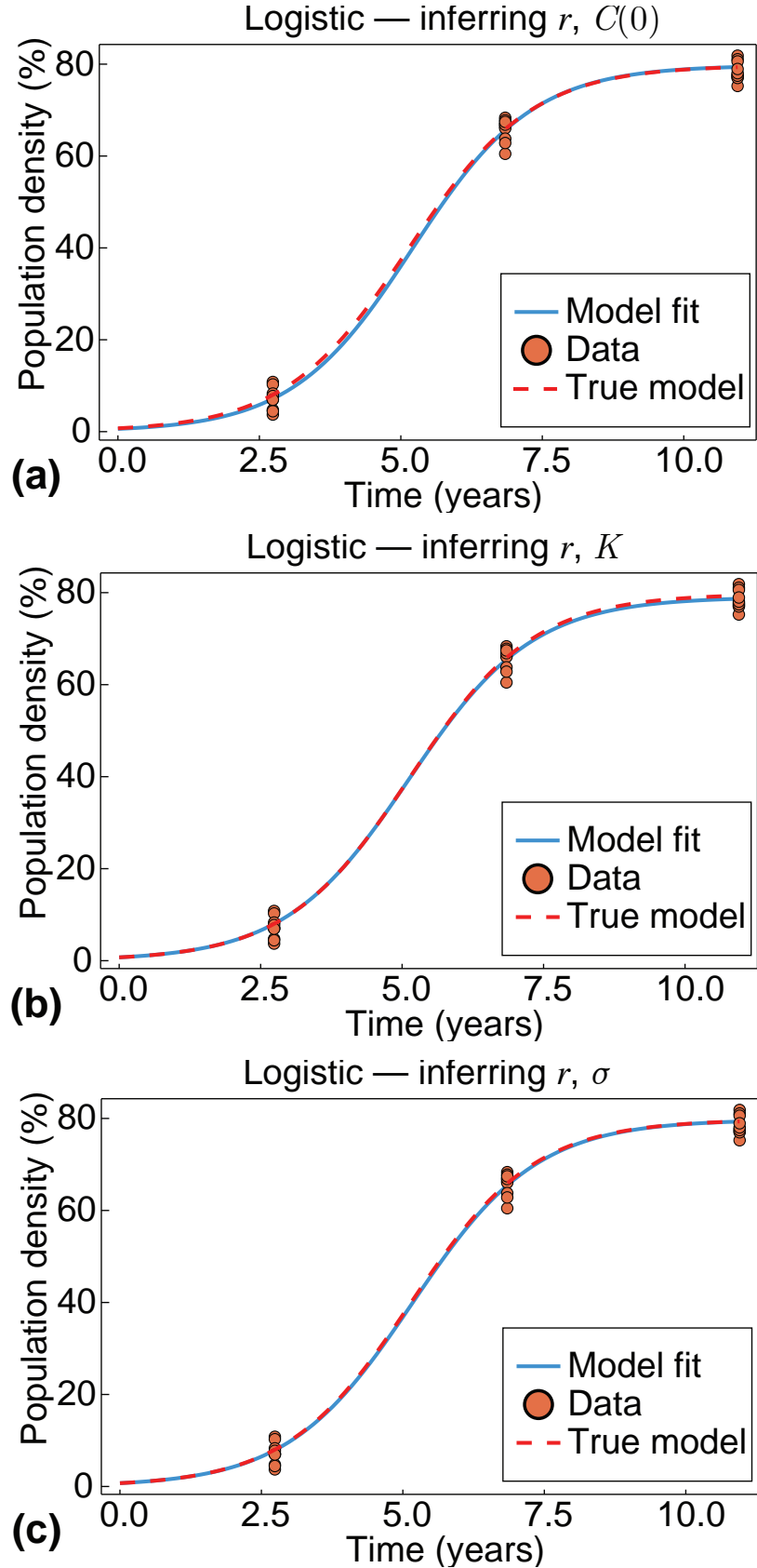


Figure 5.6: Example synthetic data generated from the logistic growth model. The logistic model is fit to the synthetic data, inferring pairwise combinations of r with $C(0)$, K and σ . Observations are made at $T = (2.74, 6.84, 10.95)$ years, with $N = 10$ observations per time-point. True parameter values are $r = 0.9131$, $C(0) = 0.7237$, $K = 79.74$ and $\sigma = 2.301$.

Linear growth

Linear growth describes growth at a constant rate, independent of the population density. The linear growth model and solution are given by

$$\frac{dC}{dt} = a, \quad C(t) = at + C(0).$$

With parameters $\Theta = (a, C(0), \sigma)$, $\mu(\Theta, t) = at + C(0)$ describes the expected model behaviour. In Figure 5.7(a-f) we present inference results for the linear model for all pairwise combinations of Θ . The partial derivatives of the linear model with respect to the parameters a and $C(0)$, required to form the Jacobians, $\mathbf{J}(\theta)$, are

$$\frac{\partial \mu(\Theta, t)}{\partial a} = t, \quad \frac{\partial \mu(\Theta, t)}{\partial C(0)} = 1.$$

Recall from Equation (5.10) that we only require the partial derivatives corresponding to unknown parameters in any given example. When estimating $\theta = (a, C(0))$ we find that, similar to the multivariate normal case where we estimate means, the scalar curvature is zero everywhere. We also observe that the end-points of the geodesics align with the likelihood-based confidence region. We stress that this arises through the relationship in Equation (5.15), and is not forced to occur via termination of the numerical solution of the ODE once it reaches the likelihood-based confidence region. However, due to the relationship between a and $C(0)$, we find that the confidence regions in this case are not symmetric about the MLE with respect to each parameter. Rather, we see that for a given normalised log-likelihood value a larger growth rate corresponds to a smaller initial condition, and vice versa. This aligns with our intuition when considering fitting a straight line through data, as presented in Figure 5.5a; lines with a greater slope (a) must start lower ($C(0)$) to fit the data.

When one of the parameters to be estimated is σ , we observe similar results to the univariate normal case; geodesic endpoints are offset in the direction of decreasing σ relative to the likelihood-based confidence regions, and there is constant scalar curvature of $Sc = -1/N$. The geodesics and confidence regions appear symmetric with respect to the model parameter, about the MLE.

Exponential growth

Exponential growth describes growth at a rate proportional to the size of the population. The exponential growth model and solution are

$$\frac{dC}{dt} = aC, \quad C(t) = C(0) \exp(at).$$

With parameters $\Theta = (a, C(0), \sigma)$, $\mu(\Theta, t) = C(0) \exp(at)$ describes the expected model behaviour. The partial derivatives of the exponential model with respect to the parameters a and $C(0)$, required to form the Jacobians, $\mathbf{J}(\boldsymbol{\theta})$, are

$$\frac{\partial \mu(\Theta, t)}{\partial a} = tC(0) \exp(at), \quad \frac{\partial \mu(\Theta, t)}{\partial C(0)} = \exp(at).$$

By construction, as detailed in Figure 5.5, the linear and exponential models with identical parameters and initial conditions produce very similar behaviours over a sufficiently small time-scale. This is seen when comparing the inference results for the exponential model, presented in Figure 5.7(g-l), to the corresponding linear results in Figure 5.7(a-f). When inferring $\boldsymbol{\theta} = (a, \sigma)$, deviations from the corresponding linear results are minimal. The likelihood-based confidence region and corresponding geodesic endpoints for $\boldsymbol{\theta} = (a, C(0))$ are marginally tighter and less elliptical. When inferring $\boldsymbol{\theta} = (C(0), \sigma)$, we find that the confidence region for the exponential model is narrower with respect to $C(0)$ than that of the linear model, though near-identical with respect to σ . As for the linear case, the scalar curvature is $Sc = -1/N$ everywhere when σ is one of the unknown parameters, and zero everywhere otherwise.

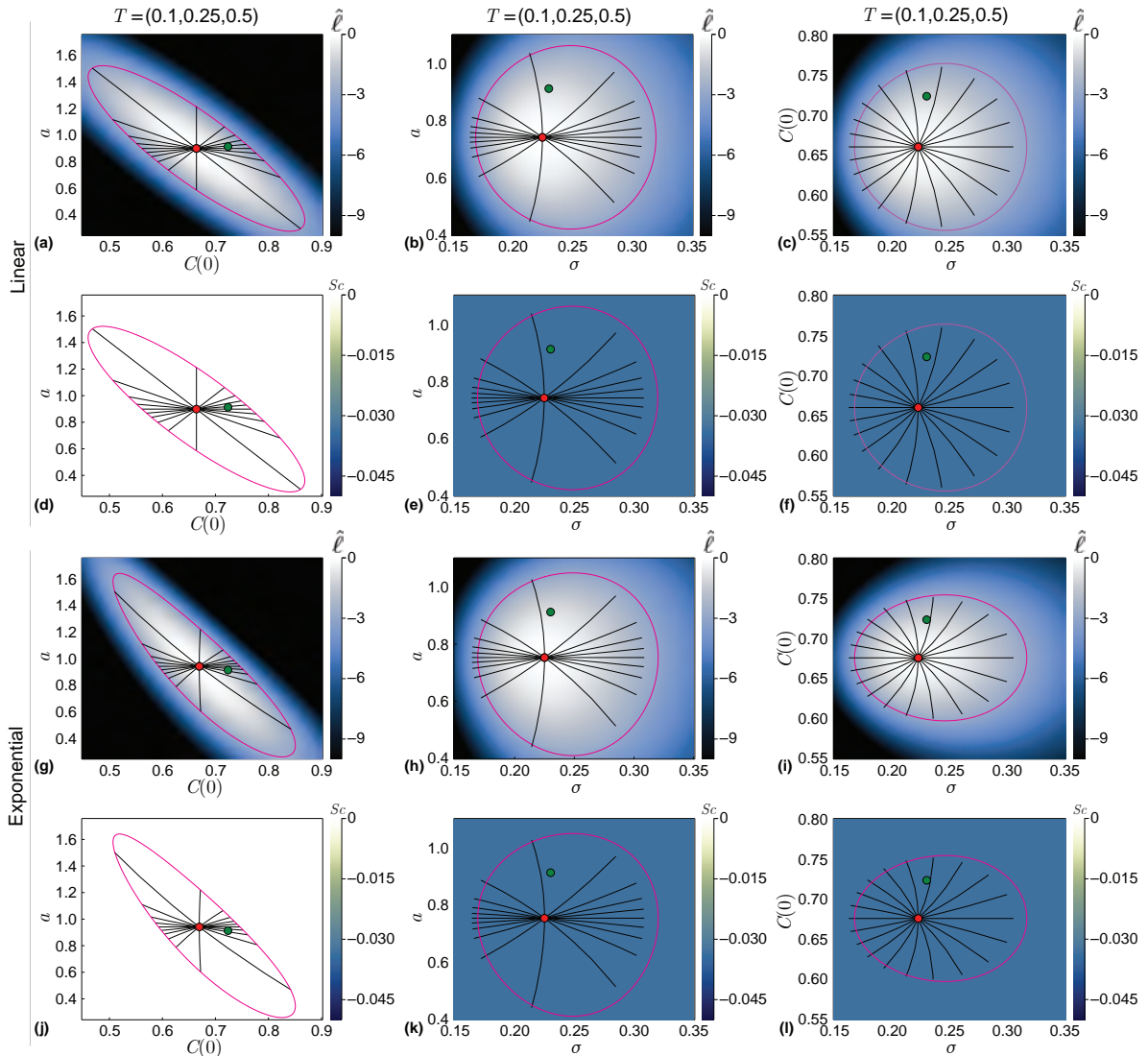


Figure 5.7: Linear (a-f) and exponential (g-l) models with inferred pairwise combinations of growth rate, a , initial condition, $C(0)$, and standard deviation, σ . Heatmaps visualise the normalised log-likelihood, $\hat{\ell}$, (a-c,g-i); and the scalar curvature, Sc , (d-f,j-l). Observations are made at $T = (0.1, 0.25, 0.5)$, with 10 observations per time-point; corresponding to the example data presented in Figure 5.5. The true parameter values are marked with green discs, with the MLEs indicated using red discs. Magenta curves correspond to likelihood-based 95% confidence regions. Black lines are geodesic curves emanating from the MLEs, with lengths corresponding to a theoretical 95% confidence distance. True values of model parameters correspond to the logistic growth parameters; $a = 0.9131$, $C(0) = 0.7237$, with reduced standard deviation $\sigma = 0.2301$.

Logistic growth

Logistic growth describes growth at a rate dependent on the size of the population, with growth ceasing once the population reaches a carrying capacity. For sufficiently small populations relative to the carrying capacity, logistic growth is approximately exponential [321]. As the population approaches the carrying capacity, the rate of growth slows. The logistic growth model is

$$\frac{dC(t)}{dt} = rC(t) \left(1 - \frac{C(t)}{K}\right),$$

with solution

$$C(t) = \frac{C(0)K}{C(0) + (K - C(0)) \exp(-rt)}. \quad (5.26)$$

The long-time limit of Equation (5.26) is $\lim_{t \rightarrow \infty} C(t) = K$. The behaviour of the logistic model can be described by the three model parameters and standard deviation: $\boldsymbol{\Theta} = (r, C(0), K, \sigma)$. We can compute the partial derivatives required to form the Jacobian matrices, $\mathbf{J}(\boldsymbol{\Theta})$, analytically:

$$\begin{aligned} \mu(\boldsymbol{\Theta}, t) &= C(r, C(0), K, t) = \frac{C(0)K}{C(0) + (K - C(0)) \exp(-rt)}, \\ \frac{\partial \mu(\boldsymbol{\Theta}, t)}{\partial r} &= \frac{C(0)Kt(K - C(0)) \exp(-rt)}{((K - C(0)) \exp(-rt) + C(0))^2}, \\ \frac{\partial \mu(\boldsymbol{\Theta}, t)}{\partial C(0)} &= \frac{K^2 \exp(rt)}{(C(0)(\exp(rt) - 1) + K)^2}, \\ \frac{\partial \mu(\boldsymbol{\Theta}, t)}{\partial K} &= \frac{C(0)^2 \exp(rt)(\exp(rt) - 1)}{(C(0)(\exp(rt) - 1) + K)^2}. \end{aligned} \quad (5.27)$$

Recall that $\boldsymbol{\theta}$ includes only the unknown parameters to be estimated, so the components required from Equation (5.27) to form $\mathbf{J}(\boldsymbol{\theta})$ depend on the specific example.

Example synthetic logistic data is presented in Figure 5.6, demonstrating the model fits for $\boldsymbol{\theta} = (r, C(0))$, $\boldsymbol{\theta} = (r, K)$ and $\boldsymbol{\theta} = (r, \sigma)$. With data at *early*, *mid* and *late* time, $T = (t_1, t_2, t_3) = (2.74, 6.84, 10.95)$ years, we observe an excellent model fit in all cases. The fit is best when $\boldsymbol{\theta} = (r, \sigma)$, as only one model parameter is unknown. Comparing $\boldsymbol{\theta} = (r, C(0))$ and $\boldsymbol{\theta} = (r, K)$ we observe a marginally better fit at late time when K is known, and at early time when C is known, as expected.

We present inference results for the logistic model for $\boldsymbol{\theta} = (r, C(0))$ in Figure 5.8(a-f) and for $\boldsymbol{\theta} = (r, K)$ in Figure 5.8(g-l). We do not present further results of inferring σ for the logistic model, as little insight is gained beyond what we glean from the linear and exponential growth results. For $\boldsymbol{\theta} = (r, C(0))$, the normalised log-likelihood reflects the same relationship between growth rate and initial condition as for the linear and

exponential case. With early-mid time data and early-mid-late time data, we are able to infer $\boldsymbol{\theta} = (r, C(0))$. With only mid-late time data, we find that the parameters are not practically identifiable. This can be seen from Figure 5.8(c); the normalised log-likelihood remains above the threshold prescribed in Equation (5.7), and a closed likelihood-based 95% confidence region cannot be constructed based on Wilks' theorem. This is also reflected in Figure 5.8(f) alongside zero scalar curvature; such that the plot appears empty. Comparing Figure 5.8(a,b), and noting that they each rely on the same total number of observations, the importance of early and mid time data when inferring $\boldsymbol{\theta} = (r, C(0))$ is reinforced. The confidence region is tighter with only early-mid data, than with the same amount of data spread across early, mid and late times.

Inferring $\boldsymbol{\theta} = (r, K)$ reflects similar behaviour. In Figure 5.8(j) and associated zoomed-in view (Figure 5.8g), inferring the carrying capacity from only early-mid time data results in an extremely wide confidence region, though the parameters remain identifiable. The geodesics emanating from the MLE match the likelihood-based confidence region very well in directions where the normalised log-likelihood is steep, however they do not quite reach the true parameter value in the direction where the normalised log-likelihood is relatively flat. Comparing Figure 5.8(g,j) to Figure 5.8(h,i), the MLE for $\boldsymbol{\theta} = (r, K)$ appears to be relatively poor when only early-mid time data is used.

When considering $\boldsymbol{\theta} = (r, C(0))$, we see that with early-mid time data and mid-late time data, the scalar curvature is zero everywhere. However, introducing a third time-point (early-mid-late data) results in a non-constant negative scalar curvature. We expect that this relates to the relationships between the parameters, and the difference between a mapping (where we have two pieces of information and two parameters to estimate), and a fit (where we have three pieces of information and two parameters to estimate). We do not observe similar behaviour for $\boldsymbol{\theta} = (r, K)$ with data at three time-points; the scalar curvature still appears to be zero everywhere. One explanation for this is that data at t_1 , where $C(t) \ll K$, may be effectively independent of K ; providing no information about K [329]. This may effectively reduce the problem to a mapping. Given that the scalar curvature is a feature of the manifold rather than the data, it is of interest to investigate what would happen, were the true parameters to lie within this region of non-constant scalar curvature.

To address this, we generate an alternate set of synthetic logistic growth data using parameter values from within the high curvature region;

$(r, C(0)) = (0.9, 0.2)$, with $(K, \sigma) = (79.74, 2.301)$ as before. Inference results are presented in Figure 5.9. We still observe correspondence between the endpoints of the geodesics and the likelihood-based confidence region, however the confidence region is now significantly narrower and reflects a more hyperbolic shaped relationship between r and $C(0)$ in terms of the normalised log-likelihood. Increasing the number of observations, as depicted in Figure 5.9c, has the expected effects of tightening the confidence

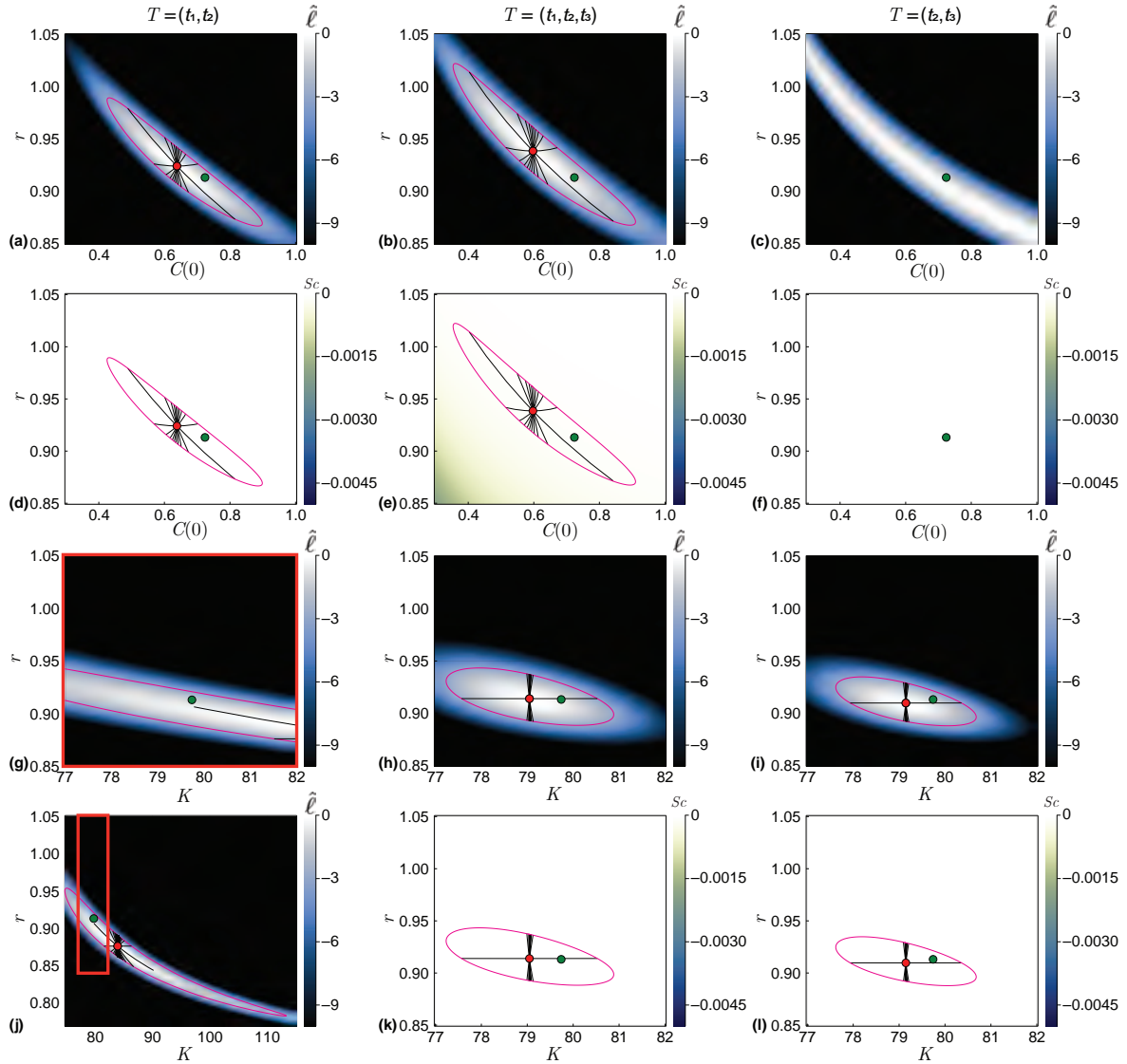


Figure 5.8: Logistic growth model with inferred growth rate, r , and initial condition, $C(0)$, (a-f); and with inferred growth rate, r , and carrying capacity, K , (g-l). True parameters are as noted in Figure 5.6, with known standard deviation, $\sigma = 2.301$. Heatmaps visualise the normalised log-likelihood (a-c,g-j) and the scalar curvature (d-f,k-l). The true parameter values are marked with green discs, with the MLEs indicated using red discs. Magenta curves correspond to likelihood-based 95% confidence regions. Black lines are geodesic curves emanating from the MLEs, with lengths corresponding to a theoretical 95% confidence distance. Columns of the figure correspond to observations from early-mid time ($T = (t_1, t_2)$), early-mid-late time ($T = (t_1, t_2, t_3)$), and mid-late time ($T = (t_2, t_3)$), where $(t_1, t_2, t_3) = (2.74, 6.84, 10.95)$ years. Each plot reflects a total of 30 observations, distributed equally between the specified time-points. The red outline in (j) corresponds to the (zoomed in) region (g), also outlined in red. In (g,j) we plot 1000 geodesics to observe the geodesic near the true parameter values. We do not present Sc corresponding to (g,j), however it is zero everywhere.

region and reducing the scalar curvature. This reduces the apparent curvature of the confidence region.

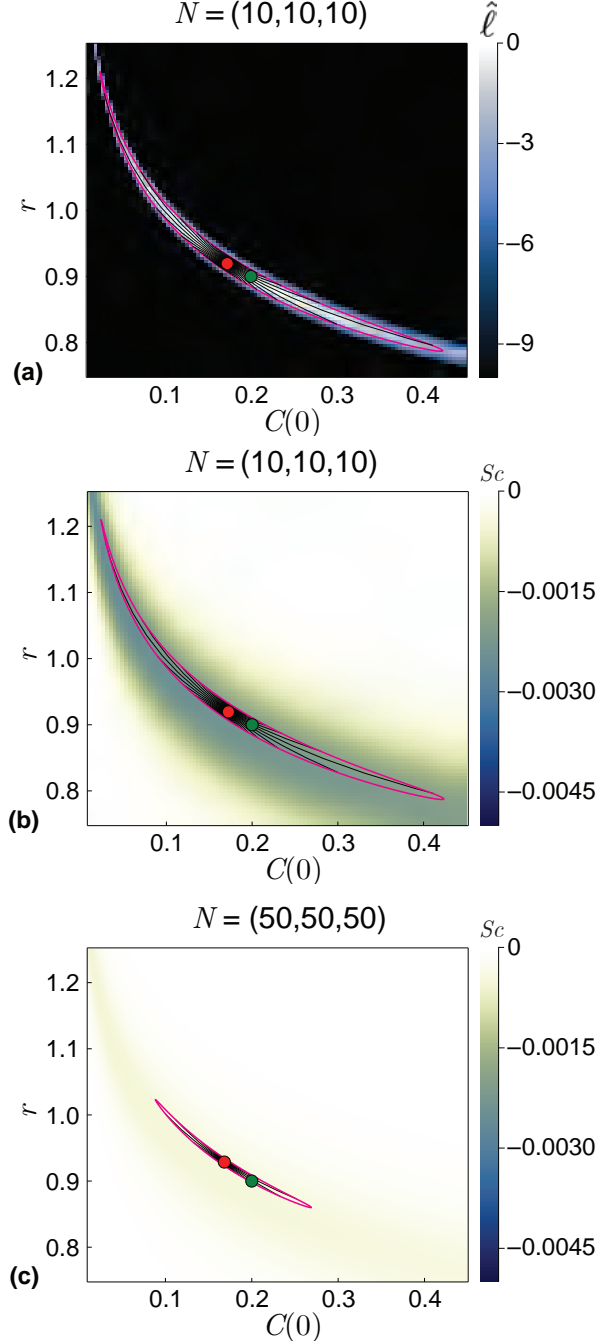


Figure 5.9: Logistic growth model with inferred growth rate, r , and initial condition, $C(0)$, with known standard deviation, $\sigma = 2.301$ and carrying capacity, $K = 79.74$. Heatmaps visualise the normalised log-likelihood (a) and the scalar curvature (b-c). Data is observed at $T = (2.74, 6.84, 10.95)$, with 10 (a-b) and 50 (c) observations per time-point. The true parameter values are marked with green discs, with MLEs indicated using red discs. Magenta curves correspond to likelihood-based 95% confidence regions. Black lines are 100 geodesic curves emanating from the MLEs, with lengths corresponding to a theoretical 95% confidence distance.

5.3.3 SIR epidemic model

The SIR model describes the dynamics of epidemic transmission through a population [235]. Populations are assumed to be comprised of susceptible, $s(t)$, infected, $i(t)$, and recovered, $r(t)$, individuals. The total population, \mathcal{N} , is held constant. When analysing the SIR model in this work, we consider each population as a proportion of the total population, such that $S(t) = s(t)/\mathcal{N}$, $I(t) = i(t)/\mathcal{N}$, and $R(t) = r(t)/\mathcal{N}$. Quantities \mathcal{N} , $s(t)$, $i(t)$ and $r(t)$ are dimensional with dimensions of number of individuals, whereas $S(t) \in [0, 1]$, $I(t) \in [0, 1]$ and $R(t) \in [0, 1]$ are dimensionless quantities with the property that $S(t) + I(t) + R(t) = 1$. While the coral re-growth process considered in the population model examples takes place over many years, epidemic occur over a timescale of days or weeks. As such, we now take t to represent time as measured in days, rather than years. The parameters of the SIR model are the infection rate, β [day $^{-1}$], and the rate at which infected individuals are removed, γ [day $^{-1}$], for example, via recovery from the infection:

$$\begin{aligned}\frac{dS}{dt} &= -\beta SI, \\ \frac{dI}{dt} &= \beta SI - \gamma I, \\ \frac{dR}{dt} &= \gamma I.\end{aligned}\tag{5.28}$$

Alongside β and γ we could also treat the initial conditions; $S(0)$, $I(0)$ and $R(0)$, as unknown parameters to be estimated. The standard SIR model presented in Equation (5.28) is sufficient for our purposes in this work, however numerous extensions to the SIR model are considered in the literature. These extensions incorporate factors such as age structure, birth and death, exposed but not yet infected individuals, seasonality, competition between infectious strains, waning immunity, vaccination and spatial structure [70, 235, 253, 281].

Data pertaining to the proportion of a population infected during an influenza outbreak in a boarding school is presented in Figure 5.10. Observations in the original data record the number of infected individuals over a 14 day period [235], in a population of $\mathcal{N} = 763$, with initial populations $(s(0), i(0), r(0)) = (762, 1, 0)$. This data is used in [235] to estimate parameters for the SIR model, which, after scaling such that $S + I + R = 1$, are $\beta = 1.6633$ and $\gamma = 0.44036$. We treat these values as the true parameters when generating synthetic data; examples of which are presented in Figure 5.11. In the context of an SIR model, the presence of multiple observations at a single time-point could reflect, for example; reporting errors, uncertainty in test accuracy or expert judgement [137, 347]. In the boarding school data considered in [235], observations pertain only to the number of infected individuals. Given that the SIR model features multiple populations, data could in theory contain observations of the other populations also. Example synthetic

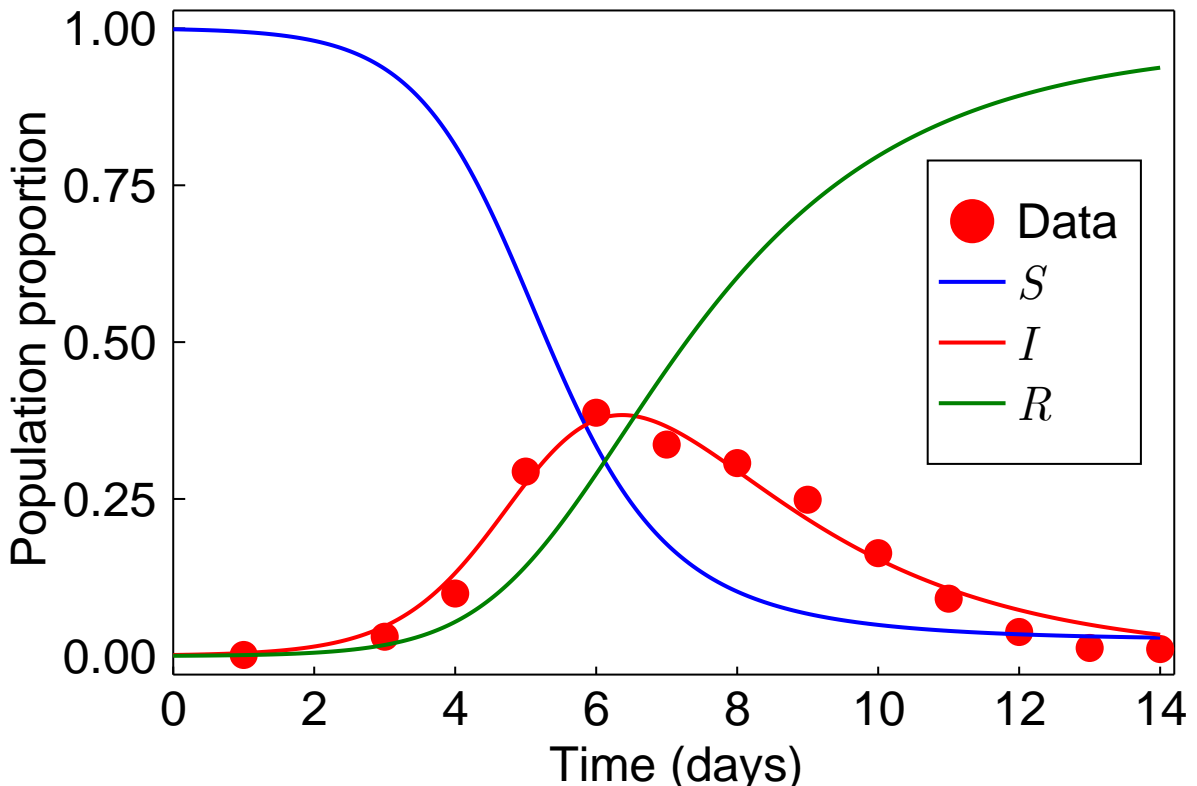


Figure 5.10: Data marked with red discs represents number of infected individuals during an influenza outbreak in a boarding school [235]. Susceptible, $S(t)$, infected, $I(t)$, and recovered, $R(t)$ populations are modelled according to Equation (5.28) based on parameters inferred in [235], $\beta = 1.6633$, $\gamma = 0.44036$; which we treat as the true parameters when generating synthetic data. Initial population proportions are $S(0) = 762/763$, $I(0) = 1/763$ and $R(0) = 0$.

data with observations on all three populations is presented in Figure 5.11b.

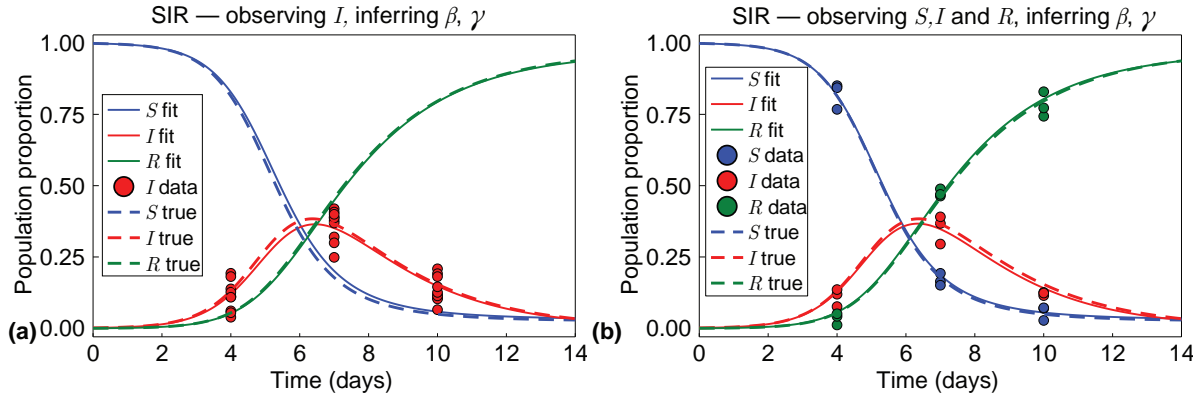


Figure 5.11: Example synthetic data generated from the SIR model under the scenarios where: (a) only the number of infected individuals is observed, and; (b) where we have observations pertaining to all three populations. Observations are marked with discs. Populations are modelled according to Equation (5.28) based on parameters inferred in [235]. Initial population proportions are $S(0) = 762/763$, $I(0) = 1/763$ and $R(0) = 0$. In (a) there are $N = 10$ observations at each time-point, and we prescribe $\sigma = 0.05$; in (b) there are three observations per time-point, per population, with prescribed $\sigma = 0.03$. The choices of σ are sufficiently small that the data generated consists only of positive observed population proportions.

The SIR model as described in Equation (5.28) does not admit a closed form analytical solution, so we apply numerical techniques to solve the system. This becomes somewhat computationally expensive, as the Fisher information computations rely on partial derivatives of the model solution with respect to the parameters to form the model Jacobian, and the information geometry computations require partial derivatives of the Fisher information up to second order. Approximating these partial derivatives using numerical techniques entails solving the system of ODEs several times. Some computational cost may be spared through taking advantage of the known relationship that $S + I + R = 1$.

For brevity, we restrict our investigation of the SIR model to the cases where $\boldsymbol{\theta} = (\beta, \gamma)$ and $\boldsymbol{\theta} = (\beta, \sigma)$. Results in Figure 5.12 correspond to the case where observations pertain only to the number of infected individuals, while those in Figure 5.13 are produced from data containing observations of all three populations. In both cases the results for $\boldsymbol{\theta} = (\beta, \sigma)$ align with that observed in previous results; the geodesics appear to define a marginally smaller area and are offset from the likelihood-based confidence regions in the direction of decreasing σ , and the scalar curvature is the constant $Sc = -1/N$.

Regardless of whether we observe only the infected population or all populations, inferring $\boldsymbol{\theta} = (\beta, \gamma)$ produces a non-constant positive scalar curvature. In Figure 5.12b, where only I is observed, we see that the geodesics emanating from the MLE extend beyond the likelihood-based confidence region. This also occurs in Figure 5.13b, where all three populations are observed, however it is difficult to perceive at this scale. Based

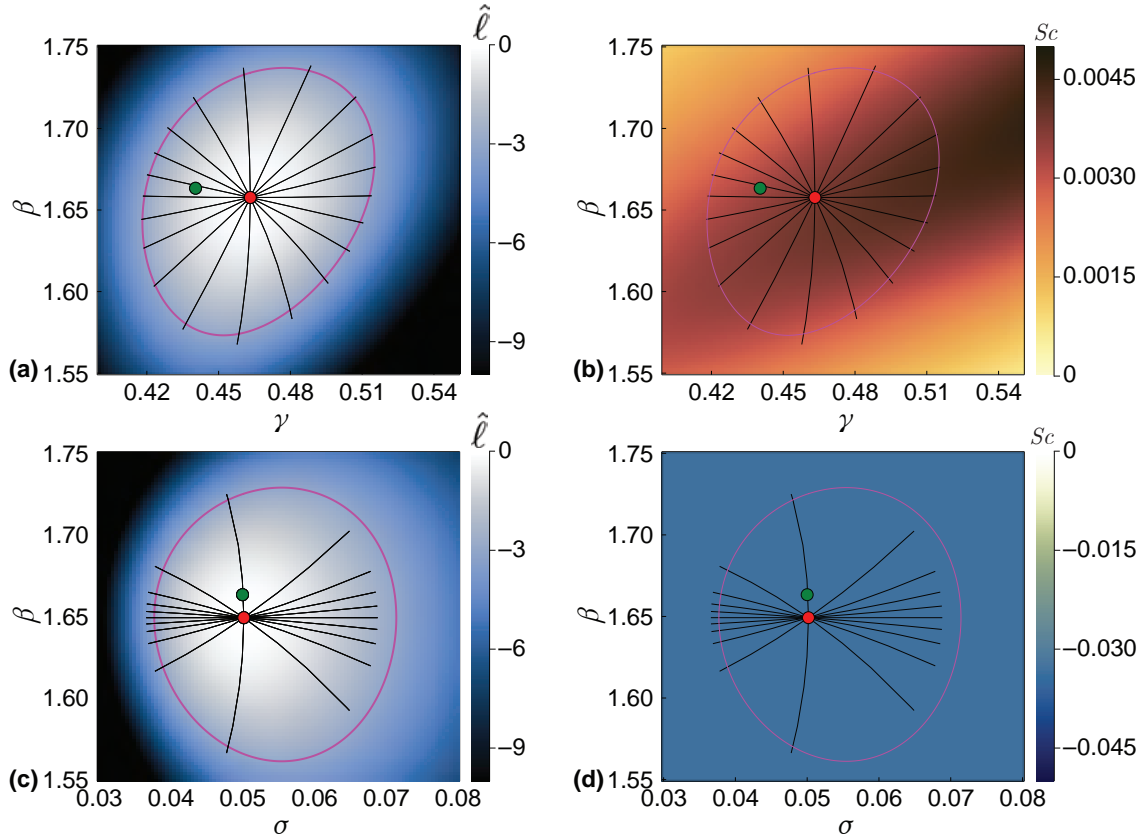


Figure 5.12: Inferring $\boldsymbol{\theta} = (\beta, \gamma)$ in (a,b) and $\boldsymbol{\theta} = (\beta, \sigma)$ in (c,d), for the SIR model with observations only on the number of infected individuals. Observations in the synthetic data occur at $T = (4, 7, 10)$, with $N = 10$ observations per time-point. True parameters, $(\beta, \gamma, \sigma) = (1.66334, 0.44036, 0.05)$, are marked with green discs, with MLEs indicated using red discs. Magenta curves correspond to likelihood-based 95% confidence regions. Black lines are geodesic curves emanating from the MLEs, with lengths corresponding to a theoretical 95% confidence distance. Initial populations are as described in Figure 5.11.

on this result, and the observations involving negative scalar curvature when inferring σ , it might seem that positive scalar curvature produces geodesics that extend beyond corresponding likelihood-based confidence regions, whereas negative scalar curvature has the opposite effect. However, repeating the analysis with different synthetic data sets—generated from a different random seed—suggests that in some cases the geodesics will extend beyond the likelihood-based confidence regions, and in some cases they will fall short, however the scalar curvature remains positive in all cases.

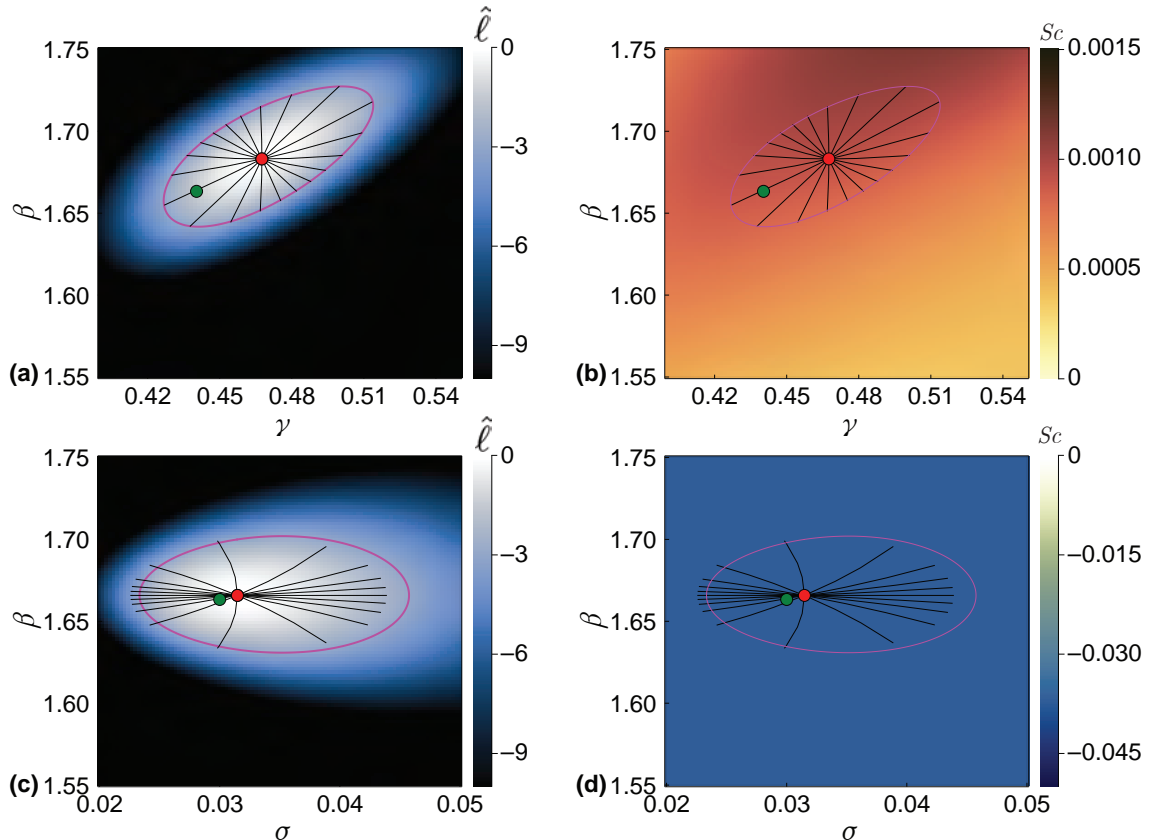


Figure 5.13: Inferring $\boldsymbol{\theta} = (\beta, \gamma)$ in (a,b) and $\boldsymbol{\theta} = (\beta, \sigma)$ in (c,d), with observations on all three variables, S , I and R . Observations in the synthetic data occur at $T = (4, 7, 10)$, with three observations of each population at each time-point; 27 observations in total, as depicted in Figure 5.11b. True parameters, $(\beta, \gamma, \sigma) = (1.66334, 0.44036, 0.03)$, are marked with green discs, with MLEs indicated using red discs. Magenta curves correspond to likelihood-based 95% confidence regions. Black lines are geodesic curves emanating from the MLEs, with lengths corresponding to a theoretical 95% confidence distance. Initial populations as described in Figure 5.11.

5.3.4 Hypothesis testing

In Figure 5.14 we present several example hypothesis tests, using both likelihood-ratio-based and geodesic-distance-based approaches, as outlined in Section 5.2. Test statistics and corresponding p -values for each hypothesis test are provided in Table 1. For the multivariate normal distribution, where we observe that the endpoints of geodesics corresponding to a theoretical 95% confidence distance align closely with the likelihood-based 95% confidence regions, we find that the results of the hypothesis tests are near-identical. Further, the hypothesis test results are consistent with our interpretation of the 95% confidence regions; test points within the confidence regions have p -values greater than 0.05, while test points outside the confidence regions have p -values less than 0.05.

We also perform hypothesis tests for the logistic model in the high curvature region of parameter space. Like before, results are comparable for different numbers of observations at each time point; $N = (10, 10, 10)$ and $N = (50, 50, 50)$, as considered in Figure 5.9. Even in this high curvature region, we find that the endpoints of geodesics corresponding to a theoretical 95% confidence distance very closely match the likelihood-based 95% confidence regions. This is again reflected in the results of the hypothesis tests, where very similar results are obtained from the likelihood-ratio-based hypothesis tests and the geodesic-distance-based hypothesis tests, even for relatively extreme θ_0 . As the number of observations increases, we observe for each θ_0 considered, that in accordance with the confidence regions tightening, the test statistics increase and accordingly p -values decrease.

Table 5.1: Hypothesis test results

Model	θ_0	λ_{LR}	λ_{GD}	p_{LR}	p_{GD}
Multivariate Normal	(0.8,1.0)	3.3737	3.3737	0.1851	0.1851
	(0.9,1.4)	10.9297	10.9297	0.0042	0.0042
Univariate Normal	(0.6,0.3)	7.5051	5.1954	0.0235	0.0744
	(0.6,0.6)	1.0460	1.2201	0.5927	0.5433
	(0.6,0.85)	4.6134	6.5226	0.0996	0.0383
	(0.6,1.0)	6.9271	10.6665	0.0313	0.0048
Logistic (10, 10, 10)	(1.0,0.095)	2.7086	2.5798	0.2581	0.2753
	(0.87,0.25)	1.6387	1.5626	0.4407	0.4578
	(0.92,0.21)	30.0130	29.9821	3.0391×10^{-7}	3.0865×10^{-7}
	(0.9,0.15)	56.2776	56.5328	6.0185×10^{-13}	5.2969×10^{-13}
Logistic (50, 50, 50)	(1.0,0.095)	31.3038	31.0222	1.5939×10^{-7}	1.8349×10^{-7}
	(0.87,0.25)	4.2062	4.2276	0.1221	0.1208
	(0.92,0.21)	97.6247	97.5164	$< 10^{-16}$	$< 10^{-16}$
	(0.9,0.15)	368.1479	368.7335	$< 10^{-16}$	$< 10^{-16}$

As we are using synthetic data and know the true parameters, we can use hypothesis testing to pedagogically investigate Wilks' theorem [255] and the asymptotic relationship given in (5.15). We generate 1000 synthetic datasets and for each dataset perform a hy-

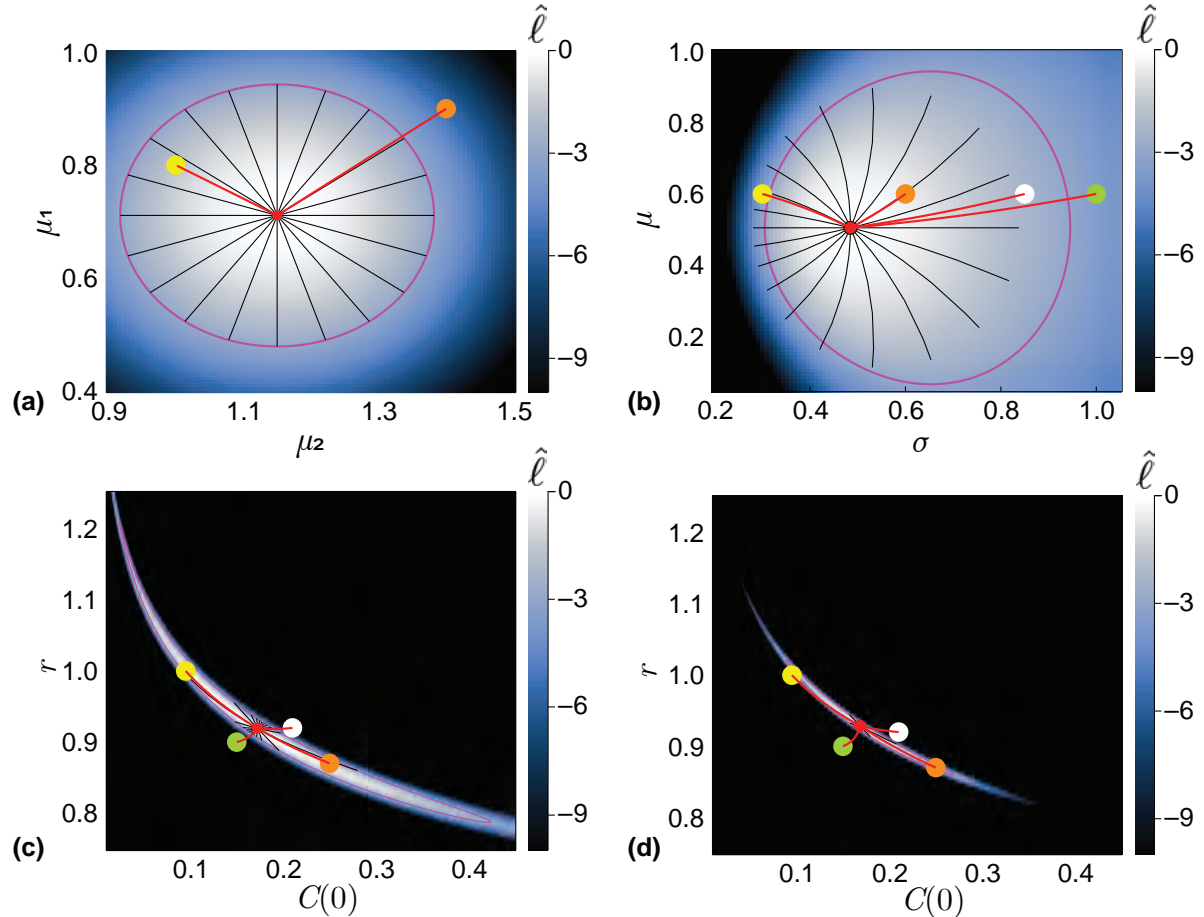


Figure 5.14: Example hypothesis tests for the: (a) univariate normal distribution, with $\theta = (\mu, \sigma)$, $\hat{\theta} = (0.5050, 0.4846)$; (b) multivariate normal distribution, with $\theta = (\mu_1, \mu_2)$, $\hat{\theta} = (0.7109, 1.1498)$; logistic model with $\theta = (r, C(0))$ in the high curvature region as considered in Figure 5.9, with (c) $N = (10, 10, 10)$, $\hat{\theta} = (0.9195, 0.1723)$, and (d) $N = (50, 50, 50)$, $\hat{\theta} = (0.9287, 0.1682)$. In each case, we test several example hypotheses, θ_0 , marked by coloured discs. Geodesics between the MLEs (red discs) and each θ_0 are shown in red. Magenta curves correspond to likelihood-based 95% confidence regions. Black lines are geodesic curves emanating from the MLEs, with lengths corresponding to a theoretical 95% confidence distance.

pothesis test for the true parameters. This is repeated for the univariate and multivariate normal distributions with $N = 10$ and $N = 1000$ observations. In Figure 5.15 we present densities for both the likelihood-ratio-based and geodesic-distance-based test statistics, alongside the probability density of $\chi^2(2)$. For the multivariate normal distribution with $\theta = (\mu_1, \mu_2)$, the density profiles for λ_{LR} and λ_{GD} are near-identical; as expected following the results in Figure 5.14 and Table 1. We also observe a good match between these profiles and $\chi^2(2)$, even with just $N = 10$. For the univariate normal distribution with $\theta = (\mu, \sigma)$, when $N = 10$ we observe differences between λ_{LR} and λ_{GD} . Both profiles are similar to $\chi^2(2)$, though there appears to be a higher density in the tails of the distributions of the test statistics. As the number of observations increases to $N = 1000$, the difference between λ_{LR} and λ_{GD} reduces significantly, and both closely match $\chi^2(2)$.

From Wilks' theorem [255] and (5.15), asymptotically 95% of the 95% confidence regions we construct should contain the true parameter values. We can determine what proportion of the likelihood-based and geodesic-distance-based 95% confidence regions that we construct contain the true parameter values using the information presented in Figure 5.15. This is done by comparing the test statistics to the critical value; $\Delta_{2,0.05}$, from (5.7). For the multivariate normal distribution with $N = 10$ we find that 95.7% of the likelihood-based and geodesic-distance-based confidence regions contain the true parameter values. With $N = 1000$ we find that 94.8% contain the true parameters, approaching the theoretical 95%. For the univariate normal distribution with $N = 10$ we find that 93.2% of the likelihood-based confidence regions contain the true parameter, while only 88.0% of the geodesic-distance-based confidence regions contain the true parameters. With $N = 1000$, we find that 95.2% of the likelihood-based confidence regions and 95.1% of the geodesic confidence regions contain the true parameters.

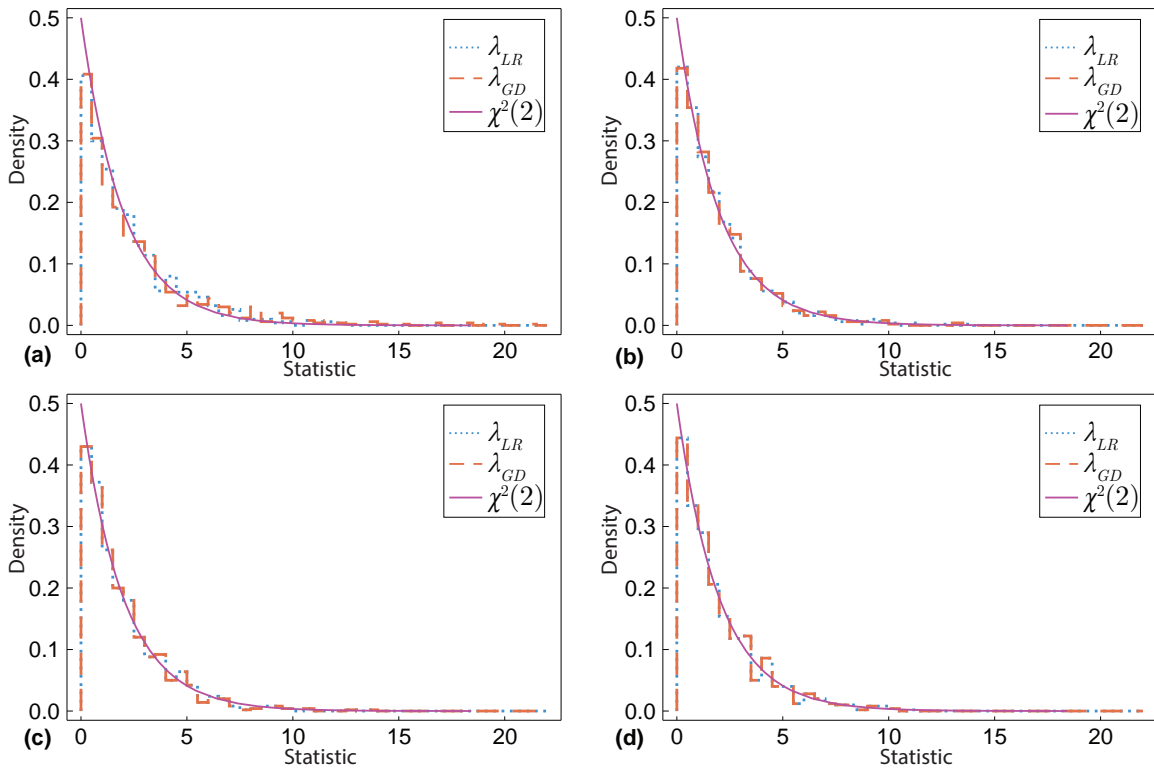


Figure 5.15: Step histograms show the density of the distribution of test statistics for each hypothesis testing approach, for (a,b): the univariate normal distribution with $\boldsymbol{\theta} = (\mu, \sigma)$, and (c,d): the multivariate normal distributions with $\boldsymbol{\theta} = (\mu_1, \mu_2)$. Test statistics are computed from the true parameter values and the MLE, for 1000 sets of synthetic data. Datasets represented in (a,c) contain $N = 10$ observations, while in (b,d) $N = 1000$. Purple curves correspond to the density of the $\chi^2(2)$ distribution, while blue dotted lines represent the likelihood-ratio-based test statistics and orange dashed lines represent the geodesic-distance-based test statistics.

5.4 Discussion

Parameter estimation is wrought with challenges relating to the availability and quality of experimental or field data [114, 145, 315, 325]. This prompts a strong consideration of uncertainty quantification to support point-estimation of model parameters [89]. In this section, we discuss the results presented in Section 5.3. We highlight opportunities for application of information geometry techniques, including geodesic curves and scalar curvature; to supplement traditional maximum likelihood based parameter inference and uncertainty quantification. We conclude by outlining areas for further investigation.

Even for relatively small sample sizes, we observe good correspondence between the likelihood-based 95% confidence regions and the end-points of geodesic curves corresponding to a theoretical 95% confidence distance, in accordance with the asymptotic relationship described in Equation (5.15); particularly when estimating model parameters. When estimating standard deviation, as outlined in Section 5.3, geodesics appear to suggest a tighter confidence region, and appear to be biased towards parameter space with smaller standard deviation. We observe this effect decreasing as the number of observations increases; in line with the known underestimation bias of minimum likelihood estimates of variance [255]. The misalignment of likelihood-based confidence regions and geodesic endpoints appears to occur more frequently in examples with non-zero scalar curvature, although we observe a good match in Figure 5.9 despite the non-constant scalar curvature.

Visualising the scalar curvature throughout a parameter space can indicate areas where there may be issues with identifiability. Areas with significant non-constant scalar curvature can suggest a complicated relationship between parameters in terms of the normalised log-likelihood, such as the hyperbolic confidence region observed in Figure 5.9. However, it is possible to produce examples, such as Figure 5.8(c,f), where there is practical non-identifiability despite zero scalar curvature everywhere. Although we do not show it here, for the logistic model with $\boldsymbol{\theta} = (r, K)$ in the region of parameter space where $C(0) \approx K$, computation of the scalar curvature breaks down as the Fisher information matrix becomes singular. Here, it may be obvious that we can not identify the growth rate, r , from a process that is initialised at its steady state ($C(0) = K$). However, observing this behaviour in general may help to detect issues with identifiability, particularly for models without analytical solutions.

The information geometry techniques we discuss are primarily implemented numerically; as such there is a computational cost to consider. For the normal distributions and population growth models in this work, where analytical solutions are available, the information geometry techniques are not disproportionately more computationally expensive than the traditional likelihood-based inference and confidence regions. Examples such as the SIR model, where no analytical solution is available, represent a significantly greater

computational burden. However, this impacts both the likelihood based inference and information geometry techniques as the underlying system of ODEs, for example Equation (5.28), must be solved numerous times. The computational cost associated with the information geometry techniques depends significantly on the desired resolution for the scalar curvature surface, and on the number of geodesic curves. A suitable approach may be to first compute the scalar curvature on a coarse grid to identify areas of interest to investigate with a refined grid. Further, the geodesic curves and scalar curvature computations are highly amenable to parallelisation, which can significantly reduce computation time.

This computational cost will generally pale in comparison to the costs associated with collecting experimental or field data, and may be easily justified if the information geometry techniques are used to guide data collection. If information geometric analysis identifies a region of parameter space with significant non-constant scalar curvature for a model, such as in Figure 5.9, and practitioners have a prior expectation that the true parameter values fall somewhere within this region, this may indicate that a greater quantity or quality of data is needed to improve identifiability for that particular model. Alternatively, such analysis may guide practitioners in choosing favourable experimental conditions; for example in cell culture experiments, where it is possible to vary the initial cell seeding density [52]. Experimental design is a process wherein experiments are performed or simulated iteratively with perturbations, such that some measure of information is maximised. Through this process the most informative experiments are identified, facilitating design of optimal experimental protocols [133, 198, 280]. Common to these approaches is the importance of quantifying and comparing information. While we do not consider optimal experimental design in this work, there is potential to incorporate information geometric techniques in the experimental design process as a means of comparing information between experimental perturbations. This is an area for further investigation.

Although we focus on how information geometry can supplement traditional maximum likelihood based inference and uncertainty quantification, primarily through visualisation, it should be noted that concepts from information geometry have also found application in the inference context from a computational efficiency standpoint. For example in Bayesian inference, by defining Monte Carlo sampling methods on a Riemann manifold, the geometric structure of the parameter space can be exploited [122]. Simulated paths across the manifold automatically adapt to local structure, facilitating efficient convergence, even in higher dimensions and in the presence of strong correlation [122, 146]. Concepts from information geometry, including geodesic curves, are also implemented in methods for model reduction [316]. These applications of information geometry techniques to improve computational algorithms highlight further utility of geometric concepts for inference in higher dimensions, beyond that which we demonstrate

through visualisation in this work.

Geodesics can be used to measure the distance between probability distributions. As demonstrated in Section 5.3, it is possible to perform hypothesis tests based on geodesic distance [162, 228, 239]. The approach for performing a hypothesis test is to solve a boundary value problem to find the geodesic connecting two points in parameter space, and use the corresponding geodesic distance to compute a test statistic. For the examples considered in this work, such boundary value problems are readily solved numerically using standard techniques, such as those included in the Julia package DifferentialEquations.jl [272]. Careful numerical handling may be required for geodesic curves close to boundaries of parameter space. For more complicated examples, particularly those in high-dimensional manifolds, achieving converging solutions to geodesic boundary value problems can prove challenging. There is scope for a review of the different numerical methods for solving boundary value problems, with a particular focus on their applicability to solving geodesic boundary value problems for hypothesis testing in high-dimensional manifolds.

In this work we only consider models that admit unimodal likelihoods. In cases where the likelihood is multimodal; provided that we are able to obtain the Fisher information required to compute the Christoffel symbols, we are still able to compute the scalar curvature and perform hypothesis tests based on geodesic distance. With multimodal likelihoods, it would not be possible to construct confidence regions from geodesics emanating from the MLE. Although, we note that constructing confidence regions for multimodal likelihoods is also problematic with traditional likelihood-based inference methods.

There are several avenues for future research in this area. Here, we consider two-dimensional manifolds to facilitate convenient visualisation, however the inference and information geometry techniques are general, and can be readily applied to higher dimensional manifolds [13, 255]; albeit with increased computational cost. Extending this analysis to three dimensions would enable consideration of situations where there is scalar curvature associated both with the variability of the observation process, σ , and also with interactions between model parameters; for example, it may be insightful to consider $\boldsymbol{\theta} = (\beta, \gamma, \sigma)$ for the SIR model, where we associate a constant negative scalar curvature with σ and non-constant positive scalar curvature due to interactions between β and γ . In three dimensions, likelihood-based confidence regions can be visualised as a series of two-dimensional slices oriented in three-dimensional space [52]; this technique could be applied to visualise slices of the scalar curvature in three-dimensions. One approach for visualisation in higher dimensions is to produce an ensemble of these two- or three-dimensional confidence regions for various combinations of parameters of interest, with other parameters fixed at their MLEs. Alternatively, in higher dimensions it may be more appropriate to use non-visual techniques, such as hypothesis testing.

While we have considered ODE models, there is appetite in the literature for pa-

parameter estimation, uncertainty quantification and identifiability analysis for more complicated models; including partial differential equations, stochastic differential equations (SDEs), delay differential equations [42, 227, 298]. This appetite extends to non-differential-equation-based models, including agent-based models [182] and network models [138]. A natural extension of this work is to present examples demonstrating how the information geometry techniques can be applied to these more complicated models. This will introduce new challenges, though it may be possible to leverage existing techniques; for example, linear noise approximation may be used to obtain a representation of the Fisher information matrix for SDEs [172]. Further, we fix σ across observation times, model parameters and populations. However, the techniques presented in this work can be generalised to handle data with non-constant variance [53]; the expression for the Fisher information matrix given in Equation (5.4) can be extended to account for a parameter-dependent covariance matrix [212]. Investigation of examples paralleling those in Section 5.3, but with non-constant standard deviation, may prove insightful.

Here, the Fisher information defines a Riemann metric on the statistical manifold. For some inference problems it is not practical to obtain the Fisher information. Where the Fisher information is not available, the sample-based *observed information*—computed as negative the Hessian of the log-likelihood function, or via Monte Carlo methods—may be available [98, 267]. The observed information has been demonstrated to equip a manifold with an *observed geometric structure* akin to the *expected geometric structure* associated with the Fisher information [34]. Further work could identify the viability of the techniques presented here in situations where only the observed information is available, particularly for local approximation about the MLE.

Data accessibility

Data and code is made available on [GitHub](#).

Competing interests

We declare we have no competing interests.

Funding

J.A.S. and A.P.B. acknowledge support from the Australian Government Research Training Program. J.A.S acknowledges support from the AF Pillow Applied Mathematics Trust. J.A.S., A.P.B. and K.B. acknowledge support from the Australian Centre of Excellence for Mathematical and Statistical Frontiers (CE140100049). M.J.S. is supported

by the Australian Research Council (DP200100177).

Acknowledgements

We thank Professor Alan Garfinkel (UCLA) for introducing K.B. to information geometry, and for numerous discussions while both were at the University of Oxford. We also thank Dr. Brodie Lawson (QUT) for some helpful discussions. Finally, we thank two anonymous referees for their helpful comments.

Chapter 6

Conclusions and future work

In this chapter we recapitulate the key outcomes of this thesis. We highlight the novel and significant contributions to the literature, and identify avenues for future research.

6.1 Summary and contribution

This thesis concerns numerical methods frequently applied in the life sciences, with a particular focus on techniques for optimal control, and parameter estimation and uncertainty quantification. We discuss in great practical detail the implementation of the forward-backward sweep method for solving two-point boundary value problems arising from application of the Pontryagin maximum principle in optimal control. Initially, we apply the FBSM to study the optimal chemotherapy treatment for a model of acute myeloid leukaemia [82], and investigate the convergence behaviour [290]. Motivated by combination therapies observed in cancer treatment [59], we consider the application of multiple optimal controls simultaneously [291]. Finally, we discuss numerical techniques to improve and accelerate the convergence of the FBSM [292]. Connecting models with data poses significant challenges, particularly in the life sciences; where data is often limited, noisy or incomplete [145]. As such, we are interested not only in point-estimates of parameters but also information characterising the associated uncertainty [325]. In the second part of this thesis we explore techniques from information geometry to supplement traditional likelihood-based uncertainty quantification for parameter inference.

In this thesis, we have addressed the following objectives:

- (1) Modify a stem cell model for AML to incorporate an immune response, and use optimal control techniques to investigate optimal chemotherapy treatment regimes.
- (2) Extend the work with the model of AML from Objective 1 to investigate the application of multiple optimal controls to interacting species.

- (3) Unify disparate parts of the optimal control and numerical methods literature and improve accessibility of optimal control techniques.
- (4) Develop novel improvements to the FBSM for optimal control, to achieve faster and more reliable convergence.
- (5) Demonstrate the insights that can be attained by supplementing likelihood-based parameter inference with information geometry techniques.
- (6) Improve the accessibility of information geometry techniques to practitioners in the life sciences.

Here, we provide a brief summary of each chapter. In Chapter 2 we introduce a biologically appropriate and mathematically convenient immune response into a haematopoietic stem cell model of AML [82, 290]; such that the model admits a stable healthy steady state, where leukaemic cells are eradicated. We demonstrate the application of continuous and bang-bang controls to the modified model under various parameter regimes, and show how the optimal controls can steer the system from an unhealthy steady state with coexistence of healthy and leukaemic cells; to a healthy steady state free from leukaemic cells. We demonstrate that the convergence behaviour of the FBSM depends both on the control update weighting parameter, ω , and the weighting parameters in the pay-off that determine the relative importance of minimising the leukaemic cell population and minimising the negative impact from the chemotherapy. We also consider how the optimal control strategies differ in the situation where the negative impact of the chemotherapy is modelled explicitly; as additional death of healthy cells. This chapter provides methodological insights that motivate Chapter 3, as it demonstrates that the optimal control techniques can be applied to situations where the control impacts multiple interacting species. Chapter 2 addresses Objective 1, and corresponds to Paper 1: *Optimal control of acute myeloid leukaemia*, published 2019 in the Journal of Theoretical Biology [290]. We provide clear and well-documented code for this chapter on [GitHub](#).

In Chapter 3 we extend our investigation of the AML model from Chapter 2, to consider multiple interacting species within an ecological niche. We consider the application of multiple optimal controls to interacting populations with resource competition; where abundance of one species is desirable and the other is undesirable. We produce results for a range of pay-off forms and weightings, corresponding to both controls being continuous, both controls being bang-bang, and a combination of continuous and bang-bang controls. We show that varying the parameters governing interaction between species can elicit a highly nonlinear response from the optimal control strategies. We demonstrate that interspecies interactions introduce complexity when designing optimal interventions; however, they also provide opportunities for exploitation if the controls can be designed

to take advantage of the particular interspecies interactions. Chapter 3 addresses Objective 2, and corresponds to Paper 2: *Designing combination therapies using multiple optimal controls*, published 2020 in the Journal of Theoretical Biology [291]. We provide clear and well-documented code for this chapter on [GitHub](#).

In Chapter 4 we comprehensively review the theory of optimal control, and numerical methods for solving control problems. We focus on the PMP approach to optimal control, and the implementation of the FBSM. Prior to completing this review, we find the literature to be fragmented and sparse in terms of practical guidance for implementation of the numerical methods for optimal control. To address this gap in the literature, we take a pedagogical approach and apply optimal control techniques to solve continuous, bang-bang, and fixed endpoint control problems for both a single-variable linear model, and a multi-variable nonlinear model. We provide detailed discussion regarding practical considerations for numerical implementation of the FBSM and analyse the convergence behaviour. We propose novel augmentations to improve and accelerate the convergence behaviour of the FBSM; including the Wegstein method, Aitken and Steffensen methods and Anderson acceleration. We demonstrate that we are able to not only accelerate convergence of the FBSM; but also improve its robustness—in some instances inducing convergence where the underlying FBSM fails to converge—without requiring prohibitively costly tuning of the acceleration techniques. We highlight that the most promising application of the acceleration techniques is not necessarily for solving individual control problems, but rather for solving families of related control problems; such as those that arise in fixed endpoint control problems, or from producing a Pareto frontier of optimal controls when facing uncertainty in pay-off weightings [10, 164, 204]. Chapter 4 addresses Objective 3 and Objective 4, and corresponds to Paper 3: *Implementation and acceleration of optimal control for systems biology*, published 2021 in the Journal of the Royal Society Interface [292]. We provide clear and well-documented code for this chapter on [GitHub](#).

In Chapter 5 we review fundamental concepts in inference and information geometry. We demonstrate how information geometry techniques can supplement traditional likelihood-based parameter estimation and uncertainty quantification, through application to pedagogical examples in the life sciences. We implement the techniques for linear and nonlinear ODE models, and systems of coupled nonlinear ODEs, with observational data that includes examples where single and multiple observations are recorded. We consider cases where combinations of model parameters, initial conditions, and the variability of observations are estimated. We demonstrate that the information geometry techniques can provide insight into uncertainty quantification and identifiability, and guide data collection. In unifying inference and information geometry concepts and improving their accessibility, we focus heavily on practical implementation and interpretation; and do not assume any prior knowledge of inference or differential geometry. Chapter 5 addresses

Objective 5 and Objective 6, and corresponds to Paper 4: *Parameter estimation and uncertainty quantification using information geometry*, accepted for publication in 2022 and currently in press at the Journal of the Royal Society Interface [293]. We provide clear and well-documented code for this chapter on [GitHub](#).

6.2 Future work

The numerical techniques and examples explored in this thesis lay a sound foundation with broad opportunity for future development. Here, we discuss some of the most promising avenues for extending the ideas explored in this work.

6.2.1 Optimal control

Biological fidelity

In Chapter 2, we model a chemotherapy control for acute myeloid leukaemia via a simple and fairly abstract mechanism; a direct increase in the death rate of the leukaemic population. We extend this in the supplementary material to Chapter 2 by considering a chemotherapy control that also directly kills healthy cells. Another approach for incorporating additional biological fidelity to this process is to introduce pharmacokinetic processes such as drug absorption and metabolism, such that the control determines the supply of the chemotherapeutic agent, but its effect is captured through mechanisms explicitly incorporated in the model. In clinical settings it has been observed that cell production may not occur for several weeks following a stem cell transplant [69]. This effect could be incorporated into the model as a delay to the impact of the stem cell transplant on the system; potentially via delay differential equations, for which the PMP has been extended [43]. Incorporating additional biological fidelity comes at the cost of increasing the number of unknown, and possibly unmeasurable parameters; as we discuss in the inference and uncertainty quantification component of this thesis. We could also reformulate the control problems presented in Chapter 2 and Chapter 3 as fixed final state problems—where the treatment continues until the leukaemic population falls below a prescribed threshold—leaving the final time free to vary. This more accurately reflects cancer treatment in a clinical setting.

With the introduction of an immune mechanism to the model of acute myeloid leukaemia in Chapter 2, it is possible to consider an immunotherapy control; we explore this in Chapter 3. However, the immune response that we introduce is phenomenological rather than mechanistic. Introducing a mechanistic immune response, for example through modelling the various populations of immune cells [3], may facilitate a more in-depth consideration of immunotherapeutic controls.

We have studied models of AML through systems of time-dependent ODEs. While informative, this approach does not allow for incorporation any spatial heterogeneity of tumours or drug concentrations, or spatially dependent cell behaviours. Recent studies suggest that spatial heterogeneity in the tumour microenvironment can significantly impact cancer development and evolution [343], and therefore may impact the optimal treatment protocol. Mathematical modelling suggests that heterogeneity of chemotherapy drugs within the tumour microenvironment and across metastases may also contribute to the emergence of drug resistance [115]. Incorporating spatial effects through a PDE model of AML and the associated optimal control could yield interesting insights.

Clinically motivated optimal controls

In Chapter 3 we discuss the application of multiple controls simultaneously, as motivated by observing combination therapies for treatment of acute myeloid leukaemia. In combination therapies for cancer treatment, patients receive two or more treatments concurrently; including chemotherapy, stem cell therapy and radiotherapy [59]. This is only one of many clinically motivated control scenarios that could be considered. A recent idea gaining traction in clinical cancer treatment settings is the introduction of an interval of time during the course of treatment where no chemotherapy is applied. This on-off style of intervention parallels bang-bang control, and is referred to in the literature as a *drug holiday* [313]. One motivation for pursuing the drug holiday line of treatment is evidence suggesting that drug resistance of tumour cells may wane, such that following a drug holiday, the patient may respond more promisingly to chemotherapy treatment [174, 180, 287]. Investigating the requirements of the mathematical model and control formulation that yields a treatment regime featuring drug holidays may provide valuable insights into clinical applicability and design of such approaches.

An emerging trend in diagnosis and treatment of acute myeloid leukaemia, and in clinical practice generally, is that of personalised or individualised medicine [132]. As technology improves, we are better equipped to measure a diverse range of biological and molecular signals (biomarkers) in patients, on a case-by-case basis. Tools could be developed to interpret these biomarkers, possibly integrated with techniques we discuss in Chapter 5, with a view to informing patient-specific model parameterisation. Optimal control strategies calibrated to models with patient-specific parameters represent a significant opportunity in personalised medicine.

Numerical methods

Throughout this thesis we have considered a broad range of control problem formulations, though the examples are not exhaustive. Further challenges can be introduced; either through the formulation of the control problem, or the behaviour of the underlying system.

Examples of such challenges include control problems with singular arcs, path constraints, multiple local solutions, discontinuous dynamics and sensitivity to the initial guess of the control [319]. Each of these challenges introduces numerical difficulties, and can introduce complications in the optimal control theory. For example, for control problems that admit solutions with singular arcs, the conditions derived from the PMP may fail to characterise optimality; as the Hamiltonian is independent of the control over the singular interval [55, 191]. A comprehensive assessment of the applicability of the FBSM for solving control problems with such complications, and any modifications required, is an avenue for further investigation.

An interesting observation in Chapter 4 is that the acceleration methods can induce convergence where the underlying FBSM does not converge; for example in the AML control problems with $\omega = 0$. It should be noted that the FBSM does converge for the particular examples considered for appropriately chosen ω . An interesting avenue for further research is to identify control problems that cannot be solved via the FBSM for any ω , to investigate whether the acceleration methods can induce convergence in these cases.

Inverse optimal control

In this thesis, we focus on the *forward problem*; given a particular model and pay-off functional or specified objectives, what is the optimal control. More recently, however, optimal control techniques have been applied in a systems biology context to further our understanding of the underlying mechanisms or processes involved in a given system. In the *inverse problem*, commonly referred to as inverse optimal control or inverse reinforcement learning, exhibited behaviour is investigated in an attempt to elicit the optimality principles that guide the underlying system [318]. Recent insights in systems biology obtained through this process include rationalisation for experimentally and numerically observed sequential activation of metabolic pathways [251]; and prediction of enzyme activation times and metabolite concentrations [319]. At a high level, inverse optimal control relates to the second part of this thesis; whereby mathematical models and inference techniques can develop our understanding—in the form of parameter values—of complex biological processes

6.2.2 Inference and uncertainty quantification

There are several avenues for future research into information geometry techniques in the context of parameter inference and uncertainty quantification. So far, we have limited ourselves to two-dimensional manifolds for ease of visualisation, however the techniques are general, and readily apply to problems concerning high-dimensional manifolds [13, 255]; albeit with increased computational cost. There is opportunity to explore this further,

with a particular focus on the performance of numerical methods in high-dimensional manifolds; and an aim to develop efficient algorithms and implementations, alongside guidance for interpretation of the results in higher dimensions.

A natural extension to the work in Chapter 5 is to consider how the information geometry techniques can be applied to more complicated models including delay differential equations, stochastic differential equations and partial differential equations. Further, the techniques we implement can be generalised to handle data with non-constant variance; investigating how this manifests—through a series of examples with increasing complexity, as we present in Chapter 5—may prove insightful.

Geodesics can be used to measure the distance between probability distributions; we can perform hypothesis tests based on this geodesic distance [162, 228, 239]. Performing hypothesis tests based on geodesic distance involves solving a boundary value problem to find the geodesic connecting two distributions. In few dimensions such as we consider in Chapter 5, these boundary value problems are readily solved via standard numerical techniques, and without significant computational expense. For more complicated examples, particularly those in high-dimensional manifolds, achieving converging solutions to geodesic boundary value problems can prove challenging. There is scope for a review of the different numerical methods for solving boundary value problems, with a particular focus on their applicability to solving geodesic boundary value problems for hypothesis testing in high-dimensional manifolds.

6.3 Final remarks

In the words of Frank Herbert’s *Dune*, “Science is made up of so many things that appear obvious after they are explained”. In this thesis we discuss, implement, and improve numerical methods frequently applied in the life sciences. We do this with a view to demystifying and unifying disparate and often sparsely explained areas of the literature; increasing the accessibility of the methods to a broad audience. At all stages we provide clear and detailed algorithms, with practical guidance related to implementation. We further support this by making code available for reproducing all examples in the thesis. We posit that this thesis serves not only as a vessel for novel ideas, but also as a pedagogical tool.

Chapter 2A

Supplementary material to Chapter 2

2A.1 Arbitrary initial conditions

Optimal control results in the Main paper are produced with an initial condition corresponding to a stable steady state of the system. In Figure 2A.1 we present results demonstrating that the optimal control techniques do not require such an initial condition. To produce these results we choose an arbitrary initial condition, solve the system numerically up to some transient time without control, $u \equiv 0$, then apply the FBSM from that transient time to the final time to determine the optimal control.

These results adhere to our intuitive expectations; with a larger initial leukaemic population, a greater amount of control is applied, for example compare Figure 2A.1d and Figure 2A.1e. Similarly, if there is a larger initial haematopoietic stem cell population, a smaller amount of control is required, for example compare Figure 2A.1a and Figure 2A.1c.

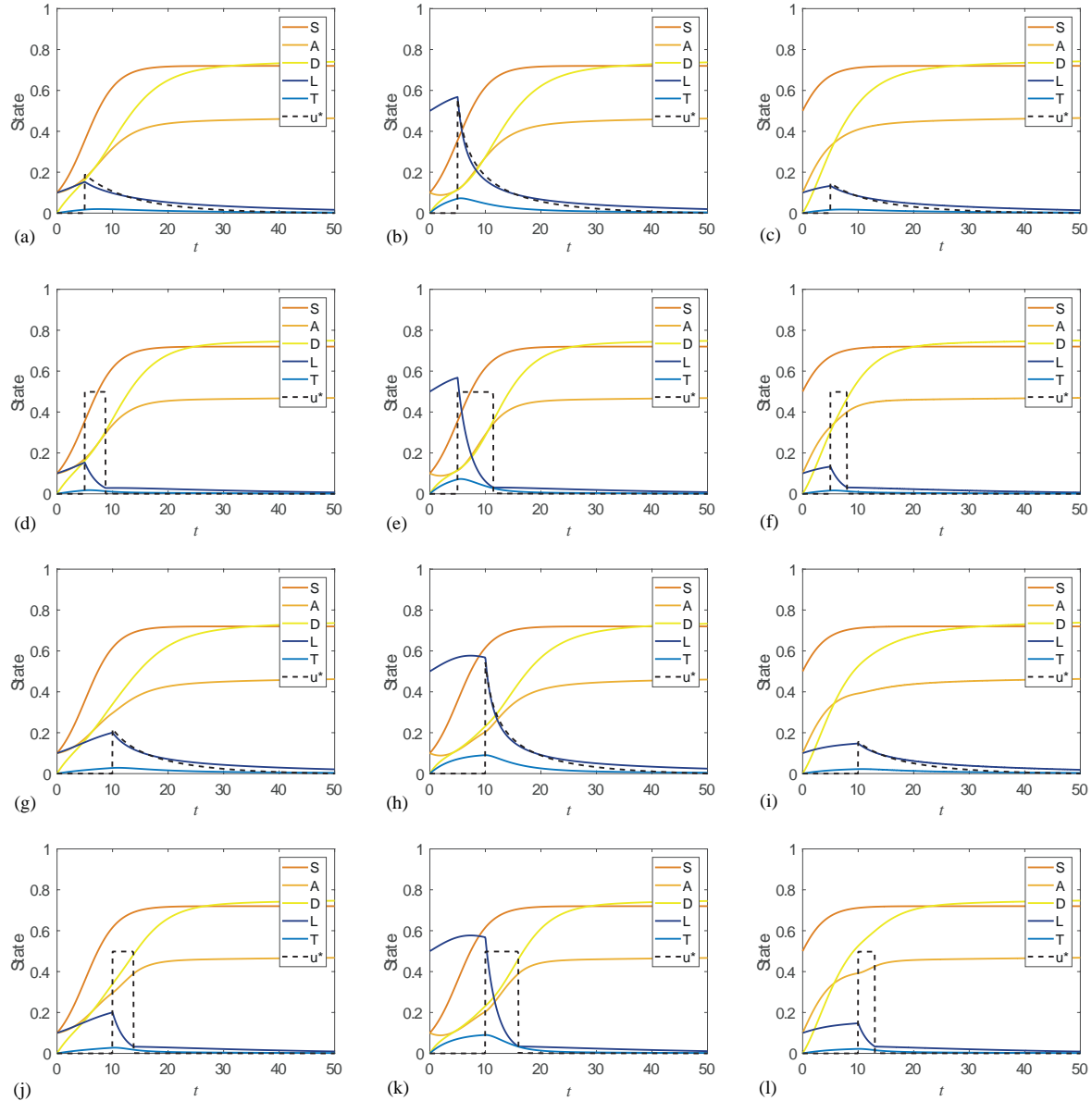


Figure 2A.1: Results are produced for a range of arbitrary initial conditions subject to a transient growth phase prior to application of a control. Columns from left to right correspond to initial conditions of $[0.1, 0.1, 0, 0.1, 0]$, $[0.1, 0.1, 0, 0.5, 0]$ and $[0.5, 0.1, 0, 0.1, 0]$. Control is applied from $t = 5$ in Figures (a-f) and from $t = 10$ in Figures (g-l). The first and third rows correspond to the continuous control case, while the second and fourth rows show the corresponding bang-bang case with an upper control bound of $u = 0.5$. For all results in this figure, $a_1 = a_2 = 1$.

2A.2 Control affects all proliferative cells

In reality, typical chemotherapy treatment of AML uses cytotoxic drugs that affect not only leukaemic cells but all proliferative cells [233]. In this section we demonstrate that our analysis can be extended to consider the case where the control also impacts the proliferative healthy cells; S and A . We extend our state equations (Equation 12, Main paper) by introducing terms with parameters r_1 and r_2 describing the rates at which the control, u , affects the S and A populations relative to its effect on the L population:

$$\begin{aligned}\frac{dS}{dt} &= \rho_S S(K_1 - Z_1) - \delta_S S - r_1 u S, \\ \frac{dA}{dt} &= \delta_S S + \rho_A A(K_2 - Z_2) - \delta_A A - r_2 u A, \\ \frac{dD}{dt} &= \delta_A A - \mu_D D, \\ \frac{dL}{dt} &= \rho_L L(K_2 - Z_2) - \delta_L L - \frac{\alpha L}{\gamma + L} - u L, \\ \frac{dT}{dt} &= \delta_L L - \mu_T T.\end{aligned}\tag{2A.1}$$

We define a pay-off function to minimise, such as

$$J = \int_0^{t_f} (a_1 u^2 + a_2 L^2) dt,\tag{2A.2}$$

for the continuous control case, or

$$J = \int_0^{t_f} (a_1 u + a_2 L) dt,\tag{2A.3}$$

for the bang-bang control case. Recalling that a_1 weights the relative importance placed on the negative impact of the control, we could at this point consider reducing a_1 relative to a_2 , as we have now explicitly accounted for the direct negative effect of the control on the healthy cells. We could also explicitly include S and A in the pay-off. The motivation for this becomes apparent when considering a control that affects S and A more than L ; $r_1, r_2 > 1$, as in Figure 2A.2g-l, as we see the healthy cell counts become very low during the treatment period, which may be clinically undesirable. These terms would need to be weighted negatively, as the pay-off is a quantity to be minimised.

Following the procedure in the Main paper we construct the Hamiltonian and find the optimal control by setting $\partial H/\partial u = 0$, or define a switching function in the bang-bang control case. Co-state equations for λ are found by setting $d\lambda/dt = -\partial H/\partial x$, giving

$$\begin{aligned}
\frac{d\lambda_1}{dt} &= 2S\lambda_1\rho_S + \delta_S\lambda_1 - \delta_S\lambda_2 - \lambda_1\rho_S + \lambda_1r_1u, \\
\frac{d\lambda_2}{dt} &= 2A\lambda_2\rho_A + L\lambda_2\rho_A + L\lambda_4\rho_L + \delta_A\lambda_2 - \delta_A\lambda_3 - \lambda_2\rho_A + \lambda_2r_2u, \\
\frac{d\lambda_3}{dt} &= \mu_D\lambda_3, \\
\frac{d\lambda_4}{dt} &= -2a_2L + \rho_AA\lambda_2 + \lambda_4\rho_LA + 2\rho_LL\lambda_4 - \lambda_4\rho_L \\
&\quad + \lambda_4\delta_L + \frac{\alpha\gamma\lambda_4}{(\gamma+L)^2} + \lambda_4u - \delta_L\lambda_5, \\
\frac{d\lambda_5}{dt} &= \mu_T\lambda_5,
\end{aligned} \tag{2A.4}$$

in the continuous control case. The corresponding co-state equations for the bang-bang control case are subtly different to Equation (2A.4), as the first term of the fourth line of Equation (2A.4) is the constant $-a_2$, and no longer depends on L . The transversality condition again provides the final time conditions on the co-state,

$[\lambda_1(t_f), \lambda_2(t_f), \lambda_3(t_f), \lambda_4(t_f), \lambda_5(t_f)] = [0, 0, 0, 0, 0]$. Given an initial state; $[S(0), A(0), D(0), L(0), T(0)]$, we can solve the resulting two-point BVP using the FBSM, as detailed in the Main paper. Results are provided in Figure 2A.2 corresponding to various parameter combinations.

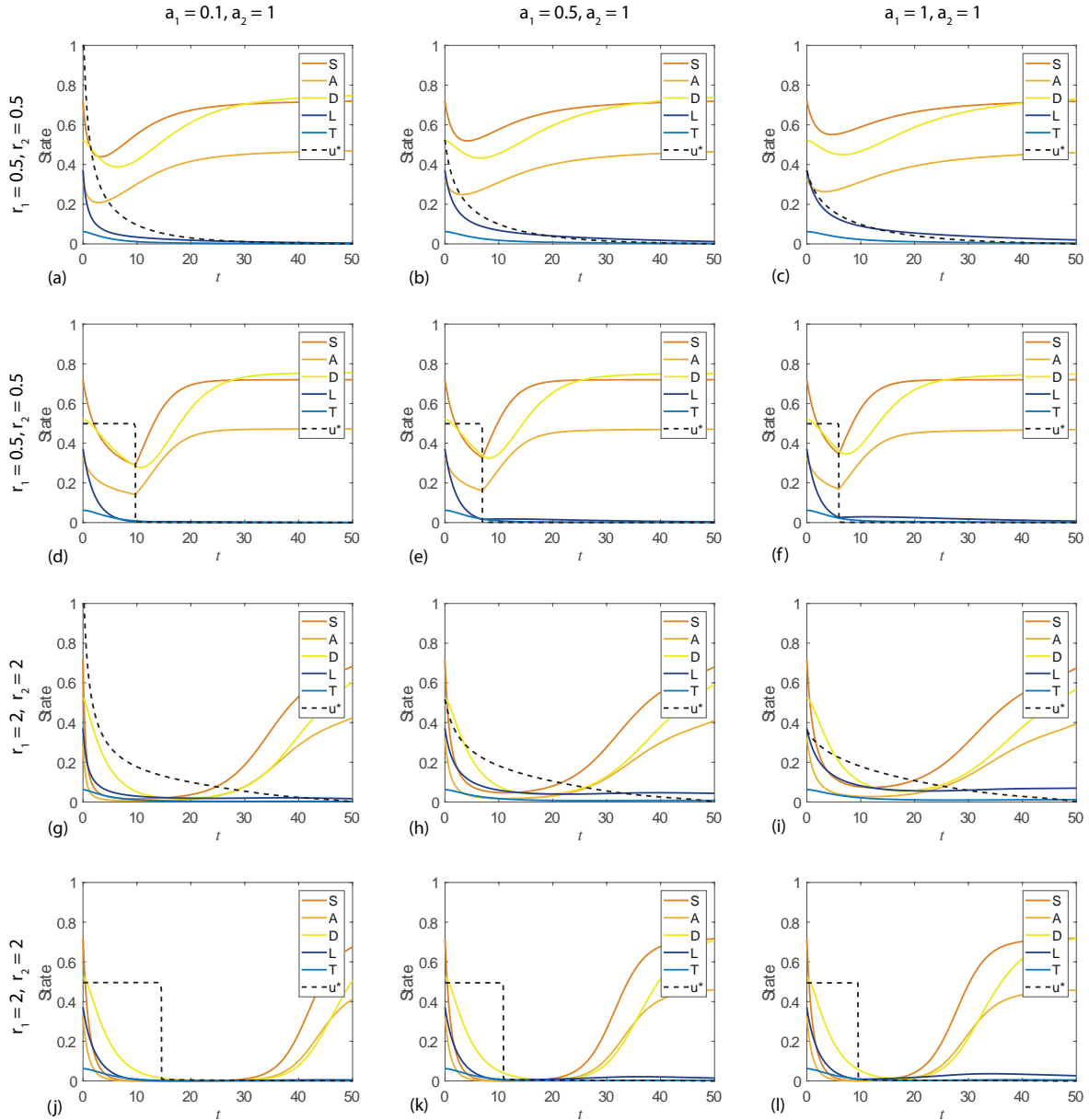


Figure 2A.2: Results are produced for a variety of parameters in the pay-off and rates that the control affects healthy cells. The continuous control case is presented in the first and third rows, while the second and fourth rows show the corresponding bang-bang case with an upper control bound of $u = 0.5$.

Chapter 3A

Supplementary material to Chapter 3

3A.1 Supplementary results

Key results are presented in the main document to highlight interesting dynamics and identify important parameters. In this section we present a broad suite of results corresponding to a wider range of parameter values. This section is divided into four subsections, with each subsection corresponding to one of the four possible combinations of control dynamics (continuous and/or bang-bang). Within each subsection, two sets of results are presented; the leukaemic term is included in the pay-off quadratically in the first set and linearly in the second set. To enable comparison, the form of the leukaemic term in the pay-off is the only difference between the central columns (sub-figures (b), (e), (h) and (k)) of figures within a subsection. Rows in each figure correspond to a different combination of pay-off weighting parameters (a_1, a_2, a_3). We explore the impact of varying a specified parameter across the rows of each figure.

3A.1.1 Continuous chemotherapy, continuous stem cell transplant controls

This Subsection contains results for pay-offs presented in Equation (3A.1) and Equation (3A.2), where both controls are continuous. These pay-offs correspond to results in Figure 3A.1 and Figure 3A.2, respectively. The pay-off functions are given by:

$$J = \int_0^{t_f} (a_1 u(t)^2 + a_2 v(t)^2 + a_3 L(t)^2) dt, \quad (3A.1)$$

$$J = \int_0^{t_f} (a_1 u(t)^2 + a_2 v(t)^2 + a_3 L(t)) dt. \quad (3A.2)$$

There are a number of intuitive results that we generally observe across all control

problems considered in this document. For continuous controls, increasing the pay-off weighting of a control reduces the amount of that control applied, and typically increases the amount of the other control applied. Increasing the weighting of leukaemia in the pay-off typically leads to a greater amount of both controls applied. With bang-bang controls the upper bound or maximum dose is fixed, so increasing the pay-off weighting causes the control to be applied for a shorter duration, or not at all. Increasing the weighting on leukaemia in the pay-off will typically increase the duration over which the bang-bang controls are applied. Incorporating leukaemia in the pay-off quadratically results in a higher level of leukaemia remaining at the terminal time. This is because linear pay-off terms are proportionally more penalising than quadratic terms; making a greater contribution to the pay-off that we are minimising ($L > L^2$ for $L \in (0, 1)$). Broadly, the nature of interactions between the controls and the state variables results in the chemotherapy control being applied to reduce the leukaemic population, and competition between progenitor blood cells, bolstered by the stem cell transplant control, and leukaemic cells prevents the leukaemic population from resurging as the chemotherapy control is reduced.

Results in Figure 3A.1 explore the impact of κ , the parameter that determines the effectiveness of the chemotherapy at killing the progenitor blood cells relative to leukaemic cells. Comparing Figure 3A.1(a) with Figure 3A.1(c), we see that κ does not appear to have a significant impact on the control dynamics. Despite the early-time decline of progenitor blood cells we observe in Figure 3A.1(c) in response to the chemotherapy control, at terminal time the remaining progenitor blood cell and leukaemic populations are not significantly different than in Figure 3A.1(a). These results are consistent for the alternative pay-off weightings considered. When leukaemia is weighted more heavily in the pay-off as in Figure 3A.1(j-l), a higher level of chemotherapy control is applied initially, although the state at terminal time does not vary significantly with κ .

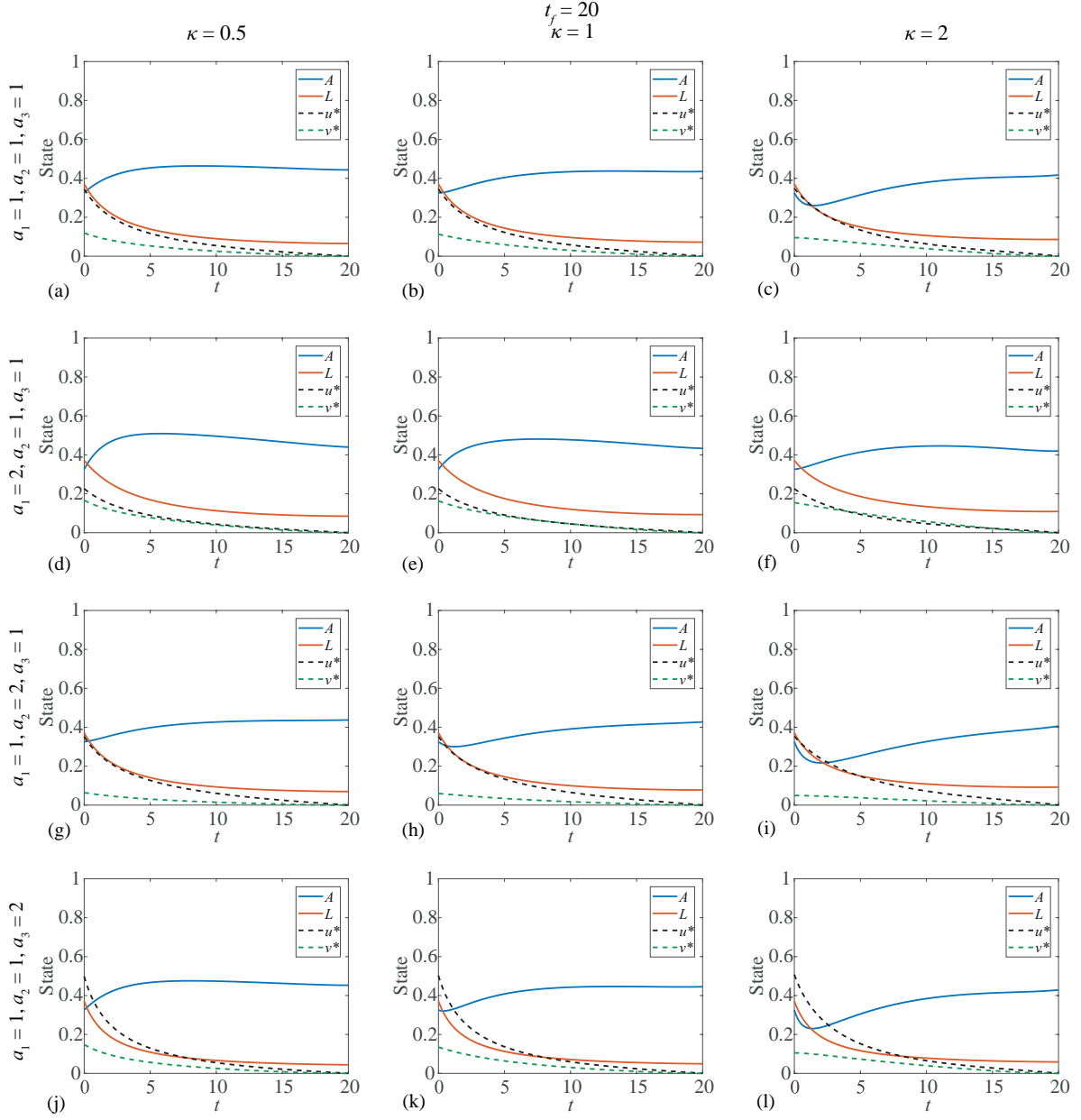


Figure 3A.1: Results are presented where both controls are applied continuously, under a range of pay-off weightings ($a_1, a_2, a_3 \in \{1, 2\}$) and where the chemotherapy control u affects the progenitor blood cell population less, equally and more than the leukaemic cell population; $\kappa \in \{0.5, 1, 2\}$, respectively. This figure corresponds to the pay-off given by Equation (3A.1), where the leukaemic term enters the pay-off quadratically. This corresponds to Equation (4) with $p = 2, q = 2, r = 2$.

In Figure 3A.2 we consider the pay-off given by Equation (3A.2), with the leukaemic term entering the pay-off linearly. Each column corresponds to a different terminal time, to investigate how this impacts the state and control dynamics. Although the results for different terminal times are not a direct scaling of one another, the dynamics are very similar. The results with larger terminal times exhibit a marginally higher initial level of control applied. We also observe a reduced leukaemic population at terminal time when the terminal time is increased. Since the pay-off considers the cumulative leukaemic burden, increasing the terminal time increases the interval over which the leukaemic population contributes to the pay-off, providing a stronger impetus to reduce it.

Comparing Figure 3A.2(b,e,h,k) with Figure 3A.1(b,e,h,k), respectively, we can investigate the impact of incorporating leukaemia in the pay-off linearly rather than quadratically. With linear weighting, leukaemia makes a greater contribution to the pay-off and motivates increased application of control. As such, a significantly higher dose of chemotherapy is applied, to more rapidly reduce the leukaemic population. As a corollary to this, a linear leukaemic term results in a lower leukaemic population at terminal time. A modest increase in the stem cell transplant control is also observed.

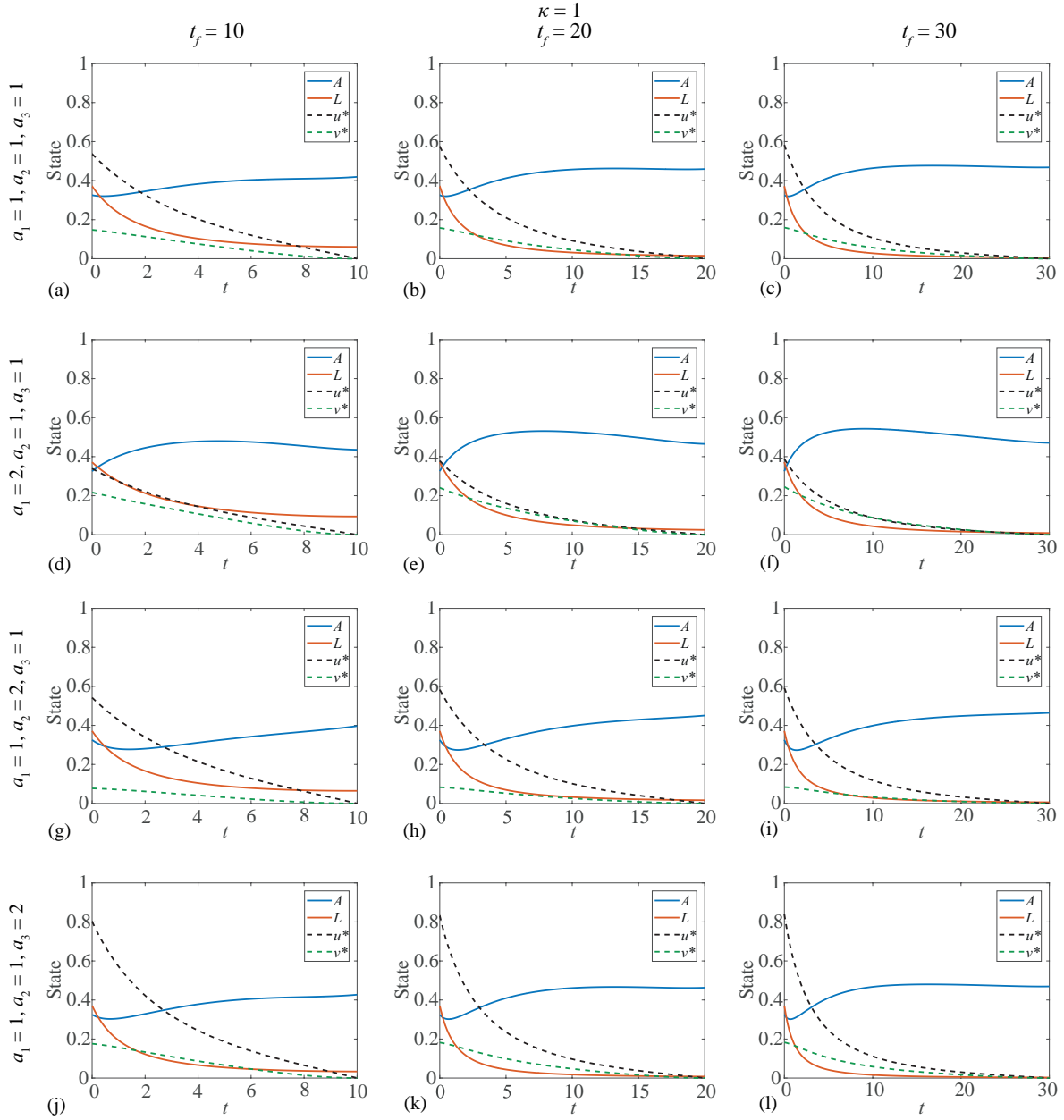


Figure 3A.2: Results are presented where both controls applied continuously, under a range of pay-off weightings ($a_1, a_2, a_3 \in \{1, 2\}$) and where each column of the figure corresponds to a different terminal time; $t_f \in \{10, 20, 30\}$. This figure corresponds to the pay-off given by Equation (3A.2), where the leukaemic term enters the pay-off linearly. This corresponds to Equation (4) with $p = 2$, $q = 2$, $r = 1$.

3A.1.2 Continuous chemotherapy, bang-bang stem cell transplant controls

This Subsection contains results for pay-offs presented in Equation (3A.3) and Equation (3A.4), where the chemotherapy control is continuous and the stem cell transplant control is bang-bang. We also apply bounds to the continuous chemotherapy control. These pay-offs correspond to results in Figure 3A.3 and Figure 3A.4, respectively. The pay-off functions are given by:

$$J = \int_0^{t_f} (a_1 u(t)^2 + a_2 v(t) + a_3 L(t)^2) dt, \quad 0 \leq u(t) \leq u_b, \quad 0 \leq v(t) \leq v_b, \quad (3A.3)$$

$$J = \int_0^{t_f} (a_1 u(t)^2 + a_2 v(t) + a_3 L(t)) dt, \quad 0 \leq u(t) \leq u_b, \quad 0 \leq v(t) \leq v_b. \quad (3A.4)$$

When the stem cell control is bang-bang, we only observe it switching on when its weighting in the pay-off is significantly lower than the weightings for the chemotherapy control and the leukaemia. Primarily, this is because the pay-off only considers the leukaemic population (and not the progenitor blood cell population), and the stem cell control is not as effective at reducing the leukaemic population as it can only achieve this indirectly through the competition between progenitor blood and leukaemia. In addition, since the bang-bang control arises from a linear term in the pay-off, it is more costly than an equivalently weighted quadratic component applied at the same level.

Bounded continuous controls allow us to incorporate physical constraints such as a maximum tolerable dose. In Figure 3A.3 an upper bound of $u_b = 0.3$ is placed on the continuous control. This leads to interesting results, particularly in combination with order of magnitude variations in κ . When all pay-off terms are weighted equally, as in Figure 3A.3(a-c), increasing κ increases the duration of the interval where chemotherapy is applied at its upper bound. Though initially counter-intuitive, this can be explained by the competition between leukaemia and progenitor blood cells; as κ is increased the progenitor population is further reduced and therefore presents weaker competition to the leukaemia.

With large κ and a low weighting on leukaemia in the pay-off relative to the controls, as in Figure 3A.4(1), we observe that only a small amount of chemotherapy control is applied, near the terminal time. This is due to a combination of not incorporating progenitor cells directly in the pay-off and having a fixed terminal time. As the chemotherapy control is quadratic in the pay-off, the small amount of chemotherapy control applied would contribute very little to the pay-off, such that the resulting minor reduction in leukaemia is worthwhile. However, this is only worthwhile near the end of the time interval. The chemotherapy control is not applied earlier in the interval as the cumulative effect of

reduced competition due to decreased progenitor population would outweigh the benefit of applying the chemotherapy. Similar behaviour appears in Figure 3A.4(i), corresponding to large κ and a low weighting on the stem cell transplant control in the pay-off.

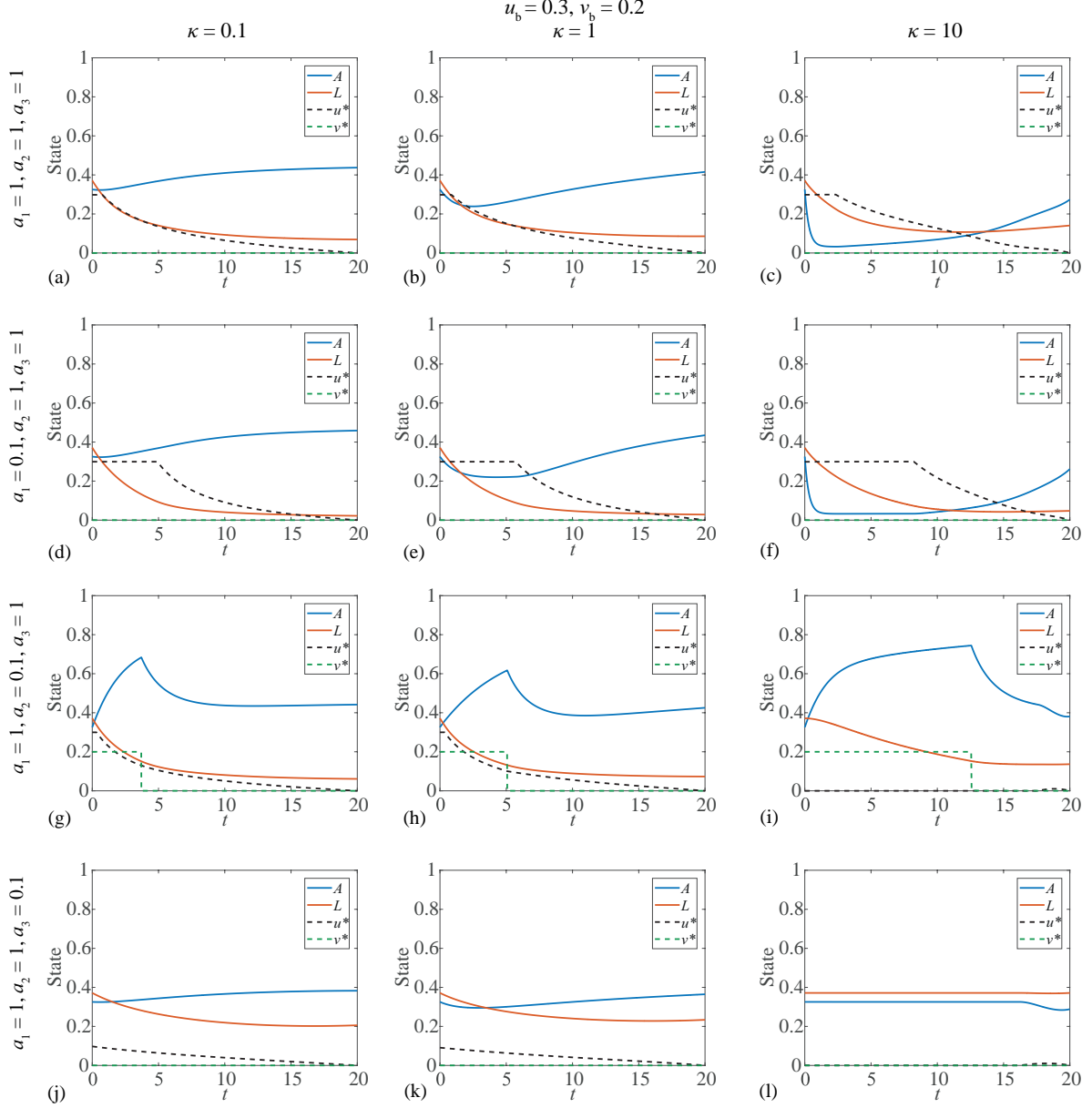


Figure 3A.3: Results are presented for a bounded continuous chemotherapy control ($u_b = 0.3$), and bang-bang stem cell transplant control ($v_b = 0.2$). Results correspond to a range of pay-off weightings ($a_1, a_2, a_3 \in \{0.1, 1\}$) and examine a more extreme variation of κ than in Figure 3A.1. This figure corresponds to the pay-off given by Equation (3A.3), where the leukaemic term enters the pay-off quadratically. This corresponds to Equation (4) with $p = 2$, $q = 1$, $r = 2$.

We investigate the impact of varying the upper bound on the continuous control in Figure 3A.4. As the upper bound is increased, the interval over which the continuous control is applied at its upper bound is reduced. Adjusting the upper bound produces a different response from the state, and therefore also alters the control dynamics over the

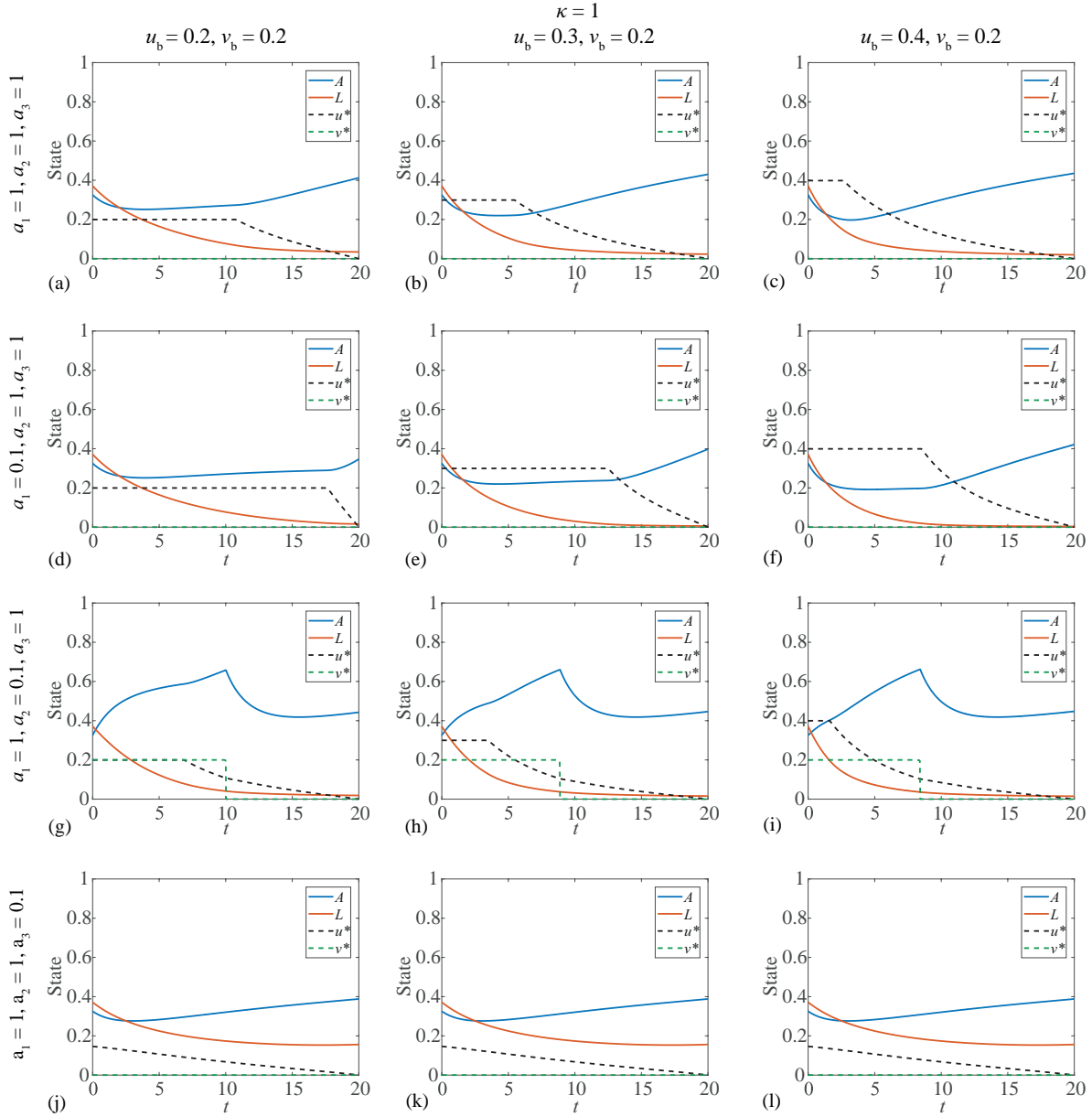


Figure 3A.4: Results are presented for a bounded continuous chemotherapy control, and bang-bang stem cell transplant control ($v_b = 0.2$). The upper bound on the continuous chemotherapy control is varied; $u_b \in \{0.2, 0.3, 0.4\}$, under a range of pay-off weightings ($a_1, a_2, a_3 \in \{0.1, 1\}$). This figure corresponds to the pay-off given by Equation (3A.4), where the leukaemic term enters the pay-off linearly. This corresponds to Equation (4) with $p = 2$, $q = 1$, $r = 1$.

intervals where the control is applied at a lower level than the upper bound. It follows that when the control is never applied at the upper bound (Figure 3A.4(j,k,l)), changing the upper bound does not impact the dynamics of the system.

Comparing Figure 3A.4(h) with Figure 3A.3(h), we see that incorporating leukaemia in the pay-off linearly rather than quadratically increases the interval over which the bounded continuous chemotherapy control is applied at its upper bound. The bang-bang stem cell transplant control is applied for longer.

3A.1.3 Bang-bang chemotherapy, continuous stem cell transplant controls

This Subsection contains results for pay-offs presented in Equation (3A.5) and Equation (3A.6), where the chemotherapy control is bang-bang and the stem cell transplant control is continuous. These pay-offs correspond to results in Figure 3A.5 and Figure 3A.6, respectively. The pay-off functions are given by:

$$J = \int_0^{t_f} (a_1 u(t) + a_2 v(t)^2 + a_3 L(t)^2) dt, \quad 0 \leq u(t) \leq u_b, \quad (3A.5)$$

$$J = \int_0^{t_f} (a_1 u(t) + a_2 v(t)^2 + a_3 L(t)) dt. \quad 0 \leq u(t) \leq u_b. \quad (3A.6)$$

We revisit varying the terminal time in Figure 3A.5 to investigate its impact on the dynamics of bang-bang controls. The dynamics are again similar with different terminal times, but are not direct scalings. As the terminal time increases, the bang-bang control is applied over a longer interval, although this interval does not necessarily increase proportionally with the terminal time. This is clear in the second row of Figure 3A.5; where the bang-bang control switches off around $t = 8$ when $t_f = 10$, and switches off around $t = 15$ when $t_f = 30$.

When the continuous stem cell transplant control is weighted much lower than the other terms in the pay-off, it is applied liberally (3A.5(g,h,i)). In this situation the bang-bang chemotherapy control is not switched on, as the leukaemic population is reduced through the competition between A and L . We note that this level of stem cell transplant control is not physically realistic, as it increases the progenitor population well above the carrying capacity of the model, resulting in a significant decline in the progenitor population as the support from the stem cell transplant control is reduced. These kind of results can provide insight regarding the quality of the model and/or the pay-off form and weightings. If we believe the model to be sufficiently realistic, then obtaining non-physical control results suggests that the pay-off form or weightings must not be realistic; in this case it would appear that applying the stem cell transplant control is not costly enough.

In Figure 3A.6, we present results exploring the continuous stem cell control and bang-bang chemotherapy control dynamics with leukaemia entering the pay-off linearly. We consider the case where the continuous stem cell transplant control is unbounded, and also consider imposing upper bounds of $v_b = 0.1$ and $v_b = 0.3$. When the stem cell transplant control is weighted lower in the pay-off, similarly to Figure 3A.5(g,h,i), the continuous stem cell transplant control is applied too liberally. This is partially mitigated through imposing the upper bounds, as in Figure 3A.6(g,i), although we still see a sharp

decline in the progenitor cell population once the support from the control is removed. This highlights a challenge in determining appropriate weightings of multiple controls with different forms; the form of the control terms in the pay-off (linear, quadratic) directly impacts their contribution to the pay-off. Pay-off terms are equally weighted in Figure 3A.6(a), and the continuous stem cell control is applied at the upper bound of $v_b = 0.1$, matching the bound of the chemotherapy control at $u_b = 0.1$. The contribution of the chemotherapy control to the pay-off is an order of magnitude greater than that of the stem cell control.

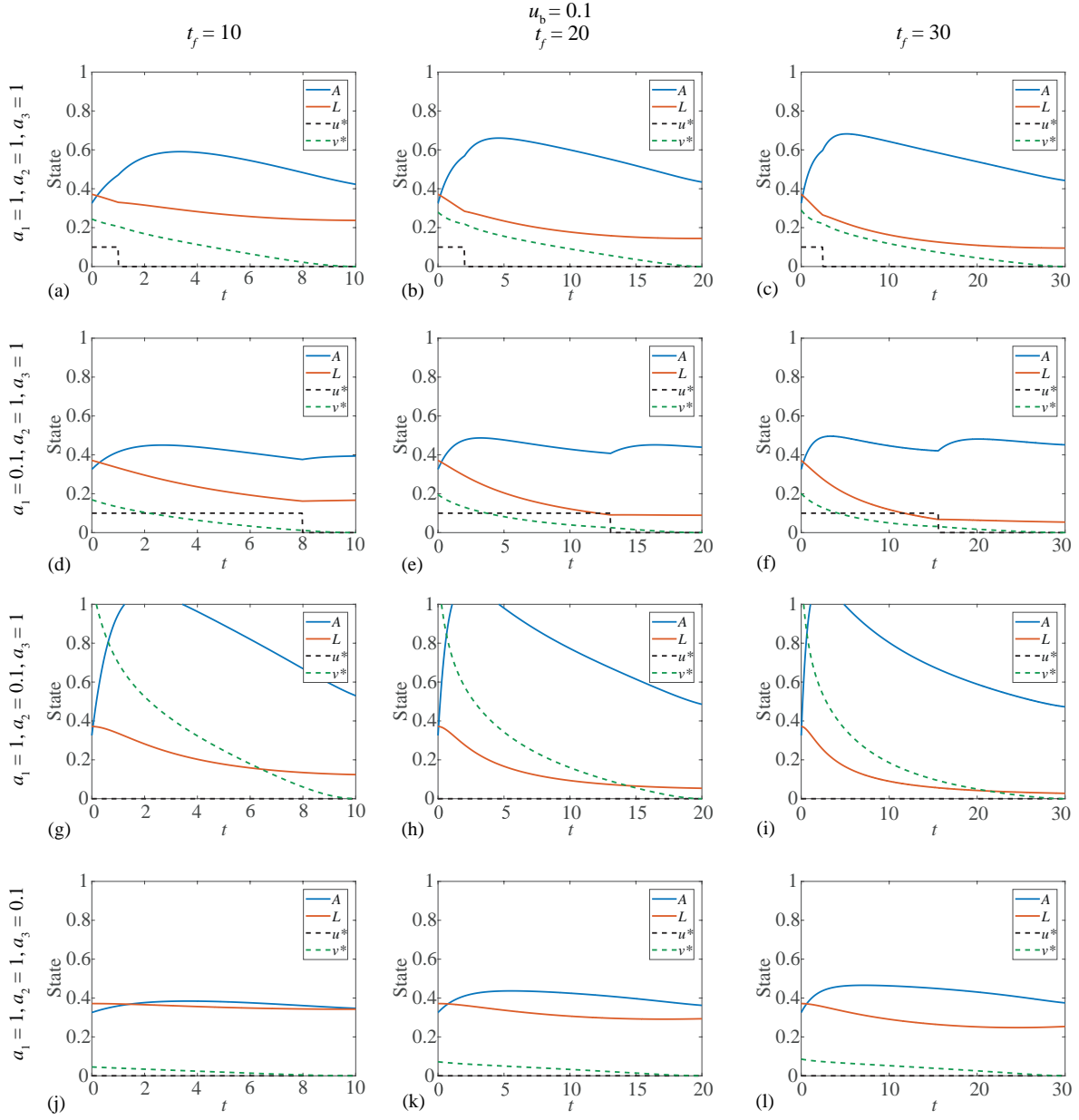


Figure 3A.5: Results are presented for a bang-bang chemotherapy control and continuous stem cell transplant control, with an upper control bound of 0.1 on the bang-bang control. Each column of the figure corresponds to a different terminal time; ($t_f \in \{10, 20, 30\}$). This figure corresponds to the pay-off given by Equation (3A.5), where the leukaemic term enters the pay-off quadratically. This corresponds to Equation (4) with $p = 1$, $q = 2$, $r = 2$.

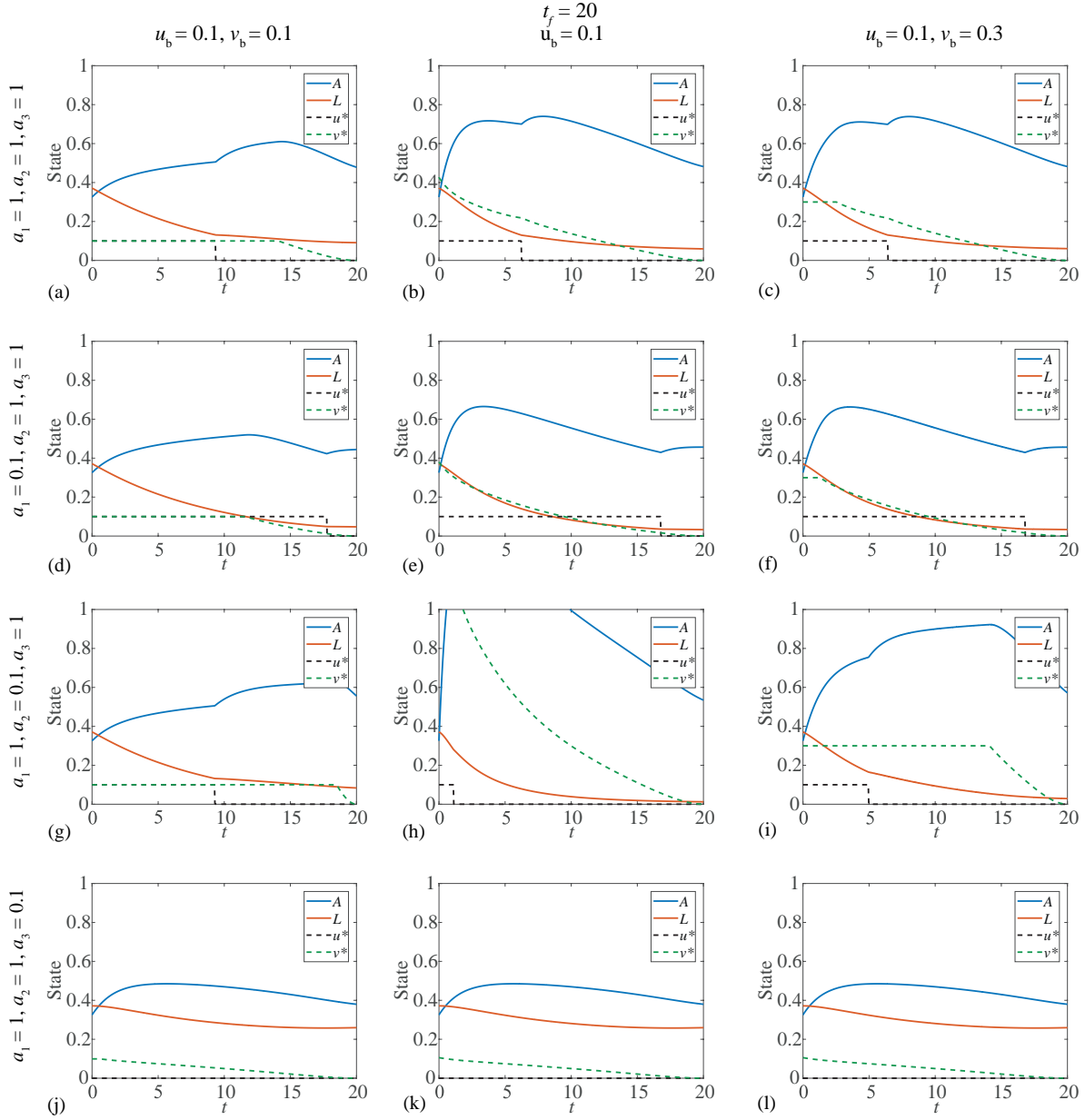


Figure 3A.6: Results are presented for a bang-bang chemotherapy control ($u_b = 0.1$) and continuous stem cell transplant control, under a range of pay-off weightings ($a_1, a_2, a_3 \in \{0.1, 1\}$). The continuous stem cell transplant control is not constrained by an upper bound in the central column, with an upper bound of $v_b = 0.1$ in the left column and $v_b = 0.3$ in the right column. This figure corresponds to the pay-off given by Equation (3A.6), where the leukaemic term enters the pay-off linearly. This corresponds to Equation (4) with $p = 1, q = 2, r = 1$.

3A.1.4 Bang-bang chemotherapy, bang-bang stem cell transplant controls

This Subsection contains results for pay-offs presented in Equation (3A.7) and Equation (3A.8), where both controls are bang-bang. These pay-offs correspond to results in Figure 3A.7 and Figure 3A.8, respectively. The pay-off functions are given by:

$$J = \int_0^{t_f} (a_1 u(t) + a_2 v(t) + a_3 L(t)^2) dt, \quad 0 \leq u(t) \leq u_b, \quad 0 \leq v(t) \leq v_b, \quad (3A.7)$$

$$J = \int_0^{t_f} (a_1 u(t) + a_2 v(t) + a_3 L(t)) dt, \quad 0 \leq u(t) \leq u_b, \quad 0 \leq v(t) \leq v_b. \quad (3A.8)$$

The intuitive results that we observe in previous subsections are reflected in Figure 3A.7 with both controls bang-bang. In the central column we consider bang-bang controls with equal upper bounds: $u_b = v_b = 0.1$. In the left column, we increase the upper bound on the stem cell transplant control to $v_b = 0.2$ and in the right column we increase the upper bound on the chemotherapy control to $u_b = 0.2$. This enables us to investigate the impact of control strength. As the upper bound on the controls increase, the duration that they are switched on decreases. When all pay-off terms are equally weighed, only the chemotherapy control is applied, as it is more effective at reducing the leukaemic population. When the pay-off weighting of a bang-bang control is reduced, it is applied for longer. Increasing the upper bound on one control can reduce the duration that the other control is required, for example compare Figure 3A.7(h) with Figure 3A.7(i). With both controls bang-bang and all terms weighed equally, the final populations indicate that the leukaemia will return to its coexisting steady state; such a result suggests that the leukaemia may not be sufficiently weighted in the pay-off.

In Figure 3A.8 we investigate the impact of varying κ when the controls are bang-bang, and when leukaemia enters the pay-off linearly. For the small variations considered in this case ($\kappa \in 0.5, 1, 2$) we notice changes in the state response, particularly of the progenitor population, but change to the control dynamics is marginal. As κ is increased, leading to a greater reduction in the progenitor population; the stem cell transplant control is applied for longer, and the chemotherapy control is applied for less time.

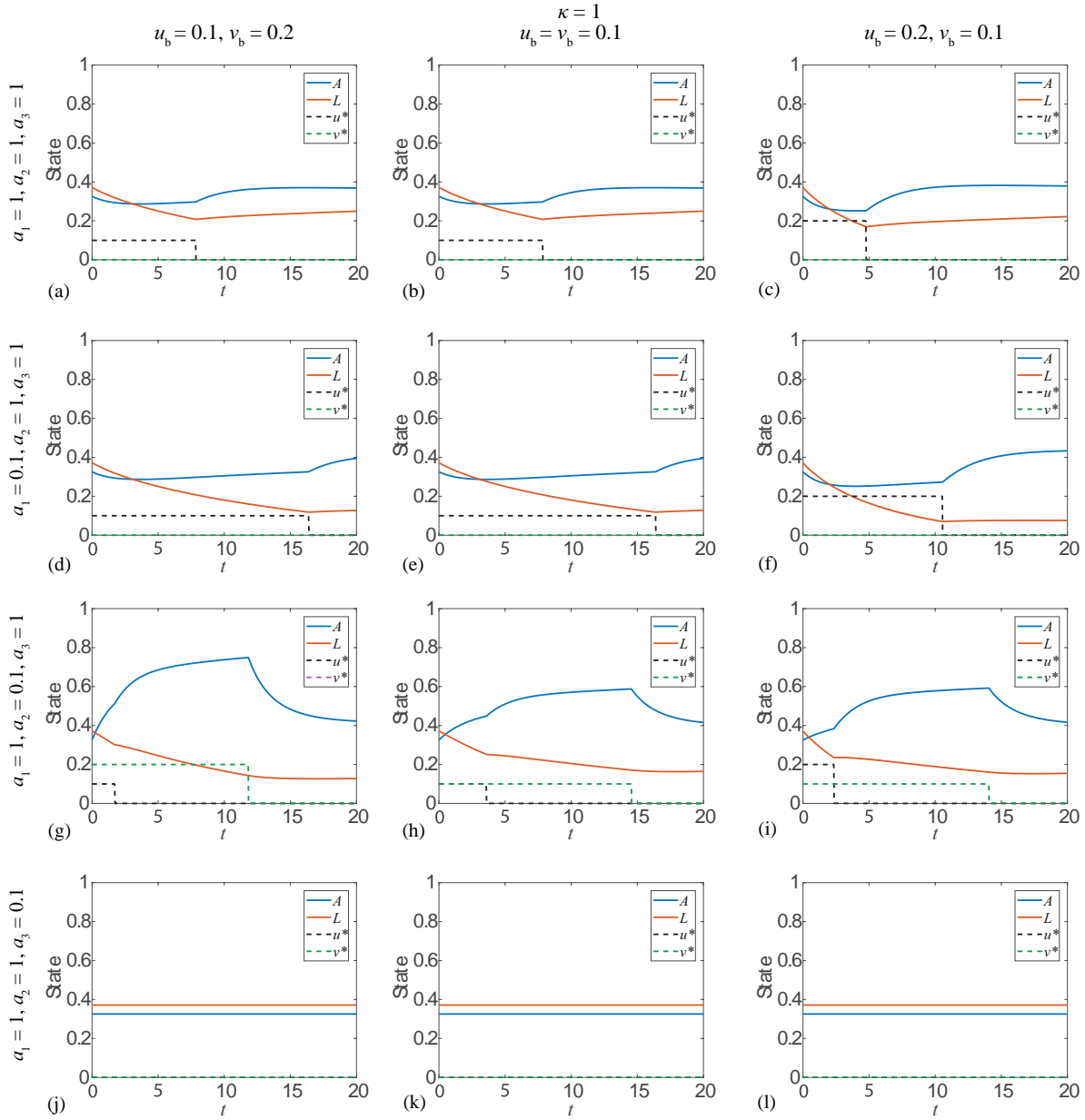


Figure 3A.7: Results are presented where both controls are bang-bang, under a range of pay-off weightings ($a_1, a_2, a_3 \in \{0.1, 1\}$). In the central column we consider equal control bounds; $u_b = v_b = 0.1$. In the left column the upper bound on the stem cell transplant control is increased ($v_b = 0.2$), and in the right column the upper bound on the chemotherapy control is increased ($u_b = 0.2$). This figure corresponds to pay-off given by Equation (3A.7), where the leukaemic term enters the pay-off quadratically. This corresponds to Equation (4) with $p = 1, q = 1, r = 2$.

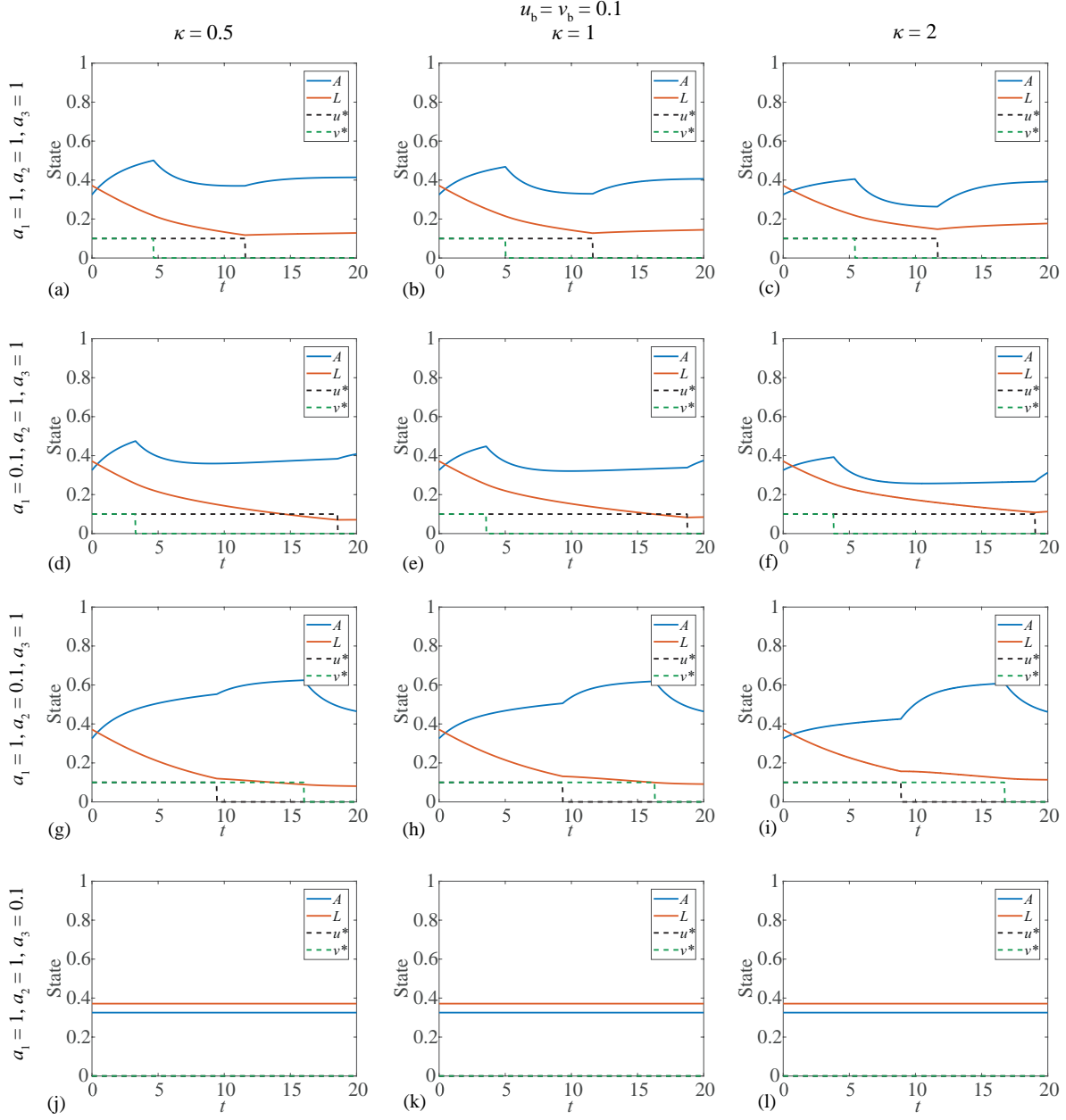


Figure 3A.8: Results are presented where both controls are bang-bang, under a range of pay-off weightings ($a_1, a_2, a_3 \in \{0.1, 1\}$) and for upper control bounds $u_b = v_b = 0.1$. We investigate how κ , the rate that chemotherapy kills progenitor blood cells relative to leukaemic cells, impacts the dynamics of bang-bang controls. This figure corresponds to the pay-off given by Equation (3A.8), where the leukaemic term enters the pay-off linearly. This corresponds to Equation (4) with $p = 1, q = 1, r = 1$.

3A.2 Steady state behaviour

The steady state behaviour of Equation (3), with no control applied ($u = v = 0$), is presented in Figure 3A.9. This phase portrait corresponds to the parameter values in Table 1. The steady state behaviour of the underlying model is discussed thoroughly in the literature, both with [290], and without [82], the immune response. We observe that there is a stable coexisting steady state with neither A nor L zero, and a stable healthy steady state (no leukaemia cells, $L = 0$). Solutions in this work are initialised at the coexisting steady state values for A and L unless otherwise specified.

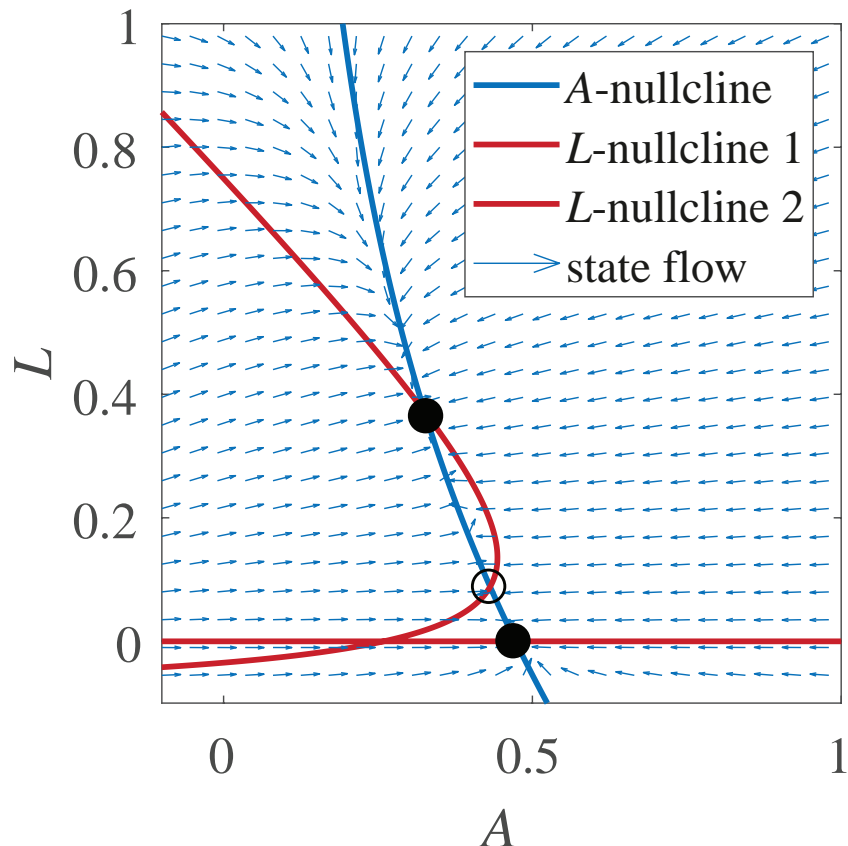


Figure 3A.9: Fixed points within the region of interest ($0 \leq A + L \leq 1$), are marked with black discs. Closed discs mark the stable fixed points and the open disc marks the unstable fixed point.

3A.3 Sensitivity

Due to the interconnected nature of optimal control; the particular aspects of the optimal control regimes that are sensitive, and the degree of sensitivity; to initial conditions, model parameters, and assumptions, depends on the pay-off that is being considered. The question of performing a sensitivity analysis for an optimal control problem is not as

straightforward as considering a sensitivity analysis for a regular uncontrolled model. As we will show, it is always straightforward to analyse the optimal solution as one or more features of the model, such as a particular parameter value, is varied. However, when we vary some features in the optimal control problem, such as weighting parameters in the pay-off, the characterisation of optimality and the associated optimal solution changes, as does the value of the pay-off. Therefore, we ought to remember that it is not straightforward to compare optimal solutions in a sensitivity analysis because each change in a control parameter value leads to a different optimal solution. In this section we explore the sensitivity of the optimal control results to the initial conditions, model parameters and the haematopoietic stem cell steady state assumption. We present a variety of sensitivity results corresponding to the pay-off in Equation (3A.4), with $a_1 = 1$, $a_2 = 0.1$, $a_3 = 1$, $\kappa = 1$ and control bounds $0 \leq u(t) \leq 0.3$ and $0 \leq v(t) \leq 0.2$. This corresponds to the optimal control problem solved to obtain Figure 3A.4(h).

We find that the optimal control regimes are relatively robust, in that a small change in the initial conditions, model parameters or steady state values leads to a small change in the optimal solution trajectories. However, we caveat this by noting that the pay-off weighting parameters also impact the sensitivity of the optimal control regimes to model parameters, and the optimal control regimes will be more sensitive under some pay-off weighting regimes than others. We explore this sensitivity at the end of this section.

3A.3.1 Initial conditions

Optimal control results presented in this work correspond to systems initialised at the coexisting steady state values for A and L . In Figure 3A.10 we demonstrate that this is not a requirement of the techniques, and that the optimal control strategies are not sensitive to moderate changes in the initial conditions. The subtle differences that do emerge between the optimal control strategies are intuitive. As $L(0)$ increases, the application of both controls increases. As $A(0)$ increases, both controls are slightly reduced. The minimum achievable pay-off, J , is marginally worse when $L(0)$ is increased or when $A(0)$ is decreased. This is to be expected, as these cases represent a less favourable initial situation.

3A.3.2 Model parameters

The parameters presented in Table 1 are used throughout this work. As outlined in Section 3, acute myeloid leukaemia (AML) is a highly heterogeneous disease, and accurate measurement and estimation of parameters is likely to change significantly from patient to patient. As such, we investigate the sensitivity of the control strategies to the model parameters in Table 1 by independently varying each parameter $\pm 10\%$ and recomputing the optimal controls and corresponding state trajectories. We perform this parameter

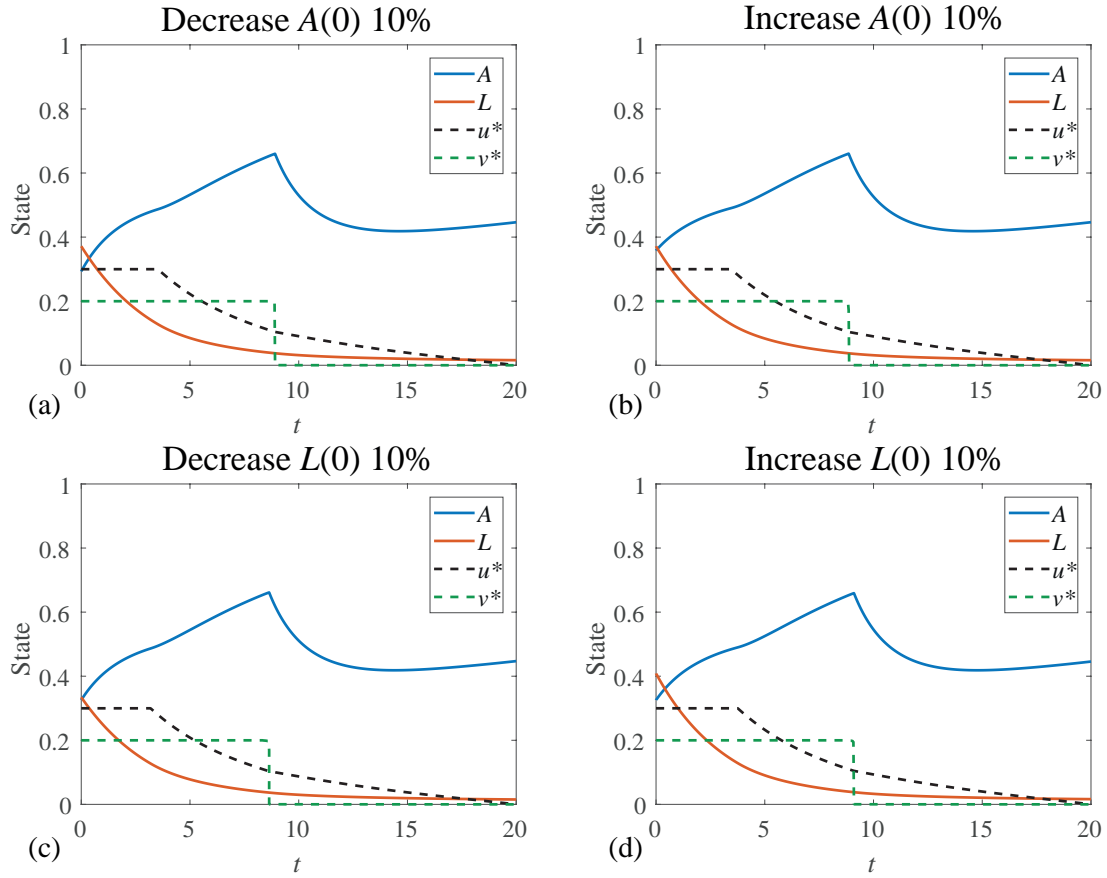


Figure 3A.10: Results are presented to explore the effect of moderate increases and decreases in the initial conditions, $A(0)$ and $L(0)$. Results correspond to the pay-off given by Equation (3A.4), where the chemotherapy control is bounded and continuous, and the stem cell transplant control is bang-bang. Control weighting parameters are $a_1 = 1$, $a_2 = 0.1$, $a_3 = 1$, with bounds $0 \leq u(t) \leq 0.3$ and $0 \leq v(t) \leq 0.2$. Figure 3A.4(h) is the corresponding optimal control regime for a system initialised at the coexisting steady state values for A and L . In (a), $[A(0), L(0)] = [0.2930, 0.3715]$, with pay-off $J = 2.1626$; in (b), $[A(0), L(0)] = [0.3581, 0.3715]$, with pay-off $J = 2.1369$; in (c) $[A(0), L(0)] = [0.3255, 0.3343]$, with pay-off $J = 2.0049$; and in (d) $[A(0), L(0)] = [0.3255, 0.4087]$, with pay-off $J = 2.2888$.

variation for the optimal control problem described in Equation (3A.4), with pay-off weightings $a_1 = 1$, $a_2 = 0.1$ and $a_3 = 1$. We find that the optimal control regimes are qualitatively robust to these moderate parameter variations. The variations that have the most noticeable impact are of the proliferation parameters, presented in Figure 3A.11; particularly that of the leukaemic population, ρ_L . Increasing ρ_L leads to a modest increase in the optimal duration of the stem cell transplant control. However, we note that in this case, it is not surprising that the stem cell transplant control is the most sensitive element, as its reduced weighting in the pay-off ($a_2 < a_1, a_3$), makes it the least *costly* means of compensating for the increased proliferation of leukaemia. It is fair to expect that the chemotherapy control would be more sensitive to this parameter variation if a_1 were to be reduced relative to a_2 and a_3 . Similarly, we also find that the

control regimes are insensitive to the other parameters in Table 1 (not shown).

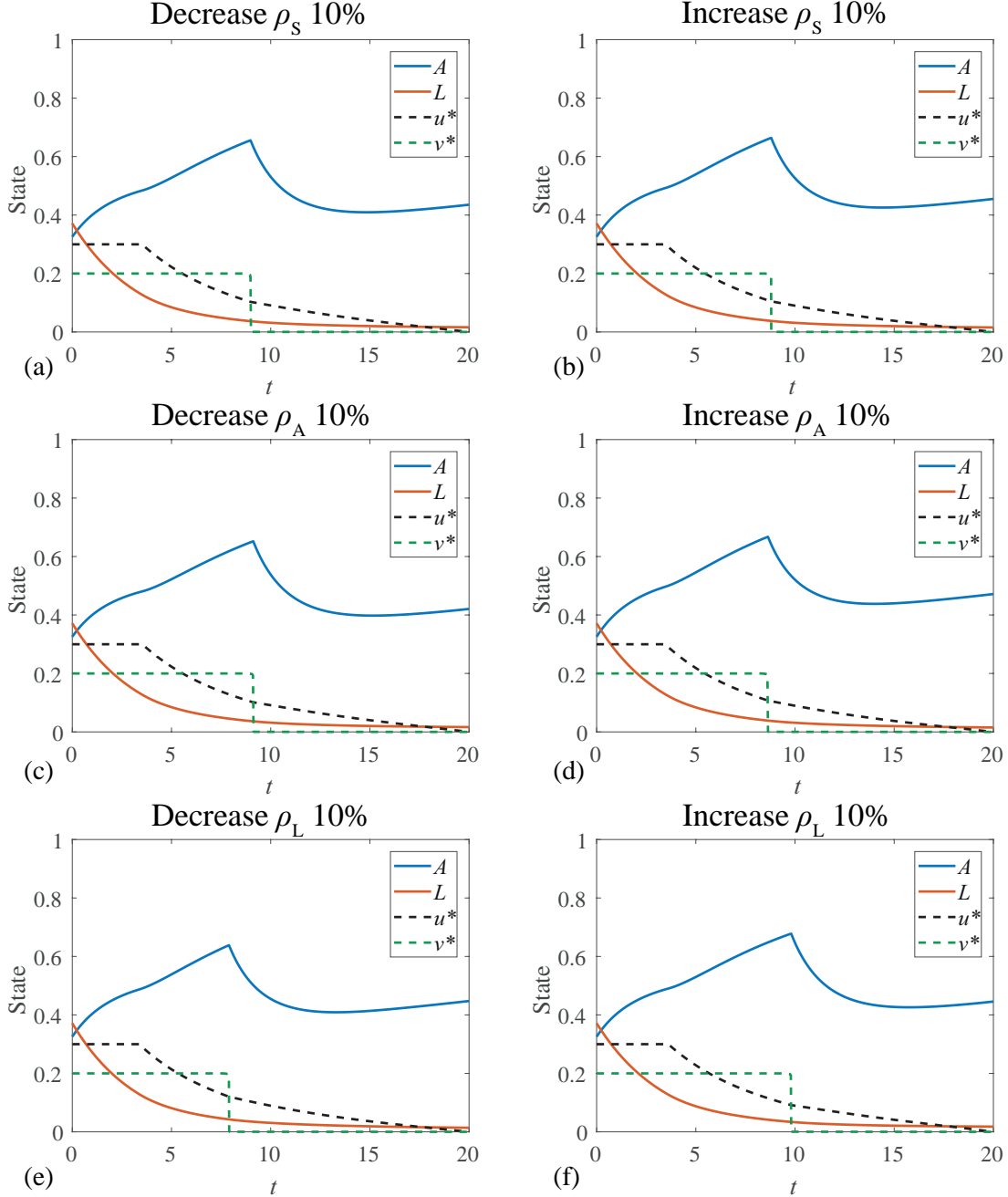


Figure 3A.11: Proliferation rates ρ_S , ρ_A and ρ_L are varied independently by $\pm 10\%$ to gain insight into the sensitivity of the control regimes to these parameters. Results in this figure are for the control problem given by Equation (3A.4) with bounded continuous chemotherapy control, $0 \leq u(t) \leq 0.3$, bang-bang stem cell transplant control, $0 \leq v(t) \leq 0.2$, and pay-off weightings $a_1 = 1$, $a_2 = 0.1$, $a_3 = 1$. The control regime and state trajectories for this pay-off with the original (unvaried) parameters are presented in Figure S4(h). The control regimes and state trajectories are qualitatively similar. The most noticeable deviation arises from variations of ρ_L ; we see that the duration over which the stem cell transplant control is applied is increased between (e) and (f).

3A.3.3 Steady state assumption

In the original model, Equation (2), a population of haematopoietic stem cells, S , grows endogenously to a steady state, and serves as a source of A . In the control results in this work we make the simplifying assumption that S is held constant at this steady state. As the haematopoietic stem cells do not face competition, they grow to this steady state quickly, even from a significantly depressed initial value. As such, provided that $S(0)$ is of a similar scale to $A(0)$ and $L(0)$ this assumption does not significantly impact the optimal control regimes. Further, this assumption permits us to focus on the interaction dynamics of A and L .

The Pontryagin Maximum Principle (PMP) and Forward-Backward Sweep Method (FBSM) both readily generalise to higher dimensional systems without prohibitive increases to the computational cost, so there would be minimal technical challenge associated with relaxing this assumption. When including S dynamically, prior to S reaching steady state, the production of A from S is proportionally reduced, resulting in less competitive pressure exerted on L by A , promoting an increased application of control. This is illustrated in Figure 3A.12.

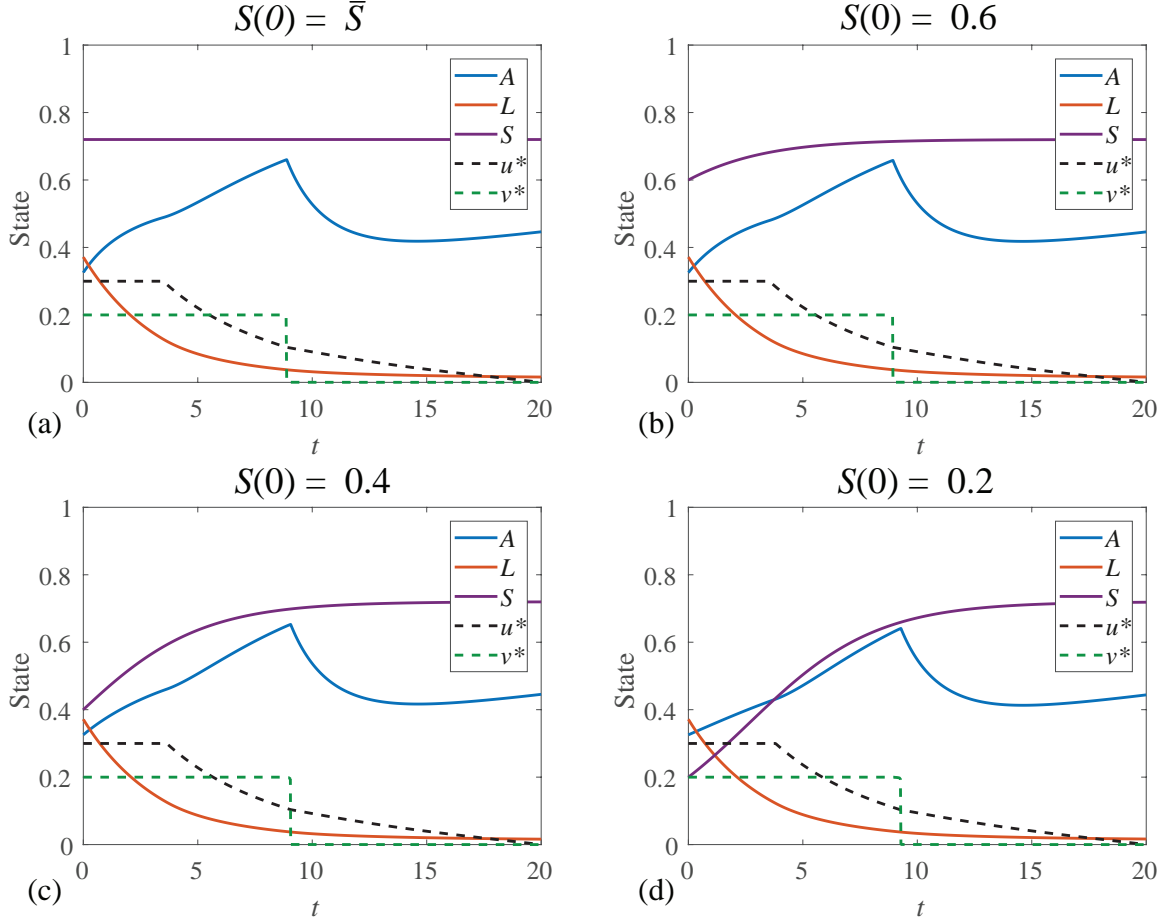


Figure 3A.12: Results are presented for various values of $S(0)$, the initial haematopoietic stem cell population, relaxing the assumption that $S(t) \equiv \bar{S}$. We relax this assumption by modelling $S(t)$ using the dynamics given in Equation (2). We present the dynamics with $S(0) = \bar{S}$ in (a), then we explore what happens as we relax this assumption and reduce $S(0)$. Even for the relatively small $S(0) = 0.2$ in (d), the optimal control regimes are qualitatively similar. The early-time growth of A is slowed as $S(0)$ is reduced, however this does not significantly impact the optimal control dynamics.

3A.3.4 Control parameters impact sensitivity

The sensitivity of the optimal control regimes depends on the pay-off weighting parameters. We present summary figures to demonstrate this behaviour. Results in Figures 3A.13 - 3A.15 correspond to the control problem given by Equation (3A.4) with bounded continuous chemotherapy control, $0 \leq u(t) \leq 0.3$, and bang-bang stem cell transplant control, $0 \leq v(t) \leq 0.2$. Figure 3A.13 has pay-off weighting parameters $a_1 = 1$, $a_2 = 0.1$, $a_3 = 1$, Figure 3A.14 has pay-off weighting parameters $a_1 = 0.5$, $a_2 = 0.1$, $a_3 = 1$, and Figure 3A.15 has pay-off weighting parameters $a_1 = 1$, $a_2 = 0.1$, $a_3 = 0.5$. In each case we vary $\kappa \in [0, 2]$ to observe the sensitivity of the optimal control regimes under different pay-off weighting parameters.

As the weighting parameter of an element in the pay-off decreases, we generally observe that it becomes more sensitive to changes in model parameters such as κ . As a corollary to this, we notice in each case that A is the most sensitive to changes in κ , partly because κ directly corresponds to an additional killing rate of A , and partly because A is not explicitly included in the pay-off.

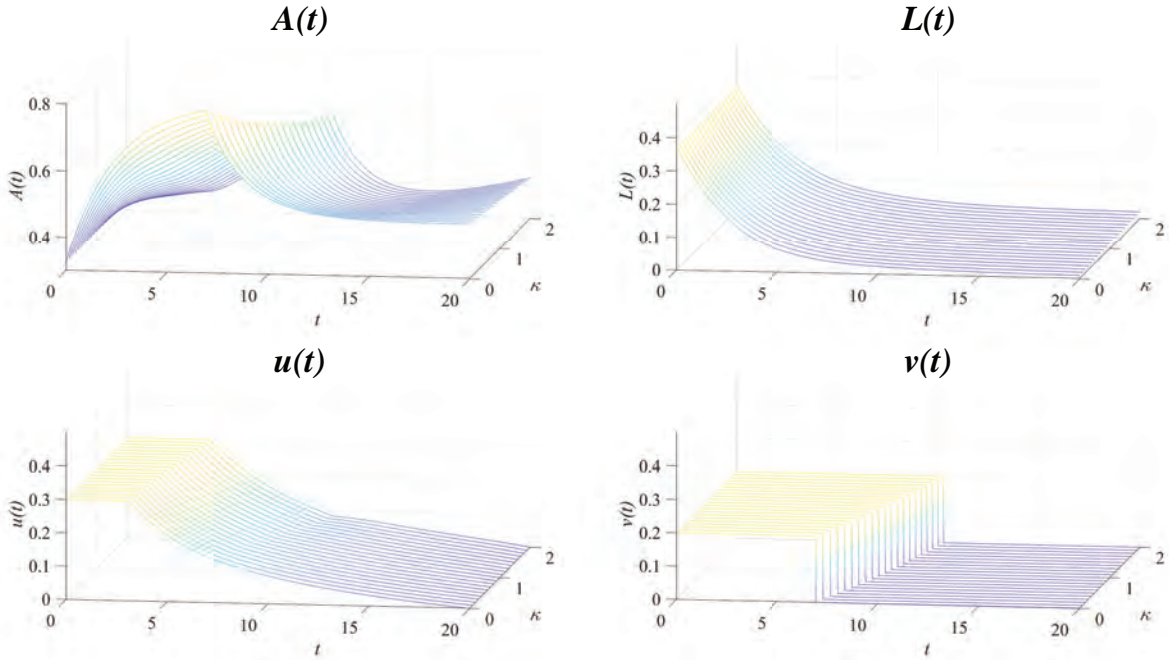


Figure 3A.13: Sets of solutions are presented for A , L , u and v as we vary $\kappa \in [0, 2]$ with pay-off weightings $a_1 = 1$, $a_2 = 0.1$, $a_3 = 1$. As κ increases, such that the chemotherapy control is effectively becoming more toxic to progenitor blood cells, we observe little change in L and u . However, we observe increasing application of the stem cell transplant control, as it mitigates the effect of the increasing toxicity on A .

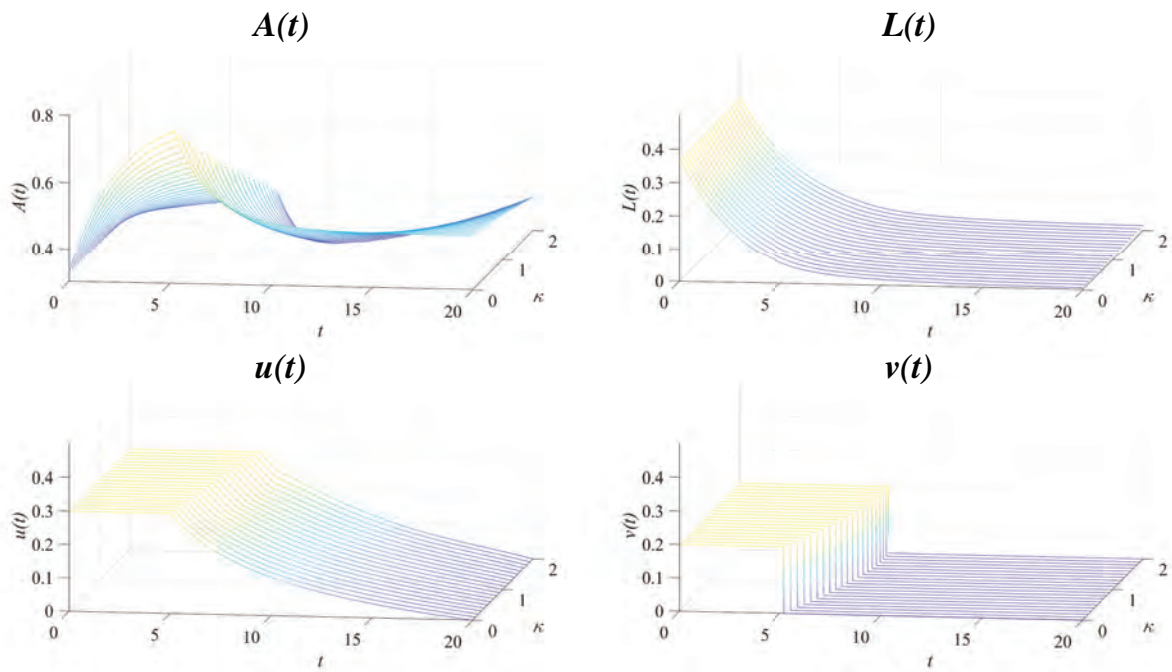


Figure 3A.14: Sets of solutions are presented for A , L , u and v as we vary $\kappa \in [0, 2]$ with pay-off weightings $a_1 = 0.5$, $a_2 = 0.1$, $a_3 = 1$. This represents a reduced cost of applying chemotherapy control relative to Figure 3A.13. As κ increases, we still observe little change in L , however u increases with κ . Relative to Figure 3A.13 we also note that the duration of the stem cell transplant control is reduced. It is also evident that the duration of the stem cell transplant control increases non-linearly with κ , at a decreasing rate.

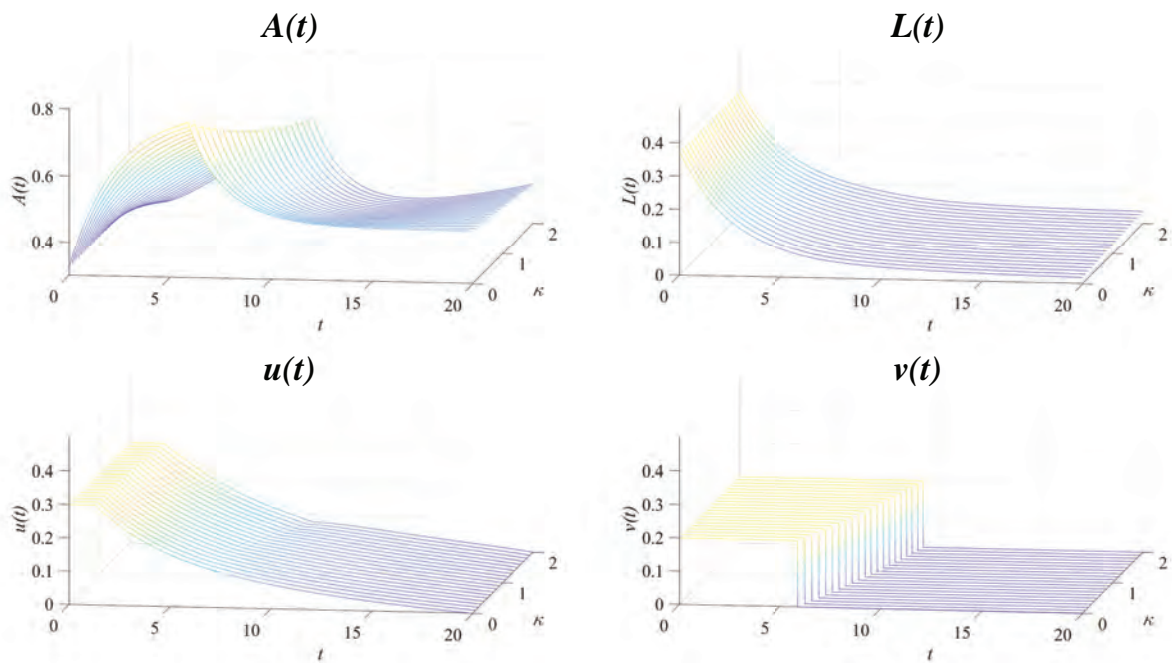


Figure 3A.15: Sets of solutions are presented for A , L , u and v as we vary $\kappa \in [0, 2]$ with pay-off weightings $a_1 = 1$, $a_2 = 0.1$, $a_3 = 0.5$. This represents a reduced cost of leukaemia relative to Figure 3A.13. As κ increases, we observe that u increases only marginally with κ , and is applied less relative to Figure 3A.13. In response to this, L is reduced more gradually over time, and the final time population of L noticeable increases with κ .

3A.4 Supporting code

Code for implementation of the optimal control algorithms in this work is made freely available on [GitHub](#).

3A.5 Forward-backward sweep method

In Algorithm 1 we present a concise algorithm for the FBSM with multiple controls [290]. We denote the system state as $\mathbf{x}(t)$, the co-state as $\boldsymbol{\lambda}(t)$, and the controls as $\mathbf{u}(t)$. For the two control model considered in this work, $\mathbf{x}(t) = [A(t), L(t)]^T$, $\mathbf{u}(t) = [u(t), v(t)]^T$, and $\boldsymbol{\lambda}(t) = [\lambda_1(t), \lambda_2(t)]^T$; where $\lambda_1(t)$ and $\lambda_2(t)$ are the co-state equations derived from the Hamiltonian [290].

Algorithm 1: FBSM for multiple controls

- i. Make an initial guess of $\mathbf{u}(t)$.
For all problems considered in this work, $u(t) \equiv v(t) \equiv 0$ is sufficient.
- ii. Using the initial condition $\mathbf{x}(0) = \mathbf{x}_0$, solve for $\mathbf{x}(t)$ forward in time using the initial guess of $\mathbf{u}(t)$.
- iii. Using the transversality condition $\boldsymbol{\lambda}(t_f)$, solve for $\boldsymbol{\lambda}(t)$ backwards in time, using the values for $\mathbf{u}(t)$ and $\mathbf{x}(t)$.
- iv. Calculate $\mathbf{u}_{\text{new}}(t)$ by evaluating the expression for the optimal control $\mathbf{u}^*(t)$ using the updated $\mathbf{x}(t)$ and $\boldsymbol{\lambda}(t)$ values.
- v. Update $\mathbf{u}(t)$ based on a combination of $\mathbf{u}_{\text{new}}(t)$ and the previous $\mathbf{u}(t)$.
- vi. Check for convergence.
If $\mathbf{x}(t)$, $\boldsymbol{\lambda}(t)$ and $\mathbf{u}(t)$ meet a specified tolerance, accept $\mathbf{x}(t)$, $\boldsymbol{\lambda}(t)$ and $\mathbf{u}(t)$, otherwise return to Step ii. using the updated $\mathbf{u}(t)$.

Chapter 4A

Supplementary material to Chapter 4

Supporting code

Code for implementing the algorithms presented in this work is freely available on [GitHub](#).

4A.1 Forward-backward sweep method algorithm

The algorithm for the forward-backward sweep method (FBSM) is adapted from [191, 290]. Recall that in the standard control notation we represent the control as $u(t)$, the state variables as $\mathbf{x}(t)$, and the co-state variables as $\boldsymbol{\lambda}(t)$.

Algorithm 1: Forward-backward sweep

- i. Make an initial guess, $u^{(0)}(t)$.
- ii. Iterate for $k = 0, 1, \dots$, until converged or iteration limit met:
- iii. Solve for $\mathbf{x}^{(k)}(t)$ forward in time using initial values $\mathbf{x}(0)$, and $u^{(k)}(t)$.
- iv. Solve for $\boldsymbol{\lambda}^{(k)}(t)$ backwards in time from the transversality condition $\boldsymbol{\lambda}(t_N)$, using $u^{(k)}(t)$ and $\mathbf{x}^{(k)}(t)$.
- v. Compute temporary update, $\hat{u}^{(k+1)}(t)$, using $\mathbf{x}^{(k)}(t)$, $\boldsymbol{\lambda}^{(k)}(t)$, and the optimality condition derived from minimising the Hamiltonian.
- vi. Update $u^{(k+1)}(t) = \omega u^{(k)}(t) + (1 - \omega)\hat{u}^{(k+1)}(t)$.
- vii. Check for convergence. If not converged, return to Step ii.

In Step i., an initial guess of $u^{(0)}(t) \equiv \mathbf{0}$ is often sufficient, though an initial guess closer to the optimal control can improve convergence. The choice of $\omega \in [0, 1)$ in Step vi. can significantly impact the rate of convergence, and whether or not the process converges at all [191, 290]. We do not prescribe a specific convergence criterion in Step vii., as there are several valid choices. A general approach is to check if $\boldsymbol{x}^{(k)}(t)$, $\boldsymbol{\lambda}^{(k)}(t)$, and $u^{(k)}(t)$ are within a specified absolute or relative tolerance of their previous iteration values. For well-behaved systems, convergence of the control terms generally implies convergence of the associated state and co-state variables.

4A.2 Single-variable linear continuous control analytical solution

Consider the linear continuous control problem posed in the main document, repeated here as Equation (4A.1).

$$\frac{dx(t)}{dt} = \gamma x(t) + u(t), \quad x(0) = x_0, \quad \gamma > 0, \quad 0 \leq t \leq 1. \quad (4A.1)$$

The co-state equation is

$$\frac{d\lambda(t)}{dt} = -2ax(t) - \lambda(t)\gamma, \quad (4A.2)$$

with transversality condition $\lambda(1) = 0$, and optimal control characterised by

$$u^*(t) = \frac{\lambda(t)}{2b}. \quad (4A.3)$$

We set model parameter $\gamma = 0.5$ and pay-off weightings $a = b = 1$, with initial condition $x_0 = 1$. In this case, we are able to solve the control problem analytically. Substituting Equation (4A.3) into Equation (4A.1) we can combine with Equation (4A.2) to form the following system:

$$\begin{bmatrix} \frac{dx(t)}{dt} \\ \frac{d\lambda(t)}{dt} \end{bmatrix} = \begin{bmatrix} \frac{1}{2} & \frac{1}{2} \\ -2 & -\frac{1}{2} \end{bmatrix} \begin{bmatrix} x(t) \\ \lambda(t) \end{bmatrix}. \quad (4A.4)$$

This system has complex eigenvalues $e_1 = (\sqrt{3}/2)i$, $e_2 = (-\sqrt{3}/2)i$ and corresponding eigenvectors $v_1 = [(\sqrt{3}i - 1)^{-1}, 1]^T$, $v_2 = [(-\sqrt{3}i - 1)^{-1}, 1]^T$. Following the standard approach for systems with complex eigenvalues [160], and noting that $v_1 = [-1/4 - \sqrt{3}i/4, 1]^T$ we are able to produce a general solution of the form

$$\begin{bmatrix} x(t) \\ \lambda(t) \end{bmatrix} = C_1 \left(\begin{bmatrix} -\frac{1}{4} \\ 1 \end{bmatrix} \cos \left(\frac{\sqrt{3}t}{2} \right) + \begin{bmatrix} \frac{\sqrt{3}}{4} \\ 0 \end{bmatrix} \sin \left(\frac{\sqrt{3}t}{2} \right) \right) \\ + C_2 \left(- \begin{bmatrix} \frac{\sqrt{3}}{4} \\ 0 \end{bmatrix} \cos \left(\frac{\sqrt{3}t}{2} \right) + \begin{bmatrix} -\frac{1}{4} \\ 1 \end{bmatrix} \sin \left(\frac{\sqrt{3}t}{2} \right) \right). \quad (4A.5)$$

Evaluating Equation (4A.5) with the initial condition $x(0) = 1$, and transversality condition $\lambda(1) = 0$, we can solve for the coefficients C_1 and C_2 .

$$C_1 = -4 - \sqrt{3}C_2, \quad \text{where}$$

$$C_2 = \frac{4 \cos \left(\frac{\sqrt{3}}{2} \right)}{\sin \left(\frac{\sqrt{3}}{2} \right) - \sqrt{3} \cos \left(\frac{\sqrt{3}}{2} \right)}.$$

We can then form the complete analytical solution for the optimal state and co-state:

$$\begin{bmatrix} x(t) \\ \lambda(t) \end{bmatrix} = \left(\frac{4 \cos \left(\frac{\sqrt{3}}{2} \right)}{\sin \left(\frac{\sqrt{3}}{2} \right) - \sqrt{3} \cos \left(\frac{\sqrt{3}}{2} \right)} \right) \left(\begin{bmatrix} 0 \\ -\sqrt{3} \end{bmatrix} \cos \left(\frac{\sqrt{3}t}{2} \right) + \begin{bmatrix} -1 \\ 1 \end{bmatrix} \sin \left(\frac{\sqrt{3}t}{2} \right) \right) \\ + \left(\begin{bmatrix} 1 \\ -4 \end{bmatrix} \cos \left(\frac{\sqrt{3}t}{2} \right) + \begin{bmatrix} -\sqrt{3} \\ 0 \end{bmatrix} \sin \left(\frac{\sqrt{3}t}{2} \right) \right). \quad (4A.6)$$

From Equation (4A.3), recalling that $b = 1$ we can also obtain an analytical expression for the optimal control that depends only on t .

$$u^*(t) = \left(\frac{2 \cos \left(\frac{\sqrt{3}}{2} \right)}{\sin \left(\frac{\sqrt{3}}{2} \right) - \sqrt{3} \cos \left(\frac{\sqrt{3}}{2} \right)} \right) \left(-\sqrt{3} \cos \left(\frac{\sqrt{3}t}{2} \right) + \sin \left(\frac{\sqrt{3}t}{2} \right) \right) \\ - 2 \cos \left(\frac{\sqrt{3}t}{2} \right). \quad (4A.7)$$

In Figure 4A.1 we plot the exact solutions against the optimal state and control obtained from the FBSM to demonstrate excellent agreement.

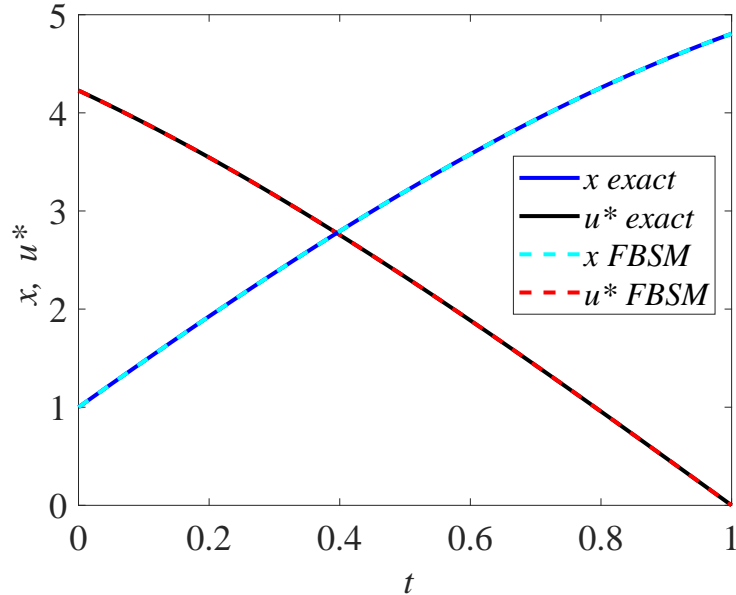


Figure 4A.1: We observe excellent agreement between the analytical and numerical solutions to the linear continuous control problem. The analytical optimal control is shown in black, with the optimal control obtained via the FBSM shown in red dash. The analytical solution for the state is plotted in blue, with the numerical solution overlaid in cyan dash. These solutions are produced with model parameter $\gamma = 0.5$, time-step $dt = 3.91 \times 10^{-3}$, over the interval $0 \leq t \leq 1$. The contributions of the state and the control to the pay-off are equally weighted, with $a = b = 1$.

4A.3 Steffensen derivation

In this section, we present the derivation of the multivariate Steffensen method, adapted from the two-variable derivation presented in [141], and then outline the proposed modification for use with accelerating convergence of the FBSM for an iterative process, $X^{(k+1)} = F(X^{(k)})$, where $X^{(k)} = [x_0^{(k)}, x_1^{(k)}, \dots, x_N^{(k)}]^T \in \mathbb{R}^{N+1}$ and $F = [f_0, f_1, \dots, f_N]^T$. Suppose $S = [s_0, s_1, \dots, s_N]^T$ is a solution, such that $S = F(S)$. Denote the error in the k th iterations as $E^{(k)} = [e_0^{(k)}, e_1^{(k)}, \dots, e_N^{(k)}]^T$ where $E^{(k)} = X^{(k)} - S$, such that

$$e_i^{(k)} = x_i^{(k)} - s_i, \quad i = 0, \dots, N.$$

Considering the first error term, and performing a Taylor expansion about s_0 we have

$$\begin{aligned} e_0^{(k+1)} &= x_0^{(k+1)} - s_0, \\ &= f_0(x_0^{(k)}, x_1^{(k)}, \dots, x_N^{(k)}) - f_0(s_0, s_1, \dots, s_N), \\ &= f_0(s_0 + e_0^{(k)}, s_1 + e_1^{(k)}, \dots, s_N + e_N^{(k)}) - f_0(s_0, s_1, \dots, s_N), \\ &= \frac{\partial f_0(s_0, s_1, \dots, s_N)}{\partial x_0} e_0^{(k)} + \frac{\partial f_0(s_0, s_1, \dots, s_N)}{\partial x_1} e_1^{(k)} + \dots \\ &\quad + \frac{\partial f_0(s_0, s_1, \dots, s_N)}{\partial x_N} e_N^{(k)} + \mathcal{O}(\|E\|^2). \end{aligned} \tag{4A.8}$$

Similarly for the j th element of E , with $j = 1, 2, \dots, N$ we have

$$\begin{aligned} e_j^{(k+1)} &= \frac{\partial f_j(s_0, s_1, \dots, s_N)}{\partial x_0} e_0^{(k)} + \frac{\partial f_j(s_0, s_1, \dots, s_N)}{\partial x_1} e_1^{(k)} + \dots \\ &\quad + \frac{\partial f_j(s_0, s_1, \dots, s_N)}{\partial x_N} e_N^{(k)} + \mathcal{O}(\|E\|^2). \end{aligned} \tag{4A.9}$$

Recalling the definition of the Jacobian, evaluated at the solution S ; J_S ,

$$J_S = \begin{bmatrix} \frac{\partial f_0}{x_0} & \frac{\partial f_0}{x_1} & \dots & \frac{\partial f_0}{x_N} \\ \frac{\partial f_1}{x_0} & \frac{\partial f_1}{x_1} & \dots & \frac{\partial f_1}{x_N} \\ \vdots & \vdots & \ddots & \vdots \\ \frac{\partial f_N}{x_0} & \frac{\partial f_N}{x_1} & \dots & \frac{\partial f_N}{x_N} \end{bmatrix}, \tag{4A.10}$$

we can express Equations (4A.8-4A.9) in matrix form:

$$E^{(k+1)} = J_S E^{(k)} + \mathcal{O}(\|E^{(k)}\|^2). \tag{4A.11}$$

In line with the approach for deriving Aitken's formula for a single variable [141], we proceed by assuming that Equation (4A.11) is true when neglecting the $\mathcal{O}(\|E^{(k)}\|^2)$ term. Then we have

$$X^{(k+1)} - S = J_S(X^{(k)} - S), \quad k = 0, 1, 2, \dots \quad (4A.12)$$

We want to determine S , however we do not know J_S . Subtracting two consecutive terms of Equation (4A.12), and denoting $\Delta X^{(k)} = X^{(k+1)} - X^{(k)}$ gives

$$\Delta X^{(k+1)} = J_S \Delta X^{(k)}, \quad k = 0, 1, 2, \dots \quad (4A.13)$$

Defining $\mathcal{X}^{(k)}$ as a matrix constructed with columns $(X^{(k)}, X^{(k+1)}, \dots, X^{(k+N)})$, such that $\mathcal{X}^{(k)} \in \mathbb{R}^{N+1 \times N+1}$,

$$\mathcal{X}^{(k)} = \begin{bmatrix} x_0^{(k)} & x_0^{(k+1)} & \dots & x_0^{(k+N)} \\ x_1^{(k)} & x_1^{(k+1)} & \dots & x_1^{(k+N)} \\ \vdots & \vdots & \ddots & \vdots \\ x_N^{(k)} & x_N^{(k+1)} & \dots & x_N^{(k+N)} \end{bmatrix}, \quad (4A.14)$$

and $\Delta \mathcal{X}^{(k)} = \mathcal{X}^{(k+1)} - \mathcal{X}^{(k)}$, then we can use Equation (4A.13) to obtain

$$J_S \Delta \mathcal{X}^{(k)} = \Delta \mathcal{X}^{(k+1)}, \quad k = 0, 1, 2, \dots, \text{ and hence:} \quad (4A.15)$$

$$J_S = \Delta \mathcal{X}^{(k+1)} (\Delta \mathcal{X}^{(k)})^{-1}. \quad (4A.16)$$

Rearranging Equation (4A.12) to solve for S , and assuming $(I - J_S)$ is non-singular, where I is the $N + 1 \times N + 1$ identity matrix, we have

$$\begin{aligned} (I - J_S)S &= X^{(k+1)} - J_S X^{(k)}, \\ (I - J_S)S &= (I - J_S)X^{(k)} + \Delta X^{(k)}, \\ S &= X^{(k)} + (I - J_S)^{-1} \Delta X^{(k)}. \end{aligned} \quad (4A.17)$$

Combining Equation (4A.17) with Equation (4A.16), and noting that $(AB)^{-1} = B^{-1}A^{-1}$ then

$$S = X^{(k)} - \Delta \mathcal{X}^{(k)} (\Delta^2 \mathcal{X}^{(k)})^{-1} \Delta X^{(k)}. \quad (4A.18)$$

To arrive at this expression for the true solution, S , we have assumed that Equation (4A.11) holds when neglecting the $\mathcal{O}(\|E^{(k)}\|^2)$ term. Though this may not be true, we assume that

$$\hat{X}^{(k)} = X^{(k)} - \Delta \mathcal{X}^{(k)} (\Delta^2 \mathcal{X}^{(k)})^{-1} \Delta X^{(k)} \quad (4A.19)$$

is closer to S than $X^{(k)}$, provided that $\Delta^2(\mathcal{X}^{(k)})^{-1}$ is non-singular. This is the form of Steffensen acceleration for multivariate systems. In the context of accelerating the FBSM, the number of iterations required to construct the $\mathcal{X}^{(k)}$ matrix in Equation (4A.14) is $\mathcal{O}(N)$. As outlined in the main document, we expect the number of iterations required for the FBSM to converge without acceleration to be fewer than $\mathcal{O}(N)$.

Suppose instead that we chose a number, $m < N + 1$, such that when we would form $\mathcal{X}^{(k)}$ in Equation (4A.14), we instead form a rectangular matrix, $\mathcal{Y}^{(k)}$ of dimension $N + 1 \times m + 2$:

$$\mathcal{Y}^{(k)} = \begin{bmatrix} x_0^{(k)} & x_0^{(k+1)} & \dots & x_0^{(k+m+1)} \\ x_1^{(k)} & x_1^{(k+1)} & \dots & x_1^{(k+m+1)} \\ \vdots & \vdots & \ddots & \vdots \\ x_N^{(k)} & x_N^{(k+1)} & \dots & x_N^{(k+m+1)} \end{bmatrix}, \quad (4A.20)$$

We can no longer follow the standard derivation, as Equation (4A.13) now gives a relationship between rectangular matrices, from which we can no longer isolate J_S via matrix inversion.

$$J_S \Delta \mathcal{Y}^{(k)} = \Delta \mathcal{Y}^{(k+1)}, \quad k = 0, 1, 2, \dots \quad (4A.21)$$

Instead, we suppose that $\mathcal{X}^{(k)} (\Delta^2 \mathcal{X}^{(k)})^{-1} \Delta X^{(k)}$ in Equation (4A.19) can be approximated by $\Delta \mathcal{Y}^{(k)} (\Delta^2 \mathcal{Y}^{(k)})^+ \Delta X^{(k)}$, such that we obtain

$$\hat{X}^{(k)} = X^{(k)} - \Delta \mathcal{Y}^{(k)} (\Delta^2 \mathcal{Y}^{(k)})^+ \Delta X^{(k)}, \quad (4A.22)$$

where $(\Delta^2 \mathcal{Y}^{(k)})^+$ is the Moore-Penrose pseudoinverse [257]. We will refer to this as the partial Steffensen method.

The Moore-Penrose pseudoinverse is a generalisation of the matrix inverse for singular or non-square matrices. The matrix A^+ is the (unique) Moore-Penrose pseudoinverse of A if it satisfies these conditions [257]:

1. $AA^+A = A,$
2. $A^+AA^+ = A^+,$
3. $(AA^+)^* = AA^+,$
4. $(A^+A)^* = A^+A.$

Here, $(\cdot)^*$ denotes the conjugate transpose. If A is an invertible square matrix, then $A^+ = A^{-1}$. It can be shown that $X = A^+B$ is the least squares solution to $AX = B$, in that it minimises the Frobenius norm; $\|A(A^+B) - B\|_F \leq \|AX - B\|_F$, for any choice of X where AX is defined [258, 261].

Suppose an $m \times n$ matrix A is expressed in the singular value decomposition (SVD) form, $A = V^*SU$, where V and U are unitary matrices of dimension $m \times m$ and $n \times n$, respectively. The $m \times n$ matrix $S = \text{diag}(\sigma_1, \dots, \sigma_p)$, where σ_i are the singular values of A , $p = \min(m, n)$, and $\sigma_1 \geq \sigma_2 \geq \dots \geq \sigma_p \geq 0$ [126]. The matrix A^+ can then be obtained via $A^+ = U^*S^+V$, where S^+ is formed by taking the reciprocal of the non-zero diagonal elements of S then transposing the resulting matrix [258].

For numerical implementation of Equation (4A.22), many popular options for matrix computation such as MATLAB, Julia and Python's NumPy library have built in `pinv()` commands that compute the Moore-Penrose pseudoinverse using SVD [157, 221, 271]. Further, it may be more efficient to instead use in-built least-squares routines, such as `lsqminnorm()` in MATLAB [221].

4A.4 Acceleration algorithms

In this section we present algorithms for the iterative acceleration methods used in this work. We present algorithms for the Wegstein, Aitken-Steffensen and Anderson methods as applied to systems. In accordance with notation used in the main document, we consider accelerating a fixed point iterative process, $X^{(k+1)} = F(X^{(k)})$, where $X^{(k)} = [x_0^{(k)}, x_1^{(k)}, \dots, x_N^{(k)}]^T$ is the k th iterate for the control, consisting of $N + 1$ values, and $F = [f_0, f_1, \dots, f_N]^T$ is the $N + 1$ dimensional operator. We refer to evaluation of $F(X)$ as one *function evaluation*, as this is analogous to the number of iterations in a FBSM process and this is what we seek to reduce. We denote the total number of function evaluations required to achieve convergence as \mathcal{N} .

4A.4.1 Wegstein method

The algorithm for the Wegstein method is adapted from [129, 334]. This method requires element-wise computations; with elements denoted by subscript i . The element-wise computations are performed on every element, and there is no interaction between elements, such that $i = 1, \dots, N + 1$, always. This range is not explicitly mentioned in Algorithm 3 as there is no ambiguity.

Algorithm 3: Wegstein method

- i. From $X^{(0)}$, generate $X^{(1)} = F(X^{(0)})$ and $X^{(2)} = F(X^{(1)})$.
- ii. Compute $A_i^{(1)}$ and $q_i^{(1)}$ element-wise; $A_i^{(1)} = \frac{x_i^{(2)} - x_i^{(1)}}{x_i^{(1)} - x_i^{(0)}}$, $q_i^{(1)} = \frac{A_i^{(1)}}{A_i^{(1)} - 1}$, bound q_i if desired.
- iii. Update $X^{(2)}$ element-wise; $x_i^{(2)} = q_i^{(1)}x_i^{(1)} + (1 - q_i^{(1)})f_i(x_i^{(1)})$.
- iv. Iterate for $k = 2, 3, \dots$, until converged or iteration limit met:
- v. Compute $A_i^{(k)}$ and $q_i^{(k)}$ element-wise; $A_i^{(k)} = \frac{f_i(x_i^{(k)}) - f_i(x_i^{(k-1)})}{x_i^{(k)} - x_i^{(k-1)}}$, $q_i^{(k)} = \frac{A_i^{(k)}}{A_i^{(k)} - 1}$, bound q_i if desired.
- vi. Update $X^{(k+1)}$ element-wise; $x_i^{(k+1)} = q_i^{(k)}x_i^{(k)} + (1 - q_i^{(k)})f_i(x_i^{(k)})$.
- vii. Check for convergence. If not converged, return to Step iv.

The Wegstein method requires two evaluations of F initially, then one more evaluation of F to update $X^{(2)}$. From Step iv. onward, only one evaluation of F is required per iteration, as the elements $f_i(x_i^{(k-1)})$ used to obtain $A_i^{(k)}$ can be stored from the previous iteration. If $A_i = 1$ in Step ii. or Step v., prescribe a value of q_i to avoid division by

zero, for example $q_i = 0$. Aside from the choice of bounds on the q_i , variations to the Wegstein method arise by altering how frequently q is updated. In the simplest case, q is determined only once, and not updated in subsequent iterations. Updating q every n th iteration can be effective for appropriately chosen n , however the choice of n that minimises \mathcal{N} appears to be highly problem dependent and must be empirically determined [283]. As the Wegstein method is implemented element-wise, no expensive matrix operations are performed. However, these element-wise computations ignore interactions between variables and can result in instability for some problems [249].

4A.4.2 Aitken-Steffensen method

The algorithm for the Steffensen method is adapted from [58, 141]. Recall that $X^{(k)} = [x_0^{(k)}, x_1^{(k)}, \dots, x_N^{(k)}]^T$ is the k th iterate, consisting of $N+1$ elements, and $F = [f_0, f_1, \dots, f_N]^T$ is the $N+1$ dimensional operator of the iterative process. Further, $\Delta X^{(k)} = X^{(k+1)} - X^{(k)}$, $\mathcal{X}^{(k)}$ is a matrix constructed with columns $(X^{(k)}, X^{(k+1)}, \dots, X^{(k+N)})$, such that $\mathcal{X}^{(k)}$ is a square matrix of dimension $N+1$, with $\Delta \mathcal{X}^{(k)} = \mathcal{X}^{(k+1)} - \mathcal{X}^{(k)}$, and $\Delta^2 \mathcal{X}^{(k)} = \Delta \mathcal{X}^{(k+1)} - \Delta \mathcal{X}^{(k)}$.

Algorithm 2a: Steffensen method

- i. Iterate for $k = 0, 1, \dots$, until converged or iteration limit met:
- ii. From $X^{(k)}$, generate $X^{(k+1)} = F(X^{(k)})$, $X^{(k+2)} = F(X^{(k+1)})$, ..., $X^{(k+N+2)} = F(X^{(k+N+1)})$.
- iii. Define $\Delta X^{(k)} = X^{(k+1)} - X^{(k)}$, $\Delta X^{(k+1)} = X^{(k+2)} - X^{(k+1)}$, ..., $\Delta X^{(k+N+1)} = X^{(k+N+2)} - X^{(k+N+1)}$.
- iv. Append results from Step iii. to construct $N+1 \times N+1$ matrices $\Delta \mathcal{X}^{(k)} = (\Delta X^{(k)}, \Delta X^{(k+1)}, \dots, \Delta X^{(k+N)})$, and $\Delta \mathcal{X}^{(k+1)} = (\Delta X^{(k+1)}, \Delta X^{(k+2)}, \dots, \Delta X^{(k+N+1)})$.
- v. Define $\Delta^2 \mathcal{X}^{(k)} = \Delta \mathcal{X}^{(k+1)} - \Delta \mathcal{X}^{(k)}$.
- vi. Compute $\hat{X}^{(k+1)} = X^{(k)} - \Delta \mathcal{X}^{(k)}(\Delta^2 \mathcal{X}^{(k)})^{-1} \Delta X^{(k)}$.
- vii. Check for convergence. If not converged, return to Step ii. starting with $X^{(k)} = \hat{X}^{(k+1)}$.

For efficient numerical implementation, the inverse matrix is not formed in Step vi. Rather, we compute $\hat{X}^{(k+1)} = X^{(k)} - \Delta \mathcal{X}^{(k)}P$, where P is obtained by solving the linear system $(\Delta^2 \mathcal{X}^{(k)})P = \Delta X^{(k)}$. To recover the Aitken method, continue to compute $\hat{X}^{(k)}$,

$k = 1, 2, \dots$, and check for convergence in the \hat{X} series, but do not set $X^{(k)} = \hat{X}^{(k+1)}$ in Step vii; instead use $X^{(k+N+2)}$, the most recently computed X from Step ii.

As noted in §4A.3, we expect the number of iterations required for the FBSM to converge without acceleration to be fewer than the number of FBSM iterations required to construct $\mathcal{X}^{(k)}$. As such, we also present the algorithm for a partial Aitken-Steffensen method outlined in §4A.3, requiring $m + 1 \ll N$ function evaluations per iteration.

Algorithm 2b: Partial Steffensen method

- i. Choose a value m such that $1 \leq m < N + 1$.
- ii. Iterate for $k = 0, 1, \dots$, until converged or iteration limit met:
- iii. From $X^{(k)}$, generate $X^{(k+1)} = F(X^{(k)})$, $X^{(k+2)} = F(X^{(k+1)})$, ..., $X^{(k+m+1)} = F(X^{(k+m)})$.
- iv. Define $\Delta X^{(k)} = X^{(k+1)} - X^{(k)}$, $\Delta X^{(k+1)} = X^{(k+2)} - X^{(k+1)}$, ..., $\Delta X^{(k+m)} = X^{(k+m+1)} - X^{(k+m)}$.
- v. Append results from Step iv. to construct $N + 1 \times m$ matrices
 $\Delta \mathcal{Y}^{(k)} = (\Delta X^{(k)}, \Delta X^{(k+1)}, \dots, \Delta X^{(k+m-1)})$, and
 $\Delta \mathcal{Y}^{(k+1)} = (\Delta X^{(k+1)}, \Delta X^{(k+2)}, \dots, \Delta X^{(k+m)})$.
- vi. Define $\Delta^2 \mathcal{Y}^{(k)} = \Delta \mathcal{Y}^{(k+1)} - \Delta \mathcal{Y}^{(k)}$.
- vii. Compute $\hat{X}^{(k+1)} = X^{(k)} - \Delta \mathcal{Y}^{(k)} (\Delta^2 \mathcal{Y}^{(k)})^+ \Delta X^{(k)}$, where $(\Delta^2 \mathcal{Y}^{(k)})^+$ is the Moore-Penrose pseudoinverse.
- viii. Check for convergence. If not converged, return to Step ii. starting with $X^{(k)} = \hat{X}^{(k+1)}$.

As noted in §4A.3, for numerical implementation of Step vii. it may be more efficient to use in-built least-squares routines, such as `lsqminnorm()` in MATLAB [221], rather than computing the Moore-Penrose pseudoinverse explicitly via SVD or other means. To recover the partial Aitken method, continue to compute $\hat{X}^{(k)}$, $k = 1, 2, \dots$, and check for convergence in the \hat{X} series, but do not set $X^{(k)} = \hat{X}^{(k+1)}$ in Step vii.; instead use $X^{(k+m+1)}$, the most recently computed X from Step iii.

4A.4.3 Anderson Acceleration

Algorithm 4: Anderson acceleration

- i. Choose a value $M \geq 1$, let $m = 1$.
- ii. From $X^{(0)}$, generate $X^{(1)} = F(X^{(0)})$ and $X^{(2)} = F(X^{(1)})$.
- iii. Define $\Delta X^{(0)} = X^{(1)} - X^{(0)}$, $\Delta X^{(1)} = X^{(2)} - X^{(1)}$, append to form the $N + 1 \times 2$ matrix $\mathcal{G} = (\Delta X^{(0)}, \Delta X^{(1)}) = (G^{(0)}, G^{(1)})$, and compute $\Delta G^{(0)} = \Delta X^{(1)} - \Delta X^{(0)}$. Note that $X^{(2)}$ and $\Delta X^{(1)}$ in this initialisation are overwritten in Step vi. when $k = 1$, by their Anderson algorithm generated counterparts.
- iv. Iterate for $k = 1, 2, \dots$ until converged or iteration limit met:
- v. Solve the least squares problem $\gamma = \arg \min_{\gamma} \|G^{(k)} - \gamma dG^{(k-1)}\|$.
- vi. Compute $X^{(k+1)} = X^{(k)} + G^{(k)} - (dX^{(k-1)} + dG^{(k-1)})\gamma$, $\Delta X^{(k)} = X^{(k+1)} - X^{(k)}$, $G^{(k+1)} = F(X^{(k+1)}) - X^{(k+1)}$, and $\Delta G^{(k)} = G^{(k+1)} - G^{(k)}$.
- vii. **if** $m < M$

Update \mathcal{G}, dX and dG by appending the results from Step vi. as the right-most column. Increment $m = m + 1$.

else

Update \mathcal{G} , dX ad dG by removing the left-most column then appending the results from Step vi. as the right-most column.
- viii. Check the condition number of the matrix dG ; if it exceeds some prescribed tolerance, update \mathcal{G} , dX and dG by removing the left-most column. Decrement $m = m - 1$. Repeat Step viii. until the condition number falls below the tolerance or $m = 1$.
- ix. Check for convergence. If not converged, return to Step iv.

The algorithm for Anderson Acceleration is adapted from [104, 326]. Recall that for a fixed point process where we seek $X = F(X)$, we can define a corresponding root finding problem; $G(X) := F(X) - X = \mathbf{0}$, where $\mathbf{0}$ is the zero column vector of length $N + 1$. For convenience of notation in the algorithm, we denote the difference between iterates; $\Delta X^{(k)} = X^{(k+1)} - X^{(k)}$, residuals; $G^{(k)} = F(X^{(k)}) - X^{(k)}$, and difference between residuals $\Delta G^{(k)} = G^{(k+1)} - G^{(k)}$. Further, $\mathcal{G}^{(k)}$ is a matrix constructed with columns $(G^{(k-m)}, G^{(k-m+1)}, \dots, G^{(k)})$, $dX^{(k)}$ is a matrix with columns $(\Delta X^{(k-m)}, \Delta X^{(k-m+1)}, \dots, \Delta X^{(k-1)})$, and $dG^{(k)}$ is a matrix with columns $(\Delta G^{(k-m)}, \Delta G^{(k-m+1)}, \dots, \Delta G^{(k-1)})$.

The algorithms for Anderson acceleration presented in the literature can vary significantly between sources depending on how the least squares problem is handled, and which commodities are stored and accessed at what stage of the process. The algorithm we present here, along with the associated MATLAB implementation, is one of many approaches, and we recommend resources such as [18, 104, 326] for a more thorough explanation and further efficiency improvements. We attempt to strike a balance between understandable implementation, efficiency and effectiveness. As we are focussed on using these acceleration techniques to reduce \mathcal{N} , we include Step viii. to check the conditioning of dG , which is straightforward to implement and can reduce \mathcal{N} . However, we do not incorporate the approach of performing QR decomposition on dG , that enables more computationally efficient updating and solutions to the least squares problems [326]; as this adds significant complexity to the algorithm and does not further our particular goal in this work of reducing \mathcal{N} . For clarity, in Step iii. $\Delta X^{(0)} = G^{(0)}$ and $\Delta X^{(1)} = G^{(1)}$, however this is only true for the initialisation. When the next iterations of these values are calculated in Step vi., X (and hence ΔX) values are updated via the Anderson formula $X^{(k)} + G^{(k)} - (dX^{(k-1)} + dG^{(k-1)})\gamma$, whereas G values are updated based on a function evaluation of the most recently computed X .

4A.5 Test nonlinear systems

We test each iterative acceleration technique on three nonlinear systems, before applying the techniques to FBSM problems. Equation (4A.23) is a 2×2 system used in [244] to test the Steffensen method. Equations (4A.24) and (4A.25) are arbitrarily constructed systems of dimension 3×3 and 4×4 , respectively. These systems all have at least one real root that can be obtained via fixed point iteration, to use as a benchmark for the effectiveness of each acceleration algorithm. We also present approximate numerical solutions for the other real roots, obtained using `vpasolve()` in MATLAB [222].

The 2×2 system is:

$$\begin{pmatrix} x_1 \\ x_2 \end{pmatrix} = \begin{pmatrix} \frac{1}{60}(3x_1^3 - 3x_1^2 x_2 + 6x_1 x_2^2 + 61.488) \\ \frac{1}{50}(-x_1^3 + 6x_1^2 x_2 + 3x_2^3 - 32.496) \end{pmatrix}. \quad (4A.23)$$

The approximate real solutions to Equation (4A.23) are:

$$\begin{pmatrix} x_1 \\ x_2 \end{pmatrix} = \begin{pmatrix} 1.4 \\ -1 \end{pmatrix}, \begin{pmatrix} -5.2024 \\ -0.9414 \end{pmatrix}, \begin{pmatrix} -2.2912 \\ -2.9166 \end{pmatrix}, \begin{pmatrix} -1.0562 \\ 4.1194 \end{pmatrix}, \\ \begin{pmatrix} 1.5442 \\ -1.1372 \end{pmatrix}, \begin{pmatrix} 3.2302 \\ 2.3117 \end{pmatrix}, \begin{pmatrix} 3.9247 \\ 1.7874 \end{pmatrix}.$$

The 3×3 system is:

$$\begin{pmatrix} x_1 \\ x_2 \\ x_3 \end{pmatrix} = \begin{pmatrix} x_1 - \frac{1}{4}(x_1^2 + x_2^2 - 5) \\ x_2 - \frac{1}{2}(x_1 x_2 - 2) \\ \frac{1}{3}(x_2 - x_1 x_3) \end{pmatrix}. \quad (4A.24)$$

The approximate real solutions to Equation (4A.24) are:

$$\begin{pmatrix} x_1 \\ x_2 \\ x_3 \end{pmatrix} = \begin{pmatrix} 1 \\ 2 \\ 0.5 \end{pmatrix}, \begin{pmatrix} -1 \\ -2 \\ -1 \end{pmatrix}, \begin{pmatrix} -2 \\ -1 \\ -1 \end{pmatrix}, \begin{pmatrix} 2 \\ 1 \\ 0.2 \end{pmatrix}.$$

The 4×4 system is:

$$\begin{pmatrix} x_1 \\ x_2 \\ x_3 \\ x_4 \end{pmatrix} = \begin{pmatrix} \sqrt{4x_1 x_4 - x_2^2 + 5} \\ \frac{2}{x_1}(1 - x_2 x_4) + \frac{x_3}{10} \\ \frac{1}{3}(x_2 - x_1) + \frac{1}{x_3} \\ \frac{1}{50}(x_1 x_3 - \frac{3}{2} x_2 x_4) \end{pmatrix}. \quad (4A.25)$$

The approximate real solutions to Equation (4A.25) are:

$$\begin{pmatrix} x_1 \\ x_2 \\ x_3 \\ x_4 \end{pmatrix} = \begin{pmatrix} 1.9325 \\ 0.9613 \\ -1.1749 \\ -0.0441 \end{pmatrix}, \begin{pmatrix} 0.9965 \\ 1.9858 \\ -0.8486 \\ -0.0160 \end{pmatrix}, \begin{pmatrix} 1.0039 \\ 2.0205 \\ 1.1837 \\ 0.0224 \end{pmatrix}, \begin{pmatrix} 2.0566 \\ 1.0233 \\ 0.8425 \\ 0.0336 \end{pmatrix}.$$

4A.5.1 Results

Tables in this section contain the number of function evaluations required for convergence for each system, using each of the acceleration algorithms and for various initial guesses. Recall that we use \mathcal{N} to refer to the number of times the right hand side of the system is evaluated for the iterative procedure to converge. The convergence criteria for all schemes except for Aitken's method is $\|F(X) - X\| < 1 \times 10^{-10}$. Where the method fails to converge within 1000 function evaluations, we note *DNC* in the table. For Aitken's method, convergence is determined based on the difference between subsequent results in the Aitken series; $\|\hat{X}^{(k+1)} - \hat{X}^{(k)}\| < 1 \times 10^{-10}$.

Wegstein method

For the Wegstein method, results are presented for a static value of q , and for updating q every n th iteration, $n \in \{1, 2, \dots, 6\}$. We consider the standard bounds of $-5 \leq q \leq 0$ [21, 283], and the unbounded case. The effectiveness varies, with some combinations significantly outperforming fixed point iteration and other combinations requiring far more function evaluations for convergence, or not converging at all. In several cases the Wegstein method converges to a different root to the fixed point iteration, as the Wegstein updating step can cause the iterates to leave the basin of attraction of the solution found via fixed point iteration. Though we are seeking real solutions, the square root term in Equation (4A.25) can introduce complex values during the iterative process. This creates

a challenge when implementing bounds, as \mathbb{C} is not ordered. We handle this by bounding the magnitude of the complex number while maintaining its angle in the complex plane. Code implementing this step is provided on [GitHub](#), though we do not discuss it in detail in this work as it does not impact the acceleration of the FBSM for optimal control problems.

		Fixed Point		Update Wegstein q every n th iteration, bounded $-5 \leq q \leq 0$							
Eq.	$X^{(0)}$	Solution	\mathcal{N}	Static	1	2	3	4	5	6	
4A.23	[0; 0]	[1.4; -1]	167	141	87	74	60	46	42	44	
	[1; 2]	[1.4; -1]	167	135	105	55	50	46	53	DNC	
	[1; 1]	[1.4; -1]	167	131	81	66	64	58	67	56	
	[-1; -1]	[1.4; -1]	167	144	91	79	DNC	50	47	44	

		Fixed Point		Update Wegstein q every n th iteration, unbounded							
Eq.	$X^{(0)}$	Solution	\mathcal{N}	Static	1	2	3	4	5	6	
4A.23	[0; 0]	[1.4; -1]	167	141	247	32	26	26	27	27	
	[1; 2]	[1.4; -1]	167	200	242	26	20	58	DNC	56*	
	[1; 1]	[1.4; -1]	167	131	247	26	DNC	58*	DNC	DNC	
	[-1; -1]	[1.4; -1]	167	144	251	28	20	22	22	26	

* indicates that the procedure converged to another root; [3.9247; 1.7874].

		Fixed Point		Update Wegstein q every n th iteration, bounded $-5 \leq q \leq 0$						
Eq.	$X^{(0)}$	Solution	\mathcal{N}	Static	1	2	3	4	5	6
4A.24	[0; 0; 0]	[2; 1; 0.2]	56	DNC	62	62	60	64	64	71
	[1; 2; 3]	[1; 2; 0.5]	23	25	25	25	25	25	25	25
	[1; 1; 1]	[2; 1; 0.2]	57	59	61	59	59	59	59	59
	[-1; -1; -1]	[2; 1; 0.2]	57	59	DNC	60	DNC	61	59	59

		Fixed Point		Update Wegstein q every n th iteration, unbounded						
Eq.	$X^{(0)}$	Solution	\mathcal{N}	Static	1	2	3	4	5	6
4A.24	[0; 0; 0]	[2; 1; 0.2]	56	DNC	90	21	20	22	24	32
	[1; 2; 3]	[1; 2; 0.5]	23	3	3	3	3	3	3	3
	[1; 1; 1]	[2; 1; 0.2]	57	53	84	22	71*	50	28	26
	[-1; -1; -1]	[2; 1; 0.2]	57	DNC	93*	22*	49	22*	27*	26*

* indicates that the procedure converged to another root; $[-2; -1; -1]$.

Results for Equation (4A.25) exclude the initial condition $[0; 0; 0; 0]$ as the system is not defined for $x_1 = 0$ or $x_3 = 0$. The solution is presented once only for each table concerning Equation (4A.25), corresponding to all initial values considered.

		Fixed Point		Update Wegstein q every n th iteration, unbounded						
Eq.	$X^{(0)}$	Solution	\mathcal{N}	Static	1	2	3	4	5	6
4A.25	$[1; 2; 3; 4]$ $[1; 1; 1; 1]$ $[0.9613; -1.1749; -0.0441]$	$[1.9325; 100; 99]$ $[99; 99^*; 70^*]$ $[59; 70; 91]$	99 100 96	DNC DNC DNC	74 99 59	74 99* 70	89 62* 360	DNC DNC DNC	DNC DNC DNC	DNC DNC DNC

* indicates that the procedure converged to another root, $[2.0566; 1.0233; 0.8425; 0.0336]$.

Aitken-Steffensen methods

For the partial Aitken and partial Steffensen methods we produce results for $m = 1, 2, \dots, N$ where N is the size of the system and $m < N$ corresponds to the partial implementation outlined in §4A.4. The Steffensen method required fewer function evaluations than the Aitken method in most cases, though the Aitken method converged for all cases while the Steffensen method did not. In one instance the partial Steffensen method converged to a different root to the fixed point iteration. All implementations of the Aitken and Steffensen methods that converged, did so with fewer function evaluations than the fixed point iteration.

		Fixed Point		Aitken		Steffensen	
Eq.	$X^{(0)}$	Solution	\mathcal{N}	$m = 1$	$m = 2$	$m = 1$	$m = 2$
4A.23	$[0; 0]$ $[1; 2]$ $[1; 1]$ $[-1; -1]$	$[1.4; -1]$ $[1.4; -1]$ $[1.4; -1]$ $[1.4; -1]$	167 167 167 167	92 92 92 92	66 63 69 66	61 55 71 59	16 19 19 19

		Fixed Point		Aitken, $m =$			Steffensen, $m =$		
Eq.	$X^{(0)}$	Solution	\mathcal{N}	1	2	3	1	2	3
4A.24	$[0; 0; 0]$ $[1; 2; 3]$ $[1; 1; 1]$ $[-1; -1; -1]$	$[2; 1; 0.2]$ $[1; 2; 0.5]$ $[2; 1; 0.2]$ $[2; 1; 0.2]$	56 23 57 57	38 4 38 38	39 6 36 39	28 8 28 28	47 3 43 DNC	22 4 25 DNC	17 5 17 DNC

		Fixed Point		Aitken, $m =$				Steffensen, $m =$			
Eq.	$X^{(0)}$	Solution	\mathcal{N}	1	2	3	4	1	2	3	4
4A.25	$[1; 2; 3; 4]$ $[1; 1; 1; 1]$ $[0.9613; -1.1749; -0.0441]$	$[1.9325; 100; 99]$ $[99; 99^*; 70^*]$ $[59; 70; 91]$	99 100 96	50 50 46	48 45 42	40 40 36	35 35 30	73 DNC 72	76 79* 57	53 61 32	21 36 15

* indicates that the procedure converged to another root, $[2.0566; 1.0233; 0.8425; 0.0336]$.

Anderson Acceleration

For Anderson acceleration we produce results for $M \in \{1, 2, \dots, 5\}$, with a tolerance of 1×10^{10} when checking the conditioning of the matrix. Convergence was achieved in all implementations of Anderson acceleration, though several cases converged to a different root to the fixed point iteration. Of all the methods considered, Anderson acceleration produced the most consistent reduction in function evaluations relative to the fixed point iteration when applied to these test nonlinear systems.

		Fixed Point		Anderson				
Eq.	$X^{(0)}$	Solution	\mathcal{N}	$M = 1$	$M = 2$	$M = 3$	$M = 4$	$M = 5$
4A.23	[0; 0]	[1.4; -1]	167	11	15	13	15	16
	[1; 2]	[1.4; -1]	167	13	12	13	16	17
	[1; 1]	[1.4; -1]	167	12	12	14	16	17
	[-1; -1]	[1.4; -1]	167	12	12	14	16	19
		Fixed Point		Anderson				
Eq.	$X^{(0)}$	Solution	\mathcal{N}	$M = 1$	$M = 2$	$M = 3$	$M = 4$	$M = 5$
4A.24	[0; 0; 0]	[2; 1; 0.2]	56	28	18	12	14	14
	[1; 2; 3]	[1; 2; 0.5]	23	3	3	3	3	3
	[1; 1; 1]	[2; 1; 0.2]	57	24	14	12	12	13
	[-1; -1; -1]	[2; 1; 0.2]	57	53*	30*	22	35*	27*

* indicates that the procedure converged to another root, [-1;-2;-1].

		Fixed Point		Anderson				
Eq.	$X^{(0)}$	Solution	\mathcal{N}	$M = 1$	$M = 2$	$M = 3$	$M = 4$	$M = 5$
4A.25	[1; 2; 3; 4]	[1.9325;	99	32	29	21	22	27
	[1; 1; 1; 1]	100	37*	27*	14*	14*	14*	16*
	[-1; -1; -1; -1]	0.9613; -1.1749; -0.0441]	96	25	19	12	13	13

* indicates that the procedure converged to another root, [2.0566; 1.0233; 0.8425; 0.0336].

4A.6 Control results

In this section we present results for the acceleration algorithms applied to control problems, for a wide range of tuning parameters. For Wegstein's method we vary ω and the frequency with which q is updated. For each problem we select a bounding on q that works reasonably, though we do not attempt to find the optimal bounds. For the Aitken and Steffensen methods we vary ω and m . For Anderson acceleration we vary ω and M , with a tolerance of 1×10^{10} when checking the conditioning of the matrix. We do not vary or attempt to optimise this tolerance. Each value in the tables correspond to \mathcal{N} , the number of function evaluations required for convergence. Simulations are terminated when \mathcal{N} reaches 100; any value in the tables that is 100 or greater corresponds to a combination of tuning parameters that did not yield convergence within this specified maximum. This does not necessarily imply that this combination would not have converged if additional function evaluations were performed. For the linear problems, we do not vary ω as the FBSM with no acceleration converges with minimum \mathcal{N} when $\omega = 0$.

A heatmap is applied to each table, with colours scaled relative to the result from the FBSM with the best tuning but without acceleration. Recall that with the tuning that minimises \mathcal{N} , the FBSM with no acceleration requires $\mathcal{N} = 57$ for the linear continuous control problem, $\mathcal{N} = 8$ for the linear bang-bang control problem, $\mathcal{N} = 38$ for the AML continuous control problem, and $\mathcal{N} = 34$ for the AML bang-bang control problem. Acceleration results that reflect a reduction in \mathcal{N} relative to these FBSM results are shaded in the green spectrum, while worse performance is shaded in the red spectrum. The midpoint of the colour spectra, yellow, corresponds to the FBSM result with the best tuning, without acceleration. In the main document we use robustness to refer to the ability of a method to reduce \mathcal{N} over a range of tuning parameters. Visually, tables with large groups of green shaded cells indicate robustness, while isolated green cells surrounded by orange-red cells suggest a lack of robustness.

For the AML bang-bang control problem with the Aitken method, for values of $\omega \leq 0.35$, we observe apparent convergence to controls that are not bang-bang. The iterative procedure terminates as the convergence criteria is met; however the resulting controls contain intermediate values between the lower and upper bounds. Similarly for the AML continuous control problem with the Aitken method, for values of $\omega \leq 0.35$, we observe apparent convergence. However, explicitly calculating the pay-off associated with these controls, and comparing it to the pay-off associated with the control obtained via the standard FBSM, indicates that the controls obtained via the Aitken method for $\omega \leq 0.35$ are not optimal. These sections of the partial Aitken method tables have been denoted as $\mathcal{N} = 100$, to indicate a failure to converge to the optimal control; regardless of the number of iterations taken to achieve the apparent convergence to controls that are not optimal.

We note that implementation of Anderson Acceleration involves computing condition numbers of matrices. Matrices that are ill-conditioned (indicated by a large condition number), are close to singular, such that significant numerical error can arise when computing the inverse, or obtaining the solution of a corresponding linear system of equations [142]. It is known that for ill-conditioned matrices, computation of the condition number can itself be highly sensitive [142]. Computing condition numbers is commonly impacted by underflow and overflow, or rounding errors [88, 142]. For this reason, users attempting to reproduce results of the Anderson Acceleration method using different software or hardware may find that in some instances convergence is achieved with a different \mathcal{N} to what is indicated in the tables, depending on whether the estimated condition number at each iteration suggests that the matrix is ill-conditioned. For a thorough discussion of condition numbers and issues arising from floating point arithmetic we direct readers to [143].

4A.6.1 Linear continuous control problem

	Wegstein, updating q every n th iteration, $-2 \leq q \leq 0$									
ω	$n=1 \quad n=2 \quad n=3 \quad n=4 \quad n=5 \quad n=6 \quad n=7 \quad n=8 \quad n=9 \quad n=10$									
0	24	32	26	23	27	38	44	42	47	62
	Partial Aitken									
ω	$m=1$	$m=2$	$m=3$	$m=4$	$m=5$	$m=6$	$m=7$	$m=8$	$m=9$	$m=10$
0	12	12	12	15	18	14	16	18	20	22
	Partial Steffensen									
ω	$m=1$	$m=2$	$m=3$	$m=4$	$m=5$	$m=6$	$m=7$	$m=8$	$m=9$	$m=10$
0	31	16	13	11	13	8	9	10	11	12
	Anderson									
ω	$M=1$	$M=2$	$M=3$	$M=4$	$M=5$	$M=6$	$M=7$	$M=8$	$M=9$	$M=10$
0	12	9	8	7	7	7	7	7	7	7

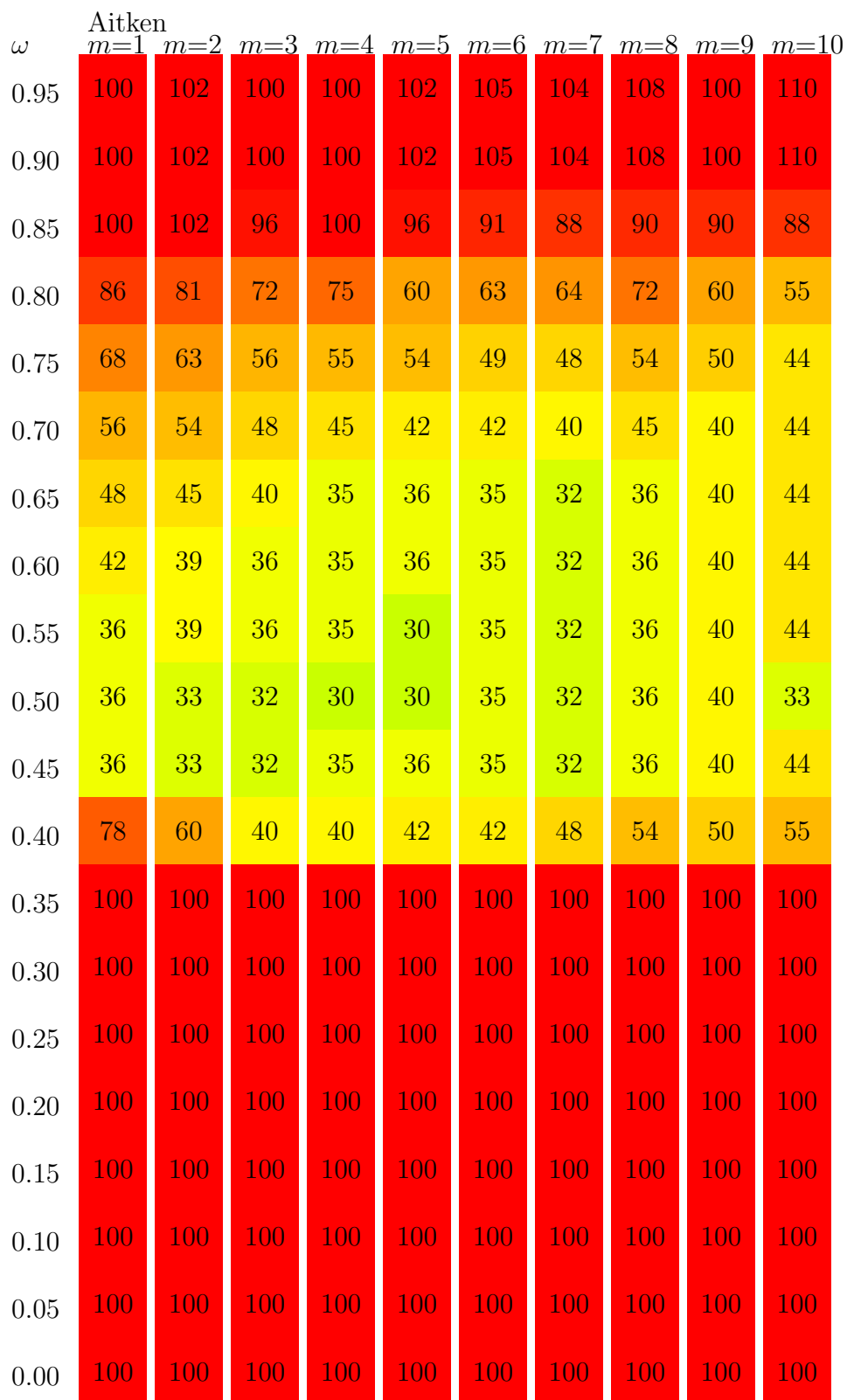
4A.6.2 Linear bang-bang control problem

	Wegstein, unbounded									
ω	$n=1 \quad n=2 \quad n=3 \quad n=4 \quad n=5 \quad n=6 \quad n=7 \quad n=8 \quad n=9 \quad n=10$									
0	9	9	9	9	9	9	9	9	9	9
	Partial Aitken									
ω	$m=1$	$m=2$	$m=3$	$m=4$	$m=5$	$m=6$	$m=7$	$m=8$	$m=9$	$m=10$
0	10	12	12	15	18	21	16	18	20	22
	Partial Steffensen									
ω	$m=1$	$m=2$	$m=3$	$m=4$	$m=5$	$m=6$	$m=7$	$m=8$	$m=9$	$m=10$
0	29	19	17	16	13	15	9	10	11	12
	Anderson									
ω	$M=1$	$M=2$	$M=3$	$M=4$	$M=5$	$M=6$	$M=7$	$M=8$	$M=9$	$M=10$
0	11	14	17	19	21	22	21	24	26	28

4A.6.3 AML continuous control problem with the Wegstein method

ω	Wegstein, updating q every n th iteration, $-1 \leq q \leq 1$									
	$n=1$	$n=2$	$n=3$	$n=4$	$n=5$	$n=6$	$n=7$	$n=8$	$n=9$	$n=10$
0.95	68	60	62	87	100	100	100	100	100	100
0.90	61	54	67	54	57	100	100	100	100	100
0.85	61	52	62	83	72	77	100	100	100	100
0.80	62	56	59	73	68	100	100	100	100	100
0.75	68	56	53	89	62	100	95	100	100	100
0.70	57	54	71	62	72	92	70	100	100	74
0.65	57	53	55	61	62	90	65	100	56	100
0.60	57	53	56	65	67	36	100	100	100	100
0.55	63	58	50	62	42	26	59	66	100	100
0.50	64	58	53	88	47	47	79	100	100	92
0.45	68	59	41	78	74	74	90	100	100	63
0.40	54	64	50	90	72	100	100	100	76	100
0.35	72	63	48	77	67	66	93	100	100	100
0.30	62	68	67	55	72	86	100	45	100	100
0.25	63	72	60	74	100	100	100	100	100	100
0.20	57	65	56	75	87	92	86	100	97	100
0.15	63	65	68	86	73	100	86	100	100	100
0.10	64	66	66	71	77	100	100	100	100	100
0.05	64	55	71	72	77	100	100	100	100	94
0.00	60	54	59	70	92	100	100	100	100	100

4A.6.4 AML continuous control problem with the partial Aitken method



4A.6.5 AML continuous control problem with the partial Steffensen method

ω	Steffensen	$m=1$	$m=2$	$m=3$	$m=4$	$m=5$	$m=6$	$m=7$	$m=8$	$m=9$	$m=10$
0.95	61	28	25	26	25	29	33	28	31	45	
0.90	53	31	21	21	25	22	25	28	31	34	
0.85	47	28	21	21	19	22	25	28	31	34	
0.80	61	28	25	21	25	22	25	28	31	34	
0.75	53	34	25	21	25	22	25	28	31	34	
0.70	49	37	25	21	25	22	25	28	31	34	
0.65	53	34	25	21	25	22	25	28	31	34	
0.60	61	34	25	21	19	22	25	28	31	34	
0.55	67	34	25	21	19	22	25	28	31	34	
0.50	69	31	25	21	19	22	25	28	31	23	
0.45	69	31	25	21	25	22	25	28	31	34	
0.40	69	31	25	21	25	22	25	28	31	34	
0.35	53	31	25	26	31	29	33	37	41	45	
0.30	67	34	29	31	37	36	49	46	51	56	
0.25	65	31	33	46	55	71	65	82	101	100	
0.20	65	34	37	56	37	106	81	100	101	100	
0.15	73	31	45	71	37	106	49	100	101	100	
0.10	51	43	57	76	79	106	105	100	101	100	
0.05	67	55	73	86	103	106	105	100	101	100	
0.00	71	64	101	61	103	106	105	100	101	100	

4A.6.6 AML continuous control problem with Anderson acceleration

ω	Anderson									
	$M=1$	$M=2$	$M=3$	$M=4$	$M=5$	$M=6$	$M=7$	$M=8$	$M=9$	$M=10$
0.95	100	100	100	33	34	32	31	28	28	27
0.90	100	40	27	25	24	26	23	20	20	20
0.85	62	45	22	22	20	17	17	18	19	19
0.80	53	34	26	23	24	21	22	19	21	22
0.75	44	30	28	29	24	26	33	27	34	31
0.70	40	31	36	30	35	33	54	44	47	55
0.65	33	26	29	58	30	35	50	41	57	54
0.60	30	26	27	28	32	45	71	45	46	71
0.55	33	25	26	26	32	32	41	40	42	54
0.50	32	29	27	28	30	28	30	39	38	37
0.45	33	25	27	25	28	27	26	29	30	28
0.40	31	23	28	27	38	29	36	31	41	41
0.35	28	24	23	26	30	30	31	39	36	38
0.30	26	24	25	29	27	29	33	33	45	51
0.25	23	21	25	28	38	33	65	49	58	56
0.20	22	21	25	28	27	57	32	46	87	75
0.15	20	21	24	32	39	52	34	44	45	53
0.10	22	19	24	32	35	36	31	42	69	50
0.05	24	22	30	34	37	45	47	74	75	48
0.00	26	25	27	80	40	56	64	43	100	94

4A.6.7 AML bang-bang control problem with the Wegstein method

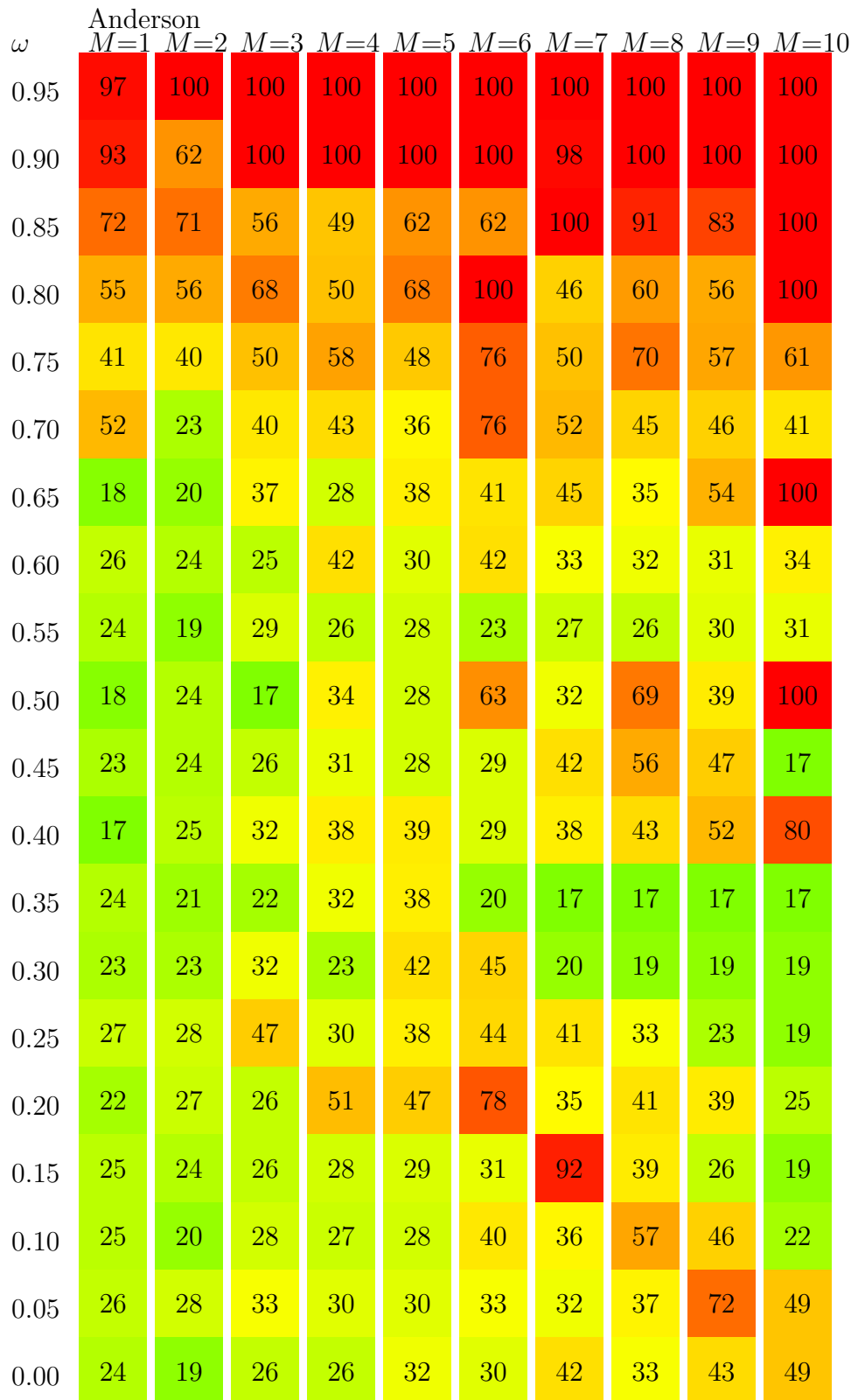
ω	Wegstein, updating q every n th iteration, $-1 \leq q \leq 1$									
	$n=1$	$n=2$	$n=3$	$n=4$	$n=5$	$n=6$	$n=7$	$n=8$	$n=9$	$n=10$
0.95	31	32	11	14	17	20	23	26	29	32
0.90	30	30	29	30	17	20	23	26	29	32
0.85	30	30	29	14	17	20	23	26	29	32
0.80	31	20	26	26	17	20	23	26	29	32
0.75	31	24	17	14	17	20	23	26	29	32
0.70	30	24	11	46	27	20	23	42	29	32
0.65	28	28	26	42	37	44	37	42	29	32
0.60	30	26	20	50	27	44	44	26	29	32
0.55	30	26	32	22	17	20	23	26	29	32
0.50	31	30	32	14	17	32	23	26	29	32
0.45	31	28	32	34	17	32	23	26	29	32
0.40	27	28	38	46	27	32	23	26	29	32
0.35	25	36	38	46	52	56	37	26	29	32
0.30	28	30	41	46	52	50	44	50	56	62
0.25	29	32	35	38	42	50	44	50	20	22
0.20	32	34	35	34	32	14	16	18	20	22
0.15	27	30	35	34	27	14	16	26	11	12
0.10	27	28	35	30	27	14	16	18	29	12
0.05	28	30	29	26	37	14	23	10	11	12
0.00	33	32	35	30	37	26	9	10	11	12

4A.6.8 AML bang-bang control problem with the partial Aitken method

4A.6.9 AML bang-bang control problem with the partial Steffensen method

ω	Steffensen									
	$m=1$	$m=2$	$m=3$	$m=4$	$m=5$	$m=6$	$m=7$	$m=8$	$m=9$	$m=10$
0.95	101	100	101	66	103	106	105	100	101	100
0.90	51	100	41	41	73	64	33	64	71	78
0.85	33	100	101	41	43	43	49	46	51	45
0.80	29	34	29	26	37	36	33	37	41	34
0.75	29	28	17	26	25	22	33	28	21	34
0.70	23	22	21	21	19	22	17	19	21	23
0.65	21	19	17	16	19	15	17	19	11	12
0.60	21	13	13	11	13	15	9	10	11	12
0.55	19	16	13	11	13	15	17	19	21	23
0.50	19	16	17	11	7	8	9	10	11	12
0.45	21	16	17	16	13	15	9	10	11	12
0.40	17	19	17	21	25	22	17	19	21	12
0.35	17	16	17	21	19	22	25	28	31	23
0.30	19	16	17	16	19	22	25	28	31	34
0.25	19	16	17	16	19	22	25	28	31	34
0.20	19	13	17	21	19	22	25	28	31	34
0.15	19	13	17	21	25	22	25	28	31	34
0.10	19	16	17	21	25	29	33	37	31	34
0.05	19	19	17	26	25	29	33	37	41	45
0.00	17	22	21	26	25	36	33	46	41	56

4A.6.10 AML bang-bang control problem with Anderson acceleration



4A.6.11 Linear fixed endpoint control problem

For the linear fixed endpoint control problem we present $\Sigma = \mathcal{N}_1 + \mathcal{N}_2 + \dots$ in the tables; the cumulative number of function evaluations required for convergence of the adapted FBSM. With no acceleration, the adapted FBSM applied to the linear fixed endpoint control problem requires solving three two-point boundary value problems (TPBVPs), incurring a total of $\Sigma = 177$ function evaluations. This value is used as the midpoint (yellow) of the heatmaps. Importantly, the acceleration techniques do not reduce the number of TPBVPs that need to be solved, but rather facilitate solving each TPBVP with reduced \mathcal{N} , leading to reduced Σ . For the Wegstein method we apply the same bounds on q as we did for the linear continuous control problem, noting that further tuning of the bounds may improve results.

		Wegstein, updating q every n th iteration, $-2 \leq q \leq 0$									
ω		$n=1$	$n=2$	$n=3$	$n=4$	$n=5$	$n=6$	$n=7$	$n=8$	$n=9$	$n=10$
0		91	105	98	95	113	120	111	102	105	126
Partial Aitken											
ω		$m=1$	$m=2$	$m=3$	$m=4$	$m=5$	$m=6$	$m=7$	$m=8$	$m=9$	$m=10$
0		42	36	36	45	54	84	48	54	60	66
Partial Steffensen											
ω		$m=1$	$m=2$	$m=3$	$m=4$	$m=5$	$m=6$	$m=7$	$m=8$	$m=9$	$m=10$
0		173	57	51	33	39	38	27	30	33	36
Anderson											
ω		$M=1$	$M=2$	$M=3$	$M=4$	$M=5$	$M=6$	$M=7$	$M=8$	$M=9$	$M=10$
0		39	30	30	24	24	24	24	24	24	24

4A.6.12 AML fixed endpoint control problem

For the AML fixed endpoint control problem with no acceleration techniques, the adapted FBSM requires solving ten TPBVPs; incurring $\Sigma = 434$ function evaluations. This is achieved using the best tuning ($\omega = 0.55$) from the AML continuous control problem. In this particular instance, $\omega = 0.55$ also happens to be the best tuning for the AML fixed endpoint control problem if holding ω constant, when considering $\omega \in [0, 1]$ at increments of 0.05. These ω values will not necessarily coincide in general, as the adapted FBSM requires solving several related but distinct TPBVPs, each potentially calling for different ideal tuning. For each of the acceleration methods we employ the tuning parameters that minimised \mathcal{N} for the AML continuous control problem. This does not imply that we are using the best tuning parameters for the acceleration methods in the context of the AML fixed endpoint control problem. This is important, as it demonstrates the effectiveness of the techniques in accelerating fixed endpoint control problems without requiring prohibitive tuning. In the following table, we present the cumulative \mathcal{N} after each FBSM within the secant steps of the adapted FBSM. In the right-most column, corresponding

to the tenth and final TPBVP, we present Σ . While Wegstein's method performs significantly worse than the case with no acceleration, we find that the Anderson, Aitken and Steffensen methods are all able to reach convergence in fewer function evaluations.

No acceleration, $\omega = 0.55$

Secant step	1	2	3	4	5	6	7	8	9	10
Cumulative \mathcal{N}	38	98	147	188	229	270	311	352	393	434

Wegstein, $\omega = 0.55$, updating q every 6th iteration, $-1 \leq q \leq 1$

Secant step	1	2	3	4	5	6	7	8	9	10
Cumulative \mathcal{N}	26	172	356	423	505	675	809	929	1045	1161

Partial Aitken, $\omega = 0.5$, $m = 5$

Secant step	1	2	3	4	5	6	7	8	9	10
Cumulative \mathcal{N}	30	72	114	144	180	216	252	288	324	360

Partial Steffensen, $\omega = 0.5$, $m = 5$

Secant step	1	2	3	4	5	6	7	8	9	10
Cumulative \mathcal{N}	19	44	69	88	113	138	163	188	213	238

Anderson, $\omega = 0.85$, $M = 6$

Secant step	1	2	3	4	5	6	7	8	9	10
Cumulative \mathcal{N}	17	45	67	86	109	128	147	166	185	204

Bibliography

- [1] Abbasi Z, Zamani I, Amiri Mehra AH, Shafieirad M, Ibeas A. 2020 Optimal control design of impulsive SQEiar epidemic models with application to COVID-19. *Chaos, Solitons & Fractals* **139**, 110054. (doi.org/10.1016/j.chaos.2020.110054).
- [2] Ackleh AS, Kearfott RB, Allen EJ, Padmanabhan S. 2010 *Classical and Modern Numerical Analysis: Theory, Methods and Practice*. London, United Kingdom: Chapman & Hall/CRC, Taylor & Francis. (doi.org/10.1201/b12332).
- [3] Adam JA, Bellomo N. 1997 *A Survey of Models for Tumor Immune System Dynamics*. Boston: Birkhäuser.
- [4] Adas M, Kemik O, Adas G, Arikan S, Kuntsal L, Kapran Y, Toklu AS. 2013 Is combined therapy more effective than growth hormone or hyperbaric oxygen alone in the healing of left ischemic and non-ischemic colonic anastomoses? *Clinics (Sao Paulo)* **68**, 1440–1445. ([doi.org/10.6061/clinics/2013\(11\)10](https://doi.org/10.6061/clinics/2013(11)10)).
- [5] Adomian G, Rach R. 1993 Analytic solution of nonlinear boundary-value problems in several dimensions by decomposition. *Journal of Mathematical Analysis and Applications* **174**, 118–137. (doi.org/10.1006/jmaa.1993.1105).
- [6] Australian Institute of Health and Welfare. 2014 *Cancer in Australia: an overview 2014*. Canberra: Australian Institute of Health and Welfare.
- [7] Aitken AC. 1927 On Bernoulli's numerical solution of algebraic equations. *Proceedings of the Royal Society of Edinburgh* **46**, 289–305. (doi.org/10.1017/S0370164600022070).
- [8] Akian, M, Sulem A. 2001 Dynamic optimization of long-term growth rate for a portfolio with transaction costs and logarithmic utility. *Mathematical Finance* **11**, 153–188. (doi.org/10.1111/1467-9965.00111).
- [9] Almocera AES, Nguyen VK, Hernandez-Vargas EA. 2018 Multiscale model within-host and between-host for viral infectious diseases. *Journal of Mathematical Biology* **77**, 1035–1057. (doi.org/10.1007/s00285-018-1241-y).

- [10] Alvarez-Vázquez LJ, García-Chan N, Martínez A, Vázquez-Méndez ME. 2010 Multi-objective Pareto-optimal control: an application to wastewater management. *Computational Optimization and Applications* **46**, 135–157. (doi.org/10.1007/s10589-008-9190-9).
- [11] Amari S. 1985 *Differential-Geometrical Methods in Statistics*. New York: Springer-Verlag.
- [12] Amari S. 1998 Natural gradient works efficiently in learning. *Neural Computation* **10**, 251–276. (doi.org/10.1162/089976698300017746).
- [13] Amari S, Nagaoka H. 2000 *Methods of Information Geometry*. Providence: American Mathematical Society.
- [14] Amari S, Andrzej C. 2010 Information geometry of divergence functions. *Bulletin of the Polish Academy of Sciences. Technical Sciences* **58**, 183–195. (doi.org/10.2478/v10175-010-0019-1).
- [15] Amari S. 2016 *Information Geometry and its Applications*. Tokyo: Springer Japan.
- [16] Anderson DG. 1965 Iterative procedures for nonlinear integral equations. *Journal of the ACM* **12**, 547–560. (doi.org/10.1145/321296.321305).
- [17] Anderson B, Moore J. 2014 *Optimal Control Linear Quadratic Methods*. New York: Dover Publications.
- [18] Anderson DG. 2019 Comments on “Anderson Acceleration, Mixing and Extrapolation”. *Numerical Algorithms* **80**, 135–235. (doi.org/10.1007/s11075-018-0549-4).
- [19] Andreeff M. 2015 *Current Cancer Research: Targeted Therapy of Acute Myeloid Leukaemia*. New York: Springer-Verlag.
- [20] Andrieu C, De Freitas N, Doucet A, Jordan MI. 2003 An introduction to MCMC for machine learning. *Machine Learning* **50**, 5–43. (doi.org/10.1023/A:1020281327116).
- [21] Arman A. 1986 *Acceleration algorithms for process design simulations*. Masters thesis, Oklahoma State University.
- [22] Arutjunjan R. 2020 *On the geometric foundation of parameter inference*. Masters Thesis. Erlangen-Nürnberg: Friedrich-Alexander University.
- [23] Arwini KA, Dodson, CTJ. 2008 *Information Geometry – Near Randomness and Near Independence*. Berlin: Springer-Verlag.

- [24] American Society of Clinical Oncology. 2017 What to Expect When Having Chemotherapy. Retrieved from www.cancer.net/navigating-cancer-care/how-cancer-treated/chemotherapy/what-expect-when-having-chemotherapy (Accessed November 2018).
- [25] Aspirin AP, de los Reyes V AA, Yangjin K. 2021 Polytherapeutic strategies with oncolytic virus–bortezomib and adjuvant NK cells in cancer treatment. *Journal of the Royal Society Interface* **18**, 20200669. (doi.org/10.1098/rsif.2020.0669).
- [26] Athans M, Falb P. 1966 *Optimal Control: An Introduction to the Theory and its Applications*. New York: McGraw-Hill.
- [27] Atlas JC, Nikolaev EV, Browning ST, Shuler ML. 2008 Incorporating genome-wide DNA sequence information into a dynamic whole-cell model of Escherichia coli: application to DNA replication. *IET Systems Biology* **2**, 369–382.
- [28] Audoly S, Bellu G, D’Angio L, Saccomani MP, Cobelli C. 2001 Global identifiability of nonlinear models of biological systems. *IEEE Transactions on Biomedical Engineering* **48**, 55–65. (doi.org/10.1109/10.900248).
- [29] Austin R, Smyth MJ, Lane SW. 2016 Harnessing the immune system in acute myeloid leukaemia. *Critical Reviews in Oncology/Hematology* **103**, 62–77. (doi.org/10.1016/j.critrevonc.2016.04.020).
- [30] Baker CM, Bode M. 2013 Spatial control of invasive species in conservation landscapes. *Computational Management Science* **10**, 1–21. (doi.org/10.1007/s10287-013-0196-0).
- [31] Baker CM, Armsworth PR, Lenhart SM. 2017 Handling overheads: optimal multi-method invasive species control. *Theoretical Ecology* **10**, 493–501. (doi.org/10.1007/s12080-017-0344-1).
- [32] Baker CM, Ferrari MJ, Shea K. 2018 Beyond dose: Pulsed antibiotic treatment schedules can maintain individual benefit while reducing resistance. *Scientific Reports* **8**, 5866. (doi.org/10.1038/s41598-018-24006-w).
- [33] Baker CM, Bode M, Dexter N, Lindenmayer DB, Foster C, MacGregor C, Plein M, McDonald-Madden E. 2019 A novel approach to assessing the ecosystem-wide impacts of reintroductions. *Ecological Applications* **29**, e01811. (doi.org/10.1002/eap.1811).
- [34] Barndorff-Nielsen OE 1986. Likelihood and observed geometries. *The Annals of Statistics* **14**, 856–873. (doi.org/10.1214/aos/1176350038).

- [35] Bast RC Jr, Holland JF, Croce CM, Hait WN, Hong WK, Kufe DW, Piccart-Gebhart M, Pollock RE, Weichselbaum RR, Wang H. 2017 *Holland-Frei Cancer Medicine*. New Jersey: Wiley.
- [36] Bellen A, Vermiglio R. 1996 Some applications of continuous Runge-Kutta methods. *Applied Numerical Mathematics* **22**, 63–80. ([doi.org/10.1016/S0168-9274\(96\)00026-8](https://doi.org/10.1016/S0168-9274(96)00026-8)).
- [37] Bellman RE. 1957 *Dynamic Programming*. Princeton: Princeton University Press.
- [38] Bellman, RE. 1961 *Adaptive Control Processes, A Guided Tour*. Princeton: Princeton University Press.
- [39] Benner P, Findeisen R, Flockerzi D, Reichl U, Sundmacher K. 2014 *Large-Scale Networks in Engineering and Life Sciences*. Basel, Switzerland: Birkhäuser Verlag.
- [40] Berryman AA. 1992 The origins and evolution of predator-prey theory. *Ecology* **73**, 1530–1535. (doi.org/10.2307/1940005).
- [41] Bezanson J, Karpinski S, Shah VB, Edelman A. 2012 Julia: a fast dynamic language for technical computing. *arXiv preprint*. (arxiv.org/abs/1209.5145)
- [42] Bishwal JPN. 2008 *Parameter Estimation in Stochastic Differential Equations*. Berlin: Springer-Verlag.
- [43] Boccia A, Vinter RB. 2016 The maximum principle for optimal control problems with time delays. *10th IFAC Symposium on Nonlinear Control Systems* **49**, 951–955. (doi.org/10.1016/j.ifacol.2016.10.290).
- [44] Boddu P, Kantarjian H, Garcia-Manero G, Allison J, Sharma P, Dauer N. 2018 The emerging role of immune checkpoint based approaches in AML and MDS. *Leukemia & Lymphoma* **59**, 790–802. (doi.org/10.1080/10428194.2017.1344905).
- [45] Bokil VA, Allen LJS, Jeger MJ, Lenhart S. 2019 Optimal control of a vectored plant disease model for a crop with continuous replanting. *Journal of Biological Dynamics* **13**, 325–353. (doi.org/10.1080/17513758.2019.1622808).
- [46] Bonyah E, Sagoe AK, Kumar D, Deniz S. 2021 Fractional optimal control dynamics of coronavirus model with Mittag-Leffler law. *Ecological Complexity* **45**, 100880. (doi.org/10.1016/j.ecocom.2020.100880).
- [47] Brezinski C, Redivo-Zaglia M. 2019 The genesis and early developments of Aitken's process, Shanks' transformation, the ε -algorithm, and related fixed point methods. *Numerical Algorithms* **80**, 11–133. (doi.org/10.1007/s11075-018-0567-2).

- [48] Brons PPT, Haanen C, Boezeman JBM, Muus P, Holdrinet RSG, Pennings AHM, Wessels HMC, de Witte T. 1993 Proliferation patterns in acute myeloid leukaemia: leukaemic clonogenic growth and in vivo cell cycle kinetics. *Annals of Hematology* **66**, 225–233. (doi.org/10.1007/BF01738470).
- [49] Brouwer AF, Meza R, Eisenberg MC. 2016 Parameter estimation for multistage clonal expression models from cancer incidence data: a practical identifiability analysis. *PLoS Computational Biology* **13**, e1005431. (doi.org/10.1371/journal.pcbi.1005431).
- [50] Browning AP, Warne DJ, Burrage K, Baker RE, Simpson MJ. 2020 Identifiability analysis for stochastic differential equation models in systems biology. *Journal of the Royal Society Interface* **17**, 20200652. (doi.org/10.1098/rsif.2020.0652).
- [51] Browning AP, Sharp JA, Mapder T, Baker CM, Burrage K, Simpson MJ. 2021 Persistence as an optimal hedging strategy. *Biophysical Journal* **120**, 133–142. ([10.1016/j.bpj.2020.11.2260](https://doi.org/10.1016/j.bpj.2020.11.2260)).
- [52] Browning AP, Sharp JA, Murphy RJ, Gunasingh G, Lawson B, Burrage K, Haass NK, Simpson MJ. 2021 Quantitative analysis of tumour spheroid structure. *eLife* **10**, e73020. (doi.org/10.7554/eLife.73020).
- [53] Browning AP, Maclaren OJ, Buentzli PR, Lanaro M, Allenby MC, Woodruff MA, Simpson MJ. Model-based data analysis of tissue growth in thin 3D printed scaffolds. *Journal of Theoretical Biology* **528**, 110852. (doi.org/10.1016/j.jtbi.2021.110852).
- [54] Broyden CG., 1965 A class of methods for solving nonlinear simultaneous equations. *Mathematics of Computation* **19**, 577–593. (doi.org/10.1090/S0025-5718-1965-0198670-6).
- [55] Bryson AE, Ho YC. 1975 *Applied Optimal Control: Optimization, Estimation, and Control*. Abingdon: Taylor & Francis.
- [56] Bryson AE. 1996 Optimal control – 1950 to 1985. *IEEE Control Systems Magazine* **16**, 26–33. (doi.org/10.1109/37.506395).
- [57] Bunimovich-Mendrazitsky S, Shklyar B. 2017 Optimization of combined leukaemia therapy by finite-dimensional optimal control modeling. *Journal of Optimization Theory and Applications* **175**, 218–235. (doi.org/10.1007/s10957-017-1161-9).
- [58] Burden RL, Faires DJ. 1985 *Numerical Analysis*. Massachusetts: PWS Publishing Company.
- [59] Burnett AK, Goldstone AH, Stevens RMF, Hann IM, Rees JHK, Gray RG, Wheatley K. 2001 Randomised comparison of addition of autologous bone-marrow transplantation to intensive chemotherapy for acute myeloid leukaemia in first remission: results of

- MRC AML 10 trial. *The Lancet* **351**, 700–708. (doi.org/10.1016/s0140-6736(97)09214-3).
- [60] Burnett AK. 2001 *Clinical Haematology: Acute Myeloid Leukaemia*. Baillière Tindall, London.
- [61] Bussell EH, Cunniffe NJ. 2020 Applying optimal control theory to a spatial simulation model of sudden oak death: ongoing surveillance protects tanoak while conserving biodiversity. *Journal of the Royal Society Interface* **17**, 20190671. (doi.org/10.1098/rsif.2019.0671).
- [62] Butcher JC. 2008 *Numerical Methods for Ordinary Differential Equations*. Chichester, United Kingdom: John Wiley & Sons, Ltd.
- [63] Byrne HM. 2010 Dissecting cancer through mathematics: from the cell to the animal model. *Nature Reviews Cancer* **10**, 221–230. (doi.org/10.1038/nrc2808).
- [64] Calin O, Udriste C. 2014 *Geometric Modeling in Probability and Statistics*. Cham: Springer International Publishing.
- [65] Calvo M, Oller JM. 1991 An explicit solution of information geodesic equations for the multivariate normal model. *Statistics & Risk Modeling* **9**, 119–138. (doi.org/10.1524/strm.1991.9.12.119).
- [66] Camacho, A, Jerez, S, 2018. Bone metastasis modeling via optimal control. *Journal of Mathematical Biology* **78**, 497–526. (doi.org/10.1007/s00285-018-1281-3).
- [67] Cancer Council Australia. 2018 Understanding acute leukaemia. Retrieved from www.cancercouncil.com.au/acute-myeloid-leukaemia/ (Accessed February 2020).
- [68] Cancer Council Australia. 2019 Stem cell transplant for acute myeloid leukaemia. Retrieved from www.cancercouncil.com.au/acute-myeloid-leukaemia/treatment/stem-cell-transplant/ (Accessed February 2020).
- [69] Cancer Research UK. 2019 Stem cell or bone marrow transplants for acute myeloid leukaemia (AML). Retrieved from www.cancerresearchuk.org/about-cancer/acute-myeloid-leukaemia-aml/treating-aml/bone-marrow-stem-cells-transplant-aml/having-transplant (Accessed February 2020).
- [70] Carcione JM, Santos JE, Bagaini C, Ba J. 2020 A simulation of a covid-19 epidemic based on a deterministic SIR model. *Frontiers in Public Health* **8**, 1–13. (doi.org/10.3389/fpubh.2020.00230).
- [71] Carmichael DG. 1990 Bang-bang control and optimum structural design. *Engineering Optimization* **15**, 205–209. (doi.org/10.1080/03052159008941153).

- [72] Carrasco LR, Baker R, MacLeod A, Knight JD, Mumford JD. 2010 Optimal and robust control of invasive alien species spreading in homogeneous landscapes. *Journal of the Royal Society Interface* **7**, 529–540. (doi.org/10.1098/rsif.2009.0266).
- [73] Carré BA. 1961 The determination of the optimum accelerating factor for successive over-relaxation. *The Computer Journal* **4**, 73–78. (doi.org/10.1093/comjnl/4.1.73).
- [74] Carrére, C. 2017 Optimization of an *in vitro* chemotherapy to avoid resistant tumours. *Journal of Theoretical Biology* **413**, 24–33. (doi.org/10.1016/j.jtbi.2016.11.009).
- [75] Castiglione F, Piccoli B. 2007 Cancer immunotherapy, mathematical modeling and optimal control. *Journal of Theoretical Biology* **247**, 723–732. (doi.org/10.1016/j.jtbi.2007.04.003).
- [76] Castro M, Lythe G, Molina-Paris C, Ribeiro RM. 2016 Mathematics in modern immunology. *Interface Focus* **6**, 20150093. (doi.org/10.1098/rsfs.2015.0093).
- [77] Chamchod F. 2018 Modeling the spread of capripoxvirus among livestock and optimal vaccination strategies. *Journal of Theoretical Biology* **437**, 179–186. (doi.org/10.1016/j.jtbi.2017.10.009).
- [78] Chapman LAC, Shipley RJ, Whiteley JP, Ellis MJ, Byrne HM, Waters SL. 2014 Optimising cell aggregate expansion in a perfused hollow fibre bioreactor via mathematical modelling. *PLoS One* **9**, e105813. (doi.org/10.1371/journal.pone.0105813).
- [79] Corthay A. 2014 Does the immune system naturally protect against cancer? *Frontiers in Immunology* **5**, 1–8. (doi.org/10.3389/fimmu.2014.00197).
- [80] Costa SIR, Santos SA, Strapasson JE. 2015 Fisher information distance: a geometrical reading. *Discrete Applied Mathematics* **197**, 59–69. (doi.org/10.1016/j.dam.2014.10.004).
- [81] Crowe CM, Nishio M. 1975 Convergence promotion in the simulation of chemical processes - The general dominant eigenvalue method. *American Institute of Chemical Engineers Journal* **21**, 528–533. (doi.org/10.1002/cjce.5450490414).
- [82] Crowell HL, MacLean AL, Stumpf MPH. 2016 Feedback mechanisms control coexistence in a stem cell model of acute myeloid leukaemia. *Journal of Theoretical Biology* **401**, 43–53. (doi.org/10.1016/j.jtbi.2016.04.002).
- [83] Cucuiaru A, Precup R. 2010 A hypothetical-mathematical model of acute myeloid leukaemia pathogenesis. *Computational and Mathematical Methods in Medicine* **2010**, 49–65. (doi.org/10.1080/17486700902973751).

- [84] Cunningham, J.J, Brown, J.S, Gatenby, R.A, Staňková, K, 2018. Optimal control to develop therapeutic strategies for metastatic castrate resistant prostate cancer. *Journal of Theoretical Biology* **459**, 67–78. (doi.org/10.1016/j.jtbi.2018.09.022).
- [85] Daly AC, Gavaghan D, Cooper J, Tavener S. 2018 Inference-based assessment of parameter identifiability in nonlinear biological models. *Journal of the Royal Society Interface* **15**, 20180318. (doi.org/10.1098/rsif.2018.0318).
- [86] Day C, Merlino G, Dyke TV. 2015 Preclinical mouse cancer models: a maze of opportunities and challenges. *Cell* **163**, 39–53. (doi.org/10.1016/j.cell.2015.08.068).
- [87] Del Vecchio D, Dy AJ, Qian Y. 2016 Control theory meets synthetic biology. *Journal of the Royal Society Interface* **13**, 20160380. (doi.org/10.1098/rsif.2016.0380).
- [88] Demmel JW, Li X. 1994 Faster numerical algorithms via exception handling. *IEEE Transactions on Computers* **43**, 983–992. (doi.org/10.1109/12.295860)
- [89] Devenish-Nelson ES, Harris S, Soulsbury CD, Richards SA, Stephens PA. Uncertainty in population growth rates: determining confidence intervals from point estimates of parameters. *PLOS ONE* **5**, e13628. (doi.org/10.1371/journal.pone.0013628).
- [90] Dexter N, Hudson M, James S, MacGregor C, Lindenmayer DB. 2013 Unintended consequences of invasive predator control in an Australian forest: overabundant wallabies and vegetation change. *PLOS ONE* **8**, e69087. (doi.org/10.1371/journal.pone.0069087).
- [91] Dobrushkin VA. 2017 *Applied Differential Equations with Boundary Value Problems*. Boca Raton: CRC Press.
- [92] Döhner H, Estey EH, Amadori S, Appelbaum FR, Büchner T, Burnett AK, Dombret H, Fenaux P, Grimwade D, Larson RA, Lo-Coco F, Naoe T, Niederwieser D, Ossenkoppele GJ, Sanz MA, Sierra J, Tallman MS, Löwenberg B, Bloomfield CD. 2010 Diagnosis and management of acute myeloid leukemia in adults: recommendations from an international expert panel, on behalf of the European LeukemiaNet. *Blood* **115**, 453–474. (doi.org/10.1182/blood-2009-07-235358).
- [93] Döhner H, Weisdorf DJ, Bloomfield CD. 2015 Acute myeloid leukaemia. *The New England Journal of Medicine* **373**, 1136–1152. (doi.org/10.1056/NEJMra1406184).
- [94] Domijan M, Rand DA. 2015 Using constraints and their value for optimization of large ODE systems. *Journal of the Royal Society Interface* **12**, 20141303. (doi.org/10.1098/rsif.2014.1303).

- [95] d'Onofrio A, Ledzewicz U, Maurer H, Schättler H. 2009 On optimal delivery of combination therapy for tumours. *Mathematical Biosciences* **222**, 13–26. (doi.org/10.1016/j.jtbi.2018.09.022).
- [96] Doyle FJ, Stelling J. 2006 Systems interface biology. *Journal of the Royal Society Interface* **3**, 603–616. (doi.org/10.1098/rsif.2006.0143).
- [97] Edelstein-Keshet L. 2005 *Mathematical Models in Biology*. Philadelphia: Society for Industrial and Applied Mathematics.
- [98] Assessing the accuracy of the maximum likelihood estimator: Observed versus expected Fisher information. *Biometrika* **65**, 457–487. (doi.org/10.1093/biomet/65.3.457).
- [99] Eguchi S, Copas J. 2006 Interpreting Kullback-Leibler divergence with the Neyman-Pearson lemma. *Journal of Multivariate Analysis* **97**, 2034–2040. (doi.org/10.1016/j.jmva.2006.03.007).
- [100] Estey E, Döhner H. 2006 Acute myeloid leukaemia. *The Lancet* **368**, 1894–1907. (doi.org/10.1016/S0140-6736(06)69780-8).
- [101] Ewald J, Bartl M, Kaleta C. 2017 Deciphering the regulation of metabolism with dynamic optimization: an overview of recent advances. *Biochemical Society Transactions* **45**, 1035–1043. (doi.org/10.1042/BST20170137).
- [102] Eyert V. 1996 A comparative study on methods for convergence acceleration of iterative vector sequences. *Journal of Computational Physics* **124**, 271–285. (doi.org/10.1006/jcph.1996.0059).
- [103] Falisse A, Serrancolí G, Dembia CL, Gillis J, Jonkers I, De Groote F. 2019 Rapid predictive simulations with complex musculoskeletal models suggest that diverse healthy and pathological human gaits can emerge from similar control strategies. *Journal of the Royal Society Interface* **16**, 20190402. (doi.org/10.1098/rsif.2019.0402).
- [104] Fang H, Saad Y. 2008 Two classes of multisecant methods for nonlinear acceleration. *Numerical Linear Algebra with Applications* **16**, 197–221. (doi.org/10.1002/nla.617).
- [105] Fernandez-de-Simon J, Díaz-Ruiz F, Rodríguez-de le Cruz M, Delibes-Mateos M, Villafuerte R, Ferreras P. 2015 Can widespread generalist predators affect keystone prey? A case study with red foxes and European rabbits in their native range. *Population Ecology* **57**, 591–599. (doi.org/10.1007/s10144-015-0510-5).
- [106] Ferson S, Ginzburg LR. 1996 Different methods are needed to propagate ignorance and variability. *Reliability Engineering and System Safety* **54**, 133–144. (doi.org/10.1016/S0951-8320(96)00071-3).

- [107] Filippov AF. 1962 On certain questions in the theory of optimal control. *SIAM Journal on Control and Optimization* **1**, 76–84. (doi.org/10.1137/0301006).
- [108] Fisher RA. 1992 *Statistical methods for research workers* In: Kotz S, Johnson NL (eds) *Breakthroughs in Statistics*, 66–70. New York: Springer.
- [109] Fister RK, Panetta JC. 2000 Optimal control applied to cell-cycle-specific cancer chemotherapy. *SIAM Journal on Applied Mathematics* **60**, 1059–1072. (doi.org/10.1137/S0036139998338509).
- [110] Fraser-Andrews G. 1989 Finding candidate singular optimal controls: a state of the art survey. *Journal of Optimization Theory and Applications* **60**, 173–190. (doi.org/10.1007/BF00940004).
- [111] Fribourg M, Hartmann B, Schmolke M, Marjanovic N, Albrecht RA, García-Sastre A, Sealfon SC, Jayaprakash C, Hayot F. 2014 Model of influenza A virus infection: dynamics of viral antagonism and innate immune response. *Journal of Theoretical Biology* **351**, 47–57. (doi.org/10.1016/j.jtbi.2014.02.029).
- [112] Frieden BR. 1990 Fisher information, disorder, and the equilibrium distribution of physics. *Physical Review A* **41**, 4265–4276. (doi.org/10.1103/PhysRevA.41.4265).
- [113] Frieden BR, Gatenby RA. 2007 *Exploratory Data Analysis Using Fisher Information*. London: Springer London.
- [114] Fröhlich F, Theis FJ, Hasenauer J. 2014 Uncertainty analysis for non-identifiable dynamical systems: profile likelihoods, bootstrapping and more. In *Computational Methods in Systems Biology: Proceedings of the 12th International Conference, 2014*. Cham: Springer.
- [115] Fu F, Nowak MA, Bonhoeffer S. 2015 Spatial heterogeneity in drug concentrations can facilitate the emergence of resistance to cancer therapy. *PLOS Computational Biology* **11**, e1004142. (doi.org/10.1371/journal.pcbi.1004142).
- [116] Gábor A, Banga JR. 2015 Robust and efficient parameter estimation in dynamic models of biological systems. *BMC Systems Biology* **9**, 1–25. (doi.org/10.1186/s12918-015-0219-2).
- [117] Galluzzi L, Bugué A, Kepp O, Zitvogel L, Kroemer G. 2015 Immunological effects of conventional chemotherapy and targeted anticancer agents. *Cancer Cell* **28**, 690–714. (doi.org/10.1016/j.ccr.2015.10.012).
- [118] Gelman A, Carlin JB, Stern HS, Dunson SB, Vehtari A, Rubin DB. 1995 *Bayesian Data Analysis*. New York: Chapman & Hall/CRC.

- [119] Gelman A, Bois F, Jiang J. 1996 Physiological pharmacokinetic analysis using population modeling and informative prior distributions. *Journal of the American Statistical Association* **91**, 1400–1412. (doi:10.2307/2291566).
- [120] Gibert K, García-Alonso C, Salvador-Carulla L. 2010 Integrating clinicians, knowledge and data: expert-based cooperative analysis in healthcare decision support. *Health Research Policy and Systems* **8**, 6490. (doi.org/10.1186/1478-4505-8-28).
- [121] Giesel E, Reischke R, Schäfer BM, Chia D. 2021 Information geometry in cosmological inference problems. *Journal of Cosmology and Astroparticle Physics* **2021**, 005. (doi.org/10.1088/1475-7516/2021/01/005).
- [122] Girolami M, Calderhead B. 2011 Riemann manifold Langevin and Hamiltonian Monte Carlo methods. *Journal of the Royal Statistical Society B* **73**, 123–214. (doi.org/10.1111/j.1467-9868.2010.00765.x).
- [123] Godfrey KR, Jones RP, Brown RF. 1980 Identifiable pharmacokinetic models: the role of extra inputs and measurements. *Journal of Pharmacokinetics and Biopharmaceutics* **8**, 633–648. (doi.org/10.1007/bf01060058).
- [124] Goh BS. 1966. Necessary conditions for singular extremals involving multiple control variables. *SIAM Journal on Control and Optimization* **4**, 716–731. (doi.org/10.1137/0304052).
- [125] Goldstine HH. 1980 *A History of the Calculus of Variations from the 17th through to the 19th Century*. New York, NY: Springer-Verlag.
- [126] Golub GH, Van Loan CF. 2013 *Matrix Computations [Fourth Edition]*. Baltimore: John Hopkins University Press.
- [127] Gooley TA, Chien JW, Pergam SA, Hingorani S, Sorror ML, Boeckh M, Martin PJ, Sandmaier BM, Marr KA, Appelbaum FR, Storb R, McDonald GB. 2010 Reduced Mortality after Allogeneic Hematopoietic-Cell Transplantation. *The New England Journal of Medicine* **363**, 2091–2101. (doi.org/10.1056/NEJMoa1004383).
- [128] Gutenkunst RN, Waterfall JJ, Casey FP, Brown KS, Myers CR, Sethna JP. 2007 Universally sloppy parameter sensitivities in systems biology models. *PLoS Computational Biology* **3**, e189. (doi.org/10.1371/journal.pcbi.0030189).
- [129] Gutzler CH. 1959 *An iterative method of Wegstein for solving simultaneous nonlinear equations*. Masters thesis, Oregon State College.
- [130] Hackbusch W. 1978 A numerical method for solving parabolic equations with opposite orientations. *Computing* **20**, 229–240. (doi.org/10.1007/BF02251947).

- [131] Hadjidimos A. 2000 Successive overrelaxation (SOR) and related methods. *Journal of Computational and Applied Mathematics* **123**, 177–199. (doi.org/10.1016/S0377-0427(00)00403-9).
- [132] Haferlach T, Schmidts I. 2019 The power and potential of integrated diagnostics in acute myeloid leukaemia. *British Journal of Haematology* **188**, 36–48. (doi.org/10.1111/bjh.16360).
- [133] Hagen DR, White JK, Tidor B. 2013 Convergence in parameters and predictions using computational experimental design. *Interface Focus* **3**, 20130008. (doi.org/10.1098/rsfs.2013.0008).
- [134] Hamelin FM, Bowen B, Bernhard P, Bokil VA. 2021 Optimal control of plant disease epidemics with clean seed usage. *Bulletin of Mathematical Biology* **83**, article 46. (doi.org/10.1007/s11538-021-00872-w).
- [135] Hanahan D, Weinberg RA. 2011 Hallmarks of cancer: the next generation. *Cell* **144**, 646–674. (doi.org/10.1016/j.cell.2011.02.013).
- [136] Hassani H, Tenriero Machado JA, Mehrabi S. 2021 An optimization technique for solving a class of nonlinear fractional optimal control problems: Application in cancer treatment. *Applied Mathematical Modelling* **93**, 868–884. (doi.org/10.1016/j.apm.2021.01.004).
- [137] Hay J, Hellewell J, Qiu X. 2021 When intuition falters: repeated testing accuracy during an epidemic. *European Journal of Epidemiology* **36**, 749–752. (doi.org/10.1007/s10654-021-00786-w).
- [138] Hazelton ML. 2010 Bayesian inference for network-based models with a linear inverse structure. *Transportation Research Part B: Methodological* **44**, 674–685. (doi.org/10.1016/j.trb.2010.01.006).
- [139] He F, Murabito E, Westerhoff HV. 2016 Synthetic biology and regulatory networks: where metabolic systems biology meets control engineering. *Journal of the Royal Society Interface* **13**, 20151046. (doi.org/10.1098/rsif.2015.1046).
- [140] Heinbockel JH. 2001 *Introduction to Tensor Calculus and Continuum Mechanics*. Victoria, BC: Trafford.
- [141] Henrici P. 1964 *Elements of Numerical Analysis*. New York: John Wiley & Sons.
- [142] Higham DJ. 1995 Condition numbers and their condition numbers. *Linear Algebra and its Applications* **214**, 193–213. (doi.org/10.1016/0024-3795(93)00066-9)

- [143] Higham NJ. 2002 *Accuracy and Stability of Numerical Algorithms [Second Edition]*. Philadelphia: Society for Industrial and Applied Mathematics.
- [144] Hines KE, Middendorf TR, Aldrich RW. 2014 Determination of parameter identifiability in nonlinear biophysical models: a Bayesian approach. *Journal of General Physiology* **143**, 401–416. (doi.org/10.1085/jgp.201311116).
- [145] Hlavacek WS. 2011 *Two Challenges of Systems Biology*. In *Handbook of Statistical Systems Biology*. Chichester: John Wiley & Sons, Ltd.
- [146] House T, Ford A, Lan S, Bilson S, Buckingham-Jeffery E, Girolami M. 2016 Bayesian uncertainty quantification for transmissibility of influenza, norovirus and ebola using information geometry. *Journal of the Royal Society Interface* **13**, 20160279. (doi.org/10.1098/rsif.2016.0279).
- [147] Huang CYF, Ferrell JE. 1996 Ultrasensitivity in the mitogen-activated protein kinase cascade. *Proceedings of the National Academy of Sciences of the United States of America* **93**, 10078–10083. (doi.org/10.1073/pnas.93.19.10078).
- [148] Ibrahim M, Kallies C, Findeisen R. 2020 Learning-supported approximated control for autonomous vehicles in the presence of state dependent uncertainties. *2020 European Control Conference*, 338–343. (doi.org/10.23919/ECC51009.2020.9143737).
- [149] Ishikawa F, Yoshida S, Saito Y, Hijikata A, Kitamura H, Tanaka S, Nakamura R, Tanaka T, Tomiyama H, Saito N, Fukata M, Miyamoto T, Lyons B, Ohshima K, Uchida N, Taniguchi S, Ohara O, Akashi K, Harada M, Shultz LD. 2007 Chemotherapy-resistant human AML stem cells home to and engraft within the bone-marrow endosteal region. *Nature Biotechnology* **25**, 1315–1321. (doi.org/10.1038/nbt1350).
- [150] Itik M, Salamuci MU, Banks SP. 2009 Optimal control of drug therapy in cancer treatment. *Nonlinear Analysis* **71**, 1473–1486. (doi.org/10.1016/j.na.2009.01.214).
- [151] Jabot F, Faure T, Dumoulin N. 2013 EasyABC: performing efficient approximate Bayesian computation sampling schemes in R. *Methods in Ecology and Evolution* **4**, 684–687. (doi.org/10.1111/2041-210X.12050).
- [152] Jain RK, 2001. Normalizing tumor vasculature with anti-angiogenic therapy: a new paradigm for combination therapy. *Nature Medicine* **7**, 987–989. (doi.org/10.1038/nm0901-987).
- [153] Jajarmi A, Baleanu D. 2019 On the fractional optimal control problems with a general derivative operator. *Asian Journal of Control* **23**, 1062–1071. (doi.org/10.1002/asjc.2282).

- [154] Jajarmi A, Ghanbari B, Baleanu D. 2019 A new and efficient numerical method for the fractional modeling and optimal control of diabetes and tuberculosis co-existence. *Chaos*, **29**, 093111. (doi.org/10.1063/1.5112177).
- [155] Janzen DH, 1966. Coevolution of mutualism between ants and acacias in Central America. *Evolution* **20**, 249–275. (doi.org/10.2307/2406628).
- [156] Jost J. 2017 *Riemannian Geometry and Geometric Analysis*. Cham: Springer International Publishing.
- [157] Julia Language. 2020 *Julia 1.5 Documentation - LinearAlgebra.pinv*. Retrieved November 2020. (<https://docs.julialang.org/en/v1stdlib/LinearAlgebra>).
- [158] Jung E, Lenhart S, Fing Z. 2002 Optimal control of treatments in a two-strain tuberculosis model. *Discrete and Continuous Dynamical Systems - Series B* **2**, 473–482. (doi.org/10.3934/dcdsb.2002.2.473).
- [159] Kalinski P, Talmadge JE. 2017 Tumor immuno-environment in cancer progression and therapy. *Advances in Experimental Medicine and Biology* **1036**, 1–18. (doi.org/10.1007/978-3-319-67577-0_1).
- [160] Kapitula T. 2015 *Ordinary Differential Equations and Linear Algebra: A Systems Approach*. Philadelphia: Society for Industrial and Applied Mathematics.
- [161] Karr JR, Sanghvi JC, Macklin DN, Gutschow MV, Jacobs JM, Bolival B, Assad-Garcia N, Glass JI, Covert MW. 2012 A whole-cell computational model predicts phenotype from genotype. *Cell* **150**, 389–401. (doi.org/10.1016/j.cell.2012.05.044).
- [162] Kass RE, Vos PW. 1997 *Geometrical Foundations of Asymptotic Inference*. New Jersey: Wiley-Interscience.
- [163] Kay SM. 1993 *Fundamentals of Statistical Signal Processing: Estimation Theory*. New Jersey: Prentice-Hall.
- [164] Keane AJ, Scanlan JP. 2007. Design search and optimization in aerospace engineering. *Philosophical Transactions of the Royal Society A* **365**, 2501–2529. (doi.org/10.1098/rsta.2007.2019).
- [165] Keller HB. 1976 *Numerical Solution of Two Point Boundary Value Problems*. Philadelphia: Society for Industrial and Applied Mathematics.
- [166] Kermack WO, McKendrick AG. 1927 A contribution to the mathematical theory of epidemics. *Proceedings of the Royal Society A* **115**, 700–721. (doi.org/10.1098/rspa.1927.0118).

- [167] Edelstein-Keshet L. 1988 *Mathematical Models in Biology*. New York: McGraw-Hill.
- [168] Kirk DE. 2004 *Optimal Control Theory: an Introduction*. New York: Dover Publications.
- [169] Kirschner DE, Lenhart S, Serbin S. 1997 Optimal control of the chemotherapy of HIV. *Journal of Mathematical Biology* **35**, 775–792. (doi.org/10.1007/s002850050076).
- [170] Kirschner DE, Linderman JJ. 2009 Mathematical and computational approaches can complement experimental studies of host-pathogen interactions. *Cell Microbiology* **11**, 531–539. (doi.org/10.1111/j.1462-5822.2008.01281.x).
- [171] Knowles G. 1981 *An Introduction to Applied Optimal Control*. Ney York: Academic Press.
- [172] Komorowski M, Costa MJ, Rand DA, Stumpf MPH. 2011 Sensitivity, robustness and identifiability in stochastic chemical kinetics models. *Proceedings of the National Academy of Sciences of the United States of America* **108**, 8645–8650. (doi.org/10.1073/pnas.1015814108).
- [173] Krupar R, Schreiber C, Offermann A, Lengerke C, Sikora AG, Thorns C, Perner S. 2018 Insilico analysis of anti-leukemia immune response and immune evasion in acute myeloid leukemia. *Leukemia & Lymphoma* **12**, 1–4. (doi.org/10.1080/10428194.2018.1434883).
- [174] Kuczynski EA, Sargent DJ, Grothe A, Kerbel RS. 2013 Drug rechallenge and treatment beyond progression: implications for drug resistance. *Nature Reviews Clinical Oncology* **10**, 571–587. (doi.org/10.1038/nrclinonc.2013.158).
- [175] Kulsrud HE. 1961 A practical technique for the determination of the optimum relaxation factor of the successive over-relaxation method. *Communications of the ACM* **4**, 184–187. (doi.org/10.1145/355578.366504).
- [176] Kumar CC. 2011 Genetic Abnormalities and Challenges in the Treatment of Acute Myeloid Leukemia. *Genes & Cancer* **2**, 95–107. (doi.org/10.1177/1947601911408076).
- [177] Kumbhari A, Kim PS, Lee PP. 2020 Optimisation of anti-cancer peptide vaccines to preferentially elicit high-avidity T cells. *Journal of Theoretical Biology* **486**, 110067. (doi.org/10.1016/j.jtbi.2019.110067).
- [178] Kuwana Y. 1995 Certainty equivalence and logarithmic utilities in consumption investment problems. *Mathematical Finance* **5**, 297–309. (doi.org/10.1111/j.1467-9965.1995.tb00069.x).

- [179] Kursawe J, Baker RE, Fletcher AG. Approximate Bayesian computation reveals the importance of repeated measurements for parameterising cell-based models of growing tissues. *Journal of Theoretical Biology* **443**, 66–81. (doi.org/10.1016/j.jtbi.2018.01.020).
- [180] Labianca R, Sobrero A, Isa L, Cortesi E, Barni S, Nicoella D, Aglietta M, Lonardi S, Corsi D, Turci D, Beretta GD, Fornarini G, Dapretto E, Floriani I, Zaniboni A. 2011 Intermittent versus continuous chemotherapy in advanced colorectal cancer: a randomised ‘GISCAD’ trial. *Annals of Oncology* **22**, 1236–1242. (doi.org/10.1093/annonc/mdq580).
- [181] Lai AKM, Dick TJM, Biewener AA, Wakeling JM. 2021 Task-dependent recruitment across ankle extensor muscles and between mechanical demands is driven by the metabolic cost of muscle contraction. *Journal of the Royal Society Interface* **18**, 20200765. (doi.org/10.1098/rsif.2020.0765).
- [182] Lambert B, MacLean AL, Fletcher AG, Combes AN, Little MH, Byrne HM. 2018 Bayesian inference of agent-based models: a tool for studying kidney branching morphogenesis. *Journal of Mathematical Biology* **76**, 1673–1697. (doi.org/10.1007/s00285-018-1208-z).
- [183] Lambert B. 2018 *A Student’s Guide to Bayesian Statistics*. London: Sage Publications Ltd.
- [184] LaRiviere J, Kling D, Sanchirico JN, Sims C, Springborn M. 2017 The treatment of uncertainty and learning in the economics of natural resource and environmental management. *Review of Environmental Economics and Policy* **12**, 92–112. (doi.org/10.1093/reep/rex021).
- [185] Ledzewicz U, Schättler H. 2016 Optimizing Chemotherapeutic Anti-cancer Treatment and the Tumor Microenvironment: an Analysis of Mathematical Models. In: Rejniak K. (eds) Systems Biology of Tumor Microenvironment. *Advances in Experimental Medicine and Biology*. Cham: Springer.
- [186] Lee JM, Gianchandani EP, Eddy JA, Papin JA. 2008 Dynamic analysis of integrated signaling, metabolic and regulatory networks. *PLoS Computational Biology* **4**, 1–20. (doi.org/10.1371/annotation/5594348b-de00-446a-bdd0-ec56e70b3553).
- [187] Lee S, Chowell G. 2017 Exploring optimal control strategies in seasonally varying flu-like epidemics. *Journal of Theoretical Biology* **412**, 36–47. (doi.org/10.1016/j.jtbi.2016.09.023).

- [188] Lee J, Kim J, Kwon H. 2013 Optimal control of an influenza model with seasonal forcing and age-dependent transmission rates. *Journal of Theoretical Biology* **317**, 310–320. (doi.org/10.1016/j.jtbi.2012.10.032).
- [189] Lee JM. 2018 *Introduction to Riemannian Manifolds*. Cham: Springer International Publishing.
- [190] Lehmann EL, Fienberg S, Casella G. 1998 *Theory of Point Estimation*. Secaucus: Springer.
- [191] Lenhart S, Workman JT. 2007 *Optimal Control Applied to Biological Models*. London: Chapman & Hall/CRC, Taylor & Francis.
- [192] Leung CY, Weitz JJ. 2017 Modeling the synergistic elimination of bacteria by phage and the innate immune system. *Journal of Theoretical Biology* **429**, 241–252. (doi.org/10.1016/j.jtbi.2017.06.037).
- [193] Li W, Todorov E. 2004 Iterative linear quadratic regulator design for non-linear biological movement systems. *Proceedings of the 1st International Conference on Informatics in Control, Automation and Robotics* **1**, 222–229. (doi.org/10.5220/0001143902220229).
- [194] Li Q, Chen L, Tai C, E W. 2018 Maximum principle based algorithms for Deep Learning. *Journal of Machine Learning Research* **18**, 1–29. (jmlr.org/papers/v18/17-653).
- [195] Liberzon D. 2011 *Calculus of Variations and Optimal Control Theory - A Concise Introduction*. Princeton: Princeton University Press.
- [196] Lichtenegger FS, Krupka C, Haubner S, Köhnke T, Subklewe M. 2017 Recent developments in immunotherapy of acute myeloid leukemia. *Journal of Hematology and Oncology* **10**, 1–20. (doi.org/10.1186/s13045-017-0505-0).
- [197] Liepe J, Barnes C, Cule E, Erguler K, Kirk P, Toni T, Stumpf MPH. 2010 ABC-SysBio—approximate Bayesian computation in Python with GPU support. *Bioinformatics* **26**, 1797–1799. (doi.org/10.1093/bioinformatics/btq278).
- [198] Liepe J, Filippi S, Komorowski M, Stumpf MPH. 2013 Maximising the information content of experiments in systems biology. *PLOS Computational Biology* **9**, e1002888. (doi.org/10.1371/journal.pcbi.1002888.g002).
- [199] Liepe J, Kirk P, Filippi S, Toni T, Barnes CP, Stumpf MPH. 2014 A framework for parameter estimation and model selection from experimental data in systems biology using approximate Bayesian computation. *Nature Protocols* **9**, 439–456. (doi.org/10.1038/nprot.2014.025).

- [200] Lill D, Timmer J, Kaschek D. 2019 Local Riemannian geometry of model manifolds and its implications for practical parameter identifiability. *PLOS ONE*, **14**: e0217837. (doi.org/10.1371/journal.pone.0217837).
- [201] Liso A, Castiglione F, Cappuccio A, Stracci F, Schlenk RF, Amadori S, Thiede C, Schnittger S, Valk PJM, Döhner K, Martelli MF, Schaich M, Krauter J, Ganser A, Martelli MP, Bolli N, Löwenberg B, Haferlach T, Ehninger G, Mandelli F, Döhner H, Michor F, Falini B. 2008 A one-mutation mathematical model can explain the age incidence of acute myeloid leukemia with mutated nucleophosmin (NPM1). *Haematologica* **93**, 1219–1226. (doi.org/10.3324/haematol.13209).
- [202] Liu JS, Chen R. 1998 Sequential Monte Carlo methods for dynamic systems. *Journal of the American Statistical Association* **93**, 1032–1044. (10.1080/01621459.1998.10473765).
- [203] Liu X, Frank J. 2021 Symplectic Runge–Kutta discretization of a regularized forward–backward sweep iteration for optimal control problems. *Journal of Computational and Applied Mathematics* **383**, 113113. (doi.org/10.1016/j.cam.2020.113113).
- [204] Logist F, Houska B, Diehl M, Van Impe JF. 2011 Robust multi-objective optimal control of uncertain (bio)chemical processes. *Chemical Engineering Science* **66**, 4670–4682. (doi.org/10.1016/j.ces.2011.06.018).
- [205] Lotka AJ. 1925 *Elements of Physical Biology*. Baltimore: Williams and Wilkins.
- [206] Loveridge LC. 2016 Physical and geometric interpretations of the Riemann Tensor, Ricci Tensor and Scalar Curvature. *arXiv preprint*. (arxiv.org/abs/gr-qc/0401099).
- [207] Löwenberg B, Downing JR, Burnett A. 1999 Acute myeloid leukaemia. *The New England Journal of Medicine* **341**, 1051–1062. (doi.org/10.1056/NEJM199909303411407).
- [208] Luscombe JH. 2018 *Core Principles of Special and General Relativity*. Boca Raton: CRC Press, Taylor & Francis.
- [209] Maclaren OJ, Nicholson R. 2020 What can be estimated? Identifiability, estimability, causal inference and ill-posed inverse problems. *arXiv preprint*. (arxiv.org/abs/1904.02826).
- [210] MacLean AL, Celso CL, Stumpf MPH. 2013 Population dynamics of normal and leukaemia stem cells in the haematopoietic stem cell niche show distinct regimes where leukaemia will be controlled. *Journal of The Royal Society Interface* **10**, 20120968. (doi.org/10.1098/rsif.2012.0968).

- [211] Maclean AL, Filippi S, Stumpf MPH. 2014 The ecology in the hematopoietic stem cell niche determines the clinical outcome in chronic myeloid leukemia. *Proceedings of the National Academy of Sciences of the United States of America* **111**, 3883–3888. (doi.org/10.1073/pnas.1317072111).
- [212] Malagò L, Pistone G. 2015 Information geometry on the Gaussian distribution in view of stochastic optimization. *Proceedings of the 2015 ACM Conference on Foundations of Genetic Algorithms XIII* **13**, 150–162. (doi.org/10.1145/2725494.2725510).
- [213] Malik T, Imran M, Jayaraman R. 2016 Optimal control with multiple human papillomavirus vaccines. *Journal of Theoretical Biology* **393**, 179–193. (doi.org/10.1016/j.jtbi.2016.01.004).
- [214] Manzoor H, Selam MA, Rahman FBA, Adham S, Castier M, Abdel-Wahab A. 2020 A tool for assessing the scalability of pressure-retarded osmosis (PRO) membranes. *Renewable Energy* **149**, 987–999. (doi.org/10.1016/j.renene.2019.10.098).
- [215] Marciniak-Czochra A, Stiehl T, Ho AD, Jäger W, Wagner W. 2009 Modelling of asymmetric cell division in hematopoietic stem cells - regulation of self renewal is essential for efficient repopulation. *Stem Cells and Development* **18**, 377–386. (doi.org/10.1089/scd.2008.0143).
- [216] Marino S, Hogue IB, Ray CJ, Kirschner DE. 2008 A methodology for performing global uncertainty analysis in systems biology. *Journal of Theoretical Biology* **254**, 178–196. (doi.org/10.1016/j.jtbi.2008.04.011).
- [217] Marjoram P, Molitor J, Plagnol V, Tavaré S. 2013 Markov chain Monte Carlo without likelihoods. *Proceedings of the National Academy of Sciences of the United States of America* **100**, 15324–15328. (doi.org/10.1073/pnas.0306899100).
- [218] Marler RT, Arora JS. 2004 Survey of multi-objective optimization methods for engineering. *Structural and Multidisciplinary Optimization* **26**, 369–395. (doi.org/10.1007/s00158-003-0368-6).
- [219] Martin TG, Burgman MA, Fidler F, Kuhnert PM, Low-Choy S, McBride M, Mengersen K. 2012 Eliciting expert knowledge in conservation science. *Conservation Biology* **26**, 29–38. (doi.org/10.1111/j.1523-1739.2011.01806.x).
- [220] Masarova L, Kanatarjian H, Garcia-Mannero G, Ravandi F, Sharma P, Daver N. 2017 Harnessing the immune system against leukemia: monoclonal antibodies and checkpoint strategies for AML. *Advances in Experimental Medicine and Biology* **995**, 73–95. (doi.org/10.1007/978-3-319-53156-4_4).

- [221] MathWorks. 2020 *Moore-Penrose pseudoinverse* (*R2020b*). Retrieved November 2020. (<https://au.mathworks.com/help/matlab/ref/pinv.html>).
- [222] MathWorks. 2020 *Solve equations numerically - vpasolve* (*R2020b*). Retrieved March 2020. (<https://au.mathworks.com/help/symbolic/vpasolve.html>).
- [223] Mayer LD, Janoff AS. 2007 Optimizing combination chemotherapy by controlling drug ratios. *Molecular Interventions* **7**, 216–223. (doi.org/10.1124/mi.7.4.8).
- [224] Mayo Clinic. 2019 Bone Marrow Transplant. Retrieved from <https://www.mayoclinic.org/tests-procedures/bone-marrow-transplant/about/pac-20384854> (Accessed February 2020).
- [225] McAsey M, Mou L, Han W. 2012 Convergence of the forward-backward sweep method in optimal control. *Computational Optimization and Applications* **43**, 207–226. (doi.org/10.1007/s10589-011-9454-7).
- [226] McGray AJR, Bramsom J. 2017 Adaptive resistance to cancer immunotherapy. *Advances in Experimental Medicine and Biology* **1036**, 213–227. (doi.org/10.1007/978-3-319-67577-0_14).
- [227] Mehrkanon S, Mehrkanon S, Suykens JAK. 2014 Parameter estimation of delay differential equations: an integration-free LS-SVM approach. *Communications in Nonlinear Science and Numerical Simulation* **19**, 830–841. (doi.org/10.1016/j.cnsns.2013.07.024).
- [228] Menéndez ML, Morales D, Pardo L, Salicrú M. 1995 Statistical tests based on geodesic distances. *Applied Mathematics Letters* **8**, 65–69. ([doi.org/10.1016/0893-9659\(94\)00112-P](https://doi.org/10.1016/0893-9659(94)00112-P)).
- [229] Miao H, Xia X, Perelson AS, Wu H. 2011 On identifiability of nonlinear models and applications in viral dynamics. *SIAM Review* **53**, 3–39. (doi.org/10.1137/090757009).
- [230] Mirams GR, Byrne HM, King JR. 2010 A multiple timescale analysis of a mathematical model of the Wnt/ β -catenin signalling pathway. *Journal of Mathematical Biology* **60**, 131–160. (doi.org/10.1007/s00285-009-0262-y).
- [231] Mitra ED, Hlavacek WS. 2019 Parameter estimation and uncertainty quantification for systems biology models. *Current Opinion in Systems Biology* **18**, 9–18. (doi.org/10.1016/j.coisb.2019.10.006).
- [232] Moore H. 2018 How to mathematically optimize drug regimens using optimal control. *Journal of Pharmacokinetics and Pharmacodynamics* **45**, 127–137. (doi.org/10.1007/s10928-018-9568-y).

- [233] Mughal TI, Goldman JM, Mughal ST. 2010 *Understanding leukaemias, Lymphomas and Myelomas*. London: Taylor & Francis.
- [234] Murphy KP. 2012 *Machine Learning: A Probabilistic Perspective*. Massachusetts: MIT Press.
- [235] Murray JD. 2002 *Mathematical Biology I: An Introduction*, 3rd ed. Heidelberg: Springer.
- [236] Mwanga GG, Haario H, Capasso V. 2015 Optimal control problems of epidemic systems with parameter uncertainties: Application to a malaria two-age-classes transmission model with asymptomatic carriers. *Mathematical Biosciences* **261**, 1–12. (doi.org/10.1016/j.mbs.2014.11.005).
- [237] Nanda S, Moore H, Lenhart S. 2007 Optimal control of treatment in a mathematical model of chronic myelogenous leukaemia. *Mathematical Biosciences* **210**, 143–156. (doi.org/10.1016/j.mbs.2007.05.003).
- [238] Neilan RLM, Schaefer E, Gaff H, Fister KR, Lenhart S. 2010 Modeling optimal intervention strategies for cholera. *Bulletin of Mathematical Biology* **72**, 2004–2018. (doi.org/10.1007/s11538-010-9521-8).
- [239] Nielsen F. 2020 An elementary introduction to information geometry. *Entropy* **22**, 1–61. (doi.org/10.3390/e22101100).
- [240] Nievergelt Y. 1991 Aitken’s and Steffensen’s accelerations in several variables. *Numerische Mathematik* **59**, 295–310. (doi.org/10.1007/BF01385782).
- [241] Nievergelt Y. 1995 The condition of Steffensen’s acceleration in several variables. *Journal of Computational and Applied Mathematics* **58**, 291–305. (doi.org/10.1016/0377-0427(94)00004-K).
- [242] Noda T. 1984 The Steffensen iteration method for systems of nonlinear equations. *Proceedings of the Japan Academy* **60**, 18–21. (doi.org/10.3792/pjaa.60.18).
- [243] Noda T. 1986 The Aitken-Steffensen formula for systems of nonlinear equations. III. *Proceedings of the Japan Academy* **62**, 174–177. (doi.org/10.3792/PJAA.62.174).
- [244] Noda T. 1987 The Steffensen iteration method for systems of nonlinear equations. II. *Proceedings of the Japan Academy* **63**, 186–189. (doi.org/10.3792/pjaa.63.186).
- [245] Normand ST, McNeil BJ, Peterson LE, Palmer RH. 1998 Eliciting expert opinion using the Delphi technique: identifying performance indicators for cardiovascular disease. *International Journal for Quality in Healthcare* **10**, 247–260. (doi.org/10.1093/intqhc/10.3.247).

- [246] Norton M. 2014 *Modern Control Engineering*. Pergamon Unified Engineering Series. Saint Louis: Elsevier Science.
- [247] Ommen HB, Nvyold CG, Brændstrup K, Andersen BL, Ommen IB, Hasle H, Hokland P, Østergaard M. 2008 Relapse prediction in acute myeloid leukaemia patients in complete remission using WT1 as a molecular marker: development of a mathematical model to predict time from molecular to clinical relapse and define optimal sampling intervals. *British Journal of Haematology* **14**, 782–791. (doi.org/10.1111/j.1365-2141.2008.07132.x).
- [248] Ommen HB, Hokland P, Haferlach T, Abildgaard L, Alpermann T, Haferlach C, Kern W, Schnittger S. 2014 Relapse kinetics in acute myeloid leukaemias with *MLL* translocations of partial tandem duplications within the *MLL* gene. *British Journal of Haematology* **165**, 618–628. (doi.org/10.1111/bjh.12792).
- [249] Orbach O, Crowe CM. 1971 Convergence promotion in the simulation of chemical processes with recycle – the dominant eigenvalue method. *Canadian Journal of Chemical Engineering* **49**, 509–513. (doi.org/10.1002/cjce.5450490414).
- [250] Østby I, Rusten LS, Kvalheim G, Grøttum P. 2003 A mathematical model for reconstitution of granulopoiesis after high dose chemotherapy with autologous stem cell transplantation. *Journal of Mathematical Biology* **47**, 101–136. (doi.org/10.1007/s00285-003-0198-6).
- [251] Oyarzún DA, Ingalls BP, Middleton RH, Kalamatianos D. 2009 Sequential activation of metabolic pathways: a dynamic optimization approach. *Bulletin of Mathematical Biology* **71**, 1851–1872. (doi.org/10.1007/s11538-009-9427-5).
- [252] Panik MJ. 2014 *Growth Curve Modeling: Theory and Applications*. New Jersey: John Wiley & Sons, Ltd.
- [253] Papst I, Earn DJD. 2019 Invariant predictions of epidemic patterns from radically different forms of seasonal forcing. *Journal of the Royal Society Interface* **16**, 20190202. (doi.org/10.1098/rsif.2019.0202).
- [254] Patil NS, Dingwell JB, Cusumano JP. 2020 Task-level regulation enhances global stability of the simplest dynamic walker. *Journal of the Royal Society Interface* **17**, 20200278. (doi.org/10.1098/rsif.2020.0278).
- [255] Pawitan Y. 2001 *In All Likelihood: Statistical Modelling and Inference Using Likelihood*. Oxford: Oxford University Press, Incorporated.

- [256] Peitz S, Dellnitz M. 2018 A Survey of Recent Trends in Multiobjective Optimal Control — Surrogate Models, Feedback Control and Objective Reduction. *Mathematical and Computational Applications* **23**, 1–33. (doi.org/10.3390/mca23020030).
- [257] Penrose R. 1955 A generalized inverse for matrices. *Mathematical Proceedings of the Cambridge Philosophical Society* **51**, 406–413. (doi.org/10.1017/S0305004100030401).
- [258] Penrose R. 1956 On best approximate solutions of linear matrix equations. *Mathematical Proceedings of the Cambridge Philosophical Society* **52**, 17–19. (doi.org/10.1017/S0305004100030929).
- [259] Pinele J, Costa SIR, Strapasson JE. 2019 *On the Fisher-Rao Information Metric in the Space of Normal Distributions*. Cham: Springer International Publishing AG.
- [260] Pinele J, Strapasson JE, Costa SIR. 2020 The Fisher-Rao distance between multivariate normal distributions: special cases, bounds and applications. *Entropy* **22**, 1–24. (doi.org/10.3390/e22040404).
- [261] Planitz M. 1979 Inconsistent systems of linear equations. *The Mathematical Gazette* **63**, 181–185. (doi.org/10.2307/3617890).
- [262] Polak E. 1973 An historical survey of computational methods in optimal control. *SIAM Review* **15**, 553–584. (doi.org/10.1137/1015071).
- [263] Pollyea DA, Jordan CT. 2017 Therapeutic targeting of acute myeloid leukaemia stem cells. *Blood* **129**, 1627–1635. (doi.org/10.1182/blood-2016-10-696039).
- [264] Pontryagin LS, Boltyanskii VG, Gamkrelidze RV, Mischenko EF. 1962 *The Mathematical Theory of Optimal Processes* [English translation]. New York: Interscience.
- [265] Popat U, Abraham J. 2011 *Emerging Cancer Therapeutics: Leukaemia*. New York: Demos Medical Publishing.
- [266] Powell MJD. 2009 The BOBYQA algorithm for bound constrained optimization without derivatives. *Technical Report DAMTP 2009/NA06, Department of Applied Mathematics and Theoretical Physics, University of Cambridge*. (https://www.damtp.cam.ac.uk/user/na/NA_papers/NA2009_06.pdf).
- [267] Poyiadjis G. 2011 Particle approximations of the score and observed information matrix in state space models with application to parameter estimation. *Biometrika* **98**, 65–80. (doi.org/10.1093/biomet/asq062).
- [268] Prangle D. 2017 Adapting the ABC distance function. *Bayesian Analysis* **12**, 289–309. (doi.org/10.1214/16-BA1002).

- [269] Press WH. 2007 *Numerical Recipes: The Art of Scientific Computing*. New York: Cambridge University Press.
- [270] Priess MC, Conway R, Choi J, Popovich, JM, Radcliffe, C. 2015 Solutions to the inverse LQR problem with application to biological systems analysis. *IEEE Transactions on Control Systems Technology* **23**, 770–777. (doi.org/10.1109/TCST.2014.2343935).
- [271] SciPy Community. 2020 *NumPy Documentation*. Retrieved November 2020. (<https://numpy.org/doc/stable/reference/generated/numpy.linalg.pinv>).
- [272] Rackauckas C, Nie Q. 2017 DifferentialEquations.jl – A Performant and Feature-Rich Ecosystem for Solving Differential Equations in Julia. *The Journal of Open Research Software* **5**, 1–10. (doi.org/10.5334/jors.151).
- [273] Ramière I, Helfer T. 2015 Iterative residual-based vector methods to accelerate fixed point iterations. *Computers and Mathematics with Applications* **70**, 2210 – 2226. (doi.org/10.1016/j.camwa.2015.08.025).
- [274] Rao CR. 1992 *Information and the Accuracy Attainable in the Estimation of Statistical Parameters*. In: Kotz S, Johnson NL (eds) Breakthroughs in Statistics, 235–247. New York: Springer.
- [275] Rao AV. 2009 A survey of numerical methods for optimal control. *Advances in the Astronautical Sciences* **135**, 497–528.
- [276] Raue A, Kreutz C, Maiwald T, Bachmann J, Schilling M, Klingmüller U, Timmer J. 2009 Structural and practical identifiability analysis of partially observed dynamical models by exploiting the profile likelihood. *Bioinformatics* **25**, 1923–1929. (doi.org/10.1093/bioinformatics/btp358).
- [277] Rawlings JS, Rosler .M, Harrison DA. 2004 The JAK/STAT signaling pathway. *Journal of Cell Science* **117**, 1281–1283. (doi.org/10.1242/jcs.00963).
- [278] Rawson T, Wilkins KE, Bonsall MB. 2020 Optimal control approaches for combining medicines and mosquito control in tackling dengue. *Royal Society Open Science* **7**, 181843. (doi.org/10.1098/rsos.181843).
- [279] Reid JK. 1966 A method for finding the optimum successive over-relaxation parameter. *The Computer Journal* **9**, 200–204. (doi.org/10.1093/comjnl/9.2.200).
- [280] Ruess J, Parise F, Milius-Argeitis A, Khammash M, Lygeros J. 2015 Iterative experiment design guides the characterization of a light-inducible gene expression circuit. *Proceedings of the National Academy of Sciences of the United States of America* **112**, 8148–8153. (doi.org/10.1073/pnas.1423947112).

- [281] Roberts MG. 2007 The pluses and minuses of \mathcal{R}_0 . *Journal of the Royal Society Interface* **4**, 949–961. (doi.org/10.1098/rsif.2007.1031).
- [282] Ruijters DM, Whiteson S. 2017 *Multi-objective Decision Making*. California: Morgan & Claypool.
- [283] Rosen EM, Pauls AC. 1977 Computer aided chemical process design: the FLOWTRAN system. *Computers and Chemical Engineering* **1**, 11–21. ([doi.org/10.1016/0098-1354\(77\)80003-3](https://doi.org/10.1016/0098-1354(77)80003-3)).
- [284] Sargent RWH. 2000 Optimal control. *Journal of Computational and Applied Mathematics* **124**, 361–371. ([doi.org/10.1016/S0377-0427\(00\)00418-0](https://doi.org/10.1016/S0377-0427(00)00418-0)).
- [285] Schättler H, Ledzewicz U. 2015 *Optimal Control for Mathematical Models of Cancer Therapies*. New York: Springer.
- [286] Schnoerr D, Sanguinetti G, Grima R. 2017 Approximation and inference methods for stochastic biochemical kinetics – a tutorial review. *Journal of Physics A: Mathematical and Theoretical* **50**, 093001. (doi.org/10.1088/1751-8121/aa54d9).
- [287] Schrödl K, Von Schilling C, Tufman A, Huber RM, Gamarra F. 2015 Response to chemotherapy, reexposure to crizotinib and treatment with a novel ALK inhibitor in a patient with acquired crizotinib resistance. *Respiration* **88**, 262–264. (doi.org/10.1159/000364949).
- [288] Seghouane A, Amari S. 2007 The AIC criterion and symmetrizing the Kullback–Leibler divergence. *IEEE Transactions on Neural Networks* **18**, 97–106. (doi.org/10.1109/TNN.2006.882813).
- [289] Sethi PS. 2019 *Optimal Control Theory – Applications to Management Science and Economics, Third Edition*. Cham, Switzerland: Springer.
- [290] Sharp JA, Browning AP, Mapder T, Burrage K, Simpson MJ. 2019 Optimal control of acute myeloid leukaemia. *Journal of Theoretical Biology* **470**, 30–42. (doi.org/10.1016/j.jtbi.2019.03.006).
- [291] Sharp JA, Browning AP, Mapder T, Baker CM, Burrage K, Simpson MJ. 2020 Designing combination therapies using multiple optimal controls. *Journal of Theoretical Biology* **497**, 110277. (doi.org/10.1016/j.jtbi.2020.110277).
- [292] Sharp JA, Burrage K, Simpson MJ. 2021 Implementation and acceleration of optimal control for systems biology. *Journal of the Royal Society Interface* **18**, 20210241. (doi.org/10.1098/rsif.2021.0241).

- [293] Sharp JA, Browning AP, Burrage K, Simpson MJ. 2022 Parameter estimation and uncertainty quantification using information geometry. *Journal of the Royal Society Interface* [in press]. ([arXiv:2111.12201](https://arxiv.org/abs/2111.12201)).
- [294] Shipley RJ, Davidson AJ, Chan K, Chaudhuri JB, Waters SL, Ellis MJ. 2011 A strategy to determine operating parameters in tissue engineering hollow fibre bioreactors. *Biotechnology and Bioengineering* **108**, 1450–1461. (doi.org/10.1002/bit.23062).
- [295] Siekmann I, Sneyd J, Crampin EJ. 2012 MCMC can detect nonidentifiable models. *Biophysical Journal* **103**, 2275–2286. (doi.org/10.1016/j.bpj.2012.10.024).
- [296] Simpson MJ, Landman KA. 2007 Analysis of split operator methods applied to reactive transport with Monod kinetics. *Advances in Water Resources* **30**, 2026–2033. (doi.org/10.1016/j.advwatres.2007.04.005).
- [297] Simpson MJ. 2009 Depth-averaging errors in reactive transport modeling. *Water Resources Research* **45**, 1–8. (doi.org/10.1029/2008WR007356).
- [298] Simpson MJ, Baker RE, Vittadello ST, Maclareen OJ. 2020 Practical parameter identifiability for spatio-temporal models of cell invasion. *Journal of the Royal Society Interface* **17**, 20200055. ([http://dx.doi.org/10.1098/rsif.2020.0055](https://dx.doi.org/10.1098/rsif.2020.0055)).
- [299] Simpson MJ, Browning AP, Warne DJ, Maclareen OJ, Baker RE. 2022 Parameter identifiability and model selection for sigmoid population growth models. *Journal of Theoretical Biology* **535**, 110998. (doi.org/10.1016/j.jtbi.2021.110998).
- [300] Singh A, Jayaraman A, Hahn J. 2006 Modeling regulatory mechanisms in IL-6 signal transduction in hepatocytes. *Biotechnology and Bioengineering* **95**, 850–862. (doi.org/10.1002/bit.21026).
- [301] Sipkins DA, Wei X, Wu JW, Runnels JM, Côté D, Means TK, Luster AD, Scadden DT, Lin CP. 2005 In vivo imaging of specialized bone marrow endothelial microdomains for tumour engraftment. *Nature* **435**, 969–973. (doi.org/10.1038/nature03703).
- [302] Sisson SA, Fan Y, Beaumont M. 2018 *Handbook of Approximate Bayesian Computation*. Boca Raton: Chapman & Hall-CRC, Taylor and Francis Group.
- [303] Skorych V, Dosta M, Heinrich S. 2020 Dyssol - An open-source flow-sheet simulation framework for particulate materials. *SoftwareX* **12**, 100572. (doi.org/10.1016/j.softx.2020.100572).
- [304] Snowden TJ, van der Graaf PH, Tindall MJ. 2017 Methods of model reduction for large-scale biological systems: a survey of current methods and trends. *Bulletin of Mathematical Biology* **79**, 1449–1486. (doi.org/10.1007/s11538-017-0277-2).

- [305] Sogbohossou EA, Kassa BD, Waltert M, Khorozyan I. 2018 Spatio-temporal niche partitioning between the African lion (*Panthera leo leo*) and spotted hyena (*crocuta crocuta*) in western African savannas. *European Journal of Wildlife Research* **64**, 1–8. (doi.org/10.1007/s10344-017-1159-5).
- [306] Steffensen JF. 1933 Remarks on iteration. *Scandinavian Actuarial Journal* **1**, 64–72. (doi.org/10.1080/03461238.1933.10419209).
- [307] Stiehl T, Baran N, Ho AD, Marciniak-Czochra A. 2015 Cell division patterns in acute myeloid leukaemia - stem-like cells determine clinical course: a model to predict patient survival. *Cancer Research* **75**, 940–949. (doi.org/10.1158/0008-5472.CAN-14-2508).
- [308] Sunnåker M, Busetto AG, Numminen E, Corander J, Foll M, Dessimoz C. 2013 Approximate Bayesian computation. *PLOS Computational Biology* **9**, e1002803. (doi.org/10.1371/journal.pcbi.1002803).
- [309] Sweilam NH, Al-Mekhlafi SM, Baleanu D. 2019 Optimal control for a fractional tuberculosis infection model including the impact of diabetes and resistant strains. *Journal of Advanced Research* **17**, 125–137. (doi.org/10.1016/j.jare.2019.01.007).
- [310] Sweilam NH, Al-Mekhlafi SM, Assiri T, Atangana A. 2020 Optimal control for cancer treatment mathematical model using Atangana-Baleanu-Caputo fractional derivative. *Advances in Difference Equations* **2020**, 1–21. (doi.org/10.1158/1055-9965.EPI-10-0437).
- [311] Sweilam NH, Al-Mekhlafi SM, Baleanu D. 2020 A hybrid fractional optimal control for a novel Coronavirus (2019-nCov) mathematical model. *Journal of Advanced Research* **32**, 149–160. (doi.org/10.1016/j.jare.2020.08.006).
- [312] Tang M, Gonen M, Quintas-Cardama A, Cortes J, Kantarjian H, Field C, Hughes TP, Branford S, Michor F. 2011 Dynamics of chronic myeloid leukemia response to long-term targeted therapy reveal treatment effects on leukemic stem cells. *Blood* **118**, 1622–1631. (doi.org/10.1182/blood-2011-02-339267).
- [313] Thakur MD, Salangsang F, Landman AS, Sellers WR, Pryer NK, Levesque MP, Dummer R, McMahon M, Stuart DD. 2013 Modelling vemurafenib resistance in melanoma reveals a strategy to forestall drug resistance. *Nature* **494**, 251–256. (doi.org/10.1038/nature11814).
- [314] Tigue CC, Fitzner KA, Alkhatib M, Schmid E, Bennett CL. 2007 The value of innovation: the economics of targeted drugs for cancer. *Targeted Oncology* **2**, 113–119. (doi.org/10.1007/s11523-007-0043-8).

- [315] Toni T, Welch D, Strelkowa N, Ipsen A, Stumpf MPH. 2009 Approximate Bayesian computation scheme for parameter inference and model selection in dynamical systems. *Journal of the Royal Society Interface* **6**, 187–202. (doi.org/10.1098/rsif.2008.0172).
- [316] Transtrum MK, Qiu P. 2014 Model reduction by manifold boundaries. *Physical Review Letters* **113**, 098701. (doi.org/10.1103/PhysRevLett.113.098701).
- [317] Treloar NJ, Fedorec AJH, Ingalls B, Barnes CP. 2020 Deep reinforcement learning for the control of microbial co-cultures in bioreactors. *PLOS Computational Biology* **16**, e1007783. (doi.org/10.1371/journal.pcbi.1007783).
- [318] Tsiantis N, Balsa-Canto E, Banga JR. 2018 Optimality and identification of dynamic models in systems biology: an inverse optimal control framework. *Bioinformatics* **34**, 2433–2440. (doi.org/10.1093/bioinformatics/bty438).
- [319] Tsiantis N, Banga JR. 2020 Using optimal control to understand complex metabolic pathways. *BMC Bioinformatics* **21**, 1–33. (doi.org/10.1186/s12859-020-03808-8).
- [320] Tsitouras C. 2011 Runge–Kutta pairs of order 5 (4) satisfying only the first column simplifying assumption. *Computers & Mathematics with Applications* **62**, 770–775. (doi.org/10.1016/j.camwa.2011.06.002).
- [321] Tsouaris A, Wallace J. 2002 Analysis of logistic growth models. *Mathematical Biosciences* **179**, 21–55. ([doi.org/10.1016/S0025-5564\(02\)00096-2](https://doi.org/10.1016/S0025-5564(02)00096-2)).
- [322] Varga RS. 2000 *Matrix Iterative Analysis, Second Revised and Expanded Edition*. Heidelberg, Germany: Springer-Verlag.
- [323] Villaverde AF, Barreiro A, Papachristodoulou A. 2016 Structural identifiability of dynamic systems biology models. *PLOS Computational Biology* **12**, e1005153. (doi.org/10.1371/journal.pcbi.1005153).
- [324] Villaverde AF. 2019 Observability and structural identifiability of nonlinear biological systems. *Complexity* **2019**, 1–12. (doi.org/10.1155/2019/8497093).
- [325] Vo BN, Drovandi CC, Pettitt AN, Simpson MJ. 2015 Quantifying uncertainty in parameter estimates for stochastic models of collective cell spreading using approximate Bayesian computation. *Mathematical Biosciences* **263**, 133–142. (doi.org/10.1016/j.mbs.2015.02.010).
- [326] Walker HF, Ni P. 2011 Anderson acceleration for fixed-point iterations. *SIAM Journal on Numerical Analysis* **49**, 1715–1735. (doi.org/10.1137/10078356X).

- [327] Walpole J, Papin JA, Peirce SM. 2013 Multiscale computational models of complex biological systems. *Annual Review of Biomedical Engineering* **15**, 137–154. (doi.org/10.1146/annurev-bioeng-071811-150104).
- [328] Warlick ED, Miller JS. 2011 Myelodysplastic syndromes: the role of the immune system in pathogenesis. *Leukemia & Lymphoma* **52**, 2045–2049. (doi.org/10.3109/10428194.2011.584002).
- [329] Warne DJ, Baker RE, Simpson MJ. 2017 Optimal quantification of contact inhibition in cell populations. *Biophysical Journal* **113**, 1920–1924. (doi.org/10.1016/j.bpj.2017.09.016).
- [330] Warne DJ, Baker RE, Simpson MJ. 2019 Simulation and inference algorithms for stochastic biochemical reaction networks: from basic concepts to state-of-the-art. *Journal of the Royal Society Interface* **16**, 20180943. (doi.org/10.1098/rsif.2018.0943).
- [331] Warne DJ, Baker RE, Simpson MJ. 2019 Using experimental data and information criteria to guide model selection for reaction–diffusion problems in mathematical biology. *Bulletin of Mathematical Biology* **81**, 1760–1804. (doi.org/10.1007/s11538-019-00589-x).
- [332] Warne DJ, Baker RE, Simpson MJ. 2020 A practical guide to pseudo-marginal methods for computational inference in systems biology. *Journal of Theoretical Biology* **496**, 110255. (doi.org/10.1016/j.jtbi.2020.110255).
- [333] Watanabe S. 2009 *Algebraic Geometry and Statistical Learning Theory*. New York: Cambridge University Press.
- [334] Wegstein JH. 1958 Accelerating convergence of iterative processes. *Communications of the ACM* **1**, 9–13. (doi.org/10.1145/368861.368871).
- [335] Wiernik PH, Dutcher JP, Goldman JM, Kyle RA. 2013 *Neoplastic Diseases of the Blood*. New York: Springer.
- [336] Wilkinson RD. 2013 Approximate Bayesian computation (ABC) gives exact results under the assumption of model error. *Statistical Applications in Genetics and Molecular Biology* **12**, 129–141. (doi.org/10.1515/sagmb-2013-0010).
- [337] Yakimov AS. 2016 *Analytical Solution Methods for Boundary Value Problems*. London: Academic Press.
- [338] Yardley DA. 2013 Drug resistance and the role of combination chemotherapy in improving patient outcomes. *International Journal of Breast Cancer* **2013**, 15. (doi.org/10.1155/2013/137414).

- [339] Yeshurun M, Wolach O. 2019 Autologous hematopoietic cell transplantation for AML in first remission – An abandoned practice or promising approach? *Seminars in Hematology* **56**, 139–146. (doi.org/10.1053/j.seminhematol.2019.01.001).
- [340] Yeung E, McFann S, Marsh L, Dufresne E, Filippi S, Harrington HA, Shvartsman SY, Wühr M. 2020 Inference of multisite phosphorylation rate constants and their modulation by pathogenic mutations. *Current Biology* **30**, 877–882. (doi.org/10.1016/j.cub.2019.12.052).
- [341] Young DM. 1971 *Iterative Solutions of Large Linear Systems*. Orlando, FL: Academic Press, Inc.
- [342] Yu H, Lee H, Herrmann A, Buettner R, Jove R. 2014 Revisiting STAT3 signalling in cancer: new and unexpected biological functions. *Nature Reviews Cancer* **14**, 736–746. (doi.org/10.1038/nrc3818).
- [343] Yuan Y. 2016 Spatial heterogeneity in the tumor microenvironment. *Cold Spring Harbour Perspectives in Medicine* **6**, a026583. ([10.1101/cshperspect.a026583](https://doi.org/10.1101/cshperspect.a026583)).
- [344] Yue H, Brown M, Knowles J, Wang H, Broomhead DS, Kell DB. Insights into the behaviour of systems biology models from dynamic sensitivity analysis: a case study of an NF- κ B signalling pathway. *Molecular Biosystems* **2**, 640–649. (doi.org/10.1039/B609442B).
- [345] Zeidan AM, Mahmoud D, Kucmin-bemelmans IT, Alleman CJ, Hensen M, Skikne B, Smith BD. 2016 Economic burden associated with acute myeloid leukemia treatment. *Expert Review of Hematology* **9**, 79–89. (doi.org/10.1586/17474086.2016.1112735).
- [346] Zennaro M. 1986 Natural continuous extensions of Runge-Kutta methods. *Mathematics of Computation* **46**, 119–133. (doi.org/10.2307/2008218).
- [347] Zimmer C, Leuba SI, Cohen T, Yaesoubi R. 2018 Accurate quantification of uncertainty in epidemic parameter estimates and predictions using stochastic compartmental models. *Statistical Methods in Medical Research* **28**, 3591–3608. (doi.org/10.1177/0962280218805780).
- [348] Zoppoli R, Sanguineti M, Gnecco G, Parisini T. 2019 *Neural Approximations for Optimal Control and Decision*. Cham, Switzerland: Springer.